Isolation and Characterization of Novel Natural Compounds from Myxobacteria

Dissertation

zur Erlangung des Grades

des Doktors der Naturwissenschaften

der Naturwissenschaftlich-Technischen Fakultät III

Chemie, Pharmazie, Bio- und Werkstoffwissenschaften

der Universität des Saarlandes

von

Suvd Nadmid

Saarbrücken
2015

Tag des Kolloquiums:	06. August 2015
Dekan:	Prof. Dr. –Ing. Dirk Bähre
Berichterstatter:	Prof. Dr. Rolf Müller
	Prof. Dr. Uli Kazmaier
Vorsitz:	Prof. Dr. Rolf W. Hartmann
Akad. Mitarbeiter:	Dr. Josef Zapp

Diese Arbeit entstand unter der Anleitung von Prof. Dr. Rolf Müller in der Fachrichtung 8.2, Pharmazeutische Biotechnologie der Naturwissenschaftlich-Technischen Fakultät III der Universität des Saarlandes von Oktober 2010 bis Juni 2015.

Acknowledgements

First of all, I would like to express my sincere gratitude to my supervisor Prof. Dr. Rolf Müller for giving me the opportunity to work in his group on the fascinating and challenging projects. I thank him for his encouragement, support and guidance throughout my PhD study.

I owe my special gratitude to Dr. Alberto Plaza for being my mentor, who introduced me to the world of natural product chemistry by spending his precious time with me in the lab. Without him, all these challenging tasks would never be completed.

I want to specially thank Prof. Dr. Uli Kazmaier for his support for the DAAD scholarship and for being my second supervisor.

I also would like to thank Deutscher Akademischer Austausch Dienst (DAAD) for the financial support during my stay in Germany without which my biggest dream would never come true. I am grateful to HZI for scholarship for the final part of the study as big support to complete the thesis.

I am particularly grateful to Dr. Kirsten Harmrolfs for her support and helpful discussion regarding tough chemical synthesis and derivatization reactions as well as her valuable comments on the thesis and translation of the abstract to german. I would like to express my gracious appreciations to Dr. Ronald Garcia for providing me the prolific myxobacterial strains, Dr. Thomas Hoffmann, and Eva Luxenburger for performing MS/MS fragmentation studies, and Dr. Jennifer Herrmann and Viktoria Schmitt for carrying out the bioactivity evaluation experiments. In addition, I would like to thank Dr. Nyan Gawas, who was mentoring me in the beginning of my study and guided me well to the analytical chemistry field.

To Hilda Sucipto and Dr. Louise Kjaerulff, thank you for spending unforgettable time together and cheering me on besides for their helpful comments and suggestion for writing the thesis.

Last but not least, my deepest thanks go to my husband Batchudur Sukhbaatar and our children Misheel and Tuguldur for their patience, support and understanding their “busy mummy” who could not always be there by you for the past few years.

Publications

T. Hoffmann, S. Müller, **S. Nadmid**, R. Garcia, and R. Müller; Microsclerodermins from Terrestrial Myxobacteria: An Intriguing Biosynthesis Likely Connected to a Sponge Symbiont; *Journal of the American Chemical Society*, **2013**, 135, 16904-16911.

S. Nadmid, A. Plaza, G. Lauro, R. Garcia, G. Bifulco and R. Müller; Hyalachelins A-C, Unusual Siderophores Isolated from the Terrestrial Myxobacterium *Hyalangium minutum; Organic Letters*, **2014**, 16, 4130-4133.

S. Nadmid, A. Plaza, R. Garcia, and R. Müller; Cystochromones, Unusual Chromone-Containing Polyketides from the Myxobacterium *Cystobacter* sp.*; Journal of Natural Products,* submitted

Conference Contributions

S. Nadmid, A. Plaza, G. Lauro, R. Garcia, G. Bifulco and R. Müller. "Hyalachelins A-C, a New Structural Class of Siderophores Isolated from Myxobacterium" 4th HIPS Symposium, Saarbrucken, Germany, 2013 (poster)

S. Nadmid, A. Plaza, G. Lauro, R. Garcia, G. Bifulco and R. Müller. "Discovery of Novel Catecholate Type of Siderophores from Myxobacterium" VAAM International Workshop, Dresden, Germany, 2014 (poster)

Zusammenfassung

Mikrobielle Naturstoffe sind bekanntermaßen eine ergiebige Quelle für neue therapeutische Wirkstoffe. Aus Myxobakterien werden fortwährend neue biologisch aktive Naturstoffe mit einzigartigen Strukturen isoliert. Ein chemisches screening dieser Gram-negativen Bakterien resultierte in der Identifizierung von zwei strukturell neuen Klassen von Sekundärmetaboliten und einem neuen Derivat eines bereits bekannten Naturstoffes. In der vorliegenden Arbeit werden die Isolierung, Strukturaufklärung und die biologischen Aktivitäten dieser Substanzen diskutiert.

Die Hyacheline A-C, neue Siderophore vom Catecholat-Typ, wurden aus einem Stamm der wenig erforschten myxobakteriellen Spezies *Hyalangium minutum* isoliert. Die dreidimensionale Struktur der Hyacheline wurde mittels Kombination von spektroskopischen Daten mit quantenmechanischen Berechnungen aufgeklärt, sowie ihr Eisen-Bindungsverhalten anhand von CAS Assays bestimmt. Die Cystochromone wurden aus Extrakten von *Cystobacter* sp. isoliert. Die chromonartigen Polyketide tragen an Position C-5 des Chromonsystems einen langkettigen aliphatischen Rest. Diese Substitution ist von natürlichen Chromonen bisher nicht bekannt. Auf Basis von Fütterungsexperimenten konnte ein Biosyntheseweg für die Cystochromone vorgeschlagen werden.

Weiterhin wurde ein neues Derivat der Mikroskleroderminе aus dem Extrakt eines terrestrischen Myxobakteriums isoliert. Diese Naturstoffe waren bisher aus Meeresschwämmen bekannt und stellen ein Beispiel des selten beschriebenen Falles eines gemeinsamen oder ähnlichen Sekundärmetabolismus von marinen und terrestrischen Mikroorganismen dar.

Abstract

Microbial secondary metabolites are known to be an excellent source for novel therapeutic agents. Among other microorganisms, myxobacteria are continuously providing new biologically active natural compounds with unique structures. Here, chemical screening of these gram-negative bacteria has resulted in the identification of two new structural classes of natural products along with a new derivative of a sponge-derived natural product. In this thesis, isolation, structural elucidation, and biological activity of these new secondary metabolites are presented.

New catecholate-type siderophores, hyalachelins A-C, were isolated from the strain belonging to the underexplored species *Hyalangium minutum*. Their complete 3D structure was obtained by combining the spectroscopic data and quantum mechanical calculations. Iron binding activity of hyalachelins was determined by CAS assay. Moreover, novel polyketides, named cystochromones, were isolated from *Cystobacter* sp. Cystochromones bear a chromone ring that is substituted by a long aliphatic chain on position C-5 which is not preceded among natural chromones. Additionally, a biosynthetic pathway was proposed on the basis of the results of the feeding experiments.

Furthermore, a new derivative of the marine sponge-derived peptide microsclerodermin was isolated from the terrestrial myxobacterium. This result represents the rare example of isolation of same compounds from terrestrial and marine sources.

Table of Contents

1. Introduction

1.1. Natural Products as Source for New Drugs

The chemical substances isolated from natural sources such as plants, animals and microorganisms, have been playing important roles in treating and preventing various human diseases due to their broad range of biological activities. Besides showing great chemical structural diversity, these organic molecules, called natural products (NPs), are considered as templates for synthetic modification for drug development.[1] [2] In the past 30 years (1981-2010), 1355 new drugs have been approved around the world by the U.S. Food and Drug Administration (FDA) and similar organizations.[3] 26.8% of these new drugs were derived from either natural products or their semisynthetic compounds whereas 24% of the new drugs were made by total synthesis based on pharmacophores of natural compounds. During this time, the majority of clinically launched new antibacterial (66%) and anticancer (61%) drugs were inspired by NPs.[3] These statistics already imply how significant natural products are in drug discovery and development.

Among natural products, microorganisms have been considered a prolific source of bioactive molecules. Since the discovery of penicillin in 1928 a number of bacteria and fungi have been screened for new antibiotics.[4] This effort has successfully brought many antibiotics, which are still in use or natural scaffold of those are semisynthetically tailored into more active generations (e.g. erythromycin→ clarithromycin →telithromycin)[5] [6] (Figure 1.1). Among microorganisms, the order Actinomycetales is known to produce a large number of bioactive secondary metabolites that have significant applications in human medicine. By 2001 roughly 3000 antibiotics have been identified from this order, more precisely 90% of those were from genus *Streptomyces*.[7]

However the resistance of pathogenic bacteria to existing drugs has become one of the main problems in hospitals. Various infectious diseases specifically caused by nosocomial pathogens abbreviated ESKAPE (*Enterococcus faecium*, *Staphylococcus aureus*, *Klebsiella pneumonia*, *Acinetobacter baumanii*, *Pseudomonas aeruginosa*, and *Enterobacter* species) are the majority of hospital infections in the USA. Methicillin-resistant *S. aureus* (MRSA) alone is the reason of more deaths than those caused by HIV/AIDS and tuberculosis combined.[8] Although many antibiotics were approved between 1960s and 2000, they were synthetic derivatives of existing molecules. Most of the core scaffolds of currently used antibiotics were introduced between 1930s and 1960s, and the ESKAPE pathogens are already resistant to most of them.[9]

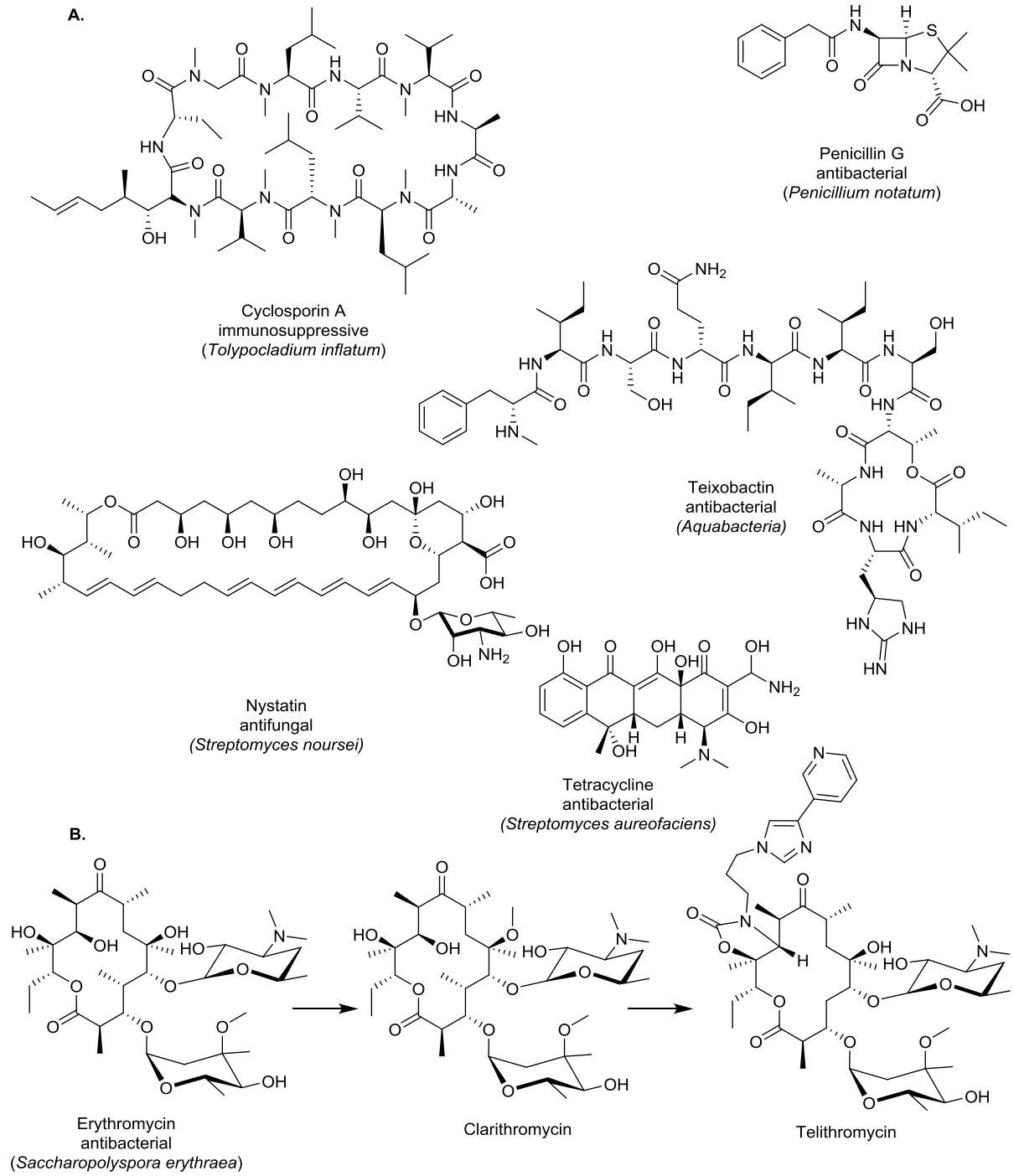

Figure 1.1 (a) Selected examples of natural products derived from microorganisms representing important antibiotics in the clinic. Name, activity, native producer are indicated below the structures. (b) Example of synthetic tailoring of natural scaffold leads to active generation of antibiotic

Therefore, there is a huge demand for new antibiotics that possess either new mode of action or novel chemical scaffold. Although terrestrial and marine microorganisms continue to provide a rich reservoir for such compounds, there is a high chance to re-isolate an already known compound. In order to minimize the rediscovery rate, different approaches are in use to discover new molecules that can fulfill the requirement for therapeutic agents, e.g. retrieving strains from underexplored

environments, screening new microbial taxa and genome-mining.[10] In this regard, within the last few years the study of marine organisms has yielded more than 22000 novel natural products bearing diverse chemical structures and biological activity.[11] It has been estimated that more than 99% of all bacteria on earth are unculturable under standard laboratory conditions and many of them could produce valuable natural products that may serve as lead structures for drug development.[12] Therefore it is believed that further attempts on drug discovery from nature remains promising. This presumption has been supported by the recent development of a new method using a multichannel device iChip which enabled the growth of unculture able soil bacteria in their natural environment. Screening of the new isolates led to a new antibiotic teixobactin (Figure 1.1) and surprisingly no resistance has been detected so far against this new antibacterial peptide.[13] Moreover, chemical studies of microbial genera and/or strains isolated from unusual ecological niches, and underexplored species appear to be an attractive source of new chemical scaffolds. Besides actinomycetes, myxobacteria attract attention due to their potential to produce natural products with wide range of biological activities.

1.2. Myxobacteria Produce Diverse Bioactive Natural Products

Myxobacteria are found in soil, dung, tree bark, decaying plants, and a small number of isolates were found from marine environment.[14] [15] This gram-negative bacteria, which belong to the delta subgroup of proteobacteria, are intriguing subjects for both academic and commercial drug discovery programs, due to their many unique characteristics.[16] [17] In general myxobacteria show a complex life cycle. Vegetative cells spread on the surface by gliding as swarm colony. When nutrients are scarce, cells aggregate and form multicellular fruiting bodies, showing various morphology which are used for taxonomic classification (Figure 1.2).

Within the fruiting body, cells alter their form into rod shaped vegetative cells and create myxospores enclosed in slimy cell wall. This life form ensures the colony to survive under extreme environmental conditions like starvation, heat and desiccation.[18]

Another noticeable behavior is that myxobacteria are able to consume biological macromolecules (e.g. cellulose), as well as other microorganisms like fungi and bacteria, as mini-predators.[19] The swarm on the solid surface allows the accumulation of extracellular enzymes so that such macro food sources can be decomposed and consumed.[14]

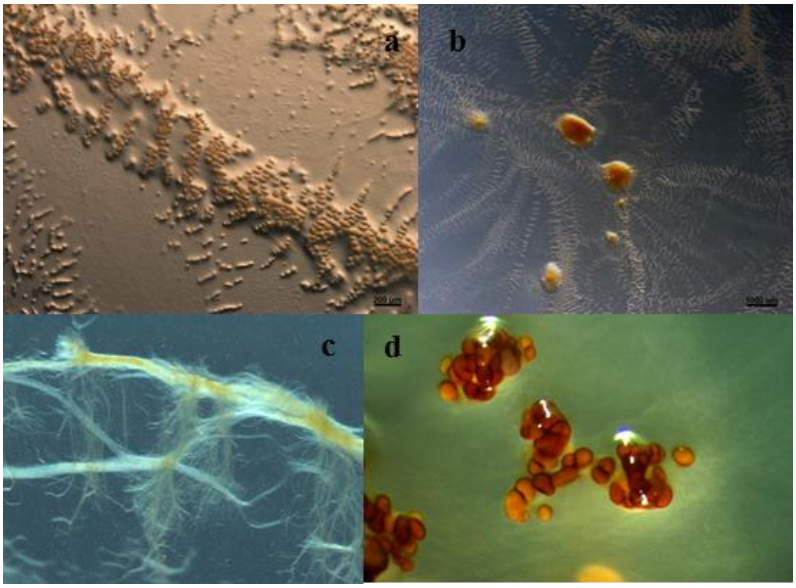

Figure 1.2 Stereo photomicrograph of (a) *Hyalangium minutum* fruiting bodies (b) *H. minutum* swarming and rippling growth pattern (c) swarm colony of *Jahnella* sp. and (d) Fruiting bodies of *Cystobacter* sp. (Pictures by Dr. R. Garcia, HIPS)

1.2.1. Myxobacterial Natural Products

The most remarkable benefit of myxobacteria is their ability to produce diverse bioactive secondary metabolites, which covers 5% of total known microbial natural products.[20] At least 100 core structures and 600 derivatives were characterized from 7500 myxobacterial strains.[14] [15] In terms of structures, myxobacterial metabolites vary from modified polyketides, alkaloids, terpenoids, phenyl-pronapoids and peptides showing a number of structural variants on each basic chemical scaffold.[21]

Antifungal/yeast activity is commonly observed with myxobacterial metabolites (~54%) and this activity arises frequently from inhibition of electron flow within the mitochondrial respiratory chain.[20] Even this is a common mode-of-action among myxobacterial compounds; it is rarely reported for natural products from other microorganism.[22] Furthermore, approximately 30% of myxobacterial compounds show antibacterial activity with different mechanisms such as inhibiting the protein synthesis and RNA polymerase etc.[20] [23] Cytotoxicity towards mammalian cells is one of the promising bioactivity exhibited by myxobacterial natural substances. This bioactivity arises mainly from acting at tubulin and with actin.[23]

Besides the secondary metabolites that are active against other pathogenic organisms, myxobacteria also produce compounds which are necessary for their own survival. For instance, DKxanthenes, a family of yellow pigments, are required for the formation of fruiting body[24] which is an essential structure for the survival under extreme condition.

Myxobacterial secondary metabolites representing diverse chemical structures are assembled by multistep biosynthetic processes catalyzed by special enzymes such as polyketide synthases (PKSs), non-ribosomal peptide synthetases (NRPSs) or hybrid thereof. These mega-enzymes are organized as several modules showing independent multi-functions which incorporate one carboxylic acid (for PKSs) or one amino acid (for NRPSs) to the growing polyketide or peptide chain.[25] Notably, the hybrid PKS-NRPS system is known to be responsible for the production of majority of myxobacterial natural products, whereas secondary metabolites isolated from actinomycetes are pure PKS and NRPS products.[16]

Polyketides – myxobacterial polyketides are classified into many structural classes such as macrocyclic lactones, polyethers, polyenes and aromatics.[25] These structurally complex organic molecules are often found from myxobacterial extracts and show diverse biological activity. For instance, potent antifungal stigmatellins were isolated from *Stigmatella aurantiaca* and they are characterized by containing a bicyclic chromone ring substituted by apolar branched side chain.[26] The antimicrobial activity arises from inhibition of electron flow in mitochondrial respiratory chain by targeting NADH dehydrogenase (complex I).[27] Isoprenoid quinoline alkaloid aurachin is a type II PKS polyketide biosynthesized by *S. aurantiaca* as well and it shows various bioactivities such as antibacterial, antifungal and anti-plasmodial properties.[28] [29]

The myxobacterial genus *Chondromyces* is well known as prolific producer of structurally unique groups of metabolites under laboratory conditions. Among them the antibacterial polyketides chondrochlorens[30] and NRPS/PKS hybrid antifungal crocacins[31] have been isolated. (Figure 1.3)

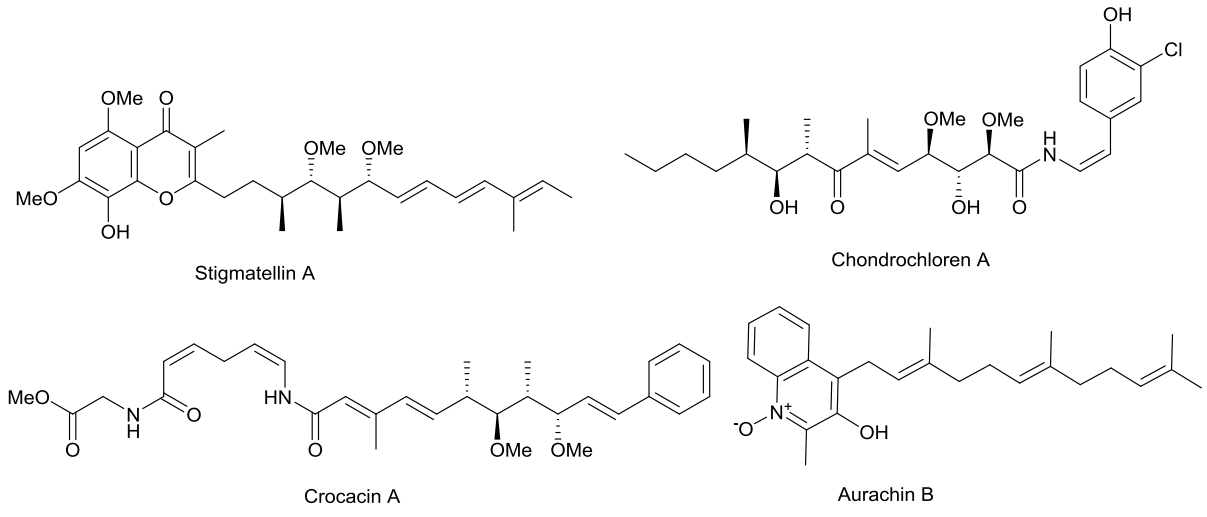

Figure 1.3 Selected polyketides isolated from myxobacteria

Macrolides – many antibacterial macrolides presenting structural diversity have been isolated from myxobacteria. A successful example of a myxobacterial macrolides approved by the FDA is

epothilone. Epothilone was isolated from *Sorangium cellulosum* by activity guided fractionation and the pure compound showed broad activity against eukaryotic cells.[32] A semi-synthetic amide derivative of epothilone B Ixempra® (ixabepilone) is in clinical use for the treatment of advanced breast cancer.[33]

Moreover, the boron-containing macrodiolide tartrolons are active against Gram positive bacteria as well as mammalian cells.[34] [35] A macrolide glycoside disciformycins were isolated by activity guided isolation approach using Gram positive indicator bacteria.[36] They exhibit antibacterial activity against methicillin- and vancomycin-resistant *S. aureus* (MRSA/VRSA) in the range of vancomycin. Remarkably, no cross-resistant was detected to vancomycin and no cytotoxicity was observed against mammalian cell, suggesting these compounds could be a lead molecule for antibiotic development. (Figure 1.4)

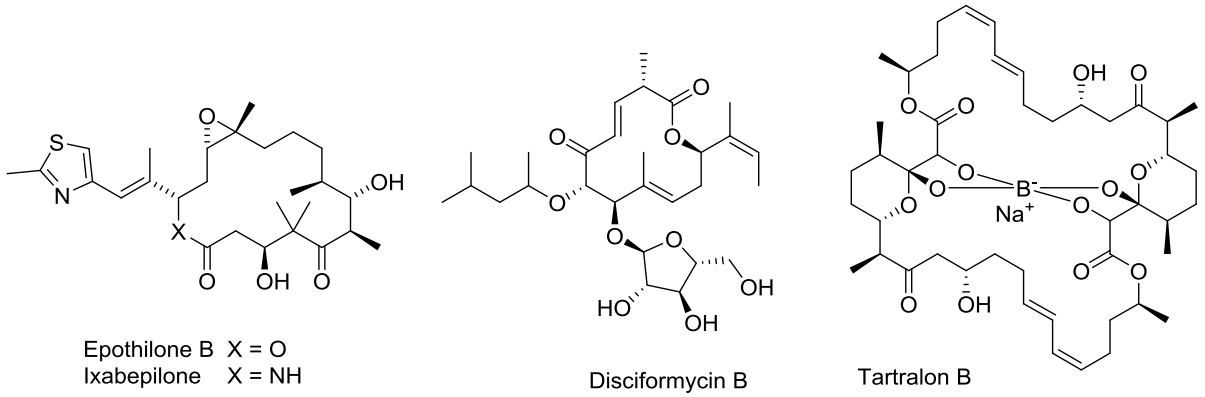

Figure 1.4 Selected macrolides isolated from myxobacteria

Peptides – even as mentioned earlier the polyketide-peptide mixed structure is the majority of myxobacterial natural products, a number of pure NRPS derived molecules were discovered from myxobacteria. The NRPs often are depsipeptides bearing unusual structural features such as hydroxy- and β-amino acids as well as homoproline etc.[25] As the representative of recent discovery of such molecule, the cyclic depsipeptide crocapeptins were isolated from *Chondromyces crocatus*.[37] (Figure 1.5) They belong to cyanopeptolins which is characterized by the presence of an unique structural unit amino-hydroxy-piperidone (Ahp)-heterocycle. This residue is known to be crucial for the protease inhibition activity[38] and crocapeptins exhibited the serine protease inhibition activity with low IC_{50} value, as predicted. Another cyclic depsipeptide aetheramides were isolated from novel myxobacterial strain *Aetherobacter fulvus*.[39] They show anti-HIV activity in low nM range and characterized by bearing the unusual fatty acid as well as modified amino acid residues.

More recently, NRPS derived potent antibiotics cystobactamides were discovered from *Cystobacter* sp. It shows broad-spectrum antibacterial activity against Gram-positive and more importantly Gram-

negative bacteria such as *E. coli* and *A. baumannii*. Cystobactamides are characterized by possessing para-aminobenzoic acid (PABA) chain which is unique for natural products. Hence, due to the novel scaffold and limited cross-resistance, cystobactamides can serve as lead structure for novel class of antibiotic development with wide range of bioactivity.[40]

The NRPS-PKS hybrid systems often yield structurally diverse molecules. Interestingly, few myxobacterial metabolites contain structural elements known from other biological source such as streptomycetes, cyanobacteria and sponges. Among them, chondramides are NRPS-PKS hybrid depsipeptides comprised of three amino acids (alanine, *N*-methyltryptophan and an unusual amino acid, either β-tyrosine or α-methoxy-β-tyrosine) and a polyketide chain (*E*-7-hydroxy-2,4,6-trimethyloct-4-enoic acid). The chondramides have been isolated from the terrestrial myxobacterial strain *Chondromyces crocatus*,[41] while their analogues, the jaspamides, were discovered from a marine sponge *Jaspis johnstoni*.[42] Both families of compounds inhibit growth of yeast and the chondramides exhibit high cytostatic activity against mammalian cells. (Figure 1.5)

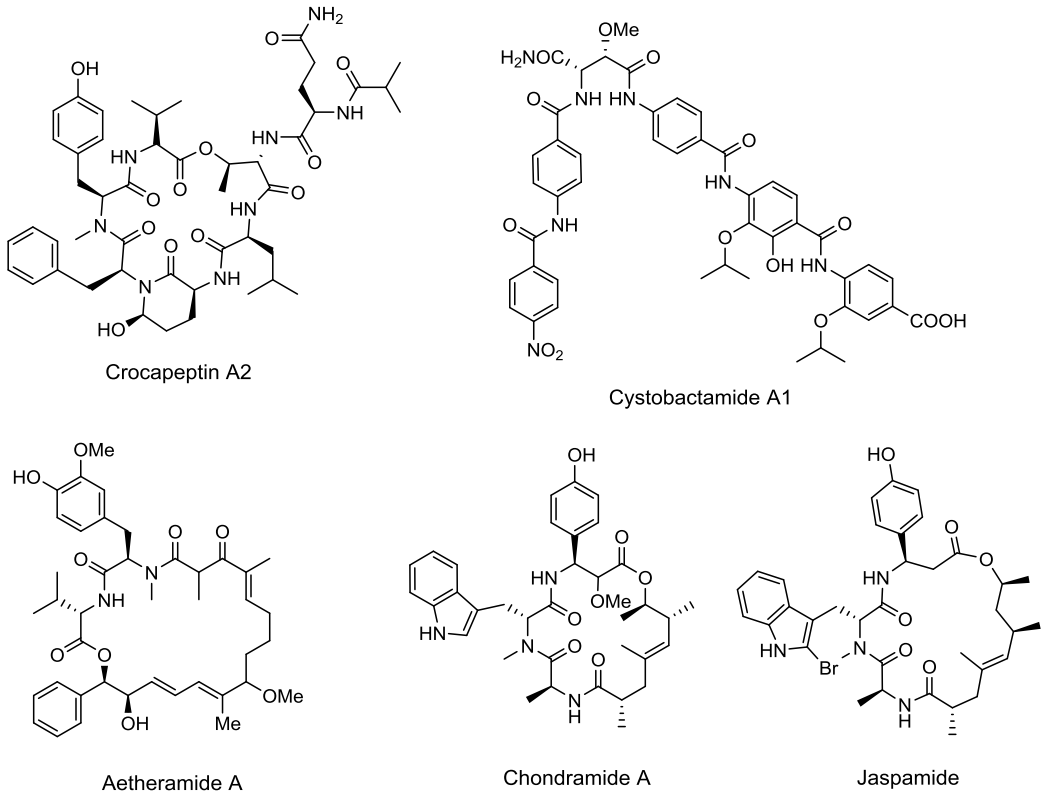

Figure 1.5 Examples of nonribosomal peptides and NRPS/PKS hydrid secondary metabolites from myxobacteria

Above mentioned metabolites are only few examples representing structural diversity of natural compounds isolated from myxobacteria. Since new compounds are continuously being discovered and characterized (60 new compounds in three years), the myxobacterial collection at HZI/HIPS

(Braunschweig and Saarbruecken) covering 8200 different strains is being partially chemically screened (1700 strains) in order to exploit the biosynthetic capacity of this intriguing microorganism by finding new anti-infectives.[43] Furthermore, investigation of novel strains and genera belonging to unexplored bacterial groups is believed to provide new interesting chemistry, the screening program at HZI/HIPS includes extensively new myxobacterial isolates.

1.2.2. Siderophores

Iron is an essential element for many important biological processes of living organisms. Even though it is considered as the fourth most abundant metal on earth, its availability is often limited for microorganisms. Under physiological pH conditions, soluble Fe(II) readily oxidizes to insoluble Fe(III). In order to overcome environmental scarcity of Fe(II), bacteria, fungi and plants produce and secrete iron scavenging molecules, called siderophores.[44] Siderophores are metal transporting agents which facilitate uptake, transport, and solubility of iron with high affinity. Their biosynthesis is triggered by low abundance of soluble iron in the environment.[45] Once the excreted siderophore is bound to a metal ion, the siderophore-iron complex is actively transported into the cell by membrane-associated ATP-dependent transport systems in bacteria. Subsequently, the iron is released by reduction and the free siderophore is again excreted from the cell.[46] [47]

Siderophores are classified due to their functional groups, e.g. hydroxamate, catecholate or α-hydroxycarboxylate which carry charged oxygen atoms as donor for iron-siderophore complex formation.[46] Over hundred structurally diverse microbial siderophores have been reported, including chatecholate-type myxochelins[48] and citrate-hydroxamate-type nannochelins[49] isolated from myxobacteria to date. Siderophores and their derivatives have potential medical applications. Deferoxamine is produced by *Streptomyces pilosus* in large scale[50] and its methane sulfonate salt (Desferal, Novartis) is used in the treatment of iron overload disease such as haemochromatosis. It binds Fe(III) ions and forms a water soluble complex which is readily excreted from the body through the kidneys.[51] In the same mechanism, it is used in the treatment of aluminium toxicity.[52] The linear trishydroxamate deferoxamine also shows potent antimalarial activity against *Plasmodium falciparum* both *in vitro* and *in vivo*.[53] [54]

Having metal chelating activity, siderophores play a major role as virulence factors of pathogenic bacteria[55] e.g. the human pathogen *Yersinia pestis* completely lose their virulence in the absence of yersiniabactin.[56] Another potential application of siderophores is “Trojan horse” strategy that brings the antibiotic in to the resistant cell as siderophore-iron-drug complex. This concept exploits the bacterial iron-siderophore uptake system as a cellular entry gateway and it is effective against the low permeability of the outer membranes of resistance strains.[57] The advantages of Trojan horse mechanism have led to the discovery of new siderophore-antibiotic conjugates, termed sideromycins,

such as trishydroxamate siderophore-ciprofloxacin conjugates (Figure 1.6, B), triscatecholate siderophore-ampicillin or amoxicillin conjugates etc. Interestingly, the latter one showed effective inhibition of the growth of the *P. aeruginosa* by introducing the ampicillin and amoxicillin in to this gram negative pathogen.[58] [59]

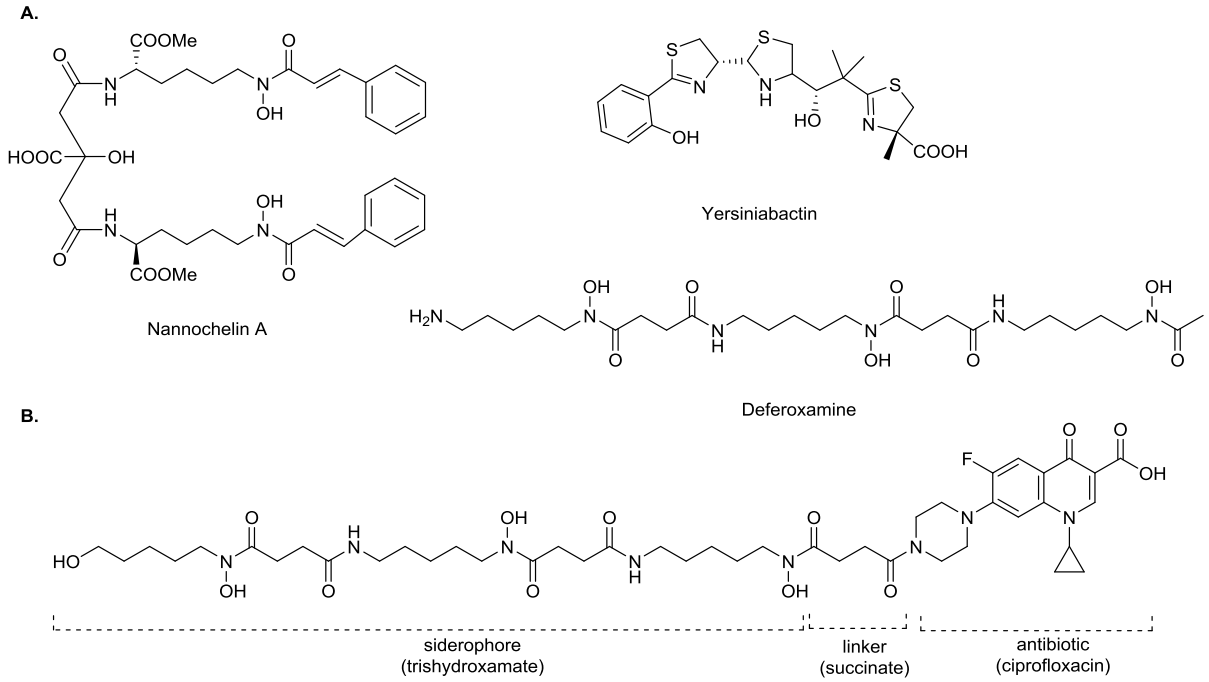

Figure 1.6 (a) Example of siderophores isolated from micoorganisms and (b) synthetic sideromycin desferrisalmycin B illustrating general structure of sideromycins

1.3. Isolation Procedure and Structure Elucidation of Natural Products

Natural products appear as a complex mixture containing many constituents in the crude extract of microorganism and plants. In the course of discovery of new natural product, identifying the right target compound that shows novel chemical structure (related to biological activity) from this complex natural matrix is crucial so that resources spent on re-isolation and re-identification of known compounds can be saved. The process that determines the known compounds present in the microbial extract is referred as dereplication, should be carried out for this purpose.[60] Thus, an effective dereplication strategy plays a vital role for the fast discovery of novel NPs from microorganism.

1.3.1. Screening and Dereplication of Microbial Extract

Dereplication process should be carried out at an early stage of NP research, and combines chromatographic and spectrometric methods with database searching. Liquid chromatography coupled with mass spectrometry (LC-MS) is the most frequently used tool for this purpose as it provides an accurate mass of every single metabolite, which can be used as a query in almost all NP databases. Further valuable information (i.e., retention time and UV/vis spectra) is obtained from a single LC-

MS run. Based on these information, the known metabolites can be identified by comparing with database. Soft ionization techniques such as electrospray ionization (ESI^+/ESI^-) and atmospheric pressure chemical ionization (APCI) provide gentle and versatile compound ionization, as e.g. ESI^+ was shown to detect 93% of natural products existing in microbial crude extract.[61] Positive and negative ionization techniques generate multiple ion adducts and simple fragments so that high resolution MS data permits unambiguous assignment of molecular weight.

LC-MS based dereplication is successfully combined with bioassay-guided isolation process to determine the active component(s) in the extract.[62] This can be conveniently achieved by performing micro-scale UHPLC-DAD-MS fractionation (usually in micro well plates) which is subsequently subjected to *in vitro* bioassays against certain test organisms that were initially identified by screening of the crude extract. On the basis of the activity result (Figure 1.7), the peak corresponding to the active area can be determined from the HPLC metabolite profile, and its spectroscopic features (UV/vis, HR-MS and retention time if applicable) should be considered to identify whether it is a known or an unreported molecule. At this stage, a good database is essential. In case of more than one hit is found from database searching, tandem MS/MS fragmentation offers a powerful solution for

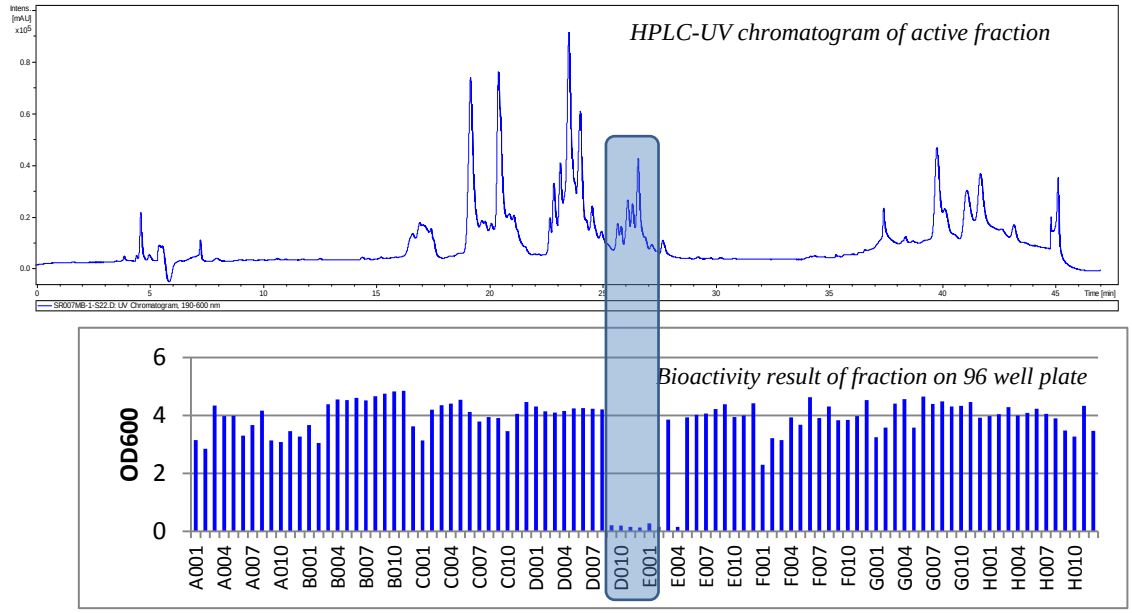

Figure 1.7 LC-MS fractionation of active fraction coupled to bioassay

obtaining structural information.[63] Besides the commercially available database Dictionary of Natural Products (The Chapman & Hall), an in-house database "Myxobase" is being developed and employed for the research of myxobacterial natural products.[64] This comprehensive database provides information regarding the producer strains (>9000 strains) and secondary metabolome dataset (ca. 2500 compounds). It contributes greatly for the dereplication of myxobacterial extracts by covering the high resolution LC-MS data linked with bioactivity and producer strains.

Another useful hyphenated technique used in the dereplication process is LC-MS coupled with solid-phase extraction (SPE) and NMR (LC-MS/SPE-NMR, Figure 1.8). The advantage of this combination is time saving by using small scale bacterial crude extract, and no initial purification is needed for the evaluation of a target compound.[65] Analytical HPLC separation with DAD and MS monitoring is used to track the peak of interest that has been previously identified by HPLC-bioassay-fractionation. A candidate peak is adsorbed on SPE cartridge and this step can be repeated multiple times in order to obtain sufficient amount of sample for NMR measurements. When the HPLC solvent is removed from the cartridge by nitrogen flow, the deuterated solvent is used to transfer the adsorbed compound via flow-probe to the NMR spectrometer. Nevertheless water and organic solvents used for HPLC cannot be removed completely, multi solvent suppression pulse programs provide reasonable NMR spectra. A NMR spectrometer equipped with a cryogenically cooled probe allows the acquisition of decent NMR spectra from few μg samples.[66]

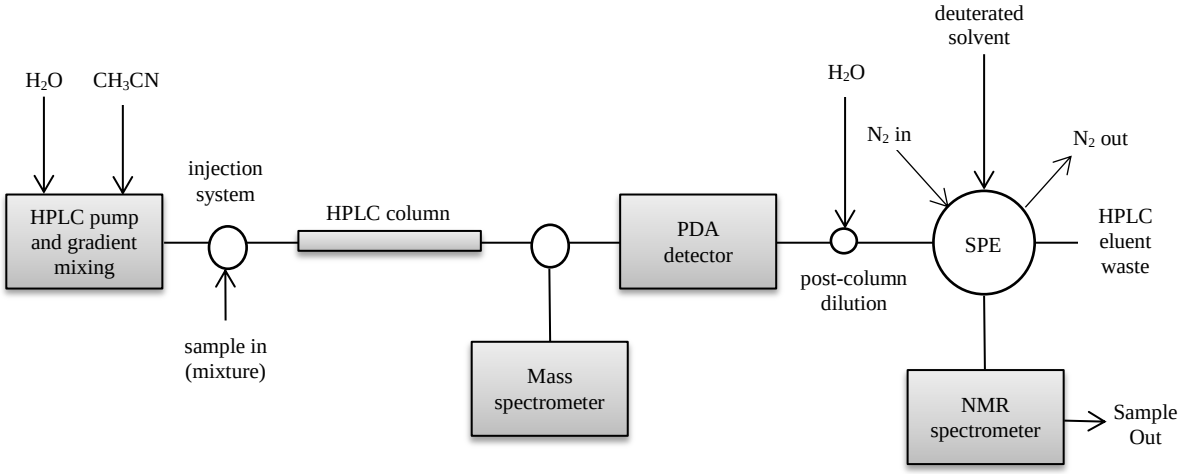

Figure 1.8 Scheme of multiple hyphenation LC-MS/SPE-NMR, reproduced from ref 67

Even though only partial (but sometimes complete) structural information is obtained from LC-MS/SPE-NMR, it facilitates the rapid identification of the desired target whether it exhibits structural novelty. Thus, the information obtained from LC-MS/SPE-NMR can play a central role for making decision on further upscaling and purification processes of compounds under examination.[68]

1.3.2. Isolation and Structure Elucidation of Novel Metabolites

Most myxobacterial secondary metabolites are extracted by adsorbing them onto resin polymer, e.g. XAD-16 which is known to capture the greatest amount of semi-polar metabolites from fermentation broth. This facilitates the isolation and structure elucidation of secondary metabolites produced in trace amount. Moreover, the production of antibiotics that acts against gram-negative bacteria can cause growth inhibition of the producer strain. To avoid this self-inhibition, sterilized XAD-16 resin is added in to the growing culture.[20]

A microbial crude extract is a reservoir of many different compounds so that it is difficult to apply a single separation step to isolate an individual compound. An efficient enrichment procedure of the target molecule facilitates the elimination of byproducts. It includes liquid-liquid partition, column chromatography on various stationary phase e.g. normal phase silica gel and Sephadex LH-20 etc.

The final isolation process is designed on the basis of physical and chemical properties of compound of interest. Preparative and semi-preparative HPLCs are employed greatly. They are usually coupled with mass spectrometric (MS) detectors besides common UV/vis detectors, and equipped with automatic fraction collectors. This hyphenation facilitates the isolation of the target compound in highest level of purity.

NMR spectroscopy is a very powerful tool for structure elucidation of natural products. The experiments rely on the quantum mechanical property of a nucleus – the spin. The nuclei such as ^{1}H, ^{13}C, ^{15}N and ^{19}F have two different spin states (energy low and high states) since they have a half spin numbers. During the irradiation of the electromagnetic wave through the sample, the nuclei flip from one state to another by absorbing or emitting the energy difference in the form of electromagnetic radiation. The frequency of the irradiation must match the energy difference between two spin states and the irradiation is applied as radio frequency (*rf*) pulses. After one or several *rf* pulses, a NMR signal can be observed. It consists of *rf* waves with frequencies that match the energy difference between two spin states of the individual nuclei involved. The different types of nuclei apply widely different resonance frequencies. Protons resonate at a four times higher frequency than ^{13}C, and ten times higher than ^{15}N nuclei. Therefore the nuclei are represented by characteristic resonance frequencies in an NMR spectrum.[69]

Due to the interaction between a nuclei and surrounding electrons, the local magnetic field is affected and thus resonance frequency of the nuclei is influenced. Therefore, a NMR spectrum exhibits the signals corresponding to different classes of protons or carbons etc.[69] Moreover, the magnetic moments of individual nuclei interact with the magnetic fields created by the spins of nearby nuclei. This spin-spin interaction is used to correlate different nuclei in the molecule with one another. Two types of interactions can be observed, either through bond or through space. Through bond interaction occurs via polarization of bonding electrons and known as *J* coupling, while through space correlation is the basis for the nuclear Overhauser effect (NOE). The latter permits distance measurement between protons and thus provides geometric information.[70]

In the case of complex organic molecules, 1D NMR data are obtained as complicated spectrum containing overlapped signals. An array of two dimensional pulse sequences has been created providing both increased resolution and correlations that are easy to analyze. A resonance in the 2D-NMR spectrum represents a pair of nuclei that interact with each other either scalar or through bond.

All 2D NMR experiments have the same scheme that consists of four phases: excitation-evolution-mixing-detection. During the excitation period, the spins are prepared, and consequently the chemical shifts of the individual nuclei are detected during the evolution period, t_1. Furthermore, the mixing period allows the correlation of spins with each other and chemical shift of one nucleus ends up on an another nucleus of which the frequency is measured during the detection period, t_2.

The skeletal structures of natural products can be deduced by number of 2D NMR experiments. ^{1}H-^{1}H homonuclear correlation spectrum combined with one-bond ^{13}C-^{1}H correlation spectrum allow determining the fragments. Furthermore, the long-range ^{13}C-^{1}H correlation links those fragments to build the planar structure of the molecule under study.

The homonuclear 2D ^{1}H-^{1}H COSY (correlation spectroscopy) experiment is used to identify the protons which are directly coupled to each other.[71] The basic COSY-90 is the most widely used experiment while its minor variant COSY-45 sequence is acquired in order to distinguish geminal and vicinal proton pairs with less sensitivity than the previous one.[72] A useful supplement to the COSY is TOCSY (total correlation spectroscopy) sequence that exhibits the sequence of coupled protons by transferring the magnetization subsequently from one proton to the next within a same spin system.[73] The extent of magnetization transfer depends on duration of the mixing time which is generally 60-100 ms. The alternate version of 2D TOCSY is selective 1D TOCSY, using shaped pulses to excite individual peaks.[74] This is a particularly helpful method in the case of the compound possessing polysaccharide units, since the subspectrum for each monosaccharide unit can be obtained including all individual protons. Furthermore, hybrid 2D HSQC-TOCSY experiment is useful in the case of extreme signal overloading in ^{1}H-NMR spectra. This relies on the better resolution of the ^{13}C signals, due to a broader chemical shift-range, to overcome the overlapping.[75]

In the early date, heteronuclear one bond ^{1}H-^{13}C correlation spectra were acquired by ^{13}C detection, using HETCOR sequence.[76] Its more sensitive analogue sequences HMQC (heteronuclear multiple quantum coherence) and HSQC (heteronuclear single quantum coherence) were developed. The advantage of these new sequences is the fact that they apply the detection of proton directly bonded to ^{13}C (inverse detection), and hence are more sensitive than the previous detection method. The gradient-selected HSQC sequence exhibits edited spectrum showing CH and CH_3 as negative, and CH_2 as positive signals. The significant advantage of this method is the elimination of additional DEPT-135 experiment.[77]

2D HMBC (heteronuclear multiple bond correlation) determines long range ^{1}H-^{13}C connectivity separated by 2-3 bonds[78] and it provides essential information for structure elucidation since it allows the linkage of the small structural fragments into the entire structure. This experiment is especially useful for the detection of quaternary carbons which are not observed in other 2D experiments.

Furthermore, ^{1}H-^{15}N HMBC provides powerful information for alkaloids and compounds with high amount of nitrogen content, although it is roughly five times less sensitive than the ^{1}H-^{13}C HMBC.[79]

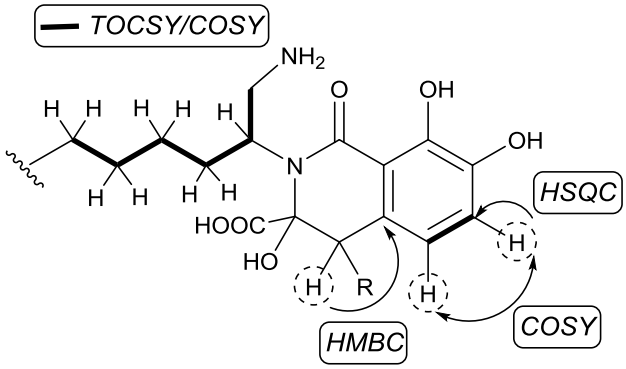

Figure 1.9 Illustration of 2D NMR correlations shown on the partial structure of hyalachelin

The major challenge for NMR spectroscopy of microbial natural products is the insufficient amount of available compound combined with the relative insensitivity of the technique. Numerous developments have been made for NMR instruments including cryogenically cooled probes and narrow probes that facilitate the performance of various insensitive 2D NMR experiments with good resolution in reasonable time with remarkably lowered amounts of sample – few micrograms.[80] By cooling the NMR probe-head with liquid helium (cryogenic probe) to 20-30 K, the signal to noise ratio (S/N) is enhanced by up to a factor of four. The acquisition time is also reduced by a factor of sixteen and enhance the signal output of the NMR instrument.[66]

1.3.3. Assignment of Stereochemical Configuration

The stereochemical configuration often determines important properties in the chemical, physical, biological and pharmaceutical aspects of the compound. Thus, obtaining an enantiomerically pure compound is a prerequisite for chemists which encouraged the development of various methods for the assignment of relative and absolute configuration of newly discovered natural molecule.

Relative configuration – The NOESY (nuclear overhauser effect spectroscopy) experiment is used very often to determine the relative configuration by observing the NOEs between protons up to 5 Å apart through space. However, the intensity of the NOE correlation is influenced by molecular weight and mixing time.[81] Since compounds of over 750 Da produce weak or negative signals, the ROESY (rotating-frame overhauser effect spectroscopy) experiment is used instead to overcome this problem.[82] In selective 1D NOE difference experiments, a proton resonance is selectively irradiated. The resulting spectra are cleaner and free of the artifacts those are observed in 2D NOE experiment, and therefore the few NOE peaks are detected.[72] [83] NOESY and ROESY data are utilized e.g. for

the establishment of geometrical configuration of double bonds (Figure 1.10, A) and cyclic substructures (Figure 1.10, B).

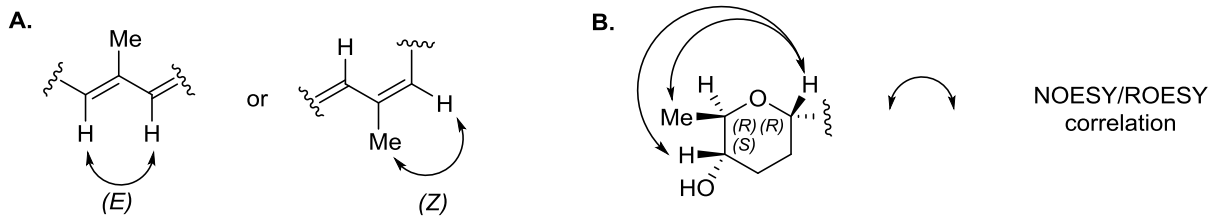

Figure 1.10 NOESY/ROESY correlation for the (a) *E* and *Z* geometry of a double bond and (b) a substituted heterocycle

Additional NMR methods for the relative configuration assignment are based on hetero- and homonuclear coupling constants ($^{n}J_{C,H}$ and $^{3}J_{H,H}$). Karplus has described that the dihedral-angle of two protons is dependent on the vicinal proton coupling constants $^{3}J_{H,H}$.[84] On the basis of this theory, Murata's *J*-based configurational analysis method has been developed and is well suited for the (1,2) or (1,3) stereogenic system on acyclic chain.[85] As an example, in a 1,2-diol system, the value of $^{3}J_{H,H}$ alone is inadequate because two H/H-gauche rotamers cannot be distinguished (Figure 1.11, A). Additional information given from $^{3}J_{C,H}$ can be used for configurational analysis in this case (Figure 1.11, C). Therefore, when an oxygen functionality on a carbon atom is gauche to its geminal proton $^{2}J_{C,H}$ is large, and when it is anti, the value becomes small (Figure 1.11, B).[85] A similar strategy combining ROESY data can be applied for relative configuration assignment of 1,3 and 1,4 methine systems.[85]

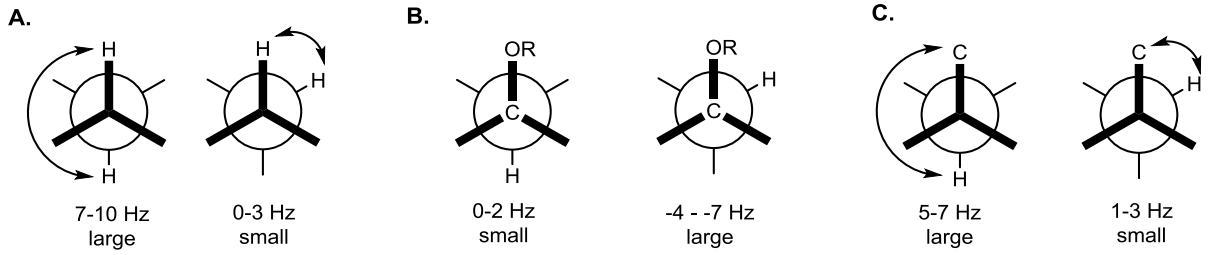

Figure 1.11 Dihedral angle dependence on hetero- and homonuclear coupling constants. (a) vicinal $^{3}J_{H,H}$ (b) germinal $^{2}J_{C,H}$ and (c) vicinal $^{3}J_{C,H}$ (adapted from ref. 85)

The $^{3}J_{H,H}$ can be extracted from a 1D ^{1}H NMR and more precisely from various 2D COSY type of experiments,[86] [87] while $^{2,3}J_{C,H}$ are accurately measured from *J*-resolved HMBC,[88] 2D hetero half-filtered TOCSY (HETLOC)[89] and many other modified pulse sequences[90]. Even though the HETLOC is one of the most sensitive experiments and most easily interpreted, it is limited to spin systems with contiguous TOCSY coherence transfer. For a structure with stereocenters at a quaternary carbon or small ^{1}H-^{1}H couplings, PS-HMBC and *J*-HMBC are more suitable.[91]

The application of Murata's method relies on the judgement on the size of coupling constant that is either large or small. In some molecules, multiple conformers exist and show averaged *J* values which are classified as medium.[92] In this case, the quantum mechanical (QM) calculation approach suggest most probable assignment of the relative configuration which is performed by calculating the relevant *J* values on all possible configurations (three *syn* and three *anti* rotamers) and quantitatively compared to the experimental ones.[93]

Recent developments in quantum chemistry enable quick, accurate, and reliable calculation of NMR parameters (coupling constants $^{2,3}J_{C,H}$, $^{3}J_{H,H}$ and ^{1}H and ^{13}C chemical shifts) which allows predicting the stereostructure.[94] [95] In brief, conformational search and geometry optimization of all significant conformers of each stereoisomer are carried out by empirical methods such as molecular mechanics (MM) or molecular dynamics (MD) at the empirical level. Furthermore, the quantum mechanical calculation of NMR chemical shifts is performed on the previously optimized geometries of all possible stereoisomers, and is compared to the experimental data. The mean absolute error (MAE) is considered to compare the calculated and experimental parameters.[92]

Another approach for the assignment of the relative configuration of a contiguous stereogenic unit is the one based on the Universal NMR Database (UDB).[96] [97] This is an empirical procedure that relies on the comparison of the experimental NMR chemical shifts of the molecule under examination with the database value. Since the local electronic environment is affected by the relative configuration, the NMR chemical shift is applicable to predict the relative configuration. Concisely, the structure under study is divided into small fragments and its chemical shifts are compared with the one of an appropriate reference compound in the database.

A widely used chemical approach for the relative configuration assignment of 1,3-diol systems is Rychnovsky's acetonide method.[98] As the result of a chemical reaction, a six membered heterocycle is obtained in a specific conformation which depends on the relative configuration of the 1,3-diol. As illustrated in Figure 1.12, a chair conformation is furnished from *syn*-1,3-diols, which is distinguished by the ^{13}C-NMR chemical shifts of CMe_2 groups (δ_C<100 ppm), axial methyl group (δ_C ~20 ppm) and equatorial methyl groups (δ_C ~30 ppm). In contrast, an *anti*-1,3-diol leads to a twisted-boat conformation, that exhibits diagnostic chemical shifts of the CMe_2 group (δ_C>100 ppm) and similar values (δ_C ~25 ppm) for both methyl groups. Moreover, standard 2D NMR experiments (NOESY/ROESY) allow this method to be applicable for more complex polyacetonide systems. In *syn*-1,3-diols, the axial methyl group shows NOE correlations to H4 and H6 axial protons. In the case of *anti*-1,3-diols, one acetonide methyl shows an NOE to H6.[99] [100] (Figure 1.12)

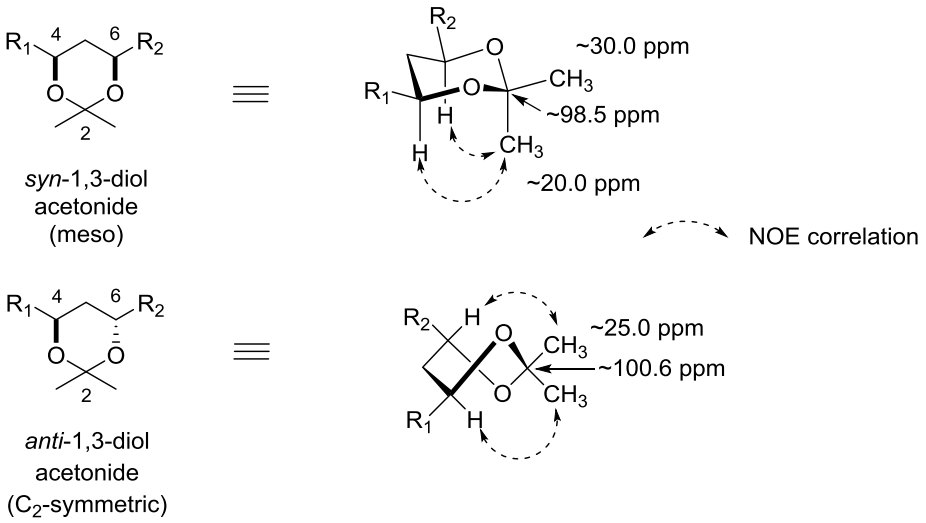

Figure 1.12 Conformations, diagnostic ^{13}C chemical shifts and NOESY correlations for *syn*-1,3-diol acetonide and *anti*-1,3-diol acetonide (reproduced from ref. 100)

Absolute configuration – several instrumental methods are available for the determination of the absolute configuration, including X-ray crystallography,[101] chiroptical methods such as circular dichroism (CD), optical rotatory dispersion (ORD) and specific optical rotation.[100] X-ray diffraction requires a monocrystal in very good quality which is unfortunately hard to obtain from natural products since the amount of available pure sample is often limited.[102] [103]

Chiroptical methods are based on the optical measurement of chiral molecules. ORD is based on the measurement of the optical rotation at various wavelengths whereas CD is the measurement of the difference of absorption intensity between right and left circularly polarized light at various wavelengths. The most specific character of ORD is that it is based on the compound skeleton. Therefore, sometimes ORD is more complicated to interpret than CD due to overlapped bands, whereas CD gives a signal only in the optically active absorption band.[104] Since light absorption is associated with electronic transitions and the presence of chromophores in the molecule, CD as a true spectroscopic technique can be made much more sensitive and can also be treated using the tools of molecular orbital calculations. CD spectra can therefore be QM calculated from known geometries and transition moments, and further compared with the one of molecule in study.[105] [106]

Mosher's method is the most widely used tool for determining the absolute configuration of secondary alcohols and amines via chemical derivatization.[107] Optically pure (*R*)- and (*S*)-α-methoxy-α-trifluoromethylphenyl acetic acid (MTPA) or its acid chloride (MTPA-Cl) are used as chiral derivatizing agents. In the corresponding (*R*)- and (*S*)-MTPA esters, anisotropic effects are observed that lead to small chemical shift differences in the ^1H-NMR spectrum. The phenyl group of the chiral auxiliary (*S*)-MTPA shields the neighboring substituent (L_1) of the chiral center, whereas the other diastereomer, the (*R*)-MTPA ester has a shielding effect on L_2. (Figure 1.13) The difference

in the chemical shift $\Delta\delta^{SR}$ between the (*S*)-MTPA and (*R*)-MTPA esters is used to express the shielding effect and its sign (+/-) is utilized for determining the absolute configuration based on the chiral center of the auxiliary MTPA. All of the protons shielded in the (*R*)-MTPA present a positive $\Delta\delta^{SR}$, while those shielded in the (*S*)-MTPA present a negative $\Delta\delta^{SR}$ value.[108]

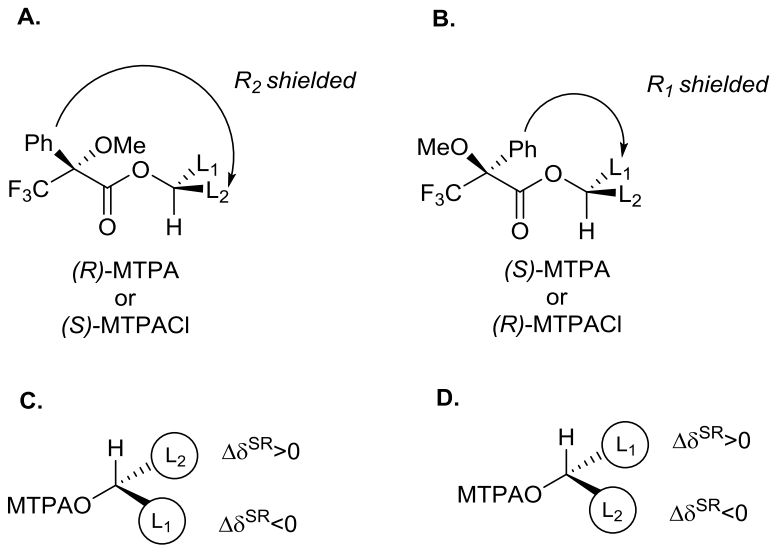

Figure 1.13 Model for the (a) (*R*)-MTPA ester and (b) (*S*)-MTPA ester of secondary alcohols, and the $\Delta\delta^{SR}$ values for (c) (*R*)-MTPA ester and (d) (*S*)-MTPA ester (reproduced from ref 108)

The absolute configuration of peptides is determined by nonempirical advanced Marfey's method using LC-MS. After hydrolysis of the peptide, the constituent amino acids are derivatized with chiral Marfey's reagents, 1-fluoro-2,4-dinitrophenyl-5-L/D-alaninamide (L/D-FDAA) or -5-L/D-leucinamide (L/D-FDLA), and further analyzed by LC-MS in comparison with corresponding derivatives of standard amino acids. Since each derivatized enantiomer results in two diastereomers, these can be separated by HPLC. The method relies on the elution order of L and D amino acid. [109] Mass spectrometry is used to detect the amino acid derivative and the retention time is considered for the absolute configuration assignment. Namely, the retention time of the L-FDLA derivative of a D amino acid (D-L type) is different than those of L-amino acid (L-L type) since they are diastereomers. Moreover, the retention time of L-D and D-L are the same, while the one for L-L and D-D are the same, since each pair acts enantiomeric. In most cases, L-amino acid derivatives elute before the corresponding D-isomers. However, for absolute configuration assignment of unusual amino acids, Marfey's method requires an enantiomerically pure standard.[110] (Figure 1.14)

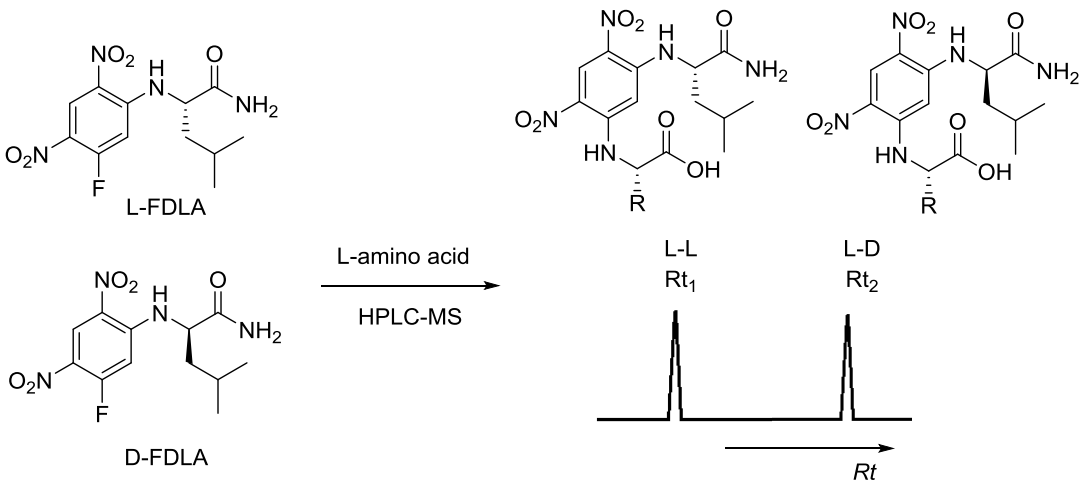

Figure 1.14 HPLC behavior of common L-amino acid after derivatized with Marfey's reagent, FDLA

Notable developments on the techniques essential for the isolation and structure elucidation of natural compounds facilitate the structure determination and characterization of novel natural compound(s) in reasonable time frame. NMR is the main method used for the unambiguous complete structure elucidation of complex molecule due to its advantages such as modern developments for the instrument sensitivity requiring low amount of samples (micrograms) which can be recovered after data acquisition. Since the natural compounds often demonstrate structural complexity and high diversity, there is no general rule to elucidate the stereochemical configuration.[100] However, successful combination of spectroscopic techniques and chemical methods enables the unequivocally elucidation of the 3D structure of novel natural compounds.

1.4. Outline of the Work

The purpose of the present thesis was the discovery of new secondary metabolites from myxobacteria, specifically from the underexplored and newly discovered myxobacterial genus – an approach that is believed to increases the discovery rate of new natural product. In this regard, the organic extract of strain MCy9135 belonging to the unexplored species *Hyalangium minutum* and the antifungal crude extract of *Jahnella* sp. strain MSr9139 were analyzed by hyphenated techniques, and revealed the presence of new metabolites. Furthermore, a chemistry guided approach was applied for the discovery of new natural products from *Cystobacter* sp. MCy9104.

The thesis describes the isolation and structure elucidation of the identified secondary metabolites from complex extracts using various analytical and comprehensive spectroscopic methods, including 1D- and 2D-NMR as well as high resolution MS, and tandem MS techniques. Absolute and relative configurations were determined using chemical derivatization methods and quantum mechanical calculations in cooperation with Prof. Giuseppe Bifulco at University of Salerno, Italy.

The crude extract of *Jahnella* sp. strain MSr9139 exhibited strong antifungal activity against *Candida albicans.* LC-MS/SPE-NMR analysis coupled to whole-cell assays enabled to trace the activity of the extract to a family of cyclic peptides. Isolation of these peptides was carried out using subsequent analytical tools and structure elucidation of these active metabolites was performed using spectroscopic instruments. Structure elucidation revealed a new microsclerodermin derivative, termed microsclerodermin L, together with a known microsclerodermin D and pedein A. The microsclerodermins family was originally discovered from lithistid sponge *Microscleroderma* sp. and *Theonella* sp. The results have contributed to the exploration of the biosynthetic pathway of these antifungal cyclic peptides as described in **Chapter 2.**

Chapter 3 deals with the isolation and full characterization of the novel catecholate-type siderophores hyalachelins A-C, from strain MCy9135 that belongs to the underexplored myxobacterial species *H. minutum*. Analysis of crude extract performed by LC-MS and LC-MS/SPE-NMR revealed the presence of unreported metabolites together with the known tartrolon D, myxochelin B and hyafurones. Scaled-up cultivation was performed in a total of 160 L since the yield of the target compounds was very low (15-30 μg/L). Reiterated purification steps yielded pure target molecules in sufficient amounts to acquire full 2D NMR datasets for structure elucidation. The relative configuration was determined (by Dr. G. Lauro and Prof. G. Bifulco, University of Salerno, Italy) by applying a QM calculation on NMR parameters such as ^{1}H and ^{13}C chemical shifts and heteronuclear coupling constants whereas the absolute configuration was analyzed by QM calculations of CD spectra. Hyalachelins are characterized by the unusual 3,7,8-trihydroxy-1-oxo-1,2,3,4-tetrahydroisoquinoline-3-carboxylic acid which has not been reported in natural products so far. Moreover, their iron chelating activity was assessed by chrome-azurol S (CAS) assay, and bioactivity evaluation was done against various Gram-negative and -positive bacteria as well as a number of fungi and mammalian cell lines towards assessing the cytotoxicity.

Chemical screening of *Cystobacter* sp. strain MCy9104 revealed the presence of a family of unknown metabolites in the crude extract. Scaled-up cultivation process enabled the isolation of seven new compounds, termed cystochromones A-G. Structure elucidation was carried out by means of comprehensive NMR data together with HR-MS/MS experiments. Cystochromones are characterized by an unusually attached pentadecyl moiety to the chromone core, which has not been reported among known chromone derivatives. The biosynthetic origin of the cystochromones was determined by feeding experiments with various stable isotope labeled precursors and a biosynthetic pathway was proposed as reported in **Chapter 4.**

1.5.References

[1] F. E. Koehn, G. T. Carter, *Nat. Rev. Drug. Discov.* **2005**, *4*, 206–220.

[2] Y. W. Chin, M. J. Balunas, H. B. Chai, A. D. Kinghorn, *AAPS J.* **2006**, *8*, E239.

[3] D. J. Newman, G. M. Cragg, *J. Nat. Prod.* **2012**, *75*, 311–335.

[4] J. W. H. Li, J. C. Vederas, *Science* **2009**, *325*, 161–165.

[5] F. von Nussbaum, M. Brands, B. Hinzen, S. Weigand, D. Habich, *Angew. Chem. Int. Ed. Engl.* **2006**, *45*, 5072–5129.

[6] J. Clardy, M. A. Fischbach, C. T. Walsh, *Nat. Biotechnol.* **2006**, *24*, 1541–1550.

[7] M. G. Watve, R. Tickoo, M. M. Jog, B. D. Bhole, *Arch. Microbiol.* **2001**, *176*, 386–390.

[8] H. W. Boucher, G. H. Talbot, J. S. Bradley, J. E. Edwards, D. Gilbert, L. B. Rice, M. Scheld, B. Spellberg, J. Bartlett, *Clin. Infect. Dis.* **2009**, *48*, 1–12.

[9] M. A. Fischbach, C. T. Walsh, *Science* **2009**, *325*, 1089–1093.

[10] S. Donadio, S. Maffioli, P. Monciardini, M. Sosio, D. Jabes, *J. Antibiot.* **2010**, *63*, 423–430.

[11] W. H. Gerwick, A. M. Fenner, *Microb. Ecol.* **2013**, *65*, 800–806.

[12] J. Kennedy, J. R. Marchesi, A. D. W. Dobson, *Microb. Cell. Fact.* **2008**, *7*, 27.

[13] L. L. Ling, T. Schneider, A. J. Peoples, A. L. Spoering, I. Engels, B. P. Conlon, A. Mueller, T. F. Schäberle, D. E. Hughes, S. Epstein et al., *Nature* **2015**, *517*, 455–459.

[14] H. Reichenbach, *J. Ind. Microbiol. Biotechnol.* **2001**, *27*, 149–156.

[15] H. Reichenbach, K. Gerth, H. Irschik, B. Kunze, *Trends Biotechnol.* **1988**, *6*, 115–121.

[16] S. C. Wenzel, R. Müller in Comprehensive Natural Products Chemistry II, Vol 2: Structural Diversity II - Secondary Metabolite Sources, Evolution and Selected Molecular Structures. B. Moore, Ed. Elsevier: Oxford, **2010**.

[17] W. Dawid, *FEMS Microbiol. Rev.* **2000**, *24*, 403–427.

[18] L. Shimkets, M. Dworkin, H. Reichenbach in *The Prokaryotes* M. Dworkin, S. Falkow, E. Rosenberg, K. Schleifer, E. Stackebrandt., Eds.; Springer Verlag: New York, **2006**.

[19] R. O. Garcia, D. Krug, R. Müller in Methods in Enzymology. Discovering Natural Products from Myxobacteria with Emphasis on Rare Prodcuer Strains in Combination with Improved Analytical Methods. Vol. 458. D. A. Hopwood, Ed. Academic Press: Burlington, **2009.**

[20] K. Gerth, S. Pradella, O. Perlova, S. Beyer, R. Müller, *J. Biotechnol.* **2003**, *106*, 233–253.

[21] M. Nett, G. M. Konig, *Nat. Prod. Rep.* **2007**, *24*, 1245–1261.

[22] Degli E. M. *Biochim. Biophys. Acta. Bioenerg.* **1998**, 1364, 222-235.

[23] K. J. Weissman, R. Müller, *Nat. Prod. Rep.* **2010**, *27*, 1276–1295.

[24] P. Meiser, H. B. Bode, R. Müller, *P. Natl. Acad. Sci. USA* **2006**, *103*, 19128–19133.

[25] S. C. Wenzel, R. Müller, *Curr. Opin. Drug. Discov. Devel.* **2009**, *12*, 220–230.

[26] B. Kunze, T. Kemmer, G. Höfle, H. Reichenbach, *J. Antibiot.* **1984**, *37*, 454–461.

[27] W. Oettmeier, D. Godde, B. Kunze, G. Höfle, *Biochim. Biophys. Acta* **1985**, *807*, 216–219.

[28] B. Kunze, G. Höfle, H. Reichenbach, *J. Antibiot.* **1987**, *40*, 258–265.

[29] A. Sandmann, J. Dickschat, H. Jenke-Kodama, B. Kunze, E. Dittmann, R. Müller, *Angew. Chem. Int. Ed.* **2007**, *46*, 2712–2716.

[30] R. Jansen, B. Kunze, H. Reichenbach, G. Höfle, *Eur. J. Org. Chem.* **2003**, 2684–2689.

[31] R. Jansen, P. Washausen, B. Kunze, H. Reichenbach, G. Hofle, *Eur. J. Org. Chem.* **1999**, 1085–1089.

[32] G. Höfle, N. Bedorf, H. Steinmetz, D. Schomburg, K. Gerth, H. Reichenbach, *Angew. Chem. Int. Ed.* **1996**, *35*, 1567–1569.

[33] A. Conlin, M. Fornier, C. Hudis, S. Kar, P. Kirkpatrick, *Nat. Rev. Drug. Discov.* **2007**, *6*, 953–954.

[34] S. I. Elshahawi, A. E. Trindade-Silva, A. Hanora, A. W. Han, M. S. Flores, V. Vizzoni, C. G. Schrago, C. A. Soares, G. P. Concepcion, D. L. Distel et al., *P. Natl. Acad. Sci. USA* **2013**, *110*, E295.

[35] M. Perez, C. Crespo, C. Schleissner, P. Rodriguez, P. Zuniga, F. Reyes, *J. Nat. Prod.* **2009**, *72*, 2192–2194.

[36] F. Surup, K. Viehrig, K. I. Mohr, J. Herrmann, R. Jansen, R. Müller, *Angew. Chem. Int. Ed.* **2014**, *53*, 13588-13591.

[37] K. Viehrig, F. Surup, K. Harmrolfs, R. Jansen, B. Kunze, R. Müller, *J. Am. Chem. Soc.* **2013**, *135*, 16885–16894.

[38] H. Yamaki, N. Sitachitta, T. Sano, K. Kaya, *J. Nat. Prod.* **2005**, *68*, 14–18.

[39] A. Plaza, R. Garcia, G. Bifulco, J. P. Martinez, S. Hüttel, F. Sasse, A. Meyerhans, M. Stadler, R. Müller, *Org. Lett.* **2012**, *14*, 2854–2857.

[40] S. Baumann, J. Herrmann, R. Raju, H. Steinmetz, K. I. Mohr, S. Hüttel, K. Harmrolfs, M. Stadler, R. Müller, *Angew. Chem. Int. Ed.* **2014**, *53*, 14605–14609.

[41] B. Kunze, R. Jansen, F. Sasse, G. Höfle, H. Reichenbach, *J. Antibiot.* **1995**, *48*, 1262–1266.

[42] T. M. Zabriskie, J. A. Klocke, C. M. Ireland, A. H. Marcus, T. F. Molinski, D. J. Faulkner, C. Xu, J. Clardy, *J. Am. Chem. Soc.* **1986**, *108*, 3123–3124.

[43] A. Plaza, R. Müller in *Natural Products* A. Osbourn, R. J. Goss, G. T. Carter., Eds.; John Wiley & Sons Inc: Hoboken, NJ, USA, **2014**.

[44] S. C. Andrews, A. K. Robinson, F. Rodriguez-Quinones, *FEMS Microbiol. Rev.* **2003**, *27*, 215–237.

[45] Sigel, A., Sigel, H., Eds.; Metal Ions in Biological Systems: Iron Transport and Storage in Microorganisms, Plants, and Animals; Dekker: New York, **1998**.

[46] R. C. Hider, X. Kong, *Nat. Prod. Rep.* **2010**, *27*, 637–657.

[47] M. Sandy, A. Butler, *Chem. Rev.* **2009**, *109*, 4580–4595.

[48] H. D. Ambrosi, V. Hartmann, D. Pistorius, R. Reissbrodt, W. Trowitzsch-Kienast, *Eur. J. Org. Chem.* **1998**, 541–551.

[49] B. Kunze, W. Trowitzsch-Kienast, G. Höfle, H. Reichenbach, *J. Antibiot.* **1992**, *45*, 147–150.

[50] G. Müller, K. N. Raymond, *J. Bacteriol.* **1984**, *160*, 304–312.

[51] B. Nagoba, D. Vedpathak, *Eur. J. Gen. Med.* **2011***;8*, 229-235.

[52] P. Ackrill, A.J. Raiston, K.C. Hoodge, *Lancet* **1980**, **2**, 692-693.

[53] S. Pollack, R. N. Rossan, D. E. Davidson, A. Escajadillo, *Proc. Soc. Exp. Biol. Med*. **1987**, *184*, 162–164.

[54] C. Raventos-Suarez, S. Pollack, R. L. Nagel. 1982. *Am. J. Trop. Med. Hyg*. **1982**, *31*, 919–922.

[55] M. Miethke, M. A. Marahiel, *Microbiol. Mol. Biol. Rev.* **2007**, *71*, 413.

[56] S. Schubert, A. Rakin, J. Heesemann, *Int. J. Med. Microbiol*. **2004**, *294*, 83–94.

[57] A. Gorska, A. Sloderbach, A. P. Marszatt, *Trends. Pharmacol. Sci.* **2014,** *35*, 442-449.

[58] C. Ji, P. A. Miller, M. J. Miller, *J. Am. Chem. Soc.* **2012**, *134*, 9898–9901.

[59] L. A. Mislin, I. J. Schalk, *Metallomics*, **2014**, *6*, 408-420.

[60] G. Lang, N. A. Mayhudin, M. I. Mitova, L. Sun, S. S. van der, J. W. Blunt, A. L. Cole, G. Ellis, H. Laatsch, M. H. Munro, *J. Nat. Prod.* **2008**, *71*, 1595–1599.

[61] K. F. Nielsen, M. Mansson, C. Rank, J. C. Frisvad, T. O. Larsen, *J. Nat. Prod.* **2011**, *74*, 2338–2348.

[62] J. L. Wolfender, K. Ndjoko, K. Hostettmann, *Phytochem. Anal*. **2001,** 12, 2-22

[63] S. D. Sarker, Z. Latif, A. I. Gray., Eds.; *Methods in Biotechnology; Natural products isolation*. Humana Press: Totowa, New Jersey, **2010**.

[64] D. Krug, R. Müller, *Nat. Prod. Rep.* **2014**, *31*, 768–783.

[65] J. -L. Wolfender, K. Ndjoko, K. Hostettmann, *J. Chromatogr. A.* **2003**, *1000*, 437-455.

[66] S. Sturm, C. Seger, *J. Chromatogr. A.* **2012**, *1259*, 50-61.

[67] J. W. Jaroszewski, *Planta. Med*. **2005**, *71*, 795-802.

[68] D. Krug, K. Harmrolfs, T. Hoffmann, N. S. Cortina, R. Müller, Screening for novel natural products from myxobacteria using LC-MS and LC-NMR, **2012**.

[69] G. Wider, *BioTechniques.* **2000**, *29*, 1278-1294.

[70] I. Solomon, *Phys. Rev*. **1955**, *99*, 559-565.

[71] A. Bax, R. Freeman, *J. Magn. Reson.* **1981**, *44*, 542-561.

[72] W. F. Reynolds, R. Enriquez, *J. Nat. Prod*. **2002**, *65*, 221-244.

[73] A. Bax, D. G. Davis, *J. Magn. Reson.* **1985**, *65*, 355-360.

[74] D. G. Davis, A. Bax, *J. Am. Chem. Soc.* **1985**, *107*, 7197-7198.

[75] K. E. Kover, O. Prakash, J. Hruby, *J. Magn. Reson.* **1993**, *A103*, 92-96.

[76] A. Bax, R. Freeman, *J. Magn. Reson.* **1981**, *44*, 542-561.

[77] R. C. Breton, W. F. Reynolds, *Nat. Prod. Rep*. **2013**, *30*, 501-524.

[78] A. Bax, M. F. Summers, *Am. Chem. Soc*. **1986**, *108*, 2093-2094.

[79] G. E. Martin, C. E. Hadden, *J. Nat. Prod.* **2000**, *63*, 543-585.

[80] T. F. Molinski, *Nat. Prod. Rep.* **2010**, *27*, 321–329.

[81] T. D. W. Claridge, *High-Resolution NMR Techniques in Organic Chemistry*, Elsevier: Amsterdam, **2009**.

[82] W. Bauer, A. Soi, A. Hirsch, *Magn. Reson. Chem.* **2000,** *38*, 500–503.

[83] K. Stott, J. Keeler, Q. N. Van, A.J. Shaka, *J. Magn. Reson.* **1997**, *125*, 302-324.

[84] M. Karplus, *J. Am. Chem. Soc.* **1963**, *85*, 2870-2871.

[85] N. Matsumori, D. Kaneno, M. Murata, H. Nakamura, K. Tachibana, *J. Org. Chem.* **1999**, *64*, 866-876.

[86] C. Griesinger, O. W. Soerensen, R. R. Ernst, *J. Am. Chem. Soc.* **1985**, *107*, 6394-6396.

[87] H. Kessler, M. Gehrke, C. Griesinger, *Angew. Chem. Int. Ed.* **1988**, *27*, 490-536.

[88] A. Meissner, O. W. Sorensen, *Magn. Reson. Chem.* **2001**, *39*, 49-52.

[89] D. Uhrín, G. Batta, V. J. Hruby, P. N. Barlow, K. E. Kövér, *J. Magn. Reson.* **1998**, *130*, 155-161.

[90] T. Parella, J. F. Espinosa, *Prog. Nucl. Magn. Reson. Spectrosc.* **2013**, *73*, 17-55.

[91] B. L. Marquez, W. H. Gerwick, R. T. Williamson, *Magn. Reson. Chem.* **2001**, *39*, 499-530.

[92] G. Bifulco, P. Dambruoso, L. Gomez-Paloma, R. Riccio, *Chem. Rev.* **2007**, *107*, 3744–3779.

[93] G. Bifulco, C. Bassarello, R. Riccio, L. Gomez-Paloma *Org. Lett.* **2004**, *6*, 1025-1028.

[94] P. Cimino, L. Gomez-Paloma, D. Duca, R. Riccio, G. Bifulco, *Magn. Reson. Chem.* **2004**, *42*, S26-33.

[95] T. Helgaker, M. Jaszunski, K. Ruud, *Chem. Rev.* **1999**, *99*, 293-352.

[96] Y. Kobayashi, J. Lee, K. Tezuka, Y. Kishi, *Org. Lett.* **1999**, *13*, 2177-2180.

[97] J. Lee, Y. Kobayashi, K. Tezuka, Y. Kishi, *Org. Lett.* **1999**, *13*, 2181-2184.

[98] S. D. Rychnovsky,J. D. Skalitzky, *Tetrahedron Lett.* **1990**, *31*, 945-948.

[99] S. D. Rychnovsky, D. J. Skalitzky, C. Pathirana, P. R. Jensen, W. Fenical, *J. Am. Chem. Soc.* **1992**, *114*, 671–677.

[100] T. F. Molinski, B. I. Morinaka, *Tetrahedron.* **2012**, *68*, 9307-9343.

[101] J. M. Bijvoet, A. F. Peerdeman, A. J. Van Bommel, *Nature*. **1951,** *168*, 271–272.

[102] M. F. C. Ladd, R. A. Palmer. Eds. *Structure determination by X-ray crystallography* 2nd ed. Plenum: NY, **1985.**

[103] N. Harada, *Chirality.* **2008**, *20*, 691-723.

[104] A. Gergely, *J. Pharmaceut. Biomed.* **1989**, *7*, 523-541.

[105] M. Masullo, C. Bassarello, G. Bifulco, S. Piacente, *Tetrahedron* **2010**, *66*, 139–145.

[106] S. G. Allenmark, *Nat. Prod. Rep.* **2000**, *17*, 145–155.

[107] T. R. Hoye, C. S. Jeffrey, F. Shao, *Nat. Protoc.* **2007**, *2*, 2451–2458.

[108] J. M. Seco, E. Quinoa, R. Riguera, *Chem. Rev.* **2004**, *104*, 17–117.

[109] K. Fujii, Y. Ikai, H. Oka, M. Suzuki, K. Harada, *Anal. Chem.* **1997**, *69*, 5146–5151.

[110] R. Bhushan, H. Bruckner, *Amino Acids* **2004**, *27*, 231–247.

Chapter 2

Microsclerodermins from Terrestrial Myxobacteria: An Intriguing Biosynthesis Likely Connected to a Sponge Symbiont

*Thomas Hoffmann, Stefan Müller, Suvd Nadmid, Ronald Garcia and Rolf Müller**

Journal of the American Chemical Society, **2013**, 135 (45), 16904–16911

DOI: 10.1021/ja4054509

Published online: October 14, 2013

Supporting information is available online at:

http://pubs.acs.org/doi/suppl/10.1021/ja4054509

2. Microsclerodermins

2.1. Abstract

The microsclerodermins are unusual peptide natural products exhibiting potent antifungal activity reported from marine sponges of the genera *Microscleroderma* and *Theonella*. We here describe a variety of microbial producers of microsclerodermins and pedeins among myxobacteria along with the isolation of several new derivatives. A retro-biosynthetic approach led to the identification of microsclerodermin biosynthetic gene clusters in genomes of *Sorangium* and *Jahnella* species, allowing for the first time insights into the intriguing hybrid PKS/NRPS machinery required for microsclerodermin formation. This study reveals the biosynthesis of a "marine natural product" in a terrestrial myxobacterium where even the identical structure is available from both sources. Thus, the newly identified terrestrial producers provide access to additional chemical diversity; moreover, they are clearly more amenable to production optimization and genetic modification than the original source from the marine habitat. As sponge metagenome data strongly suggest the presence of associated myxobacteria, our findings underpin the recent notion that many previously described "sponge metabolites" might in fact originate from such microbial symbionts.

2.2. Introduction

Natural products have a longstanding tradition as leads for the development of new medicines.[1] In addition to well-established and extensively investigated plant, fungal, and bacterial producers of secondary metabolites, newer screening campaigns increasingly include organisms from less studied taxa and previously underexploited habitats such as terrestrial myxobacteria and marine sponges.[2–5] Their potential as sources of novel chemical scaffolds has been clearly demonstrated and despite the impressive structural diversity originating from these organisms, the overall picture has emerged that structural types obtained from phylogenetically distant producers usually show little overlap.[6] However, as an exception to this general notion the production of several strikingly similar compounds by unrelated species has also been reported. Some of these findings are parallel discoveries of initially sponge-derived metabolite classes from microbial sources, leading to the assumption that the respective natural products might in fact be produced by bacterial sponge symbionts.[7–9] Support for this theory comes from the identification of filamentous bacteria growing within intercellular space inside the sponge.[8,10] However, studies which unambiguously prove the production of a "sponge metabolite" by a symbiotic bacterium are exceedingly rare.[10,11] The same holds true for marine natural products of other host organisms.[12–14] This shortcoming may be

attributed to difficulties with isolation and cultivation of symbiotic microbes under laboratory conditions. Notably, the ability to independently cultivate the "real" producer of a specific secondary metabolite holds great promise, not only for sustained production but also for improving yields using both biotechnological and genetic engineering approaches. These opportunities present an invaluable advantage when further investigating a compound of interest, as the marine organism itself usually faces critical supply limitations and is poorly amenable to genetic manipulation. Moreover, access to a microbial producer facilitates the identification of biosynthetic genes underlying the formation of the metabolite of interest - a crucial prerequisite for understanding the biosynthetic machinery and a promising step toward transferring these genes into a suitable heterologous expression host.[15]

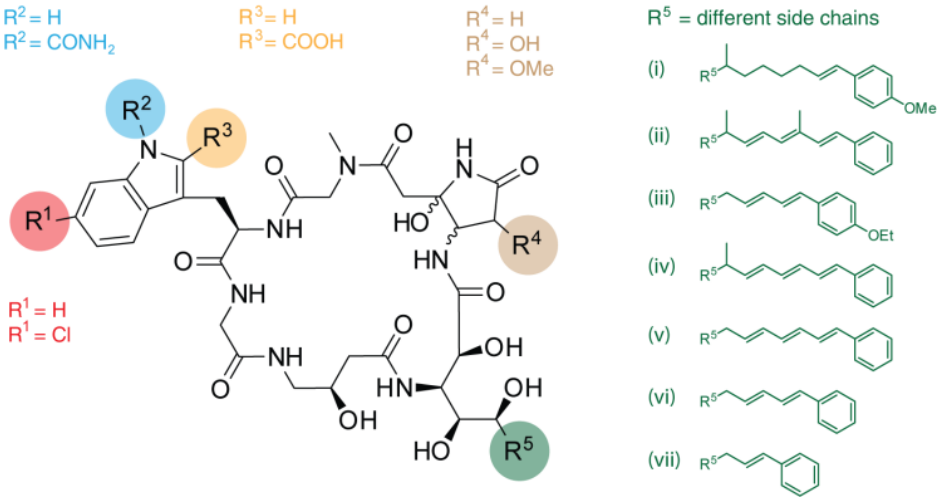

Figure 2.1 The microsclerodermin scaffold with an overview of the different residues identified so far. Groups R^1-R^4 are related to the presence of tailoring enzymes during biosynthesis whereas the side chain R^5 is derived by the PKS part of the biosynthetic machinery. The pyrrolidone is reported to have R,R- or S,S-configuration, respectively.

Looking at those natural products from marine sources having apparent microbial counterparts, several cases exist where structures of myxobacterial secondary metabolites are indeed strikingly similar to previously discovered sponge-derived compounds. For example, the cyclodepsipeptide jaspamide (jasplakinolide) isolated from the marine sponge *Jaspis*.[16,17] is closely related to the structure of chondramides produced by the myxobacterium *Chondromyces crocatus* Cm c5, suggesting that the biosynthetic pathways responsible for production of these molecules should be largely similar.[18] The same holds true for renieramycin and saframycin MX1, isolated from a *Reniera* sponge and a myxobacterium of the genus *Myxococcus*.[19,20] Moreover, the macrolides salicylihalamide and apicularen were isolated from a *Halicona* sp. sponge and a *Chondromyces* species, respectively.[21,22] Very recently, bengamides were described from a *Jaspis* sponge and a cultured myxobacterium.[23,24] Adding to the list of "biosynthetic look-alikes", the structure of pedein from the terrestrial myxobacterium *Chondromyces pediculatus* Cm p3 closely resembles that of microsclerodermin,[25] which was isolated in 1994 from *Microscleroderma* sp., a lithistid sponge

harvested in New Caledonia.[26] Upon their finding of pedeins in myxobacteria, Kunze *et al.* suggested that the origin of microsclerodermins could be a bacterial sponge symbiont closely related to myxobacteria.[25] Indeed, pedein and microsclerodermin are highly similar, and both exhibit potent antifungal activity. To date several new derivatives belonging to the microsclerodermin class of peptides have been identified from various *Microscleroderma* species as well as from a *Theonella* sponge.[27–30] Nevertheless, the biosynthetic machinery behind this natural product remains so far elusive.

Table 2.1 Overview of Different Microsclerodermins and Pedeins and Their Origin

derivative	R^1	R^2	R^3	R^4	R^5	pyrrolidone confign	sum formula	$(M+H)^+$ [m/z]	[*a*]	[*b*]	[*c*]	[*d*]	[*e*]	ref.
A	H	H	COOH	OH	i	S, S	$C_{47}H_{62}N_8O_{16}$	995.4357	•					26,29
B	H	H	COOH	H	i	S, S	$C_{47}H_{62}N_8O_{15}$	979.4407	•					26,29
C	Cl	$CONH_2$	H	H	vii	R, R	$C_{41}H_{50}N_9O_{13}Cl$	912.3289	•	•				27
D	Cl	H	H	H	vii	R, R	$C_{40}H_{49}N_8O_{12}Cl$	869.3231	•	•	•	•		27, this study
E	H	H	COOH	H	iii	R, R	$C_{45}H_{54}N_8O_{14}$	931.3832	•					27
F + G [f]	H	H	H	H	iv	R, R	$C_{45}H_{56}N_8O_{12}$	901.4090	•					28
H + I [f]	H	H	H	H	ii	R, R	$C_{46}H_{58}N_8O_{12}$	915.4247	•					28
J	H	H	H	H	i	S, S	$C_{46}H_{60}N_8O_{12}$	917.4403	•					29
K	H	H	H	OH	i	S, S	$C_{46}H_{60}N_8O_{13}$	933.4353	•					29
L	Cl	H	H	OMe	vii	R, R	$C_{41}H_{51}N_8O_{13}Cl$	899.3337			•	•		this study
M	H	H	H	H	v	R, R	$C_{44}H_{54}N_8O_{12}$	887.3934					•	this study
Pedein A [g]	Cl	H	H	OMe	vi	R, R	$C_{43}H_{53}N_8O_{13}Cl$	925.3493			•	•		25, this study
Pedein B [g]	H	H	H	OMe	vi	R, R	$C_{43}H_{54}N_8O_{13}$	891.3883			•	•		25, this study

[a] *Microscleroderma* sp. (3 species) [b] *Theonella* sp. (1 species) [c] *Chondromyces* sp. (2 species) [d] *Jahnella* sp. (2 species) [e] *Sorangium* sp. (11 species) [f] The tryptophan side chain is reduced to an α-β-unsaturated amino acid. [g] Based on their same biosynthetic origin, we implicitly include pedeins when referring to the microsclerodermin family in this study.

In this study we present several terrestrial myxobacteria as alternative producers of microsclerodermins and pedeins. Our data show that *Jahnella* and *Chondromyces* species can produce the identical derivate also known from a *Microscleroderma* species. In addition, they produce new derivatives not previously reported from other sources. Access to genomic sequences for two myxobacterial producers allowed us to establish for the first time a biosynthetic model for microsclerodermin formation and also provided us with an opportunity to probe the molecular basis responsible for the structural diversity observed from microsclerodermins. Moreover, it was shown that the myxobacterial pedeins[25] originate from the same biosynthetic machinery as the microsclerodermins; hence, they belong to the same compound family. Taken together with recent metagenomic studies providing evidence that myxobacterial taxa may even exist as sponge symbionts,[31] our results underpin the assumption that a myxobacterium is the real biosynthetic source of the "marine" natural product microsclerodermin.

2.3.Experimental Section

2.3.1. Bacterial Strains and Culture Conditions

Sorangium cellulosum So ce38 was cultivated in H-medium (2 g/L soybean flour, 2 g/L glucose, 8 g/L starch, 2 g/L yeast extract, 1 g/L $CaCl_2 \cdot 2H_2O$, 1 g/L $MgSO_4 \cdot 7H_2O$, 8 mg/L Fe-EDTA, 50 mM HEPES, adjusted to pH 7.4 with 10N KOH). Mutants of *S. cellulosum* So ce38 were cultivated in H-medium supplemented with hygromycin B (100 µg/mL) and 1% (w/v) adsorber resin (XAD-16, Rohm & Haas) at 180 rpm and 30^0C. *Jahnella* sp. MSr9139 was cultivated in buffered yeast broth medium VY/2 (5 g/L baker's yeast, 1 g/L $CaCl_2 \cdot 2H_2O$, 5 mM HEPES pH 7.0 with 10N KOH) at 180 rpm and 30^0C.[32] The *Escherichia coli* strains DH10B and ET12567 harboring the plasmids pUB307 and pSUP*mscH*_KO for conjugation purposes were cultivated in Luria-Bertani (LB) medium at 37^0C. Transformation of strains was performed according to the standard methods described elsewhere.[33] Antibiotics were added with the following final concentrations: chloramphenicol (25 µg/mL), kanamycin sulfate (25 µg/mL) and hygromycin B (100 µg/mL).

2.3.2. Disruption of the *msc*H Locus in Soce38

Gene disruption in So ce38 using biparental mating was carried out according to a previously established protocol.[34] For construction of the plasmid pSUP*mscH*_KO a homologous fragment with the size of 2472 bp was amplified from genomic DNA using the oligonucleotides *mscH*_KO_for (GAT CCA GCG CTG GTT CCT CG) and *mscH*_KO_rev (ACG AGG CTG TCG AAG AGC G) and cloned into pCR-TOPO II-vector, resulting in the plasmid pTOPO_*mscH*_KO. The genomic segment was subsequently recovered from this plasmid using the restriction enzymes *Hind*III and *Eco*RV and further integrated into the prepared vector pSUPHyg.

2.3.3. Isolation of Microsclerodermin M from So ce38

The production medium for So ce38 was P38X medium (2 g/L peptone, 2 g/L glucose, 8 g/L starch, 4 g/L probion, 1 g/L $CaCl_2$ $2H_2O$, 1 g/L $MgSO_4 \cdot 7H_2O$, 8 mg/L Fe-EDTA, 50 mM HEPES, adjusted to pH 7.5 with 10 N KOH). A 100 L fermenter with 2% (w/v) XAD-16 adsorber resin (Rohm & Haas) was harvested after 14 days of fermentation. The cells were removed from the XAD before extraction with 3 x 3 L of methanol followed by 1 x 3 L of acetone. The combined fractions yielded 47.2 g dry weight of crude extract. Five grams of this extract was suspended in cold water, the suspension was centrifuged immediately, and the remaining pellet was dissolved in DMSO/MeOH (1:1, v/v) to give a product-enriched solution which was subjected to preparative HPLC using a Waters Autopurifier System equipped with a Waters XBridge C18, 150x19 mm, 5 µm d_p column operated at room temperature. The gradient started at 30% B, increased to 50% B in 2 min and to 51 % B in another 2 min before increasing to 95% B in 4min for column flushing. The combined fractions of interest were

lyophilized, dissolved in DMSO/MeOH (1:1, v/v), and forwarded to a semipreparative Dionex HPLC system (P680 pump, TCC100 thermostat, and PDA100 detector) equipped with a Phenomenex Fusion C18, 250x4.6 mm, 4 µm d_p column. Separation was achieved by a linear gradient using (A) H_2O and (B) ACN at a flow rate of 5 mL/min and 30^0C. The gradient started at 10 % B and increased to 30% B in 3 min, followed by an increase to 38% B in 15 min (0.9% B/column volume). UV data were acquired at 316 nm. A maximum of 100 µL of the sample was manually injected before fraction collection, yielding 8.1 mg of microsclerodermin M. Microsclerodermin M: white amorphous solid, $[\alpha]_D^{20}$ - 55.7 (c 0.10, DMSO/MeOH 8:2).

2.3.4. Isolation of Microsclerodermins from MSr9139

The strain MSr9139 was cultivated in 3 x 1 L shaking flasks containing 500 mL of buffered VY/2 medium for 30 days. The medium was changed every 24 h by pipetting out the liquid broth. The cell pellet was harvested by centrifugation and lyophilized overnight, followed by extraction with 3 x 300 mL of methanol. The combined fractions yielded an orange-brown crude extract which was further partitioned between hexane and MeOH/H_2O 7:3 (v/v) to yield 170 mg of crude extract out of the aqueous phase. Subsequently, the extract was purified by semipreparative HPLC using an Agilent 1260 Infinity system (G1311C quaternary pump, G1330B thermostat, G1315D DAD detector and G1328C manual injector) equipped with a Phenomenex Jupiter Proteo, 250x10 mm, 4 µm d_p column. Separation was achieved by a linear gradient using (A) H_2O and (B) ACN at a flow rate of 2.5 mL/min and 22^0C. The gradient started at 20% B and increased to 50% B in 35 min (5.7% B/column volume). UV data were acquired at 280 nm. A maximum of 100 µL of the sample was manually injected before fraction collection yielding 0.7 mg of microsclerodermin D, 0.45 mg of microsclerodermin L, and 0.85 mg of pedein A. Microsclerodermin L: white amorphous solid, $[\alpha]_D^{20}$ - 77.7 (c 0.12, MeOH).

2.3.5. LC-MS data acquisition

All measurements were performed on a Dionex Ultimate 3000 RSLC system using a BEH C18, 100 x 2.1 mm, 1.7 µm d_p column (Waters, Germany). Separation of 1 µL sample was achieved by a linear gradient from (A) H_2O + 0.1% FA to (B) ACN + 0.1% FA at a flow rate of 600 µL/min and 45^0C. The gradient was initiated by a 0.5 min isocratic step at 5% B, followed by an increase to 95% B in 18 min to end up with a 2 min step at 95% B before reequilibration under the initial conditions. UV spectra were recorded by a DAD in the range from 200 to 600 nm. The LC flow was split to 75 µL/min before entering the maXis 4G hr-ToF mass spectrometer (Bruker Daltonics, Germany) using the Apollo II ESI source. Mass spectra were acquired in centroid mode ranging from 150–2500 m/z at 2 Hz scan rate.

2.3.6. 16S rRNA Gene and Phylogenetic Analysis

Extraction of the 16S rRNA gene was performed in representative microsclerodermin producing strains of *Sorangium, Jahnella* and *Chondromyces*. Sequences of other myxobacterial strains used in the analysis were obtained from GenBank. The 16S rRNA gene was amplified using a set of universal primers, and phylogenetic analysis was performed as described in a previous study, but using the MUSCLE alignment algorithm and Neighbor-Joining tree method (JC69) as implemented in the Geneious Pro program version 5.6.5.[35]

2.3.7. Genome Data

The *msc* gene cluster sequence was deposited in the GenBank with the accession no KF657738 for *S. cellulosum* So ce38 and accession no KF657739 for *Jahnella* sp. MSr9139.

2.4. Results and Discussion

2.4.1. Production of Microsclerodermins by Terrestrial Myxobacteria

In the course of our screening for bioactive natural products from myxobacteria, we observed antifungal activity in extracts from strain MSr9139, a newly isolated *Jahnella* species. Subsequent HPLC-based purification led to several fractions showing antifungal activity which contained compounds featuring an isotopic pattern typical for chlorination in MS analysis. Two compounds from these fractions could be assigned by their exact mass, fragmentation pattern, and retention time as pedein A (925.3493 *m/z*, $[M+H]^+$) and pedein B (891.3883 *m/z*, $[M+H]^+$), antifungal metabolites known from the myxobacterium *Chondromyces pediculatus* Cm p3.[25] Full structure elucidation was carried out for a compound with 869.3231 *m/z* obtained from another bioactive fraction, and the data unambiguously revealed this candidate as the known marine natural product microsclerodermin D (Table 2.1 and Figure S1). In addition to this, analysis of the MSr9139 extract led to the isolation and structure elucidation of the new derivative microsclerodermin L, differing from microsclerodermin D by an additional methoxy group, which is also reported for the pedein structure (Table 2.1 and Figure S3). Notably, the microsclerodermins are the first family of compounds found in the unexplored genus *Jahnella*, a member of the notable secondary metabolite producer myxobacterial family *Polyangiaceae*.[36]

Almost simultaneously, extracts from the myxobacterial strain *Sorangium cellulosum* So ce38 underwent biological profiling and HPLC fractionation, highlighting antifungal activity in the same chromatographic region as previously found from the MSr9139 extract. HPLC purification could narrow down the putatively active compounds to a candidate with 887.3934 *m/z*, and subsequent NMR analysis identified a peptide featuring the pyrrolidone moiety also known from microsclerodermins. NMR data revealed the presence of a new non-chlorinated derivative,

microsclerodermin M (Table 2.1 and Figure 2.2, S4). It shares the typical cyclic core structure with other microsclerodermins but features an unbranched side chain with three double bonds in conjugation to a phenyl moiety. Like the known microsclerodermins, the newly identified derivatives show potent activity against *Candida albicans* (microsclerodermin M, MIC 0.16 µg/mL; microsclerodermin L, MIC 18 µg/mL, microsclerodermin D, MIC 6.8 µg/mL). The stereochemistry of the isolated microsclerodermins was identified by acetonide formation and chemical degradation experiments followed by advanced Marfey analysis (see supporting information). It is identical to that reported for the microsclerodermins C – I and pedeins.[25,27,28]

Having discovered that myxobacteria from three different genera *Jahnella*, *Sorangium*, and *Chondromyces* are able to produce microsclerodermin congeners including even the exact same structure as previously described from two species of lithistid sponges (microsclerodermin D) was surprising for two reasons: examples of myxobacteria producing an identical scaffold also known from a phylogenetically distant organism are to date exceedingly rare (even when counting among the bacterial kingdom), and according to previous studies the secondary metabolite profiles from strains belonging to different myxobacterial genera usually exhibit little overlap.[6] In order to shed light on the occurrence of microsclerodermins within the myxobacteria, we conducted a search across high-resolution LC-MS data sets measured from almost 800 extracts, thus covering a sufficiently representative sample including most known myxobacterial taxa (Figure S20). On the basis of the evaluation of exact masses, isotope patterns and retention times we could identify a panel of 15 strains from the suborder *Sorangineae* (no single producer was found within the *Cystobacterineae*) as producers of microsclerodermins. Interestingly, our comprehensive LC-MS survey of myxobacterial secondary metabolomes revealed that producers of microsclerodermins form two mutually exclusive groups: one group comprises 11 *Sorangium* species producing solely the new microsclerodermin M, while the second group includes two strains of *Jahnella* sp. and two *Chondromyces* sp. that produce a variety of different derivatives: i.e. the "marine" microsclerodermin D in addition to the new microsclerodermin L and pedeins A/B (Figures S21 and S22). The various microsclerodermins differ in side chain, tryptophan modification and oxidation state at the pyrrolidone ring, whereas the peptidic core structure is always identical (Figure 2.1).

The fact that all microsclerodermins, irrespective of their origin, exhibit an identical macrocycle and in most cases even the same stereochemistry supports the idea of a shared biosynthetic origin or even a shared evolutionary ancestor. Moreover, the finding of a group of terrestrial myxobacteria producing exactly the same compound as found in lithistid sponges[27] (microsclerodermin D) fuels speculation about the actual biosynthetic origin of marine microsclerodermins. We herein propose that the marine microsclerodermins actually originate from a myxobacterium phylogenetically related to the *Sorangineae* suborder – possibly a yet uncultured species of the *Chondromyces*, *Jahnella*, or

Sorangium taxa living in symbiosis with the sponges from which microsclerodermins were previously isolated.

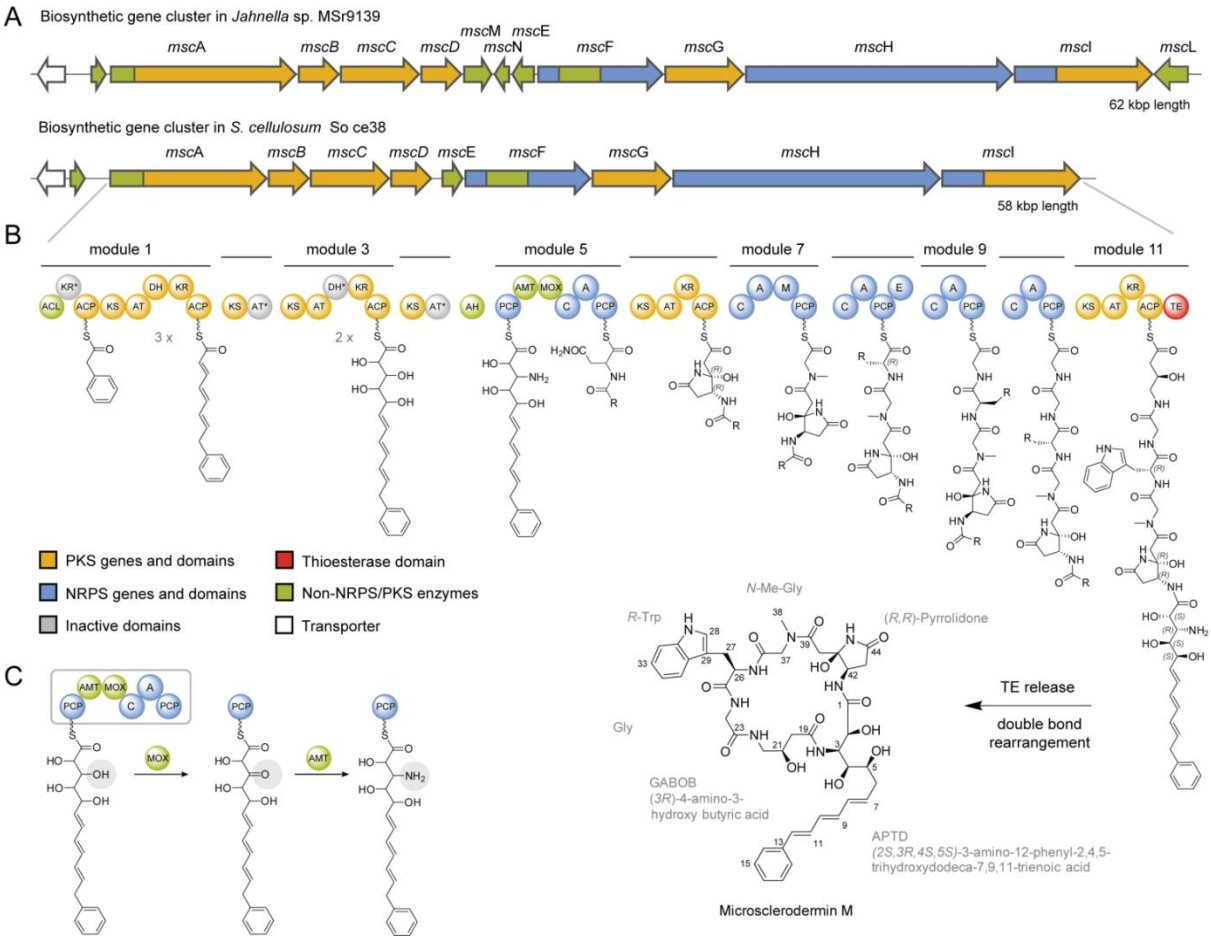

Figure 2.2 (A) Organization of the msc biosynthetic gene cluster in *Jahnella* sp. MSr9139 compared to *Sorangium cellulosum* So ce38. (B) Proposed biosynthetic route to microsclerodermin formation in So ce38. (C) Postulated biosynthetic steps leading to the amino group that is involved in macrolactam formation. A, adenylation domain; AMT, aminotransferase; ACP, acyl-carrier-protein domain; AT, acyltransferase; C, condensation domain; CoA-Lig, coenzyme A Ligase; DH, dehydratase; E, epimerase; KR, ketoreductase; KS, ketosynthase; MT, methyltransferase; MOX, monooxygenase; PCP, peptidyl-carrier-protein domain.

In coincidence with this hypothesis, phylogenetic studies of sponge metagenomes recently identified δ-proteobacteria in the sponge holobiont.[31] Indeed, the phylogenetic tree presented in the work of Simister *et al*. lists a clade containing nine myxobacterial species of terrestrial origin, including *Sorangium cellulosum* and *Chondromyces pediculatus*.[31] These data underpin our assumption that an evolutionary link exists between microsclerodermin biosynthesis in terrestrial and marine producers. Notably, 13 out of 15 producers identified by our LC-MS metabolome survey belong to the genera *Sorangium* or *Chondromyces*. In addition, the new *Jahnella* sp. MSr9139 was isolated from a soil sample collected from the same Philippine island where the sponge *Microscleroderma* was initially

found.[27] This intriguing finding suggests that myxobacteria are possibly flushed to the ocean and adapted to an association with a sponge. The diversity and density of microbial flora present in sponges appears to be a good niche for a predator and proteo-bacteriolytic myxobacterium;[7] thus it is expected that in the future myxobacteria will be isolated from this underexplored source.

Access to myxobacterial producers holds a remarkable benefit, as these bacteria may be cultivated in large-scale fermentations, thereby allowing efficient production of the compounds of interest. Microsclerodermin M is produced at 12 mg/L in *S. cellulosum* So ce38 without optimization of growth conditions or genetic modification of the strain. Moreover, it allows us to investigate their biosynthesis, which has not been elucidated from any marine source to date. Thus, we set out to mine genome sequences of the new terrestrial producers for the presence of putative microsclerodermin biosynthetic pathways, using a retrobiosynthetic analysis as the starting point. The genome sequence of the strain *Sorangium cellulosum* So ce38, producer of the new microsclerodermin M, was already available from a previous study.[37] The newly isolated *Jahnella* sp. MSr9139 was selected for additional genome sequencing, as it produces the new microsclerodermin L in addition to known pedeins A and B and the "marine" microsclerodermin D.

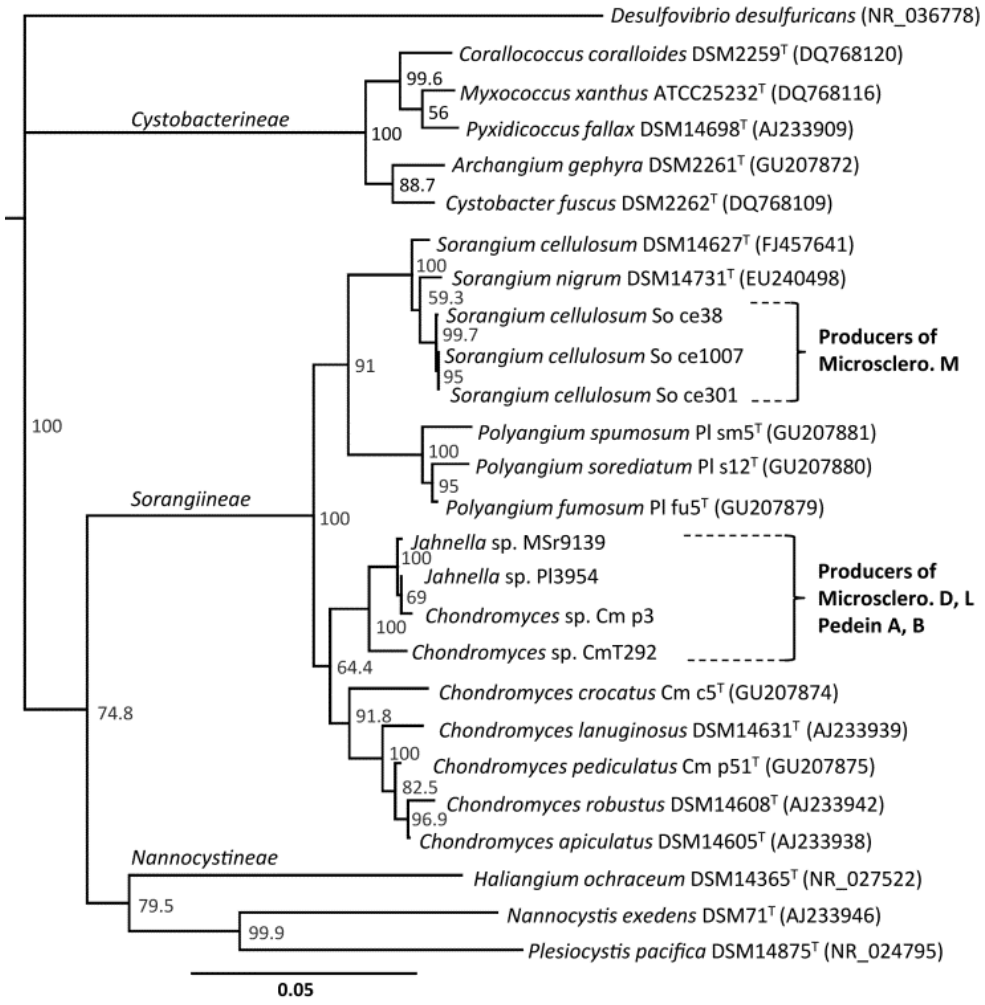

Figure 2.3 Neighbor-joining tree of myxobacteria inferred from 16S rRNA gene sequences showing the clades of microsclerodermin producing strains in suborder *Sorangiineae*. The numbers at branch points indicate percentage bootstrap support based on 1000 resamplings. GenBank accession numbers are indicated in parentheses. Bar = 0.05 substitutions per nucleotide position.

2.4.2. Microsclerodermin Biosynthetic Machinery

All microsclerodermins share the same cyclic peptide core but feature different lipophilic side chains and modifications of amino acid residues. On the basis of retrobiosynthetic considerations, the biosynthetic machinery for microsclerodermin formation was expected to consist of a multimodular PKS/NRPS system accompanied by a set of enzymes involved in side chain biosynthesis and post assembly line modification. The core PKS/NRPS modules should be conserved between producers, while enzymes involved in side chain biosynthesis and additional tailoring enzymes – responsible for modifications such as halogenation or oxidation of the pyrrolidone ring – should occur differentially between the two producer groups, as a consequence of evolutionary diversification of the microsclerodermin pathway.

Using *S. cellulosum* So ce38 and *Jahnella* sp. MSr9139 as representative strains from both microsclerodermin producer groups, we sought to identify microsclerodermin biosynthetic pathways in their genomes and subsequently elaborate on the molecular basis for the observed structural variations. The genome sequences of both strains were searched *in silico* for secondary metabolite gene clusters using the antiSMASH analysis pipeline.[38] The assignment of a matching candidate cluster to microsclerodermin biosynthesis was verified in So ce38 via targeted gene disruption by single crossover integration using biparental conjugation (Figure S24). Sequence comparison on the protein and nucleotide level revealed high similarity between gene clusters from both strains (Table 2.2), and comparison of operons permitted the tentative assignment of cluster boundaries. The microsclerodermin cluster spans a region of 58 kbp (74.7 % GC) in So ce38 and 62 kbp (72.4 % GC) in MSr9139, respectively. In both strains, genes encoding a major facilitator superfamily transporter (*mscK*) followed by a type II thioesterase (*mscJ*) are located upstream to *msc*A. The core biosynthetic assembly line covers five NRPS modules and three PKS modules encoded on genes *mscA* to *mscI*. An additional halogenase is encoded by *mscL* near the downstream boundary of the cluster in MSr9139 (Figure 2.2 A).

Microsclerodermin biosynthesis is initiated at the side chain to build up a phenyl group in conjugation to a double bond. An activated starter unit such as benzoyl-CoA or *trans*-cinnamoyl-CoA is usually recruited by the enzyme in such a case. However, a retrobiosynthetic proposal tells us that the observed double bond order of the side chain is likely different during biosynthesis (Figure 2.2, B). The biosynthetic logic requests the incorporation of C2 units, which is only possible if the double bonds are rearranged (Figure S23). A rearrangement of double bonds has already been reported for other natural products like bacillaen, rhizoxin, corallopyronin and ansamitocin where isomerization is likely catalyzed by a dehydratase domain.[39–42] The reason for isomerization of the microsclerodermin side chain remains elusive; however, it is supported by an energetic benefit of a conjugated π-system. On the basis of this hypothesis, the only suitable starter unit is phenylacetyl-CoA, which has already been reported for other natural product biosynthesis.[43] The incorporation of a phenylacetate starter unit was indeed verified by feeding experiments using isotope-labeled precursors. Feeding ring-labeled $^{13}C_6$-L-phenylalanine resulted in a mass increase of 6 Da, whereas the fully labeled $^{15}N,^{13}C_9$-L-phenylalanine led to a mass shift of 8 Da, indicating the incorporation of two side chain carbons (Figure S27). Feeding d5-benzoic acid or d7-*trans*-cinnamic acid resulted in no mass increase (Figure S25). We can conclude that the α and β carbon atoms of phenylalanine - but not the carboxyl carbon - is incorporated into microsclerodermin. Elongation of the phenylacetate unit is catalyzed by modules MscA and MscC using three times malonate and two times 3-hydroxymalonate as extender units in an iterative manner. Modules 2 (MscB) and 4 (MscD) do only exhibit a combination of a functional KS domain attached to an inactive AT domain as identified by consensus sequence analysis, likely a relic of a former PKS complex.

Table 2.2 Proteins involved in microsclerodermin biosynthesis as identified in two myxobacterial strains.

		Sorangium cellulosum So ce38		*Jahnella* sp. MSr9139	
protein	length [aa]	domains and position in sequence	length [aa]	domains and position in sequence	identity [%]
MscA	3275	CoA-Lig (264-701), KR*(1034-1197), ACP (1348-1411), KS (1441-1828), AT (1976-2286), DH (2342-2505), KR' (2870-3047), ACP' (3149-3214)	3535	CoA-Lig (215-649), KR*(1032-1126), MT (1229-1509), ACP (1613-1676), KS (1712-2147), AT (2244-2555), DH (2610-2774), KR*' (3132-3309), ACP' (3411-3476)	65.4
MscB	870	KS (27-451), AT* (548-772)	878	KS (39-464), AT* (561-792)	73.4
MscC	1551	KS (36-460), AT (557-859), DH* (956-1076), KR (1158-1336), ACP (1436-1505)	1549	KS (39-464), AT (561-865), DH* (956-1076), KR (1157-1335), ACP (1436-1499)	75.0
MscD	900	KS (36-461), AT* (565-678)	848	KS (36-461), AT* (564-675)	72.0
MscE	446	Putative amidohydrolase	386	Putative amidohydrolase	82.9
MscF	2273	PCP (27-98), AMT (329-660), MOX (828-1127), C (1185-1529), A (1673-2082), PCP' (2169-2237)	2189	PCP (4-75), AMT (280-614), MOX (758-1057), C (1105-1397), A (1594-2000), PCP' (2088-2149)	76.5
MscG	1548	KS (14-439), AT (534-828), KR (1156-1330), ACP (1441-1509)	1511	KS (14-439), AT (531-850), KR (1136-1312), ACP (1404-1472)	72.1
MscH	4141	C (76-377), A (564-966), MT (1037-1256), PCP (1469-1531), C' (1554-1850), A' (2037-2426), PCP' (2515-2574), E (2591-2905), C'' (3074-3374), A'' (3558-3967), PCP'' (4054-4121)	4106	C (48-346), A (534-936), MT (1007-1225), PCP (1442-1505), C' (1526-1827), A' (2013-2405), PCP' (2492-2551), E (2568-2872), C'' (3043-3343), A'' (3527-3932), PCP'' (4019-4083)	78.8
MscI	2904	C (48-346), A (533-936), PCP (1023-1087), KS (1111-1535), AT (1638-1936), KR (2266-2465), ACP (2549-2612), TE (2634-2888)	2945	C (77-375), A (563-965), PCP (1053-1116), KS (1150-1573), AT (1676-1970), KR (2309-2509), ACP (2597-2660), TE (2683-2945)	77.8
MscJ	257	thioesterase type II	263	thioesterase type II	43.5
MscK	415	major facilitator superfamily (MFS) transporter	450	major facilitator superfamily (MFS) transporter	24.5
MscL	-	-	535	Tryptophan halogenase	-
MscM	-	-	438	Fe(II)/α-ketoglutarate dependent oxygenase	-
MscN	-	-	277	methyltransferase	-

A, adenylation domain; AMT, aminotransferase; ACP, acyl-carrier-protein domain; AT, acyltransferase; C, condensation domain; CoA-Lig, coenzyme A Ligase; DH, dehydratase; E, epimerase; KR, ketoreductase; KS, ketosynthase; MT, methyltransferase; MOX, monooxygenase; PCP, peptidyl-carrier-protein domain. * inactive domain

The PKS-derived unit is forwarded to the first PCP domain of module MscF. This module harbors two additional domains of rather uncommon type showing high homology to the amino transferase family (AMT) and to the monooxygenase family, both located downstream to the PCP domain. A biosynthetic proposal to account for this domain order is based on oxidation of the β-hydroxyl group of the bound intermediate to the respective β-keto functionality followed by conversion to a β-amino moiety that undergoes macrocyclization (Figure 2.2, C). The use of an aminotransferase is known from other natural product biosynthetic pathways, however, not in combination with the initial oxidation step.[44]

Thereafter, biosynthesis continues with a set of NRPS- and PKS-based reaction cycles. Analysis of the A domain specificities *in silico* is consistent with the amino acids incorporated.[45] We propose the uncommon pyrrolidone moiety is built up by asparagine cyclization. To the best of our knowledge, such an asparagine-derived pyrrolidone system is only found in microsclerodermins and koshikamides, a natural product that was isolated from a *Theonella* species.[46] Indeed, the A domain of MscF is specific for asparagine activation and we did a feeding experiment with fully labeled $^{15}N_2$-$^{13}C_4$-L-asparagine to prove this biosynthetic step. We observed a mass increase of 6 Da according to the incorporation of all carbon and nitrogen atoms of asparagine into the compound (Figures S26, S28). On the basis of this result, a plausible biosynthetic hypothesis requires the nucleophilic attack of the asparagine side chain to the backbone carbonyl atom. A suitable mechanism is known from the intein-mediated peptide cleavage, where intein initiates an intra-molecular asparagine cyclization, notwithstanding the poor reactivity of the side chain's amide.[47] In microsclerodermin biosynthesis, this reaction likely is accompanied by an inversion of the stereochemistry at the α-carbon of the former (*S)*-asparagine. The relative configuration of the pyrrolidone ring was identified by NOE correlations, whereas the absolute (*R,R*)-configuration is derived from degradation experiments (see supporting information). The stereochemistry at this position is thereby identical with that of microsclerodermins C – I. The protein MscE is most likely responsible for the cyclization step, as it is found in both microsclerodermin clusters and shows similarity to the amidohydrolase class, a fairly promiscuous enzyme family able to act on a variety of substrates. However, the exact mechanism involved in this biosynthetic step remains elusive at present.

The forthcoming NRPS modules correspond to the observed structure of microsclerodermin in terms of domain order and predicted substrate specificity (Figure 2.2, B). For both new microsclerodermins an *R*-configured tryptophan was identified by means of the advanced Marfey method, which is in agreement with the epimerization domain found in module 8. The (3*R*)-configuration of the γ-amino butyric acid (GABA) subunit was identified by the same technique (see Figures S13, S14). Both stereogenic centers have the same configuration as identified in all microsclerodermins so far.

2.4.3. Genetic Basis for the Structural Diversity of Microsclerodermins

The derivatives found in *Jahnella* sp. MSr9139 feature side chains with either one or two double bonds while the side chain in So ce38 comprises strictly three double bonds**.** As the number of PKS modules encoded in the gene cluster does not match the number of required elongation cycles, an iterative function of the type I PKS subunits MscA and MscC as described for the stigmatellin megasynthase may explain this finding.[48] The KS domains of each module are highly identical for both strains and do not comprise any of the postulated sequence-based identifiers of iterative KS domains.[49] Nevertheless, MscB is grouping with iterative KS domains in a phylogenetic analysis

(Figure S11). Comparing the entire module MscA of both clusters revealed the insertion of an additional methyl transferase-like domain into the first part of the protein in MSr9139. This domain is likely inactive on the basis of *in silico* analysis as judged by the presence of a corrupted SAM-binding motif (Table S13).[50] Currently, we cannot rule out the possibility that the presence of this additional methyl transferase may influence the iteration process within MscA. In addition to this difference, there is no obvious reason why biosynthesis in So ce38 results in a triene whereas MSr9139 is less strict in iteration. As another hint for a shared origin of the biosynthetic cluster, some of the sponge-derived derivatives exhibit a methyl-branched side chain which could be attributed to this methyl transferase being active in some of the marine producers. Eventually, the variable side chains of the microsclerodermin family are in agreement with the alternating PKS functionality. Halogenation of tryptophan as well as oxidation of the pyrrolidone ring is catalyzed by tailoring enzymes. The halogenase MscL is located downstream to the cluster in MSr9139 and is responsible for chlorination of the tryptophan. It shows 32 % identity on a protein level to a tryptophan halogenase from a Streptomyces species (PDB entry 2WET_A). There is no analogue of MscL found in So ce38, which is in agreement with the absence of chlorinated products in this strain. Supplementing KBr or NaBr to the MSr9139 cultivation broth led to the production of brominated microsclerodermins on the basis of LC-MS analysis. Another difference is the inter-region between the main PKS and NRPS parts. In MSr9139 two additional proteins are found in this region. MscN is a member of the SAM-dependent methyl transferase family, and MscM shows homology to Fe(II)/α-ketoglutarate-dependent dioxygenases. On the basis of the structures produced by MSr9139, we conclude that MscM and MscN are responsible for oxidation and methylation of the pyrrolidone ring, respectively. Modifications at the tryptophan as known from some marine-derived microsclerodermins were not observed in this study. Such modifications are attributed to promiscuous acting enzymes that could be related to the producer strain or even to enzymes related to some sponge symbiont.

2.5. Conclusion

The discovery of microsclerodermins/pedeins from several myxobacteria represents one of the few findings of identical compounds from marine organisms and terrestrial bacteria reported to date. This study thus strengthens the notion that certain natural products, which have been isolated from marine sources such as sponges or other invertebrates, actually originate from associated microbes. Notably, the identification of microsclerodermin-producing myxobacteria provides meaningful hints for future attempts to isolate the symbiotic microbe. This knowledge is considered particularly helpful because isolation success in many cases critically depends on methods well adapted to the requirements of the genus targeted for isolation, especially when aimed at the rather challenging isolation of slow-growing myxobacteria. Availability of an alternative microbial producer as a sustainable source is an advantage for realizing the potential of a marine natural product for therapeutic applications.

Moreover, the myxobacterial producers come along with additional chemical diversity and are amenable to genetic manipulation, as demonstrated in this study. Finally, the identification of two slightly different microsclerodermin biosynthetic gene clusters from two myxobacteria allowed us to establish a conclusive model for microsclerodermin biosynthesis and provided insights into the molecular basis for structural diversity within this compound family. A detailed understanding of microsclerodermin biosynthesis is an important prerequisite for any future efforts toward engineering the pathway for yield improvement or for the production of new derivatives: whether in the native producer, by heterologous expression, or by using synthetic biology approaches.

2.6. References

[1] Newman, D. J.; Cragg, G. M. *J. Nat. Prod.* **2012**, *75*, 311–35.

[2] Wenzel, S. C.; Müller, R. *Mol. Biosyst.* **2009**, *5*, 567–74.

[3] Weissman, K. J.; Müller, R. *Bioorg. Med. Chem.* **2009**, *17*, 2121–36.

[4] Lane, A. L.; Moore, B. S. *Nat. Prod. Rep.* **2011**, *28*, 411–28.

[5] Winder, P. L.; Pomponi, S. A.; Wright, A. E. *Mar. Drugs.* **2011**, *9*, 2643–82.

[6] Wink, J.; Müller, R. *Int. J. Med. Microbiol.* **2013**, in press.

[7] Hentschel, U.; Piel, J.; Degnan, S. M.; Taylor, M. W. *Nat. Rev. Microbiol.* **2012**, *10*, 641–54.

[8] Taylor, M. W.; Radax, R.; Steger, D.; Wagner, M. *Microbiol. Mol. Biol. Rev.* **2007**, *71*, 295–347.

[9] Bewley, C. A.; Faulkner, D. J. *Angew. Chem. Int. Ed.* **1998**, *37*, 2162–2178.

[10] Schmidt, E. W.; Obraztsova, A. Y.; Davidson, S. K.; Faulkner, D. J.; Haygood, M. G. *Mar. Biol.* **2000**, *136*, 969–977.

[11] Unson, M. D.; Faulkner, D. J. *Experientia* **1993**, *49*, 349–353.

[12] Elshahawi, S. I.; Trindade-Silva, A. E.; Hanora, A.; Han, A. W.; Flores, M. S.; Vizzoni, V.; Schrago, C. G.; Soares, C. A.; Concepcion, G. P.; Distel, D. L.; Schmidt, E. W.; Haygood, M. G. *Proc. Natl. Acad. Sci. U.S.A.* **2013**, *110*, E295–304.

[13] Lin, Z.; Torres, J. P.; Ammon, M. A.; Marett, L.; Teichert, R. W.; Reilly, C. A.; Kwan, J. C.; Hughen, R. W.; Flores, M.; Tianero, M. D.; Peraud, O.; Cox, J. E.; Light, A. R.; Villaraza, A. J. L.; Haygood, M. G.; Concepcion, G. P.; Olivera, B. M.; Schmidt, E. W. *Chem. Biol.* **2013**, *20*, 73–81.

[14] Kwan, J. C.; Donia, M. S.; Han, A. W.; Hirose, E.; Haygood, M. G.; Schmidt, E. W. *Proc. Natl. Acad. Sci. U.S.A.* **2012**, *109*, 20655–60.

[15] Wenzel, S. C.; Müller, R. In Comprehensive Natural Products II, Vol. 2: Natural Products Structural Diversity-II Secondary Metabolites: Sources, Structures and Chemical Biology; Moore, B. S.; Crews, P., Eds.; Elsevier, 2010; pp 189-222.

[16] Crews, P.; Manes, L. V; Boehler, M. *Tetrahedron Lett.* **1986**, *27*, 2797–2800.

[17] Zabriskie, T. M.; Klocke, J. A.; Ireland, C. M.; Marcus, A. H.; Molinski, T. F.; Faulkner, D. J.; Xu, C.; Clardy, J. *J. Am. Chem. Soc.* **1986**, *108*, 3123–3124.

[18] Kunze, B.; Jansen, R.; Sasse, F.; Höfle, G.; Reichenbach, H. *J. Antibiot.* **1995**, *48*, 1262–6.

[19] Irschik, H.; Trowitzsch-Kienast, W.; Gerth, K.; Höfle, G.; Reichenbach, H. *J. Antibiot.* **1988**, *41*, 993–8.

[20] Frincke, J. M.; Faulkner, D. J. *J. Am. Chem. Soc.* **1982**, *104*, 265–269.

[21] Erickson, K. L.; Beutler, J. A.; Cardellina, J. H.; Boyd, M. R. *J. Org. Chem.* **1997**, *62*, 8188–8192.

[22] Kunze, B.; Jansen, R.; Sasse, F.; Höfle, G.; Reichenbach, H. *J. Antibiot.* **1998**, *51*, 1075–80.

[23] Hoffmann, H.; Haag-Richter, S.; Kurz, M.; Tietgen, H. Bengamide derivatives, method for the production thereof and use thereof for the treatment of cancer. WO2005044803 A1, 2005.

[24] Johnson, T. A.; Sohn, J.; Vaske, Y. M.; White, K. N.; Cohen, T. L.; Vervoort, H. C.; Tenney, K.; Valeriote, F. A.; Bjeldanes, L. F.; Crews, P. *Bioorg. Med. Chem.* **2012**, *20*, 4348–55.

[25] Kunze, B.; Böhlendorf, B.; Reichenbach, H.; Höfle, G. *J. Antibiot.* **2008**, *61*, 18–26.

[26] Bewley, C. A.; Debitus, C.; Faulkner, D. J. *J. Am. Chem. Soc.* **1994**, *116*, 7631–7636.

[27] Schmidt, E. W.; John Faulkner, D. *Tetrahedron* **1998**, *54*, 3043–3056.

[28] Qureshi, A.; Colin, P. L.; Faulkner, D. J. *Tetrahedron* **2000**, *56*, 3679–3685.

[29] Zhang, X.; Jacob, M. R.; Ranga Rao, R.; Wang, Y. H.; Agarwal, A. K.; Newman, D. J.; Khan, I. A.; Clark, A. M.; Li, X. C. *Res. Rep. Med. Chem.* **2012**, *2012*, 7–14.

[30] Zhang, X.; Jacob, M. R.; Ranga Rao, R.; Wang, Y. H.; Agarwal, A. K.; Newman, D. J.; Khan, I. A.; Clark, A. M.; Li, X. C. *Res. Rep. Med. Chem.* **2013**, 9.

[31] Simister, R. L.; Deines, P.; Botté, E. S.; Webster, N. S.; Taylor, M. W. *Environ. Microbiol.* **2012**, *14*, 517–24.

[32] Garcia, R. O.; Krug, D.; Müller, R. *Meth. Enzymol.* **2009**, *458*, 59–91.

[33] Sambrook, J.; Russell, D. W. *Molecular cloning: A laboratory manual*; Cold Spring Harbor Laboratory Press: Cold Spring Harbor, NY, 2001.

[34] Kopp, M.; Irschik, H.; Gross, F.; Perlova, O.; Sandmann, A.; Gerth, K.; Müller, R. *J. Biotechnol.* **2004**, *107*, 29–40.

[35] Garcia, R.; Gerth, K.; Stadler, M.; Dogma, I. J.; Müller, R. *Mol. Phylogenet. Evol.* **2010**, *57*, 878–87.

[36] Garcia, R.; Müller, R. In *The Prokaryotes: Deltaproteobacteria and Epsilonproteobacteria*; Rosenberg, E.; DeLong, E. F.; Lory, S.; Stackebrandt, E.; Thompson, F., Eds.; Springer: Heidelberg, 2014, in press.

[37] Jahns, C.; Hoffmann, T.; Müller, S.; Gerth, K.; Washausen, P.; Höfle, G.; Reichenbach, H.; Kalesse, M.; Müller, R. *Angew. Chem. Int. Ed.* **2012**, *51*, 5239–43.

[38] Medema, M. H.; Blin, K.; Cimermancic, P.; de Jager, V.; Zakrzewski, P.; Fischbach, M. A.; Weber, T.; Takano, E.; Breitling, R. *Nucleic Acids Res.* **2011**, *39*, W339–46.

[39] Butcher, R. A.; Schroeder, F. C.; Fischbach, M. A.; Straight, P. D.; Kolter, R.; Walsh, C. T.; Clardy, J. *Proc. Natl. Acad. Sci. U.S.A.* **2007**, *104*, 1506–9.

[40] Kusebauch, B.; Busch, B.; Scherlach, K.; Roth, M.; Hertweck, C. *Angew. Chem. Int. Ed.* **2010**, *49*, 1460–4.

[41] Erol, O.; Schäberle, T. F.; Schmitz, A.; Rachid, S.; Gurgui, C.; El Omari, M.; Lohr, F.; Kehraus, S.; Piel, J.; Müller, R.; König, G. M. *Chem. Bio. Chem.* **2010**, *11*, 1253–65.

[42] Taft, F.; Brünjes, M.; Knobloch, T.; Floss, H. G.; Kirschning, A. *J. Am. Chem. Soc.* **2009**, *131*, 3812–3.

[43] Magarvey, N. A.; Beck, Z. Q.; Golakoti, T.; Ding, Y.; Huber, U.; Hemscheidt, T. K.; Abelson, D.; Moore, R. E.; Sherman, D. H. *ACS Chem. Biol.* **2006**, *1*, 766–79.

[44] Tillett, D.; Dittmann, E.; Erhard, M.; von Döhren, H.; Börner, T.; Neilan, B. A. *Chem. Biol.* **2000**, *7*, 753–64.

[45] Röttig, M.; Medema, M. H.; Blin, K.; Weber, T.; Rausch, C.; Kohlbacher, O. *Nucleic Acids Res.* **2011**, *39*, W362–7.

[46] Plaza, A.; Bifulco, G.; Masullo, M.; Lloyd, J. R.; Keffer, J. L.; Colin, P. L.; Hooper, J. N. A.; Bell, L. J.; Bewley, C. A. *J. Org. Chem.* **2010**, *75*, 4344–55.

[47] Mujika, J. I.; Lopez, X.; Mulholland, A. J. *Org. Biomol. Chem.* **2012**, *10*, 1207–18.

[48] Gaitatzis, N.; Silakowski, B.; Kunze, B.; Nordsiek, G.; Blöcker, H.; Höfle, G.; Müller, R. *J. Biol. Chem.* **2002**, *277*, 13082–90.

[49] Yadav, G.; Gokhale, R. S.; Mohanty, D. *PLoS Comput. Biol.* **2009**, *5*, e1000351.

[50] Kozbial, P. Z.; Mushegian, A. R. *BMC Struct. Biol.* **2005**, *5*, 19.

Table S2.1. NMR chemical shifts of microsclerodermin D.

Amino acid	Assignment	δ_C [a]	δ_H (mult., *J* in Hz) [b]
APTO	1	172.3	
	2	69.2	4.39 (d, 3.2)
	3	53	4.13 (d, 11.3)
	4	69.5	3.32 (m)
	5	68.8	3.57 (m)
	6	36.3	2.35 (m)
	7	128.0	6.24 (m)
	8	130.5	6.40 (d, 15.8)
	9	137.2	
	10, 14	125.4	7.35 (d, 7.3)
	11, 13	128.2	7.29 (t, 7.6)
	12	126.5	7.19 (t, 7.3)
	OH-2		6.58 (brs)
	OH-4		4.17 (m)
	OH-5		4.36 (d, 4.5)
	NH-3		7.47 (d, 6.0)
GABOB	15	172.3	
	16	40.7	2.43 (d, 14.0)
			2.15 (d, 14.0)
	17	66.8	3.72 (m)
	18	44.7	3.39 (m)
			2.61 (m)
	OH-17		4.88 (d, 4.8)
	NH-18		7.50 (m)
Gly	19	168.5	
	20	42.3	3.75 (d, 7.0)
			3.34 (d, 7.0)
	NH-20		8.54 (t, 6.0)
6-Cl-Trp	21	171.5	
	22	55.1	4.17 (m)
	23	25.8	3.10 (dd, 5.7, 14.7)
			2.98 (dd, 5.7, 14.7)
	24	124.6	7.26 (d, 1.8)
	25	109.5	
	26	125.6	
	27	119.4	7.52 (d, 8.3)
	28	118.4	7.00 (dd, 1.5, 8.3)
	29	c	
	30	110.7	7.37 (s)
	31	136.1	
	NH-22		8.64 (d, 4.3)
	NH-24		11.04 (brs)
N-Me-Gly	32	169.9	
	33	49.5	4.08 (d, 16.3)
			3.84 (d, 16.3)
	34	36.2	2.93 (s)
Pyrrolidone	35	170.2	
	36	38.6	2.84 (d, 17.1)
			2.69 (d, 17.1)
	37	85.2	
	38	50.3	4.47 (m)
	39	35.0	2.27 (m)

	40	172.3
	NH-37	7.96 (brs)
	NH-38	7.56 (m)
	OH-37	c

[a] Recorded at 175 MHz, referenced to residual solvent DMSO-d_6 at 39.51 ppm.
[b] Recorded at 700 MHz, referenced to residual solvent DMSO-d_6 at 2.50 ppm.
[c] Not observed. [ov] overlapping signals.

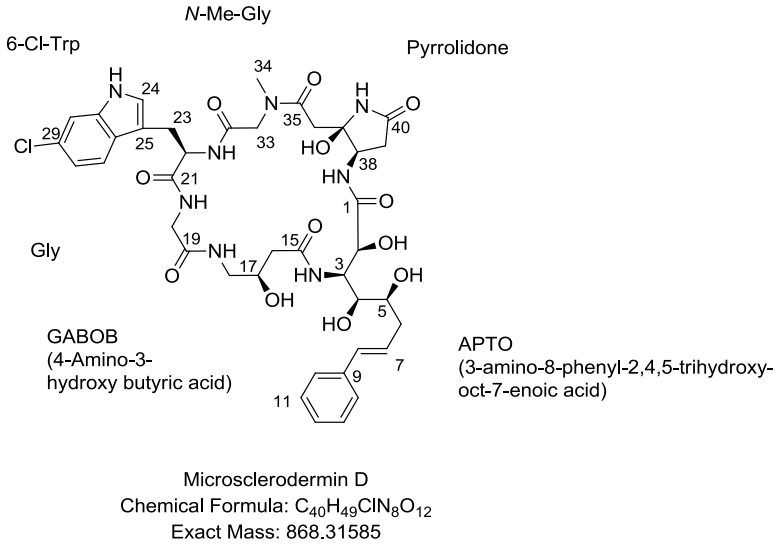

Figure S2.1 Structure and atom numbering of microsclerodermin D. Compound isolated from marine sponges of the genera *Microscleroderma* sp. and *Theonella* sp. and the myxobacterium *Jahnella* sp. MSr9139

Table S2.2 NMR chemical shifts of microsclerodermin L.

Amino acid	Assignment	δ_C [a]	δ_H (mult., *J* in Hz) [b]	HMBC	ROESY
APTO	1	172.9			
	2	69.2	4.43 (brs)	1	
	3	53	4.19 (d, 11.3)	4	4
	4	69.7	3.32 (m)		
	5	68.7	3.59 (q, 6.5)		
	6	36.6	2.38 (m)	4, 5, 7, 8	
			2.33 (m)		
	7	128	6.26 (m)	6, 9	
	8	130.5	6.40 (d, 15.8)	6, 9, 10, 14	6
	9	137.2			
	10, 14	125.6	7.36 (d, 7.0)	8, 12	7, 8
	11, 13	128.3	7.29 (t, 7.6)	9, 10, 14	
	12	126	7.19 (t, 7.4)	10, 11, 13, 14	
	OH-2		6.57 (brs)		
	OH-4		4.85 (d, 4.9)		
	OH-5		4.30 (brs)		
	NH-3		7.42 (brs)		16
GABOB	15	172.1			
	16	40.6	2.43 (d, 14.0)	15	
			2.12 (d, 14.0)		
	17	66.6	3.77 (m)	16, 18	OH-17
	18	44.8	3.33 (m)	17	
			2.65 (m)		
	OH-17		4.85 (brs)		
	NH-18		7.43 (brs)		20
Gly	19	168.5			
	20	42.5	3.72 (d, 7.0)	19, 21	
			3.36 (d, 7.0)		
	NH-20		8.51 (t, 6.0)		22
6-Cl-Trp	21	171.6			
	22	55.2	4.17 (m)		NH-20
	23	25.8	3.10 (dd, 5.7, 15.0)	21, 22, 24, 25, 26	
			2.98 (dd, 5.7, 15.0)		
	24	124.7	7.26 (d, 2.0)	25, 31, 32	
	25	109.3			
	26	125.5			
	27	119.4	7.52 (d, 8.5)	31	
	28	118.5	7.00 (dd, 1.8, 8.5)	30, 26	
	29	c			
	30	110.7	7.37 (s)	27	
	31	136.3			
	NH-22		8.68 (d, 4.3)		22, 23, 24, 33
	NH-24		11.03 (d, 2.0)	24, 25, 31, 26	24, 30
N-Me-Gly	32	172.2			
	33	49.6	4.28 (d, 16.4)	32, 34	
			3.69 (d, 16.4)		
	34	35.9	2.92 (s)	33, 35	
Pyrrolidone	35	170.4			
	36	38.6	2.83 (d, 16.9)	35, 37	38
			2.61 (d, 16.9)		
	37	82.3			
	38	55.8	4.44 (d, 9.0)	39	NH-38
	39	79.0	4.04 (d, 8.8)	40, 41	NH-38

40	56.6	3.39 (s)	39	
41	171.0			
NH-37		8.18 (brs)	37, 38, 39	
NH-38		7.61 (d, 9.6)		2, 39
OH-37		c		

[a] Recorded at 175 MHz, referenced to residual solvent DMSO-d_6 at 39.51 ppm.
Recorded at 700 MHz, referenced to residual solvent DMSO-d_6 at 2.50 ppm.
[c] Not observed. [ov] overlapping signals.

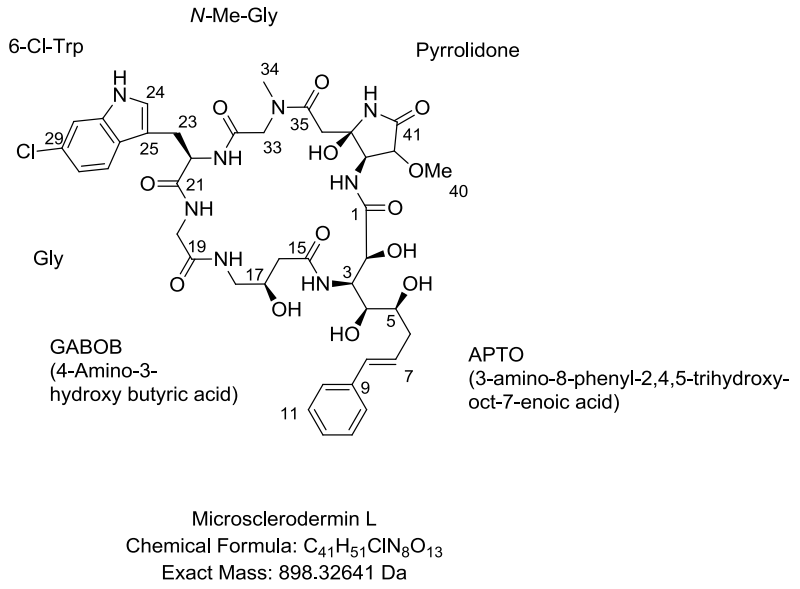

Figure S2.2 Structure and atom numbering of microsclerodermin L. Compound isolated from the myxobacterium *Jahnella* sp. MSr9139

Chapter 3

Hyalachelins A-C, Unusual Siderophores Isolated from the Terrestrial Myxobacterium *Hyalangium minutum*

Suvd Nadmid,[†,§] Alberto Plaza,[†,§] Gianluigi Lauro,[‡] Ronald Garcia,[†,§] Giuseppe Bifulco,[,‡] and Rolf Müller[*,†,§]*

Organic Letters. **2014**, *16*, 4130–4133.

DOI 10.1021/ol501826a

Published online: July 14, 2014

3. Hyalachelins

3.1. Abstract

Three new siderophores, termed hyalachelins A-C (**1-3**), were isolated from the terrestrial myxobacterium *Hyalangium minutum*. Their structures were determined by 2D NMR and HR-MS/MS experiments and their stereochemical configuration was established by a combination of NMR data, quantum mechanical calculations, and circular dichroism experiments. Hyalachelins are unusual catecholate-type siderophores that bear an 3,7,8-trihydroxy-1-oxo-1,2,3,4-tetrahydroisoquinoline-3-carboxylic acid. Their iron chelating activities were evaluated in a CAS assay showing EC_{50} values of around 30 μM.

3.2. Main Text

Most bacteria require iron for growth. In response to iron limitation which is caused by low solubility of Fe^{+3} at physiological pH, bacteria produce and secrete iron chelating small molecules, termed siderophores. The siderophore-iron complex exhibits improved solubility and enables the transport of ferric iron into the cell through outer-membrane receptor proteins.[1,2] To date only two different structural classes of siderophores, the catecholates myxochelin A and B,[3,4] and the citrate-hydroxamates nannochelins,[5] have been reported from myxobacteria.

Over the course of our research aimed at the discovery of new bioactive natural products from myxobacteria by using NMR and MS profiling,[6] our attention was drawn to screen novel and unexplored strains, which led to the isolation of new structural varieties.[7,8] Strain MCy9135 was isolated from a soil sample collected in Xiamen, China and it is phenotypically and phylogenetically related to the unexplored species *Hyalangium minutum* by 16S rDNA analysis. An ethyl acetate extract of the strain MCy9135 was analyzed by LC-MS and LC-NMR and revealed the presence of four different classes of natural products, including three new catecholate siderophores, termed hyalachelins A-C (**1-3**), together with the known tartrolon D[9], myxochelin B[4], and hyafurones[10].

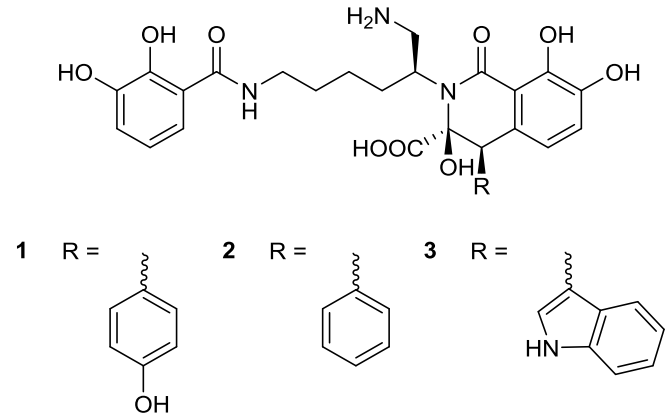

Figure 3.1. Hyalachelins A-C (**1**-**3**)

Hyalachelin A (**1**) was isolated as colorless amorphous solid. Its molecular formula was determined to be $C_{29}H_{32}N_3O_{10}$, based on a molecular ion at *m/z* 582.2074 $[M+H]^+$observed in HR-ESI-MS (calculated 582.2088, Δppm 2.4), requiring 16 degrees of unsaturation. The ^{1}H NMR spectrum of **1** in CD_3OD (see Table 3.1) exhibited aromatic proton signals including two doublets at δ 7.17 (2H, d, J = 8.5 Hz) and 6.72 (2H, d, J = 8.5 Hz) corresponding to a *para*-substituted aromatic ring and a pair of doublets at δ 6.80 (1H, d, J = 8.2 Hz) and 6.12 (1H, d, J = 8.2 Hz), characteristic of tetrasubstituted benzene ring. Moreover, a set of signals comprising two doublets at δ 7.17 (1H, d, J = 8.0 Hz), 6.90 (1H, dd, J = 8.0, 1.0 Hz), and a triplet at δ 6.68 (1H, t, J = 8.0 Hz) was observed and suggested presence of 1,2,3-trisubstituted benzene ring. Examination of the HSQC spectrum revealed the presence of two methines ($\delta_{C\text{-}4}$ 52.2, $\delta_{H\text{-}4}$ 4.70; $\delta_{C\text{-}2'}$ 59.6, $\delta_{H\text{-}2'}$ 3.51) and two aminomethylenes ($\delta_{C\text{-}1'}$ 41.3, $\delta_{H\text{-}1'}$ 3.87, 3.13; $\delta_{C\text{-}6'}$ 40.1, $\delta_{H\text{-}6'}$ 3.36, 3.31).

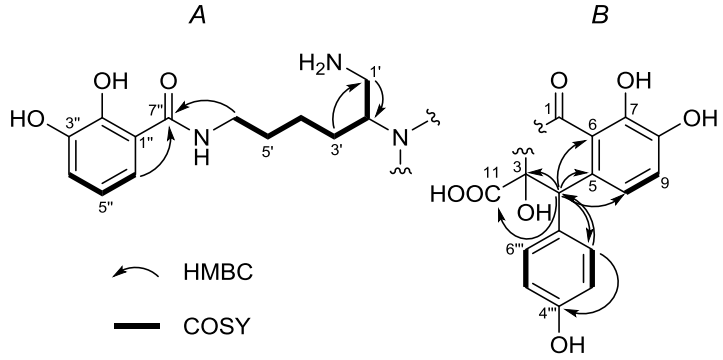

Figure 3.2 Selected key HMBC and COSY correlations for fragment A and B of hyalachelin A (**1**)

Analysis of TOCSY and COSY cross peaks yielded four spin systems, three of which comprise aromatic protons. HMBC and HSQC correlations together with splitting patterns of the aromatic protons at δ 6.12-7.17 were indicative of two 2,3-dihydroxybenzoyl moieties (DHB-1 and DHB-2, respectively) and a phenol moiety. Finally, the last spin system comprising protons H-1' to H-6' was

deduced as a hexane-1,2,6-triamine moiety. A long-range correlation from the proton at δ 3.36 (H-6'a) to the carbonyl resonance at δ 171.2 linked the triamine moiety to DHB-1 forming the partial structure A (see Figure 3.2). Partial structure B was assembled on the basis of HMBC correlations. In particular, key correlations from the methine proton H-4 to the aromatic carbons at δ 132.1 (C-5), 113.0 (C-6), 118.4 (C-10), and 133.4 (C-2''') connected DHB-2 to the phenol residue via the methine at C-4. ROESY correlations from H-10 to H-4 and H-2''' supported this connectivity (see Figure 3.3). Further HMBC correlations from H-4 to the carbon resonances at δ 94.3 (C-3) and 175.2 (C-11), attached C-4 to the α-hydroxy acid at C-3, completing the partial fragment B as depicted in Figure 3.3.

Inspection of the partial fragments A and B revealed that together they contained 15 of the required 16 degrees of unsaturation indicating that linkage between fragments A and B involved formation of a ring to satisfy the unsaturation index and the molecular formula. HMBC correlations from H-2' to the carbon resonances at δ 172.3 (C-1) and 94.3 (C-3) linked fragments A and B, which form a six-membered ring containing both an amide and a hemiaminal functional group. Therefore, the structure of **1** was established as a linear catecholate siderophore that contains a hexasubstituted tetrahydroisoquinoline ring linked to a phenol moiety at position 4.

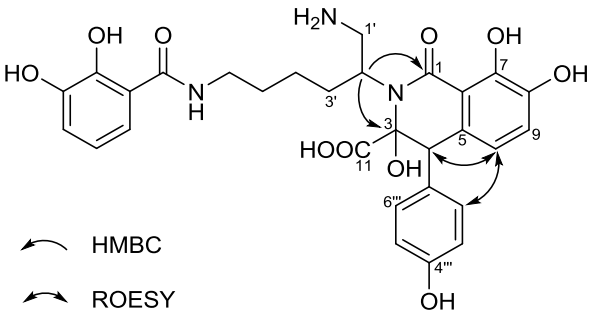

Figure 3.3 Key HMBC correlations used to link two fragments and ROESY correlations.

Tandem mass spectrometry provided further evidence to support the structure of **1**. The MS^2 fragmentation of the major ion peak at *m/z* 582 $[M+H]^+$ displayed an intense ion at *m/z* 564 $[M+H-H_2O]^+$. MS of the daughter ion peak displayed a predominant fragment at *m/z* 503 $[M+H-H_2O-44-17]^+$ corresponding to loss of CO_2 and NH_2. Finally, MS^4 fragmentation of this ion peak produced a fragment ion at *m/z* 367 $[M+H-H_2O-44-17-136]^+$ corresponding to the loss of a DHB residue along with an ion peak at *m/z* 270 $[M+H-H_2O-44-17-233]^+$ corresponding to the loss of fragment A (see Figure S3.1). Thus, the MS^n fragmentation patterns were in complete agreement with the structure of **1** as determined by NMR.

Table 3.1 NMR spectroscopic data for hyalachelin A (1) in CD_3OD

pos	δ_H[a], mult (*J* in Hz)	δ_C[b]	HMBC[c]
1		172.3	
2			
3		94.3	
4	4.70, s	52.2	3, 5, 6, 10, 11, 1'", 2'"
5		132.1	
6		113.0	
7		150.6	
8		145.3	
9	6.80, d (8.2)	120.1	5, 7, 8
10	6.12, d (8.2)	118.4	1, 4, 6, 7, 8
11		175.2	
1'a	3.87, t (11.7)	41.3	2'
1'b	3.13, dd (12.5, 3.3)		
2'	3.51, m	59.6	1, 3, 1', 3', 4'
3'a	2.16, m	31.5	1', 2', 4', 5'
3'b	2.03, m		2', 4'
4'a	1.41, m	25.1	2', 3', 6'
4'b	1.36, m		
5'	1.60, m	30.0	3', 4', 6'
6'a	3.36, m	40.1	4', 5', 7"
6'b	3.31, m		
1"		116.5	
2"		150.1	
3"		147.0	
4"	6.90, dd (8.0, 1.0)	119.3	2", 3", 6"
5"	6.68, t (8.0)	119.3	1", 3", 6"
6"	7.17, d (8.0)	118.4	1", 2", 4", 5", 7"
7"		171.2	
1'"		128.4	
2'", 6'"	7.17, d (8.5)	133.4	4, 1'", 4"
3'", 5'"	6.72, d (8.5)	115.6	1'", 4'"
4'"		157.8	

[a]Recorded at 700 MHz, referenced to residual CD_3OD at δ 3.31 ppm; [b]recorded at 175 MHz, referenced to residual CD_3OD at δ 49.15 ppm; [c]proton showing HMBC correlation to indicated carbon

HR-ESI-MS analysis of hyalachelin B (**2**) showed a molecular ion peak at *m/z* 566.2127 $[M+H]^+$ appropriate for a molecular formula of $C_{29}H_{32}N_3O_9$ (calculated 566.2139, Δppm 2.12), which is 16 mass units lower than that of **1**. The 2D NMR data for **2** closely resembled those of **1** with the

exception that resonances belonging to the phenol of **1** were replaced by resonances belonging to a phenyl group in **2**.

Hyalachelin C (**3**) showed a molecular ion peak at 605.2235 $[M+H]^+$ observed in HR-ESI-MS (calculated 605.2248, Δppm 2.15), which corresponded to a molecular formula of $C_{31}H_{33}N_4O_9$. ^1H NMR spectrum exhibited significant differences on the downfield region in comparison to that of **1**, displaying proton signals consistent with the presence of an indole ring. On the basis of the 2D NMR data **3** was identified as the indole-derivative of **1**.

Due to the lack of possible diagnostic ROE effects in the cyclic and flexible portions of the molecule, the relative configuration of representative hyalachelin B (**2**) was assigned by quantum mechanical calculations of ^{13}C and ^1H NMR chemical shifts.[11,12] By using Monte-Carlo Molecular Mechanics (MCMM) and Molecular Dynamics (MD) simulations, an extensive conformational search at the empirical level was performed for each of the four possible relative stereoisomers (see Figure S3.3), termed **2a** (2'*S**,3*R**,4*R**), **2b** (2'*S**,3*S**,4*R**), **2c** (2'*S**,3*R**,4*S**), and **2d** (2'*S**,3*S**,4*S**). All the non-redundant conformers were subsequently geometry and energy optimized at the density functional level (DFT) using the MPW1PW91 functional and 6-31G(d) basis set and using IEFPCM for simulating the DMSO solvent (Gaussian 09 software package).[13] On the previously optimized geometries of all four possible relative stereoisomers (**2a-d**), we performed quantum mechanical calculations of ^{13}C and ^1H NMR chemical shifts (see Table S3.5 and Table S3.6) and compared them to the experimental data in order to have indications on the relative configuration of **2**. The mean absolute error (MAE) value was used to impartially compare calculated and experimental ^1H and ^{13}C NMR chemical shifts (see Figure 3.4). Indeed, isomer **2b** displayed the lowest MAE values (^{13}C MAE = 2.35 ppm, ^1H MAE = 0.15 ppm) suggesting that the relative configuration of **2** is 2'*S**,3*S**,4*R**. To further confirm this result, a comparison of the calculated and experimental $^2J_{C\text{-}H}$ heteronuclear coupling constant for C-3 and H-4 was considered. It is worth mentioning that no other significant experimental coupling constants and/or dipolar effects were observed for the tetrahydroisoquinolinic ring. A $^2J_{C3\text{-}H4}$ value of -5.8 Hz was obtained from a *J*-resolved HMBC[14] spectrum, which was in good accordance with the -4.3 Hz calculated value of **2b**. On the other hand, the experimental $^2J_{C3\text{-}H4}$ value significantly differed with respect to the calculated values for the remaining stereoisomers (-8.7 Hz for 2a, -2.8 Hz for 2c, and -8.9 Hz for 2d, see Figure S3.4 and Table S3.7).

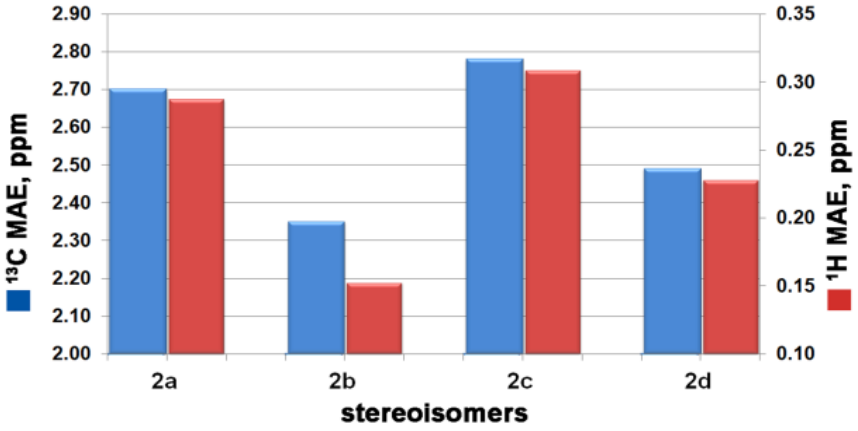

Figure 3.4 Mean absolute errors (MAE) histograms obtained by comparison of the ^{13}C (blue bars) and ^{1}H (red bars) chemical shifts for stereoisomers **2a**, **2b**, **2c** and **2d** with the experimental data. MAE=$\Sigma[|(\delta_{exp}-\delta_{calcd})|]/n$, summation through n of the absolute error values (difference of the absolute values between corresponding experimental and ^{13}C, ^{1}H chemical shifts), normalized to the number of the chemical shifts considered. The lowest MAE is reflected by the **2b** relative stereoisomer.

Finally, the absolute configuration of **2** was analyzed by comparing the calculated and experimental circular dichroism (CD) spectra of the two possible enantiomers, 2'*S*,3*S*,4*R* and 2'*R*,3*R*,4*S*.[15,16] Starting from the previously obtained conformation of **2b**, a new optimization of the geometries was performed at DFT level using the IEFPCM methanol model. Boltzmann-weighted CD spectrum was calculated for 2'*S*,3*S*,4*R*, and its enantiomer 2'*R*,3*R*,4*S*. As shown in Figure 3.5, the experimental curve closely fits with that of 2'*S*,3*S*,4*R*, thereby suggesting the absolute configuration of **2**. CD spectra were also calculated for all the other six possible stereoisomers. None of them showed significant similarity to the experimental spectrum (see Figure S3.5).

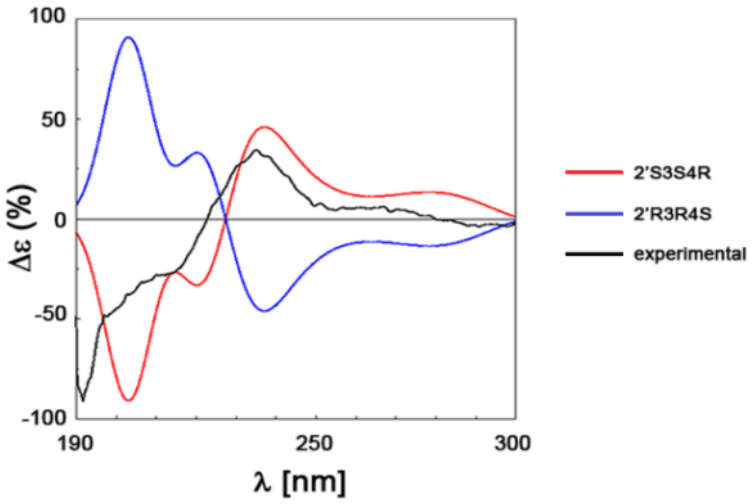

Figure 3.5 Comparison of experimental CD spectrum and 2'*S*,3*S*,4*R* and 2'*R*,3*R*,4*S* CD calculated spectra.

Furthermore, hyalachelin B skeleton shows slight similarities to the known myxobacterial-derived myxochelins. These catechol-type siderophores are biosynthetically derived from L-lysine and show an *S* configuration.[17] Interestingly, our results point out an *S* configuration at C-2', additionally supporting our analysis. The relative configurations of **2** and **3** were assumed identical to those of **1** because their structures and NMR data are very similar. Formally, the hyalachelins might be derived from myxochelins by addition of phenylalanine, tyrosine or tryptophan, respectively. How exactly this intriguing biosynthesis is achieved is currently under investigation in our laboratory.

The structural features of hyalachelins suggested that these natural products may possess iron chelating properties. Indeed, compounds **1-3** showed iron chelating activity in a liquid chrome azurol S (CAS)[18] assay with EC_{50} values approximately 5-fold higher than those of myxochelin and deferoxamine (see Table 3.2).

It has been shown that available iron in the growth medium affects the production of siderophore secondary metabolites.[19] Cultivation of strain MCy9135 in growth medium containing Fe-EDTA (20 µM) resulted in the loss of the production of compounds **1-3** (see Figure S3.2). This result demonstrates that hyalachelins are most likely biologically relevant siderophores of *H.minutum.*

Table 3.2 Iron chelating activities (EC_{50}) of 1-3 and positive controls

siderophore	EC_{50} [µM]
1	39.4± 4.29
2	28.1 ± 7.32
3	30.1 ± 0.29
myxochelin B	4.6 ± 2.18
deferoxamine mesylate	6.7 ± 0.78

Representative compound **3** was tested against *Staphylococcus aureus* and *Bacillus subtilis* on the basis of the slight structural similarities to myxochelins.[3] However, no inhibition was observed up to concentrations of 64 µg/mL. Besides, cytotoxic activity of **3** was evaluated toward HCT-116 and CHO-K1 cell lines resulting in IC_{50} values of 29.2 and 82.7 µM, respectively.

In summary, hyalachelins are a new class of catecholate siderophores that contain an unusual isoquinoline ring bearing an oxo group at C-1 and α-hydroxy acid at C-3. To our knowledge this is the first report of an 3,7,8-trihydroxy-1-oxo-1,2,3,4-tetrahydroisoquinoline-3-carboxylic acid residue present in a natural product. The relative and absolute configuration of **2** was elucidated by means of quantum mechanical calculations of NMR and CD parameters in comparison to experimental data.

The discovery of this new suite of secondary metabolites reconfirms the notion that unexplored myxobacteria are a promising source of new scaffolds. It also highlights the abundant biosynthetic capabilities of these gram-negative microorganisms.

3.3. References

[1] Sandy, M.; Butler, A. *Chem. Rev.* **2009,** *109*, 4580-4595.

[2] Kong, X.; Hider, R. C. *Nat. Prod. Rep.* **2010,** *27*, 637-657.

[3] Kunze, B.; Bedorf, N.; Kohl, W.; Höfle, G.; Reichenbach, H. *J. Antibiot.* **1989,** *42*, 14-17.

[4] Silakowski, B.; Kunze, B.; Nordsiek, G.; Blöcker, H.; Höfle, G.; Müller, R. *Eur. J. Biochem.* **2000,** *267*, 6476-6485.

[5] Kunze, B.; Trowitzsch-Kienast, W.; Höfle, G.; Reichenbach, H. *J. Antibiot.* **1992,** *45*, 147-150.

[6] Plaza, A.; Müller, R. In *Natural Products: Discourse, Diversity, and Design;* Osbourn, A., Goss, R., Carter, G.T., Eds.; John Wiley & Sons: 2014; Chapter 6, 103-124.

[7] Plaza, A.; Viehrig, K.; Garcia, R.; Müller, R. *Organic Letters* **2013,** *15*, 5882-5885.

[8] Plaza, A.; Garcia, R.; Bifulco, G.; Martinez, J. P.; Hüttel, S.; Sasse, F.; Meyerhans, A.; Stadler, M.; Müller, R. *Organic Letters* **2012,** *14*, 2854-2857.

[9] Perez, M.; Crespo, C.; Schleissner, C.; Rodriguez, P.; Zuniga, P.; Reyes, F. *J. Nat. Prod.* **2009,** *72*, 2192-2194.

[10] Okanya, P. W.; Mohr, K. I.; Gerth, K.; Kessler, W.; Jansen, R.; Stadler, M.; Müller, R. *J. Nat. Prod.* **2014,** *77*, 1420-1429.

[11] Cimino, P.; Duca, D.; Gomez-Paloma, L.; Riccio, R.; Bifulco, G. *Magn. Reson. Chem.* **2004**, *42*, S26–S33.

[12] Bifulco, G.; Dambruoso, P.; Gomez-Paloma, L.; Riccio, R. *Chem. Rev.* **2007**, *107*, 3744–3779. b) Bagno, A.; Rastrelli, F.; Saielli, G. *Chem. Eur. J.* **2006**, *12*, 5514–5525.

[13] Gaussian 09, Revision **D.01**, Frisch, M. J.; Trucks, G. W.; Schlegel, H. B.; Scuseria, G. E.; Robb, M. A.; Cheeseman, J. R.; Scalmani, G.; Barone, V.; Mennucci, B.; Petersson, G. A.; Nakatsuji, H.; Caricato, M.; Li, X.; Hratchian, H. P.; Izmaylov, A. F.; Bloino, J.; Zheng, G.; Sonnenberg, J. L.; Hada, M.; Ehara, M.; Toyota, K.; Fukuda, R.; Hasegawa, J.; Ishida, M.; Nakajima, T.; Honda, Y.; Kitao, O.; Nakai, H.; Vreven, T.; Montgomery, J. A., Jr.; Peralta, J. E.; Ogliaro, F.; Bearpark, M.; Heyd, J. J.; Brothers, E.; Kudin, K. N.; Staroverov, V. N.; Kobayashi, R.; Normand, J.; Raghavachari, K.; Rendell, A.; Burant, J. C.; Iyengar, S. S.; Tomasi, J.; Cossi, M.; Rega, N.; Millam, N. J.; Klene, M.; Knox, J. E.; Cross, J. B.; Bakken, V.; Adamo, C.; Jaramillo, J.; Gomperts, R.; Stratmann, R. E.; Yazyev, O.; Austin, A. J.; Cammi, R.; Pomelli, C.; Ochterski, J. W.; Martin, R. L.; Morokuma, K.; Zakrzewski, V. G.; Voth, G. A.; Salvador, P.; Dannenberg, J. J.; Dapprich, S.; Daniels, A. D.; Farkas, Ö.; Foresman, J. B.; Ortiz, J. V.; Cioslowski, J.; Fox, D. J. Gaussian, Inc., Wallingford CT, 2009.

[14] Meissner, A.; Soerensen, O. W. *Magn. Reson. Chem*. **2001**, *39*, 49-52.

[15] Bringmann, G.; Bruhn, T.; Maksimenka, K.; Hemberger, Y. *Eur. J. Org. Chem.* **2009**, *17*, 2717–2727.

[16] Masullo, M.; Bassarello, C.; Bifulco, G.; Piacente, S. *Tetrahedron* **2010**, *66*, 139-145.

[17] Miyanaga, S.; Obata, T.; Onaka, H.; Fujita, T.; Saito, N.; Sakurai, H.; Saiki, I.; Furumai, T.; Igarashi, Y. *J. Antibiot.* **2006,** *59*, 698-703.

[18] Schwyn, B.; Neilands, J. B. *Analytical Biochemistry* **1987,** *160*, 47-56.

[19] Metal Ions in Biological Systems: Iron Transport and Storage in Microorganisms, Plants, and Animals; Sigel, A., Sigel, H., Eds.; Dekker: New York, 1998.

3.4. Supporting Informations

3.4.1. General Experimental Procedures

Optical rotations were measured at Jasco polarimeter, IR spectra were obtained on Perkin-Elmer FT-IR Spectrum One spectrometer and UV spectra were recorded on an Agilent 8453 spectrophotometer. NMR spectra were acquired on a Bruker Ascend 500 MHz and 700 MHz spectrometers equipped with a 5 mm TXI cryoprobe in CD_3OD and DMSO-d_6 deuterated solvents. HSQC, HMBC, COSY, TOCSY and ROESY spectra were recorded using standard pulse programs. LC-HRMS data were obtained on a maXis 4G mass spectrometer (Bruker Daltonics, Germany) coupled with Dionex Ultimate 3000 RSLC system, using a BEH C18, 100 x 2.1 mm, 1.7 mm d_p column (Waters, Germany) with linear gradient of 5-95% MeCN + 0.1% FA in H_2O + 0.1% FA at 600 µL/min in 18 min with UV detection in 200-600 nm range. Mass spectra were acquired using the ESI source in the range from 150‑2000 m/z at 2 Hz scan speed. CD spectrum was recorded on a Jasco J-1500 CD spectrometer.

3.4.2. Isolation and Cultivation of Strain

Hyalangium minutum strain MCy9135 was isolated in May 2008 from a gift soil sample collected in China. The strain appears on standard isolation set-up for myxobacteria by bacterial baiting method. Series of subcultivations of sample taken from the colony edge led to the isolation of the strain. Growth maintenance is performed by cultivation of the strain in MD1G liquid medium and by plating on buffered yeast agar.[1] Identification of the strain was performed by morphology characterization of different growth stages and by 16S rDNA molecular-phylogenetic analysis. Strain MCy9135 shows characteristic features of type strain *Hyalangium minutum* NOCB-2^T and was determined to be in the same cluster with 99.3% similarity suggesting that they belong to same species. The strain was cultivated in MD1G medium (3 g/L casitone, 0.7 g/L $CaCl_2$ x $2H_2O$, 2 g/L $MgSO_4$ x $7H_20$ and 5 g/L soluble starch) for up-scaled fermentation at 30^0C on rotary shaker at 180 rpm for 10d after 4% v/v preculture inoculation.

3.4.3. Isolation of Hyalachelins

XAD and cell mass were harvested by centrifugation, lyophilized and subsequently defatted by 300 ml n-hexane which was followed by extraction with water/acetone 1:1 (v/v, three portions of 500 ml mixture). The combined extracts were evaporated to yield 2 g of crude extract. A solvent-solvent partition was further performed between n-butanol and water and the collected butanol layer was then evaporated to obtain 1.7g crude butanol extract. This was further suspended in water/acetone 1:1 (v/v), centrifuged and fractionated by preparative HPLC using Waters AutoPurification system equipped with XBridge Prep 19 x 150 mm, 5 µm d_p C18 column. Linear gradient initiated with 10% solvent B (MeCN + 0.1% FA) in solvent A (H_2O + 0.1% FA) and increased to 45% B in 19 min with

25ml/min flow rate. The automatically collected fractions of interest were dried in Genevac EZ-2 evaporator and subsequently subjected to semi-preparative HPLC Agilent system for final purification on Jupiter Proteo 90Å, 10 x 250 mm, 4 µm d_p C12 column. Separation was achieved utilizing same eluents as preparative HPLC with linear gradient started with 30% B and increased to 40% B over 20 min with 2.5 ml/min at 30^0C to afford pure compound **1** (t_R = 8.4 min), **2** (t_R = 12.9 min) and **3** (t_R = 13.3 min).

3.4.4. CAS Assay

Iron chelating activity of hyalachelins was evaluated by chrome-azurol S (CAS) assay. The CAS assay solution was prepared as previously described.[2] For CAS assay, 50 µl of freshly prepared assay solution was added into 96 well plate. Stock solutions (1 mM) of compound **1**-**3** were prepared in 20% MeOH in water and considered amount of which was added into CAS solution. Millipore water was filled up to total assay volume of 100 µL that contain test compounds in 0, 2, 4, 8, 15, 30, 60, 125, 200 and 250 µM final concentrations. UV-vis absorbance was measured at the PHERAstar FS microplate reader (BMG labtech) at 630 nm every 5 minutes for 30 minutes in total. Iron chelating activity was determined as EC_{50} value which is the concentration of compound that reduces the absorbance of CAS solution by 50% at 630 nm. EC_{50} value calculations were performed by OriginPro 8.5G software. CAS assays for myxochelin B and deferoxamine mesylate have been done simultaneously in 0, 1, 2, 4, 8, 15, 20, 30 and 50 µM final concentrations.

Hyalachelin A (1): colorless amorphous solid, $[\alpha]^{20}_D$ + 35.9 (*c* 0.06, MeOH), IR (film) ν_{max} 3356, 2921, 1595, 1445, 1381, 1261, 1023 cm^{-1}, UV (ACN) λ_{max} 206, 256, 320 nm, ^{1}H and ^{13}C NMR data see Table S3.1, HR-ESI-MS *m/z* 582.2074 $[M+H]^+$ (calcd for $C_{29}H_{32}N_3O_{10}$, 582.2088)

Hyalachelin B (2): colorless amorphous solid, $[\alpha]^{20}_D$ + 16.5 (*c* 0.12, MeOH), IR (film) ν_{max} 3281, 2970, 1738, 1598, 1445, 1365, 1217 cm^{-1}, UV (ACN) λ_{max} 208, 256, 320 nm, ^{1}H and ^{13}C NMR data see Table S3.2 and S3.3, HR-ESI-MS *m/z* 566.2127 $[M+H]^+$ (calcd for $C_{29}H_{32}N_3O_9$, 566.2139)

Hyalachelin C (3): colorless amorphous solid, $[\alpha]^{20}_D$ + 14.4 (*c* 0.06, MeOH), IR (film) ν_{max} 3344, 2941, 1737, 1595, 1456, 1368, 1227, 1046 cm^{-1}, UV (ACN) λ_{max} 224, 256, 320 nm, ^{1}H and ^{13}C NMR data see Table S3.4, HR-ESI-MS *m/z* 605.2235 $[M+H]^+$ (calcd for $C_{31}H_{33}N_4O_9$, 605.2248)

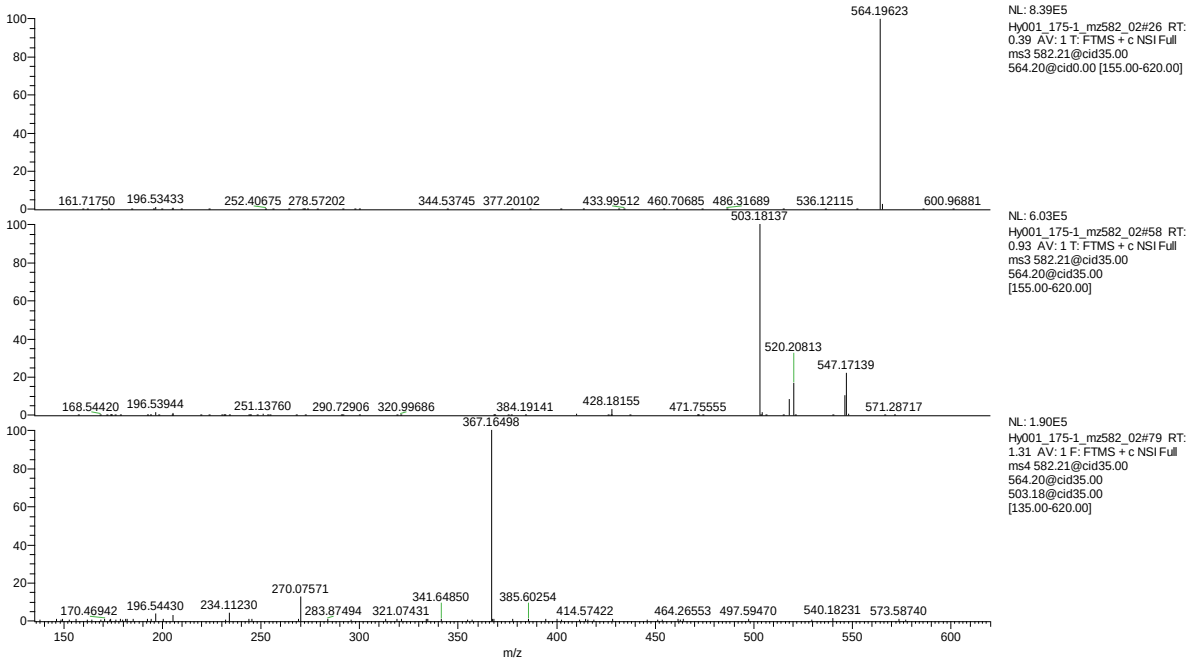

Figure S3.1 MSn fragmentation data of hyalachelin A (**1**)

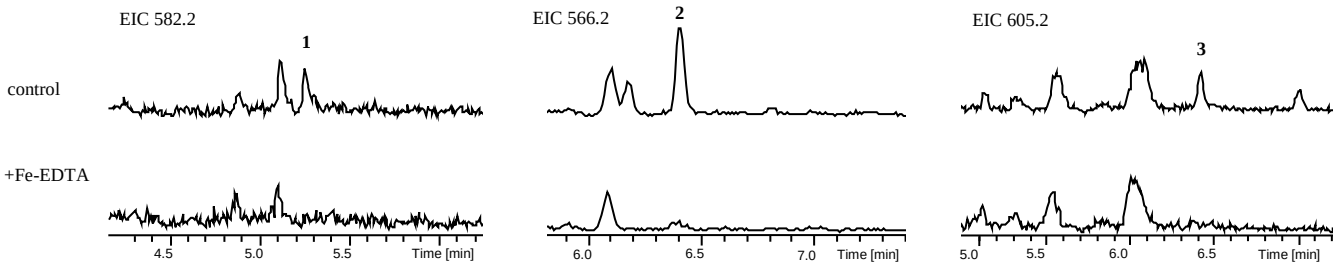

Figure S3.2 LC-MS extracted ion chromatograms (EIC) of hyalachelins A-C (**1**-**3**) in crude extract of MCy9135 cultivated in MD1G medium with presence of 20 µM Fe-EDTA (bottom) in comparison with culture without additional iron as control (top).

Table S3.1 NMR data of hyalachelin A (1) in CD_3OD

pos	δ_H[a], mult (*J* in Hz)	δ_C[b]	HMBC[c]	COSY[d]	ROESY[e]
1		172.3			
2					
3		94.3			
4	4.70, s	52.2	3, 5, 6, 10, 11, 1'", 2'", 6'"		10, 2'", 6'"
5		132.1			
6		113.0			
7		150.6			
8		145.3			
9	6.80, d (8.2)	120.1	5, 7, 8	10	
10	6.12, d (8.2)	118.4	1, 4, 6, 7, 8	9	4
11		175.2			
1'a	3.87, t (11.7)	41.3	2'	1'b, 2'	
1'b	3.13, dd (12.5, 3.3)			1'a, 2'	
2'	3.51, m	59.6	1, 3, 1', 3', 4'	1'a, 1'b, 3'a, 3'b	
3'a	2.16, m	31.5	1', 2', 4', 5'	2', 3'b, 4'	
3'b	2.03, m		2', 4'	2', 3'a, 4'	
4'a	1.41, m	25.1	2', 3', 6'	3'a, 3'b, 4'b, 5'	
4'b	1.36, m			3'a, 4'a	
5'	1.60, m	30.0	3', 4', 6'	4'a, 4'b, 6'a, 6'b	
6'a	3.36, m	40.1	4', 5', 7"	5'	
6'b	3.31, m			5'	
1"		116.5			
2"		150.1			
3"		147.0			
4"	6.90, dd (8.0, 1.0)	119.3	2", 3", 6"	5"	
5"	6.68, t (8.0)	119.3	1", 3", 6"	4", 6"	
6"	7.17, d (8.0)	118.4	1", 2", 4", 5", 7"	5"	
7"		171.2			
1'"		128.4			
2'", 6'"	7.17, d (8.5)	133.4	4, 1'", 4"	3'", 5'"	10
3'", 5'"	6.72, d (8.5)	115.6	1'", 4'"	2'", 6'"	
4'"		157.8			

[a]recorded at 700 MHz, referenced to residual CD_3OD at δ 3.31 ppm
[b]recorded at 175 MHz, referenced to residual CD_3OD at δ 49.15 ppm
[c]proton showing HMBC correlation to indicated carbon
[d]proton showing COSY correlation to indicated proton
[e]proton showing ROESY correlation to indicated proton

Table S3.2 NMR data of hyalachelin B (2) in CD_3OD

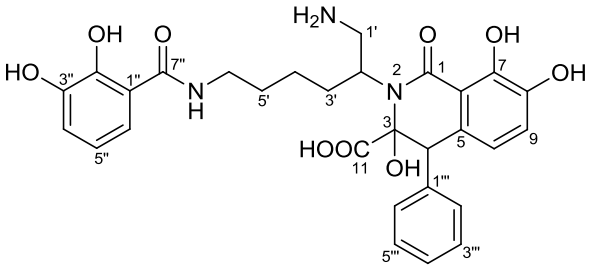

pos	δ_H[a], mult (*J* in Hz)	δ_C[b]
1		172.5
2		
3		94.2
4	4.79, s	53.0
5		131.6
6		113.0
7		150.7
8		145.5
9	6.80, d (8.2)	120.1
10	6.07, d (8.2)	118.4
11		175.2
1'a	3.88, t (11.7)	41.4
1'b	3.14, dd (12.5, 3.3)	
2'	3.53, m	59.4
3'a	2.16, m	31.5
3'b	2.03, m	
4'a	1.40, m	25.2
4'b	1.36, m	
5'	1.60, m	29.9
6'a	3.34, m	40.0
6'b	3.31, m	
1"		116.5
2"		150.3
3"		147.2
4"	6.90, dd (8.0, 1.0)	119.0
5"	6.68, t (8.0)	119.3
6"	7.17, d (8.0)	118.4
7"		171.4
1'''		138.1
2''', 6'''	7.36, d (8.5)	132.4
3''', 5'''	7.28[c]	128.5
4'''	7.29[c]	128.8

[a]recorded at 700 MHz, referenced to residual CD_3OD at δ 3.31 ppm
[b]recorded at 175 MHz, referenced to residual CD_3OD at δ 49.15 ppm
[c]overlapping signals

Table S3.3 NMR data of hyalachelin B (2) in DMSO-d_6

pos	δ_H[a], mult (*J* in Hz)	δ_C[b]	HMBC[e]	COSY[f]
1		[c]		
2				
3		91.8		
4	4.71, s	50.7	3, 6, 5, 1‴, 2‴	
5		130.5		
6		111.8		
7		149.0		
8		143.8		
9	6.76, d (8.2)	118.8	5, 7, 8	10
10	5.84, d (8.2)	116.1	4, 6, 8	9
11		[c]		
1'a	3.58, t (11.2)	39.0		1'b, 2'
1'b	2.97, dd (11.2, 4.1)			1'a, 2'
2'	3.42, m	57.6		1'a, 1'b, 3'
3'	1.92, m	29.7	4'	**2'**, 4'
4'	1.26, m	23.7	2', 3', 6'	3', 5'
5'	1.41, m	29.1	4', 6'	4', 6'
6'	3.17, m	37.7	4', 5'	5'
1"		[c]		
2"		[c]		
3"		[c]		
4"	[c]	[c]		
5"	[c]	[c]		
6"	7.08, d (7.7)	118.1		
7"		168.6		
1‴		137.4		
2‴, 6‴	7.25[d]	130.8	4, 1‴	
3‴, 5‴	7.26[d]	127.1	1‴	
4‴	7.23[d]	126.6	2‴, 3‴	

[a]recorded at 700 MHz, referenced to residual DMSO-d_6 at δ 2.50 ppm
[b]recorded at 175 MHz, referenced to residual DMSO-d_6 at δ 39.51 ppm
[c]not observed
[d]overlapping signals
[e]proton showing HMBC correlation to indicated carbon
[f]proton showing COSY correlation to indicated proton

Table S3.4 NMR data of hyalachelin C (3) in CD_3OD

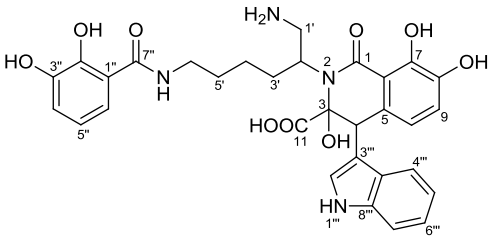

pos	δ_H[a], mult (*J* in Hz)	δ_C[b]
1		172.6
2		
3		95.4
4	5.14, s	45.3
5		131.8
6		112.7
7		150.2
8		145.2
9	6.75, d (8.2)	120.2
10	6.17, d (8.2)	118.5
11		175.7
1'a	3.87, t (11.7)	41.3
1'b	3.14, dd (12.5, 3.3)	
2'	3.52, m	59.8
3'a	2.21, m	31.4
3'b	2.06, m	
4'a	1.42, m	25.2
4'b	1.36, m	
5'	1.60, m	30.0
6'a	3.36, m	40.0
6'b	3.31, m	
1"		116.7
2"		150.3
3"		147.4
4"	6.90[c]	119.3
5"	6.68, t (8.0)	119.3
6"	7.17, d (8.0)	118.5
7"		171.4
1'''		
2'''	7.19, s	126.7
3'''		110.8
4'''	7.48, d (8.0)	121.6
5'''	6.90[c]	119.3
6'''	7.05, t (7.6)	122.0
7'''	7.33, d (8.0)	112.0
8'''		138.0
9'''		129.0

[a]recorded at 700 MHz, referenced to residual CD_3OD at δ 3.31 ppm
[b]recorded at 175 MHz, referenced to residual CD_3OD at δ 49.15 ppm
[c]overlapping signals

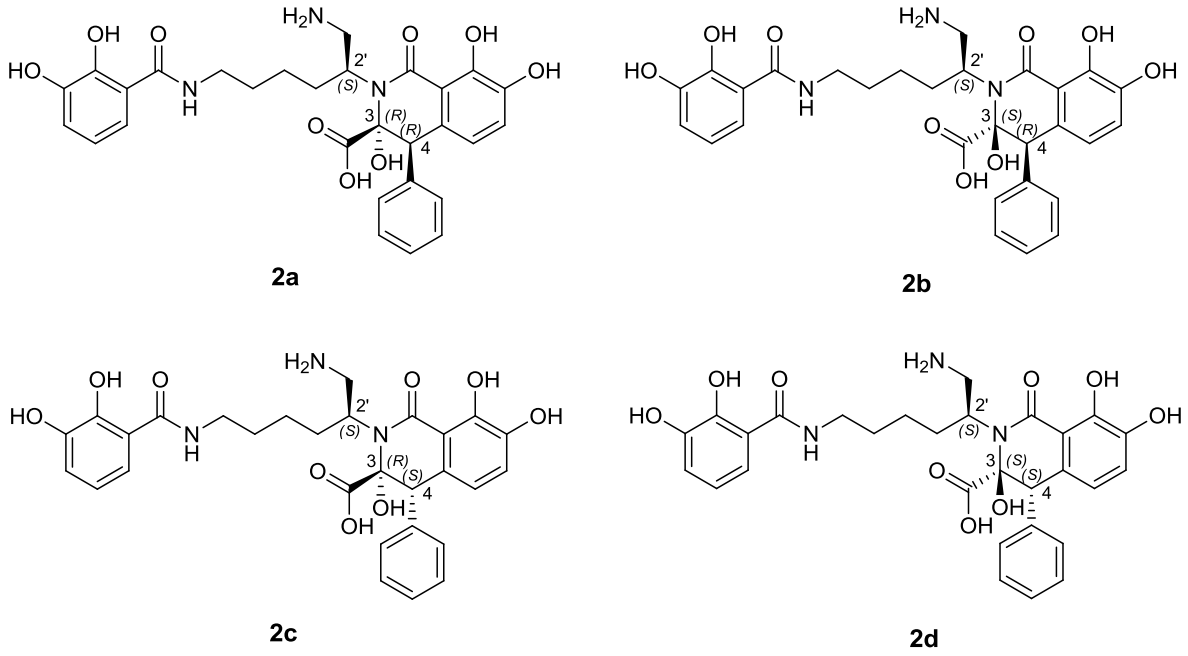

Figure S3.3 The four relative stereoisomers **2a, 2b, 2c** and **2d** of hyalachelin B (**2**)

3.4.5. Computational Details

Chemical structures of the four possible relative stereoisomers of **2**: **2a** (2'*S**,3*R**,4*R**), **2b** (2'*S**,3*S**,4*R**), **2c** (2'*S**,3*R**,4*S**), and **2d** (2'*S**,3*S**,4*S**) (see Figure S3.3) were built using Maestro 9.6[3] and optimized through the MacroModel 10.2[4] software package, using the OPLS force field and the Polak-Ribier conjugate gradient algorithm (PRCG, maximum derivative less than 0.001 kcal/mol). Starting from the obtained 3D structures, exhaustive conformational searches were performed at the empirical molecular mechanics (MM) level following the subsequent scheme:

a) Monte Carlo Multiple Minimum (MCMM) method (50,000 steps) of the MacroModel 10.2 package was used in order to allow a full exploration of the conformational space;

b) Low mode Conformational Search (LMCS) method (50,000 steps) as implemented in MacroModel 10.2 software was used to integrate the conformational sampling.

For each stereoisomer, all the obtained conformers were then minimized (PRCG, maximum derivative less than 0.001 kcal/mol) and compared. The selection of non-redundant conformers was performed using the "Redundant Conformer Elimination" module of Macromodel 10.2, choosing a 1.0 Å RMSD (root-mean-square deviation) minimum cutoff for saving structures and excluding the conformers differing more than 13.0 kJ/mol (3.11 kcal/mol) from the most energetically favored conformation. In this way, we obtained 17 conformers for **2a**, 10 for **2b**, 11 for **2c**, and 19 for **2d**.

Next, the obtained conformations of **2a**, **2b**, **2c**, **2d** were optimized at quantum mechanical (QM) level by using the MPW1PW91 functional and the 6-31G(d) basis set. Experimental solvent effects (DMSO) were reproduced using the integral equation formalism version of the polarizable continuum model (IEFPCM). On the obtained geometries, the MPW1PW91 functional and the 6-31G(d,p) basis set and IEFPCM were used for calculating the ^{1}H and ^{13}C chemical shifts. The final ^{13}C and ^{1}H NMR spectra for each of the investigated stereoisomers were built considering the influence of each conformer on the total Boltzmann distribution taking into account the relative energies. Calibration of calculated ^{13}C and ^{1}H chemical shifts was performed following the multi-standard approach (MSTD) as reported by Pellegrinet et al.;[5] in particular, aromatic ^{13}C and ^{1}H chemical shifts were scaled using benzene as reference compound, while we considered C-1 and C-2 of ethylamine for C-1' and C-2', respectively. All the other ^{13}C and ^{1}H calculated chemical shifts were scaled to TMS (tetramethylsilane) (see Table S3.5 and Table S3.6).

For each relative stereoisomer, starting from the most energetically favored QM optimized conformer, $^{2}J_{C\text{-}H}$ heteronuclear coupling constants value for C-3 and H-4 was calculated accounting the Fermi contact (FC) contributions by adding tighter polarization functions for the s and d orbitals to the original 6-311+G(d,p) basis set, which was accomplished in Gaussian 09 with the "mixed" keyword.

Regarding CD spectra calculations, in order to reproduce the experimental solvent environment (methanol), all the conformers previously obtained from MM calculations were optimized at the QM level by using the MPW1PW91 functional and the 6-31G(d) basis set, in methanol IEFPCM. Then, CD calculations were performed at TDDFT MPW1PW91/6-31g(d,p) level. The final CD spectra for each of the investigated relative stereoisomers were built considering the influence of each conformer on the total Boltzmann distribution taking into account the relative energies, and were graphically plotted using SpecDis software. In order to simulate the experimental CD curve, a Gaussian band-shape function was applied with the exponential half-width (σ/γ) of 0.26 eV.[6]

All QM calculations were performed using Gaussian 09 software package.

Table S3.5 ^{1}H NMR experimental and calculated chemical shifts for 2a, 2b, 2c, and 2d with $|\Delta\delta|(^1H)$ and MAE values.

	δ_{calc} (^{1}H), ppm				δ_{exp} (^{1}H), ppm	$\|\Delta\delta\|(^1H)$, ppm[a]			
Position	**2a**	**2b**	**2c**	**2d**		**2a**	**2b**	**2c**	**2d**
4	4.23	4.65	4.21	4.45	4.71	0.48	0.06	0.50	0.26
9	6.58[b]	6.59[b]	6.63[b]	6.50[b]	6.76	0.18	0.17	0.13	0.26
10	6.11[b]	5.92[b]	5.93[b]	6.19[b]	5.84	0.27	0.08	0.09	0.35
1'a	3.35	3.49	3.43	3.46	3.58	0.23	0.09	0.15	0.12
1'b	2.51	2.92	3.28	2.91	2.97	0.46	0.05	0.31	0.06
2'	4.05	2.94	2.71	3.42	3.42	0.63	0.48	0.71	0.00
3'	2.27	1.99	2.49	2.19	1.92	0.35	0.07	0.57	0.27
4'	1.38	1.22	1.55	1.75	1.26	0.12	0.04	0.29	0.49
5'	1.61	1.84	1.83	1.61	1.41	0.20	0.43	0.42	0.20
6'	3.37	3.37	3.74	3.62	3.17	0.20	0.20	0.57	0.45
2'''	7.48[b]	7.31[b]	7.24[b]	7.50[b]	7.25	0.23	0.06	0.01	0.25
3'''	7.45[b]	7.35[b]	7.35[b]	7.37[b]	7.23	0.22	0.12	0.12	0.14
4'''	7.43[b]	7.39[b]	7.39[b]	7.37[b]	7.26	0.17	0.13	0.13	0.11
MAE[c]						0.29	**0.15**	0.31	0.23

[a] $|\Delta\delta|(^1H) = |\delta_{exp} - \delta_{calc}|$ (^{1}H), ppm: absolute differences for experimental versus calculated ^{1}H NMR chemical shifts

[b] ^{1}H calculated values were referenced to benzene H, following the multi-standard approach (MSTD);[3] all the remaining calculated values were referenced to TMS (tetramethylsilane).

[c] MAE = $\Sigma[|(\delta_{exp} - \delta_{calcd})|]/n$, summation through n of the absolute error values (difference of the absolute values between corresponding experimental and ^{1}H chemical shifts), normalized to the number of the chemical shifts considered

Table S3.6 ^{13}C NMR experimental and calculated chemical shifts for 2a, 2b, 2c, and 2d with $|\Delta\delta|(^{13}C)$, and MAE values.

	δ_{calc} (^{13}C), ppm				δ_{exp} (^{13}C), ppm	$\|\Delta\delta\|(^{13}C)$, ppm[a]			
Position	**2a**	**2b**	**2c**	**2d**		**2a**	**2b**	**2c**	**2d**
3	89.0	93.0	95.5	89.4	91.8	2.76	1.15	3.67	2.39
4	59.6	55.1	55.6	57.5	50.7	8.88	4.39	4.93	6.82
5	130.1[b]	127.6[b]	127.2[b]	130.0[b]	130.5	0.43	2.91	3.26	0.49
6	113.5[b]	112.3[b]	111.6[b]	113.5[b]	111.8	1.69	0.51	0.18	1.68
7	149.9[b]	150.9[b]	151.7[b]	152.6[b]	149.0	0.86	1.85	2.72	3.56
8	144.7[b]	145.9[b]	146.2[b]	144.7[b]	143.8	0.94	2.06	2.43	0.89
9	118.0[b]	120.9[b]	121.8[b]	119.3[b]	118.8	0.82	2.14	3.01	0.50
10	117.3[b]	119.1[b]	119.6[b]	117.6[b]	116.1	1.24	2.99	3.52	1.48
1'	45.6[c]	42.6[c]	45.0[c]	44.8[c]	39.0	6.58	3.62	5.98	5.75
2'	58.9[d]	63.8[d]	64.2[d]	56.6[d]	57.8	1.10	6.00	5.98	1.16
3'	24.5	29.7	27.5	29.7	29.7	5.22	0.03	2.22	0.04
4'	27.7	24.3	23.1	29.8	23.7	3.99	0.65	0.59	6.07
5'	32.0	28.0	28.3	32.0	29.1	2.87	1.13	0.81	2.86
6'	41.9	42.3	36.3	41.9	37.7	4.19	4.62	1.37	4.16
1'''	137.1[b]	135.5[b]	135.0[b]	137.0[b]	137.4	0.25	1.91	2.43	0.38
2'''	132.0[b]	132.4[b]	131.9[b]	132.4[b]	130.8	1.20	1.56	1.11	1.63
3'''	129.7[b]	129.1[b]	129.3[b]	129.2[b]	126.6	3.14	2.54	2.74	2.62
4'''	129.6[b]	129.4[b]	129.7[b]	129.3[b]	127.1	2.46	2.29	2.62	2.24
MAE[e]						2.70	**2.35**	2.78	2.49

[a] $|\Delta\delta|(^{13}C) = |\delta_{exp} - \delta_{calc}|$ (^{13}C), ppm: absolute differences for experimental versus calculated ^{13}C NMR chemical shifts

[b] ^{13}C calculated values were referenced to benzene C; [c] referenced to ethylamine C1; [d] referenced to ethylamine C2, following the multi-standard approach (MSTD);[3] all the remaining calculated values were referenced to TMS (tetramethylsilane)

[e] MAE = $\Sigma[|(\delta_{exp} - \delta_{calcd})|]/n$, summation through n of the absolute error values (difference of the absolute values between corresponding experimental and ^{13}C chemical shifts), normalized to the number of the chemical shifts considered.

Table S3.7 $^2J_{C3\text{-}H4}$ heteronuclear coupling constants experimental and calculated values for 2a, 2b, 2c, and 2d, with $|\Delta\delta|(^2J)$ values.

	$^2J_{calc}$, Hz				$^2J_{exp}$, Hz	$\lvert\Delta\delta\rvert(^2J)$, Hz [a]			
	2a	2b	2c	2d		2a	2b	2c	2d
$^2J_{C3\text{-}H4}$	-8.7	-4.3	-2.8	-8.9	-5.8	2.9	1.5	3.0	3.1

[a] **$|\Delta\delta|(^2J)$, Hz = $|^2J_{exp} - {}^2J_{calc}|$, Hz**

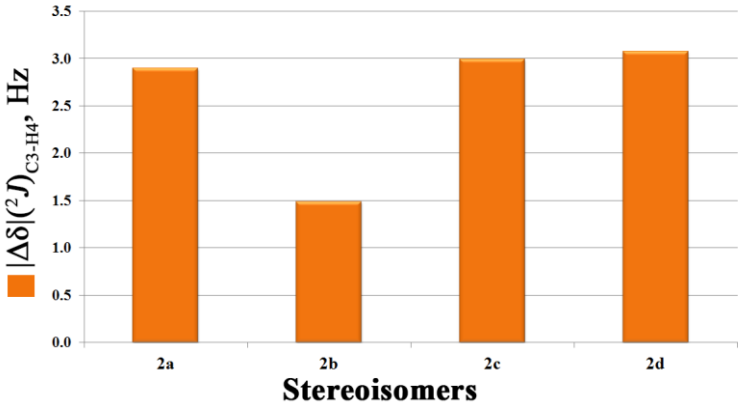

Figure S3.4 Histogram of the $|\Delta\delta|(^2J)$ values of $^2J_{C3\text{-}H4}$ heteronuclear coupling constants

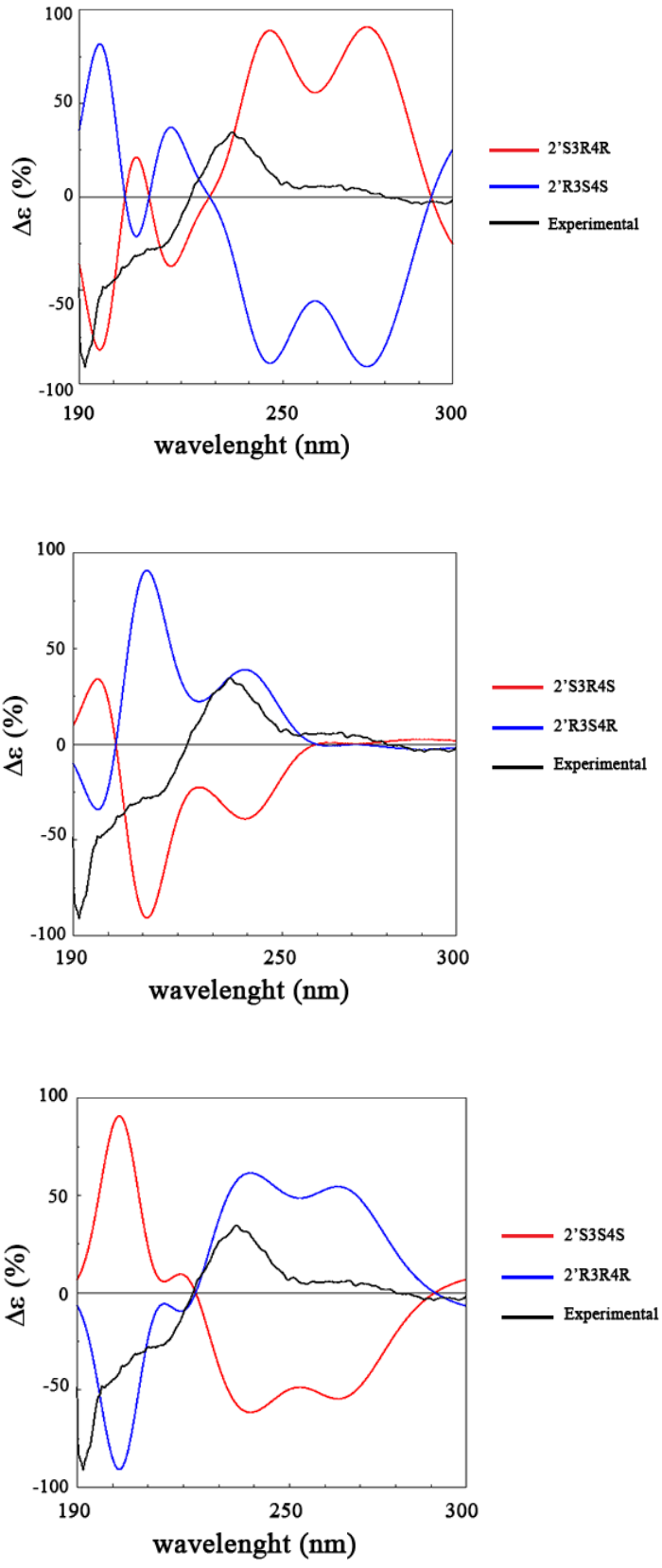

Figure S3.5 Comparison of experimental CD spectrum and calculated CD spectra of 2'*S*,3*R*,4*R;* 2'*R*,3*S*,4*S;* 2'*S*,3*R*,4*S;* 2'*R*,3*S*,4*R*; 2'*S*,3*S*,4*S*, and 2'*R*,3*R*,4*R*.

3.5. References of Supporting Information

[1] Garcia, R. O.; Krug, D.; Müller, R. In *Methods in Enzymology*; Hopwood D.A., Ed., Complex Enzymes in Microbial Natural Product Biosynthesis, Vol 458, Part A; Academic: Burlington, 2009; pp 59-91.

[2] Schwyn, B.; Neilands, J. B. *Analytical Biochemistry* **1987,** *160*, 47-56.

[3] Schrödinger, LLC: New York, NY, **2013**.

[4] MacroModel, version 10.2, Schrödinger LLC, New York, NY, **2013**.

[5] Sarotti, A. M.; Pellegrinet, S. C. *J. Org. Chem.* **2009**, *74*, 7254–7260.

[6] Bruhn, T.; Schaumlöffel, A.; Hemberger, Y.; Bringmann, G.; SpecDis version 1.61, University of Wuerzburg, Germany, **2013**.

[7] Gaussian 09, Revision **D.01**, Frisch, M. J.; Trucks, G. W.; Schlegel, H. B.; Scuseria, G. E.; Robb, M. A.; Cheeseman, J. R.; Scalmani, G.; Barone, V.; Mennucci, B.; Petersson, G. A.; Nakatsuji, H.; Caricato, M.; Li, X.; Hratchian, H. P.; Izmaylov, A. F.; Bloino, J.; Zheng, G.; Sonnenberg, J. L.; Hada, M.; Ehara, M.; Toyota, K.; Fukuda, R.; Hasegawa, J.; Ishida, M.; Nakajima, T.; Honda, Y.; Kitao, O.; Nakai, H.; Vreven, T.; Montgomery, J. A., Jr.; Peralta, J. E.; Ogliaro, F.; Bearpark, M.; Heyd, J. J.; Brothers, E.; Kudin, K. N.; Staroverov, V. N.; Kobayashi, R.; Normand, J.; Raghavachari, K.; Rendell, A.; Burant, J. C.; Iyengar, S. S.; Tomasi, J.; Cossi, M.; Rega, N.; Millam, N. J.; Klene, M.; Knox, J. E.; Cross, J. B.; Bakken, V.; Adamo, C.; Jaramillo, J.; Gomperts, R.; Stratmann, R. E.; Yazyev, O.; Austin, A. J.; Cammi, R.; Pomelli, C.; Ochterski, J. W.; Martin, R. L.; Morokuma, K.; Zakrzewski, V. G.; Voth, G. A.; Salvador, P.; Dannenberg, J. J.; Dapprich, S.; Daniels, A. D.; Farkas, Ö.; Foresman, J. B.; Ortiz, J. V.; Cioslowski, J.; Fox, D. J. Gaussian, Inc., Wallingford CT, **2009**.

Chapter 4

Cystochromones, Unusual Chromone-Containing Polyketides from the Myxobacterium *Cystobacter* sp. MCy9104

Suvd Nadmid,[†,§] Alberto Plaza,[†,§,‡] Ronald Garcia,[†,§] and Rolf Müller[†,§,]*

Journal of Natural Products, submitted

4. Cystochromones

4.1. Abstract

Seven new chromone-containing polyketides, termed cystochromones A-G, were isolated from the myxobacterial strain *Cystobacter* sp. MCy9104. Their structures were elucidated by comprehensive NMR spectroscopy and HR-MS/MS. Cystochromones bear a pentadecyl moiety unusually attached at C-5 of the chromone ring. Moreover, feeding experiments and NMR analysis suggested a hybrid iso-fatty acid and polyketide synthase biosynthetic pathway for these secondary metabolites.

4.2. Main Text

Over the past years, myxobacteria have attracted the attention of the scientific community due to their enormous biosynthetic capabilities and the potent biological activity of their secondary metabolites.[1,2] The investigation of these gram negative bacteria has resulted in numerous lead structures with diverse biological activities, including the HIV inhibitors aetheramides,[3] the unusual catecholate type of siderophores hyalachelins,[4] and the potent antibiotics disciformycins[5] and cystobactamides.[6] During our ongoing screening program aimed at the discovery of novel metabolites from terrestrial myxobacteria, strain MCy9104 *Cystobacter* sp. stood out due to its LC-HR-MS chromatographic profile which showed a number of unreported metabolites. Herein, we report the isolation, structure elucidation, and first insights into the biosynthesis of a new group of chromone-containing natural products, named cystochromones A-G (**1**-**7**). Their structures were elucidated by a combination of HR-MS/MS and 2D NMR experiments. Moreover, a biosynthetic scheme was proposed on the basis of results from feeding experiments employing isotopically labeled precursors.

4.3. Results and Discussion

The myxobacterial strain MCy9104 was cultivated in CLF production medium in the presence of 2.5% v/v of the neutral adsorber resin Amberlite XAD-16. After 10 days the resin was harvested by sieving, lyophilized, defatted with hexane, and subsequently extracted with ethyl acetate. The resultant dark brown oily crude extract was fractionated by size exclusion chromatography, and further subjected to semi preparative HPLC yielding seven new chromone derivatives, termed cystochromones A-G (**1**-**7**).

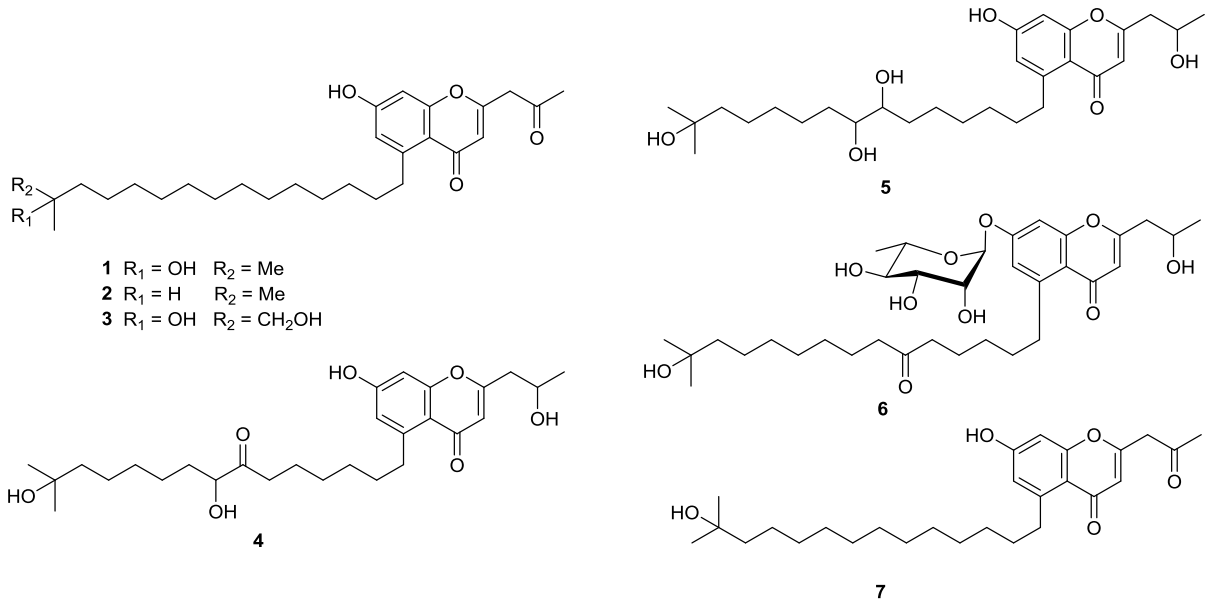

HR-ESI-MS of cystochromone A (**1**) gave a molecular ion at *m/z* 459.3115 $[M+H]^+$ corresponding to a molecular formula of $C_{28}H_{43}O_5$ requiring eight degrees of unsaturation. ^{1}H-NMR spectrum of **1** exhibited two doublets ascribable to two meta coupled aromatic protons at δ 6.65 (1H, d, J = 2.3 Hz, H-6) and 6.63 (1H, d, J = 2.3 Hz, H-8), an olefinic singlet at δ 6.07 (1H, s, H-3), a downfield shifted methylene singlet at δ 3.60 (2H, s, H-3'), and two singlets corresponding to three methyl groups at δ 2.26 (3H, s, H-1') and 1.21 (6H, s, H-15"/H-16") (Table 4.1). Additionally, highly overlapped signals corresponding to methylene protons were observed at δ 1.25-1.35 (H-3" – H-12") indicating the presence of a saturated alkyl chain. ^{13}C-NMR spectrum of **1** showed signals corresponding to two carbonyls at δ 201.8 (C-2') and 179.3 (C-4), three oxygenated aromatic quaternary carbons at δ 160.21 (C-7), 160.19 (C-9) and 159.4 (C-2), an oxygenated sp^3 quaternary carbon at δ 72.0 (C-14"), and overlapped carbon resonances at δ 29-30 (C-3" – C-12") (Table 4.1).

Analysis of the HMBC correlations from the olefinic proton H-3, and the aromatic protons H-6 and H-8 established the occurrence of a 2,5,7-trisubstituted chromone ring (Figure 4.1). Furthermore, long range correlations from the proton signal at δ 3.60 (H-3') to the ketone carbonyl at δ 201.8 (C-2') and to the methyl carbon at δ 29.7 (C-1') revealed the presence of a propan-2-one moiety. Connectivity of the propan-2-one moiety to the chromone ring was deduced via long range correlations from H-3' to the aromatic carbons at δ 159.4 (C-2) and 113.7 (C-3) (Figure 4.1). The structure of the remaining $C_{16}H_{33}O$ unit was established as 2-methylpentadecan-2-ol residue (C-1" – C-16") on the basis of HMBC and COSY correlations. Linkage of this saturated alkyl chain to the chromone ring was secured by strong HMBC correlations from the equivalent methylene protons at δ 3.18 (H-1") to the aromatic carbon resonances at δ 148.4 (C-5), 116.5 (C-6), and 115.3 (C-10) (Figure 4.1). Thereby, the

planar structure of **1** was established as a chromone ring bearing an alkyl chain in position C-5 and a propane-2-one moiety at C-2.

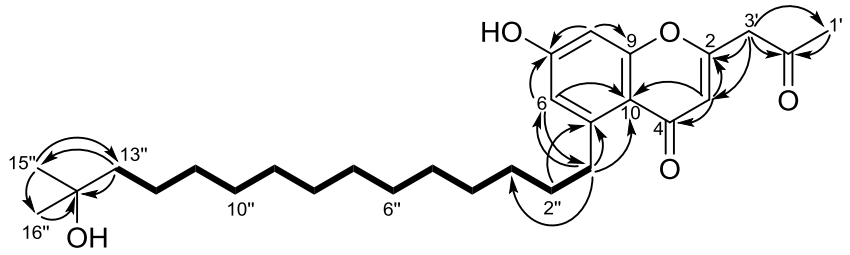

Figure 4.1 Key HMBC (arrow) and COSY (bold line) correlations of **1**

HR-ESI-MS supported the molecular formulae $C_{28}H_{43}O_4$ and $C_{28}H_{43}O_6$ for cystochromone B (**2**) and C (**3**), respectively. Detailed analysis of 2D NMR data of **2** and **3** in comparison to that of **1** clearly indicated that cystochromone B and C were the 14"-deoxy and 15"-hydroxy derivatives of **1**, respectively (Table S4.2).

Cystochromone D (**4**) showed a molecular ion peak at *m/z* 491.3001 $[M+H]^+$ ascribable to a molecular formula of $C_{28}H_{43}O_7$. The HSQC spectrum of **4** closely resembled to that of **1** only differing by the existence of two additional oxymethine signals ($\delta_{H\text{-}2'}$ 4.19, $\delta_{C\text{-}2'}$ 66.1 and $\delta_{H\text{-}8''}$ 4.06, $\delta_{C\text{-}8''}$ 77.9) (Table 4.1). Moreover, COSY correlations observed between protons H-1'/H-2'/H-3' established the presence of a propan-2-ol moiety (Figure 4.2). In turn, HMBC correlations from methylene protons H-3' to the carbons C-2 and C-3, together with HMBC correlations from H-2' to C-2 linked the propanol moiety to C-2 of the chromone ring (Figure 4.2).

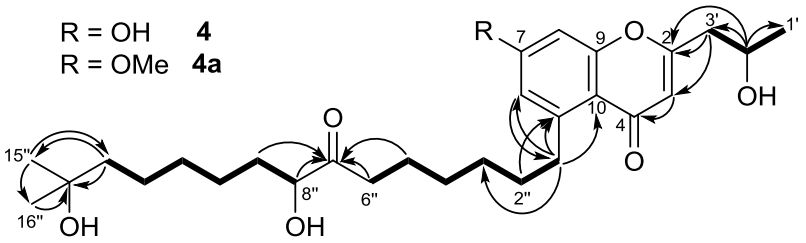

Figure 4.2 Key COSY (bold line) and HMBC (arrow) correlations of **4**

HMBC, COSY correlations, and MS^2 fragmentation experiment allowed us to identify the alkyl chain of **4** as 8,14-dihydroxy-14-methylpentadecan-7-one. In particular, HMBC correlations from the methylene protons H-9" (δ 1.53, 1.72), H-6" (δ 2.55), and H-5" (δ 1.58), and from the oxymethine proton H-8" (δ 4.06) to the ketone carbon resonance at δ 215.2 (C-7") determined the presence of an α-ketol functionality (Figure 4.2). The exact position of this functionality was proposed by an ESI-MS^2 fragmentation experiment. Indeed, the ESI-MS^2 spectrum of the molecular ion peak at *m/z* 491 $[M+H]^+$ gave a daughter ion peak at *m/z* 455 $[M+H-36]^+$ corresponding to loss of two water

molecules. Additionally, a daughter ion peak at *m/z* 331 $[M+H-160]^+$ was observed, which suggested an α-cleavage at C-7" (Figure S4.1). Taken together, MS^2 and NMR data indicated that the keto group should be placed at C-7" and the hydroxyl group at C-8". Finally, linkage of the 8,14-dihydroxy-14-methylpentadecan-7-one residue at C-5 of the chromone ring was deduced through the strong HMBC correlations from the proton at δ 3.16 (H-1") to the aromatic carbons δ 148.2 (C-5), 117.6 (C-6), and 114.8 (C-10).

Table 4.1 NMR spectroscopic data for cystochromone A (1) and D (4)

pos	**1**[a]		**4**[b]	
	δ_C,[c] type	δ_H[d] (*J* in Hz)	δ_C,[e] type	δ_H[f] (*J* in Hz)
2	159.4, C		166.5, C	
3	113.7, CH	6.07, s	112.4, CH	6.06, s
4	179.3, C		181.3, C	
5	148.4, C		148.2, C	
6	116.5, CH	6.65, d (2.3)	117.6, CH	6.64, d (2.3)
7	160.21, C		163.4, C	
8	101.5, CH	6.63, d (2.3)	101.7, CH	6.67, d (2.3)
9	160.19, C		161.5, C	
10	115.3, C		114.8, C	
1'	29.7, CH_3	2.26, s	23.4, CH_3	1.28, d (6.2)
2'	201.8, C		66.1, CH	4.19, m
3'a	48.7, CH_2	3.60, s	44.0, CH_2	2.66, dd (7.9, 14.4)
3'b				2.72, dd (4.9, 14.4)
1"	35.3, CH_2	3.18, t (7.5)	36.1, CH_2	3.16, t (7.5)
2"	31.3, CH_2	1.56, m	32.4, CH_2	1.57, m
3"-4"	29.2-30.1, CH_2	1.25-1.35, m	30.3-30.7, CH_2	1.31-1.40, m
5"	29.2-30.1, CH_2	1.25-1.35, m	24.2, CH_2	1.58, m
6"	29.2-30.1, CH_2	1.25-1.35, m	38.5, CH_2	2.55, m
7"	29.2-30.1, CH_2	1.25-1.35, m	215.2, C	
8"	29.2-30.1, CH_2	1.25-1.35, m	77.9, CH	4.06, q (3.8)
9"a	29.2-30.1, CH_2	1.25-1.35, m	34.5, CH_2	1.53, m
9"b				1.72, m
10"-12"	29.2-30.1, CH_2	1.25-1.35, m	30.3-30.7, CH_2	1.35-1.40, m
13"	44.1, CH_2	1.46, t (6.7)	44.5, CH_2	1.44, t (6.7)
14"	72.0, C		71.2, C	
15"/16"	29.3, CH_3	1.21, s	29.0, CH_3	1.16, s

[a]recorded in $CDCl_3$. [b]recorded in $MeOD_4$. [c]acquired at 125 MHz, referenced to solvent signal $CDCl_3$ at δ 77.23 ppm. [d]acquired at 500 MHz, referenced to solvent signal $CDCl_3$ at δ 7.24 ppm. [e]acquired at 175 MHz, referenced to solvent signal $MeOD_4$ at δ 49.15 ppm. [f]acquired at 700 MHz, referenced to solvent signal $MeOD_4$ at δ 3.31 ppm.

Cystochromone E (**5**) showed a molecular ion peak at *m/z* 493.3164 $[M+H]^+$ corresponding to a molecular formula of $C_{28}H_{45}O_7$ which was two mass units higher than **4**. 2D NMR data of **5** were almost identical to those of **4**, except for the substitution of a hydroxyl group at C-7" in **5** for the keto group in **4** (Table S4.4).

HR-ESI-MS at *m/z* 621.3650 $[M+H]^+$ of cystochromone F (**6**) suggested a molecular formula of $C_{34}H_{53}O_{10}$. HSQC, TOCSY, and COSY data of **6** indicated the presence of an α-rhamnose moiety (Table S4.5). Moreover, 2D NMR data of the aglycon unit of **6** was almost identical to those of **4**, only differing by the resonances belonging to the alkyl chain. Indeed, sequential COSY correlations from H-1" to H-5" along with HMBC correlations from H-5" and the proton signals at δ 1.60 (H-4"), δ 2.44 (H-7") and δ 1.55 (H-8") to the keto resonance at δ 214.2 (C-6") clearly determined the alkyl chain of **6** to be 14-hydroxy-14-methylpentadecan-6-one (Figure 4.3). A HMBC correlation from the anomeric proton at δ 5.57 (H-1"') to the carbon resonance at δ 160.6 (C-7) attached the rhamnose moiety to C-7 of the chromone ring, thereby completing the planar structure of **6** as depicted in Figure 4.3.

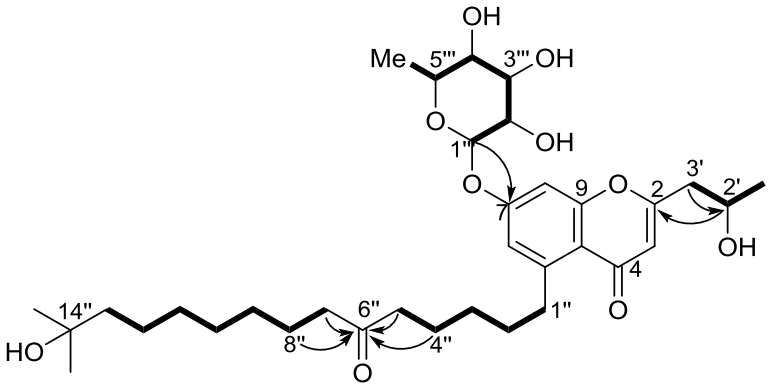

Figure 4.3 Key HMBC (arrow) and TOCSY/COSY (bold line) correlations of **6**

The absolute configuration of α-rhamnose was determined to be L by GC-MS analysis of trimethylsilylated (+)-2-butyl derivative of hydrolyzed **6** in comparison to trimethylsilylated (-)-2- and (+)-2-butyl derivative of authentic L standard[7] (Figure S4.3).

Cystochromone G (**7**) displayed an ion peak at *m/z* 445.2965 which was 14 mass units lower than that of **1**. In addition, its NMR data showed high similarity to those of **1** indicating **7** to differentiate from **1** only by having one methylene unit less in the saturated alkyl chain (Table S4.2).

In order to determine the absolute configuration of C-2' and C-8" in **4** by applying Mosher's method,[8] we first prepared its 7-*O*-methyl derivative **4a** (Figure 4.2) by treatment with iodomethane and sodium methoxide at room temperature. Subsequent esterification of **4a** (0.3 mg) was performed with *R*-(+)- and *S*-(-)-MTPA acid to produce the respective triesters in less than ca. 30% final yield. MS analysis

of both derivatives showed a formal elimination of one MTPA-ester residue. NMR spectra corroborated the elimination from C-2'/C-3' position, resulting a *trans*-$\Delta^{2'}$unsaturation (Table S4.6). Furthermore, ^{1}H-NMR and HSQC spectra of both di-MTPA esters (*S* and *R*) exhibited two sets of signals each. This led us to speculate that keto-enol tautomerization might have occurred during the esterification reaction inducing epimerization at C-8", and therefore we were unable to establish the configuration of C-8".

4.3.1. Biosynthesis of Cystochromones

The biosynthetic origin of cystochromones was studied by feeding experiments using ^{13}C labeled acetates and [D_{10}]-deuterated leucine. ^{13}C-NMR spectrum of **1** isotope labeled with [1-^{13}C] acetate clearly showed enhanced signal intensity of every second carbon starting from the C-2' keto carbonyl, including chromone carbons C-2, C-4, C-5, C-7, C-9, and part of the alkyl carbons C-1" to C-10" (Scheme 4.1). In similar fashion, incorporation of [2-^{13}C] acetate was observed for the remaining carbons in the chromone ring, C-11", C-1', and C-3'. This result was in agreement with the expected polyketide origin of **1**. Careful analysis of ^{13}C-^{13}C coupling constants resulting from [$^{13}C_2$] acetate feeding experiment, allowed us to establish the incorporation of intact acetate units (Scheme 4.1 and Table 4.2). Surprisingly, the carbon resonance of C-1' was observed as singlet although it was enriched by feeding with [2-^{13}C] acetate.

Table 4.2 ^{13}C-NMR data indicating the incorporation of [1,2-^{13}C]acetate into cystochromone A (1)

carbon	δ_C [a]	$J_{C\text{-}C}$ (Hz)	correlated carbon	carbon	δ_C	$J_{C\text{-}C}$ (Hz)	correlated carbon
2	159.4	71.2	C-3	1'	29.7	[b]	
3	113.7	71.3	C-2	2'	201.8	37.0	C-3'
4	179.3	57.0	C-10	3'	48.7	37.6	C-2'
5	148.4	41.3	C-1"	1"	35.3	41.1	C-5
6	116.5	63.1	C-7	2"	31.3	[c]	
7	160.21	63.4	C-6	3"-12"	29.2-30.1	[c]	
8	101.5	73.0	C-9	13"	44.1	[d]	
9	160.19	73.0	C-8	14"	72.0	[d]	
10	115.3	56.7	C-4	15"/16"	29.3	[d]	

[a]referenced to solvent signal $CDCl_3$ at 77.23 ppm. [b]enriched, but appeared as singlet. [c]overlapped signals. [d]not enriched with ^{13}C-acetates

Altogether, these data suggested a decarboxylation from the polyketide chain. Moreover, the C-12" – C-16" portion of the molecule was not labeled with acetate carbons, suggesting that its origin could be derived from leucine via isovaleryl-CoA being used as starter molecule. Indeed, LC-MS analysis of an extract prepared from culture fed with L-[D_{10}] leucine revealed a mass shift of 8 daltons for compounds **4** and **6**, presenting intact incorporation of isovalerate (Figure S4.4). It is worth

mentioning that the shift of 8 daltons is in concordance with loss of two deuterium atoms due to the transamination of leucine to [D_9]-α-ketoisocaproic acid[9] and oxidation at C-14". These results indicate that cystochromones are assembled from a leucine-derived fatty acid (FA)[10] which serves as a starter unit for the respective polyketide synthase (PKS).

Scheme 4.1 Proposed biogenetic pathway for 1 deduced from feeding studies

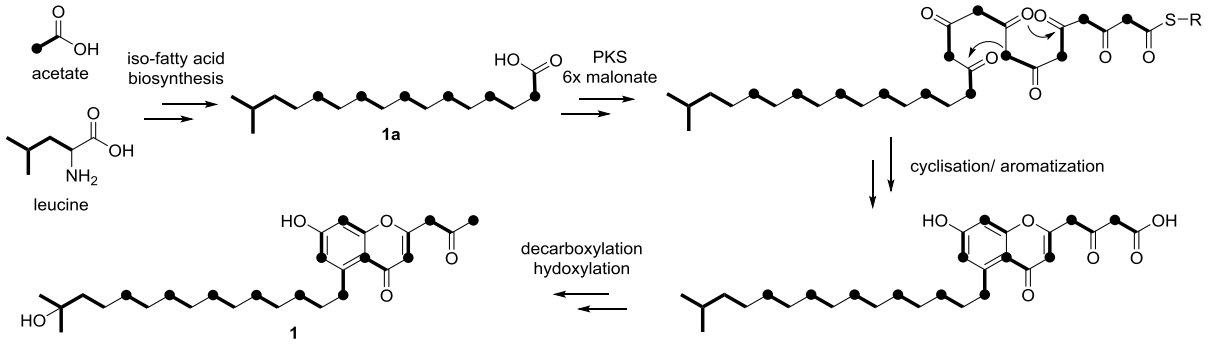

On the basis of our feeding experiments, we postulate that the presumed hybrid biosynthetic pathway of **1** initiates with the formation of leucine derived isovaleryl-CoA which further undergoes branched chain FA biosynthesis to yield a 15-methylhexadecanoic acid (**1a**)[10] (Scheme 4.1). Furthermore, the extension of this FA with six malonyl-CoA units is carried out using standard polyketide biochemistry. The resulting polyketide structure undergoes cyclisation and aromatization steps to form a characteristic chromone moiety, followed by post-PKS modifications *i.e.*, decarboxylation, regiospecific hydroxylation and glycosylation to form **5**. However, we cannot exclude the possibility that the complete molecule is formed by PKS.

Cystochromone A (**1**) was tested for activities against both Gram negative and Gram positive bacteria, cancer cell lines, and various fungal strains. It did not show significant inhibitory activity up to concentrations as high as 64 μg/mL.

In conclusion, seven new polyketides, named cystochromone A-G, were identified from the culture of the myxobacterial strain *Cystobacter* sp. Cystochromones are characterized by containing an unusual pentadecyl substitution at C-5 and an oxygenated propane moiety at C-2 of the chromone ring. To the best of our knowledge, this is the first report of a chromone-containing secondary metabolite with a pentadecyl substitution at C-5.[11] Chromones, including stigmatellin X, a chromone derivative also isolated from myxobacteria,[12] usually bear an alkyl chain in position 2. Stigmatellins are assembled by a polyketide synthase utilizing acetate and propionate as building blocks while aromatization occurs while or after the polyketide chain is generated.[13] Our feeding experiments show that the cystochromones are likely to be formed by a hybrid iso-fatty acid and polyketide synthase biosynthetic pathway.

4.4. Experimental Section

4.4.1. General Experimental Procedure

The specific optical rotations were measured on JASCO P-2000 polarimeter. UV spectra were measured on an Agilent 8453 spectrophotometer and IR spectra were obtained on Perkin-Elmer FT-IR spectrum One spectrometer. NMR spectra were acquired on Bruker Ascend 500 MHz and 700 MHz NMR spectrometers equipped with a 5 mm TXI cryoprobe. Deuterated $MeOD_4$ and $CDCl_3$ were used as NMR solvents and HSQC, HMBC, ^1H-^1H COSY, 2D TOCSY, ROESY spectra were recorded using standard pulse programs. LC-HRMS data were obtained on a maXis 4G mass spectrometer (Bruker Daltonics, Germany) coupled with Dionex Ultimate 3000 RSLC system, using a BEH C18, 100 × 2.1 mm, 1.7 mm d_p column (Waters, Germany) with linear gradient of 5-95% ACN + 0.1% FA in H_2O + 0.1% FA at 600 μL/min in 18 min with UV detection in 200-600 nm range. Mass spectra were acquired using the ESI source in the range from 150–2000 *m/z* at 2 Hz scan speed.

4.4.2. Strain Isolation and Identification

The strain MCy9104 was isolated in 2006 from a soil sample collected in Manila, Philippines. The bacterium was discovered by a standard myxobacterial baiting method using rabbit dung pellets which were half-burrowed in the soil.[14,15] It was recognized as myxobacterium by the development of rounded and brownish fruiting bodies on the baits. By picking them up using a sterile fine needle and inoculating onto buffered water agar baited with *Escherichia coli* and for successive transfers of the farthest swarm colony edge,[16] the strain was finally purified. The isolate was maintained in buffered VY/2 agar and permanently stored in -80ºC freezer using 50% glycerol as cryo protectant. Based on complete 16S rRNA gene sequence (1524bp), strain MCy9104 shows closest similarity (99%) with *Cystobacter fuscus* DSM 2262^T (GenBank accession number: NR_043941), *Cystobacter ferrugineus* Cb fe18^T (NR_025343), and *Cystobacter badius* DSM14723^T (NR_043940). The strain's affiliation to genus *Cystobacter* was also supported by morphological characteristics, and phylogenetic analysis (Figure S4.2).

4.4.3. Strain Cultivation

Preculture of strain MCy9104 *Cystobacter* sp. grew in CLF medium (4 g fructose, 6 g glucose, 10 g skim milk, 2 g yeast extract, 1 g $CaCl_2 \times 2H_2O$, 1 g $MgSO_4 \times 7H_2O$, 11.9 g HEPES per liter, pH 7.0 adjusted with 10N KOH) on rotary shaker at 30^0C. 4d old preculture was inoculated (2% v/v) in to 12 L CLF production medium (distributed in 6 × 5 L shaking flasks), and placed on rotary shaker at 180 rpm in 30^0C room, and adsorber resin Amberlite XAD-16 (2.5% w/v) was added on day nine. XAD was collected on next day by sieving, and lyophilized overnight.

4.4.4. Extraction and Isolation

Dry XAD was defatted with n-hexane and extracted with ethyl acetate 3 × 500 mL. 1 g dark brown oily crude extract was obtained after evaporation of ethyl acetate *in vacuo*, and the crude extract was then subjected to Sephadex-LH 20 column chromatography with MeOH as eluent. The fractions containing cystochromones were dried in Genevac and purified by semi-prep HPLC Agilent system equipped with Luna C18(2), 250 × 10 mm, 5 μm d_P column. Linear gradient started with 10% of B (ACN + 0.1% FA) for 5 mins, increased to 50% in 15 mins, and to 100% in 30 mins at 2.5 mL/min, followed by isocratic run for 10 mins at 3 mL/min to afford compounds **1** (1 mg, t_R = 39.1 mins), **2** (0.2 mg, t_R = 53.7 mins), **3** (0.4 mg, t_R = 31.0 mins), **4** (0.3 mg, t_R = 20.5 mins), **5** (0.3 mg, t_R = 19.8 mins), **6** (0.7 mg, t_R = 21.6 mins), and **7** (0.5 mg, t_R = 37.2 mins).

*Cystochromone A (**1**):* colorless solid, $[\alpha]^{20}_D$ -12.9 (*c* 0.2 in MeOH), IR (film) ν_{max} 3681, 2938, 2865, 1455, 1346, 1055, 1032 cm^{-1}, UV(ACN) λ_{max} 220, 250, 292 nm, ^1H and ^{13}C NMR data see Table 4.1 and S4.1, HR-ESI-MS *m/z* 459.3103 $[M+H]^+$ (calcd for $C_{28}H_{43}O_5$ 459.3105)

*Cystochromone B (**2**):* colorless solid, $[\alpha]^{20}_D$ -22.5 (*c* 0.15 in MeOH:CH_2Cl_2/1:1), IR (film) ν_{max} 2920, 2851, 1652, 1611, 1352 cm^{-1}, UV(ACN) λ_{max} 222, 250, 292 nm, ^1H and ^{13}C NMR data see Table S4.2, HR-ESI-MS *m/z* 443.3150 $[M+H]^+$ (calcd for $C_{28}H_{43}O_4$ 443.3155)

*Cystochromone C (**3**):* colorless solid, $[\alpha]^{20}_D$ -11.6 (*c* 0.2 in MeOH), IR (film) ν_{max} 3372, 2923, 2853, 1647, 1600 cm^{-1}, UV(ACN) λ_{max} 220, 251, 288 nm, ^1H and ^{13}C NMR data see Table S4.2, HR-ESI-MS *m/z* 475.3051 $[M+H]^+$ (calcd for $C_{28}H_{43}O_6$ 475.3054)

*Cystochromone D (**4**):* colorless solid, $[\alpha]^{20}_D$ -4.7 (*c* 0.2 in MeOH), IR (film) ν_{max} 3328, 2932, 2857, 1643, 1598, 1390 cm^{-1}, UV(ACN) λ_{max} 220, 251, 286 nm, ^1H and ^{13}C NMR data see Table 4.1 and S4.3, HR-ESI-MS *m/z* 491.3001 $[M+H]^+$ (calcd for $C_{28}H_{43}O_7$ 491.3003)

*Cystochromone E (**5**):* colorless solid, $[\alpha]^{20}_D$ -8.0 (*c* 0.2 in MeOH), IR (film) ν_{max} 3708, 2923, 2866, 1738, 1455, 1365, 1228, 1055 cm^{-1}, UV(ACN) λ_{max} 220, 250, 288 nm, ^1H and ^{13}C NMR data see Table S4.4, HR-ESI-MS *m/z* 493.3164 $[M+H]^+$ (calcd for $C_{28}H_{45}O_7$ 493.3159)

*Cystochromone F (**6**):* colorless solid, $[\alpha]^{20}_D$ -28.0 (*c* 0.2 in MeOH), IR (film) ν_{max} 3352, 2926, 2851, 1643, 1598, 1395 cm^{-1}, UV(ACN) λ_{max} 220, 251, 282 nm, ^1H and ^{13}C NMR data see Table S4.5, HR-ESI-MS *m/z* 621.3650 $[M+H]^+$ (calcd for $C_{34}H_{53}O_{10}$ 621.3633)

*Cystochromone G (**7**):* colorless solid, $[\alpha]^{20}_D$ -20.8 (*c* 0.1 in MeOH:CH_2Cl_2/1:1), IR (film) ν_{max} 2929, 2851, 1646, 1598 cm^{-1}, UV(ACN) λ_{max} 220, 251, 290 nm, ^1H and ^{13}C NMR data see Table S4.2, HR-ESI-MS *m/z* 445.2965 $[M+H]^+$ (calcd for $C_{27}H_{41}O_5$ 445.2954

4.4.5. Stable Isotope Feeding

Feeding experiments were carried out using [1-^{13}C]-, [2-^{13}C]- and [1,2-$^{13}C_2$] acetates, each in 5mM final concentration in 2 L cultures. Precursors were dissolved in mixture of 7 mL sterile water and 2 mL DMSO, and added into the culture as three equal portions at 20, 28 and 44h after inoculation. Simultaneously, positive and negative control cultures were prepared with 5mM unlabeled sodium acetate, and 2 mL DMSO, respectively. After 5 days of inoculation, 50 mL XAD-16 was added, and harvested after another 2 days. XAD was collected by sieving, lyophilized, defatted with n-hexane, and extracted with 3 × 300 mL ethyl acetate. EtOAc extracts were then subjected to Agilent semi-prep HPLC equipped with an automatic fraction collector and Luna C18(2), 250 × 10 mm, 5 μm d_P column. Fractionation was carried out using linear gradient started with 10% B (ACN+0.1% FA) increased to 50% in 15 mins and to 100% B in 30 mins. Fractions of interest were combined, and concentrated under reduced pressure and final purification was achieved on the semi-prep HPLC system equipped with Synergi Fusion 250 × 10 mm, 4 μm d_P column with linear gradient of 75%-100% B in 20 mins at 2.5 mL/min flow rate to yield enriched **1** in 1.0 mg ([1-^{13}C]-acetate), 1.2 mg ([2-^{13}C]-acetate) and 0.3 mg ([1,2-^{13}C]-acetate).

Feeding experiment with L-[D_{10}]leucine was achieved with 0.1mM labeled precursor as final concentration that was dissolved in 2 mL DMSO. It was added as two equal portions to the culture at 18h and 24h after cultivation initiation. MeOH extract of XAD was analyzed by LC-HR-MS.

4.4.6. Methylation and Preparation of (*R*) and (*S*)-MTPA esters of 4.

Starting material **4** (1 mg) was mixed in methyl iodide (100 μL) with 0.5M sodium methoxide solution in methanol (30 μL) at room temperature. After 2, 24 and 29h another 3 portions of both reagents were added. Mixture was dried under N_2 stream after 46h, and resuspended in MeOH. The methylated product **4a** was purified by semi-prep HPLC equipped with Luna C18(2) 250 × 10 mm, 5 μm d_P column with linear gradient of 10-100% B (ACN+0.1% FA) in 25 mins.

To the solution of **4a** (0.35 mg in 100 μL dried chloroform) was added (*R*)-(+)- and (*S*)-(-)-α-methoxy-α-trifluoromethyl phenylacetic acid (MTPA, 150 μL), extra dry pyridine (20 μL), *N*,*N*'-diisopropylcarbodiimide (DIC, 140 μL), and excess amount of dimethylaminopyridine in four portions at 0, 24, 48, 72h. The reactions were monitored by LC-MS. After 4 days, the reaction was dried under N_2, dissolved in water, and extracted with ethyl acetate. Organic layer was concentrated, and analyzed by LC-MS. Purification of (*R*)- and (*S*)-Mosher ester of **4a** were carried out by semi-prep HPLC equipped with Luna C18(2) 250 × 10 mm, 5 μm d_P column under linear gradient of 10-65% B in 15 mins, increased up to 100% in 30 mins followed by isocratic run at 100% for another 9 mins with 2.5 mL/min. Mosher esters were eluted at 56 min.

4.4.7. Assigment of Absolute Configuration of Rhamnose.

Approximately 0.3 mg of **6** was hydrolyzed with 1 N HCl (0.25 mL) at 60^0C for 4h. After cooled down to room temperature, the solution was concentrated by Speedvac concentrator (Eppendorf). The residue was dissolved in (+)-2-butanol (0.3 mL) and acetyl chloride (5 μL), and stirred for 8h at 80^0C. After cooling, the reaction was quenched with sat. aqueous $NaHCO_3$ (0.5 mL) and subsequently extracted with ethyl acetate (2 × 0.5 mL). The organic layer was dried first with stream of N_2, followed by overnight drying *in vacuo* and then threated with 1-(trimethylsilyl)imidazole (40 μL) and pyridine (160 μL) for 15 mins at 60^0C. The solution was dried by Speedvac concentrator, and the residue was separated by H_2O and EtOAc (2 × 400 μL, 1:1 v/v). The organic layer was analyzed by GC-MS on an Agilent 6890N gas chromatograph with a 5973 electron impact mass selective detector and a 7683B injector (Agilent) using a dimethyl-(5% phenyl)-polysiloxane capillary column (Agilent DB-5ht, 0.25 mm by 30 m by 0.1 μm). Helium was used as the carrier gas at a flow rate of 1 mL/min. 5 μl of the sample was injected in split mode (split ratio, 10:1). The column temperature was increased from 50°C to 180°C at a rate of 5°C/min. Other temperatures were as follows: inlet, 275°C; GC-MS transfer line, 280°C; ion source, 230°C; and quadrupole, 150°C. The mass selective detector was operated in scan mode, scanning the mass range from *m*/*z* 40 to 700. Peaks corresponding to the trimethylsilylated (+)-2-butyl rhamnoside was co-eluted with same derivative of authentic L-rhamnose (eluted at 22.26 mins) that was treated in same manner. Since the retention times of (+)-2-butyl L-rhamnoside and (-)-2-butyl D-rhamnoside are the same, the authentic L standard was derivatized with (-)-2-butanol, and analysed by GC-MS (eluted at 22.07 mins).

4.5. References

[1] Wenzel, S. C.; Müller, R. *Mol. Biosyst*. **2009**, *5*, 567–574.

[2] Weissman, K. J.; Müller, R. *Nat. Prod. Rep*. **2010**, *27*, 1276–1295.

[3] Plaza, A.; Garcia, R.; Bifulco, G.; Martinez, J. P.; Hüttel, S.; Sasse, F.; Meyerhans, A.; Stadler, M.; Müller, R. *Org. Lett.* **2012**, *14*, 2854–2857.

[4] Nadmid, S.; Plaza, A.; Lauro, G.; Garcia, R.; Bifulco, G.; Müller, R. *Org. Lett*. **2014**, *16*, 4130–4133.

[5] Surup, F.; Viehrig, K.; Mohr, K. I.; Herrmann, J.; Jansen, R.; Müller, R. *Angew. Chem. Int. Ed*. **2014**, *53*, 13588-13591.

[6] Baumann, S.; Herrmann, J.; Raju, R.; Steinmetz, H.; Mohr, K. I.; Hüttel, S.; Harmrolfs, K.; Stadler, M.; Müller, R. *Angew. Chem. Int. Ed.* **2014**, *53*, 14605–14609.

[7] Gerwig, G. J.; Kamerling, J. P.; Vliegenthart, J. F. **1978**, 349–357.

[8] Hoye, T. R.; Jeffrey, C. S.; Shao, F. *Nat. Protoc.* **2007**, *2*, 2451–2458.

[9] Dickschat, J. S.; Bode, H. B.; Kroppenstedt, R. M.; Müller, R.; Schulz, S. *Org. Biomol. Chem*. **2005**, *3*, 2824–2831.

[10] Bode, H. B.; Dickschat, J. S.; Kroppenstedt, R. M.; Schulz, S.; Müller, R. *J. Am. Chem. Soc*. **2005**, *127*, 532–533.

[11] Gaspar, A.; Matos, M. J.; Garrido, J.; Uriarte, E.; Borges, F. *Chem. Rev*. **2014**, *114*, 4960–4992.

[12] Kunze, B.; Kemmer, T.; Höfle, G.; Reichenbach, H. *J. Antibiot.* **1984**, *37*, 454–461.

[13] Gaitatzis, N.; Silakowski, B.; Kunze, B.; Nordsiek, G.; Blöcker, H.; Höfle, G.; Müller, R. *J. Biol. Chem.* **2002**, *277*, 13082–13090.

[14] Krzemieniewska, H.; Krzemieniewski, S.; Myxobacteria of the species Chondromyces *Bull Acad Polon Sci Lettr Classe Sci Math Nat Ser B*; Berkeley and Curtis, 1946, 1:31–48

[15] Shimkets, L.; Dworkin, M.; Reichenbach, H. The myxobacteria. In *The Prokaryotes*; Dworkin, M.; Falkow, S.; Rosenberg, E.; Schleifer, K-H.; Stackebrandt, E., Eds.; Springer-Verlag: Berlin, 2006; Vol. 7, 3rd edn. pp 31–11.

[16] Garcia, R.; Müller, R. Family Polyangiaceae. In *The Prokaryotes*; Rosenberg, E.; DeLong, E.; Lory, S.; Stackebrandt, E.; Thompson, F., Eds.; Springer-Verlag: Berlin Heidelberg, 2014, pp 247–279.

4.6. Supporting Informations

Table S4.1 NMR spectroscopic data for cystochromone A (1)

pos	δ_C,[a] type	δ_H[b] (*J* in Hz)	HMBC[c]	COSY[d]
2	159.4, C			
3	113.7, CH	6.07, s	2, 2', 3', 4, 10	
4	179.3, C			
5	148.4, C			
6	116.5, CH	6.65, d (2.3)	1", 4, 7, 8, 10	
7	160.21, C			
8	101.5, CH	6.63, d (2.3)	4, 6, 7, 9, 10	
9	160.19, C			
10	115.3, C			
1'	29.7, CH_3	2.26, s	2, 2', 3'	
2'	201.8, C			
3'	48.7, CH_2	3.60, s	1', 2, 2', 3	
1"	35.3, CH_2	3.18, t (7.5)	2", 3", 5, 6, 10	2"
2"	31.3, CH_2	1.56, m	1", 3"	1", 3"
3"-12"	29.2-30.1, CH_2	1.25-1.35, m	[e]	[e]
13"	44.1, CH_2	1.46, t (6.7)	14", 15", 16"	12"
14"	72.0, C			
15"/16"	29.3, CH_3	1.21, s	13", 14", 15/16"	

[a]recorded at 125 MHz, referenced to solvent signal $CDCl_3$ at δ 77.23 ppm. [b]recorded at 500 MHz, referenced to solvent signal $CDCl_3$ at δ 7.24 ppm. [c]proton showing HMBC correlation to indicated carbons. [d]proton showing COSY correlation to indicated protons. [e]overlapped signals

Table S4.2 NMR spectroscopic data for cystochromone B (2), C (3) and G (7)

pos	**2**[a]		**3**[b]		**7**[b]	
	δ_C,[c] type	δ_H[d] (*J* in Hz)	δ_C,[e] type	δ_H[f] (*J* in Hz)	δ_C,[e] type	δ_H[f] (*J* in Hz)
2	159.2, C		162.3, C		162.4, C	
3	113.9, CH	6.07, s	113.5, CH	6.09, s	113.5, CH	6.09, s
4	[g]		181.1, C		181.2, C	
5	148.6, C		148.6, C		148.6, C	
6	116.0, CH	6.60, d (2.3)	117.5, CH	6.65, d (2.3)	117.5, CH	6.65, d (2.3)
7	159.8, C		163.3, C		163.2, C	
8	101.4, CH	6.63, d (2.3)	101.6, CH	6.64, d (2.3)	101.6, CH	6.64, d (2.3)
9	159.0, C		161.4, C		161.6, C	
10	115.7, C		114.9, C		115.1, C	
1'	29.9, CH_3	2.26, s	29.7, CH_3	2.27, s	29.8, CH_3	2.27, s
2'	201.3, C		204.1, C		204.1, C	
3'	48.6, CH_2	3.60, s	48.0, CH_2	3.31[h]	48.0, CH_2	3.31[h]
1"	35.3, CH_2	3.18, t (7.5)	36.2, CH_2	3.16, t (7.9)	36.2, CH_2	3.16, t (7.9)
2"	31.5, CH_2	1.55, m	32.5, CH_2	1.56, m	32.5, CH_2	1.56, m
3"-11"	29.2-30.1, CH_2	1.25-1.35, m	29.2-30.5, CH_2	1.25-1.35, m	29.2-30.5, CH_2	1.25-1.35, m
12"	29.2-30.1, CH_2	1.25-1.35, m	29.2-30.5, CH_2	1.25-1.35, m	44.6, CH_2	1.43, m (6.7)
13"	39.3, CH_2	1.12, m	39.5, CH_2	1.45, m (6.7)	71.4, C	
14"	28.0, CH	1.49, m	73.5, C		28.9, CH_3	1.16, s
15"	22.8, CH_3	0.84, d (6.6)	70.2, CH_2	3.35, s	28.9, CH_3	1.16, s
16"	22.8, CH_3	0.84, d (6.6)	23.5, CH_3	1.11, s		

[a]recorded in $CDCl_3$. [b]recorded in $MeOD_4$. [c]acquired at 175 MHz, referenced to solvent signal $CDCl_3$ at δ 77.23 ppm. [d]acquired at 700 MHz, referenced to solvent signal $CDCl_3$ at δ 7.24 ppm. [e]acquired at 125 MHz, referenced to solvent signal $MeOD_4$ at δ 49.15 ppm. [f]acquired at 500 MHz, referenced to solvent signal $MeOD_4$ at δ 3.31 ppm. [g]not observed. [h]overlapped with solvent signal

Table S4.3 NMR spectroscopic data for cystochromone D (4)

pos	δ_C,[a] type	δ_H[b] (J in Hz)	HMBC[c]	COSY[d]
2	166.5, C			
3	112.4, CH	6.06, s	2, 4	
4	181.3, C			
5	148.2, C			
6	117.6, CH	6.64, d (2.3)	1", 7, 8, 10	
7	163.4, C			
8	101.7, CH	6.67, d (2.3)	6, 7, 9, 10	
9	161.5, C			
10	114.8, C			
1'	23.4, CH_3	1.28, d (6.2)	2', 3'	2'
2'	66.1, CH	4.19, m	1', 2, 3'	1', 3'a, 3'b
3'a	44.0, CH_2	2.66, dd (7.9, 14.4)	1', 2', 2, 3	2', 3'b
3'b		2.72, dd (4.9, 14.4)	1', 2', 2, 3	2', 3'a
1"	36.1, CH_2	3.16, t (7.5)	2", 3", 5, 6, 10	2"
2"	32.4, CH_2	1.57, m	5	1", 3"
3"-4"	30.3-30.7, CH_2	1.31-1.40, m	[e]	[e]
5"	24.2, CH_2	1.58, m	7"	4", 6"
6"	38.5, CH_2	2.55, m	7"	5"
7"	215.2, C			
8"	77.9, CH	4.06, q (3.8)	7", 9"	9"a, 9"b
9"a	34.5, CH_2	1.53, m	7", 8"	8", 9"b
9"b		1.72, m	7"	8", 9"a
10"-12"	30.3-30.7, CH_2	1.35-1.40, m	[e]	
13"	44.5, CH_2	1.44, t (6.7)	14", 15"/16"	
14"	71.2, C			
15"/16"	29.0, CH_3	1.16, s	13", 14"	

[a]recorded at 175 MHz, referenced to solvent signal $MeOD_4$ at δ 49.15 ppm. [b]recorded at 700 MHz, referenced to solvent signal $MeOD_4$ at δ 3.31 ppm. [c]proton showing HMBC correlation to indicated carbons. [d]proton showing COSY correlation to indicated protons. [e]overlapped signals

Table S4.4 NMR spectroscopic data for cystochromone E (5)

pos	δ_C,[a] type	δ_H[b] (J in Hz)	HMBC[c]	COSY[d]
2	166.7, C			
3	112.3, CH	6.06, s	2, 4	
4	181.4, C			
5	148.6, C			
6	117.4, CH	6.64, d (2.3)	1", 7, 8, 10	
7	163.1, C			
8	101.6, CH	6.67, d (2.3)	6, 7, 9, 10	
9	161.6, C			
10	115.1, C			
1'	23.5, CH_3	1.28, d (6.3)	2', 3'	2'
2'	66.4, CH	4.20, m	1', 2,	1', 3'a, 3'b
3'a	44.0, CH_2	2.65, dd (7.9, 14.3)	1', 2', 2, 3	2', 3'b
3'b		2.73, dd (4.9, 14.3)	1', 2', 2, 3	2', 3'a
1"	36.0, CH_2	3.15, m	2", 3", 5, 6, 10	2"
2"	32.5, CH_2	1.55, m	5	1", 3"
3"	30.5, CH_2	1.40, m	[e]	[e]
4"	30.8, CH_2	1.32, m	[e]	[e]
5"	24.4, CH_2	1.58, m	[e]	[e]
6"a	33.6, CH_2	1.43, m	7", 8"	[e]
6"b		1.51, m	7", 8"	[e]
7"	75.4, CH	3.38, m	5", 6", 8", 9"	6"a, 6"b
8"	75.4, CH	3.38, m	5", 6", 7", 9"	9"a, 9"b
9"a	33.6, CH_2	1.43, m	7", 8"	[e]
9"b		1.51, m	7", 8"	[e]
10"	26.9, CH_2	1.51, m	[e]	[e]
11"-12"	30.1, CH_2	1.35, m	[e]	[e]
13"	44.1, CH_2	1.45, t (6.7)	14", 15", 16"	[e]
14"	71.5, C			
15"/16"	29.0, CH_3	1.16, s	13", 14", 15"/16"	

[a]recorded at 125 MHz, referenced to solvent signal $MeOD_4$ at δ 49.15 ppm. [b]recorded at 500 MHz, referenced to solvent signal $MeOD_4$ at δ 3.31 ppm. [c]proton showing HMBC correlation to indicated carbons. [d]proton showing COSY correlation to indicated protons. [e]overlapped signals

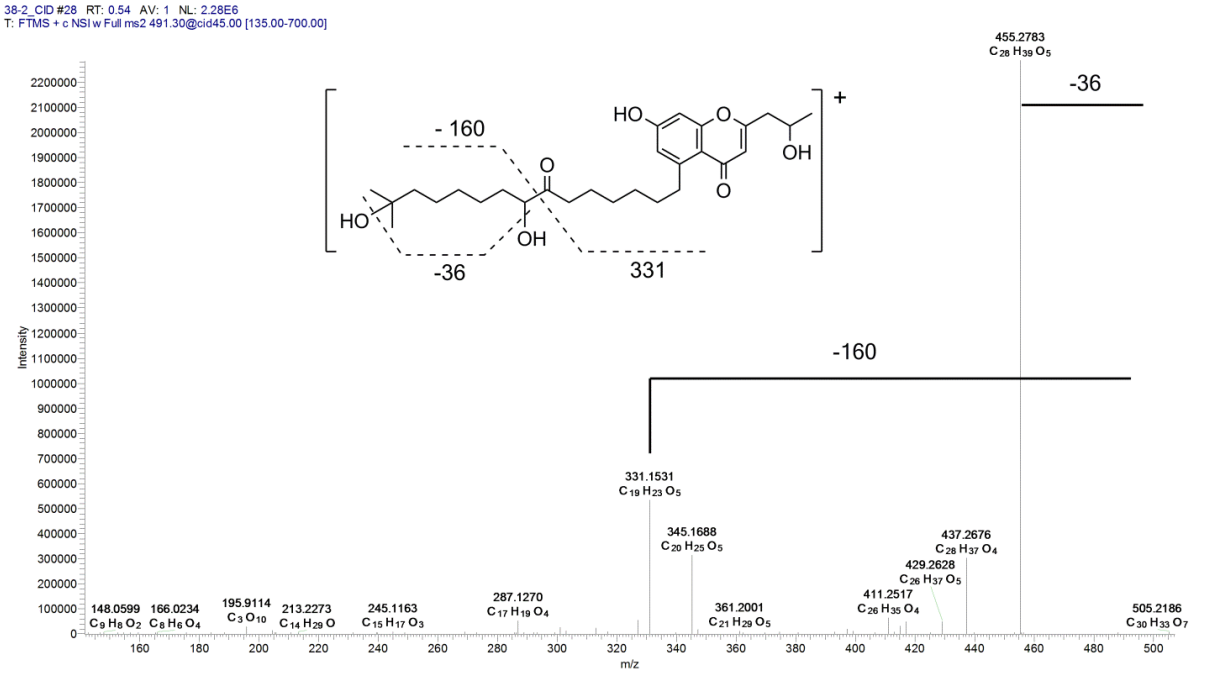

Figure S4.1ESI-MS^2 fragmentation of cystochromone D (**4**)

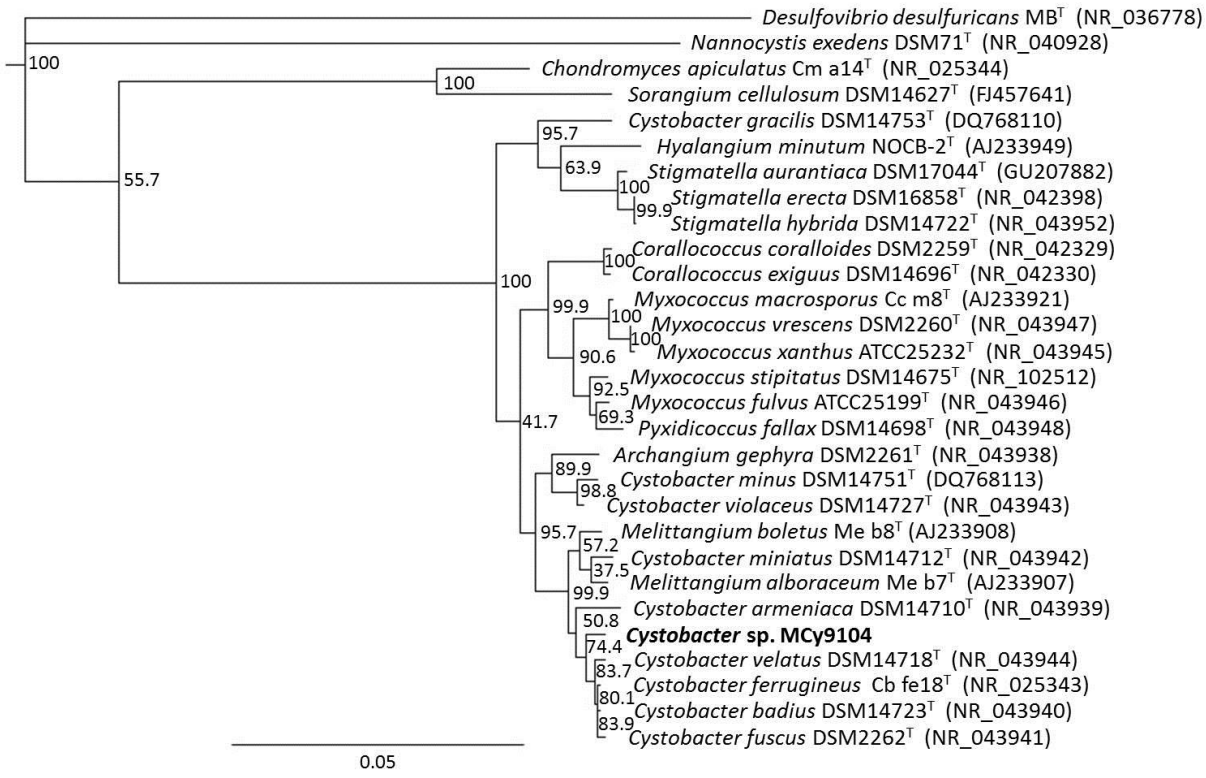

Figure S4.2 Neighbor-joining tree of myxobacteria based on 16S rRNA gene sequences showing the position of *Cystobacter* sp. MCy9104 (bold) in suborder *Cystobacterineae*. Values at the branch points represent the bootstrap support based on 1000 resamplings. *Desulfovibrio desulfuricans* strain MBT was used as an outgroup to root the tree. GenBank accession number of the 16S rRNA gene sequence is shown in parenthesis. Bar, 0.05 nucleotide substitution per site.

Table S4.5 NMR spectroscopic data for cystochromone F (6)

pos	δ_C,[a] type	δ_H[b] (J in Hz)	HMBC[c]	COSY[d]	TOCSY[f]	ROESY[g]
2	167.4, C					
3	112.7, CH	6.13, s	2, 3', 4, 5, 10			2', 3'b
4	181.3, C					
5	148.2, C					
6	118.0, CH	6.88, d (2.3)	1", 4, 7, 8, 10		8	1"', 1", 2"
7	160.6, C					
8	102.7, CH	7.07, d (2.3)	6, 7, 9, 10		6	1"'
9	160.2, C					
10	116.9, C					
1'	23.4, CH_3	1.28, d (6.3)	2', 3'	2'	2', 3'a, 3'b	
2'	66.2, CH	4.21, m	1', 2, 3'	1', 3'a, 3'b	1', 3'a, 3'b	
3'a	44.0, CH_2	2.68, dd (7.9, 14.3)	1', 2', 2, 3	2', 3'b	1', 2'	3
3'b		2.75, dd (4.9, 14.3)	1', 2', 2, 3	2', 3'a	1', 2'	3
1"	36.0, CH_2	3.20, m	2", 3", 5, 6, 10	2"	2", 3", 4", 5"	6
2"	32.3, CH_2	1.58, m	1"	1", 3"	1", 3", 4", 5"	6
3"	30.0, CH_2	1.40, m	1"	2", 4"	1", 2", 4", 5"	
4"	24.5, CH_2	1.60, m	5", 6"	3", 5"	1", 2", 3", 5"	
5"	43.3, CH_2	2.46, t (7.44)	3", 4", 6"	4"	1", 2", 3", 4"	
6"	214.3, C					
7"	43.3, CH_2	2.44, t (7.46)	6", 8"	8"	8", 9"	
8"	24.6, CH_2	1.55, m	6", 7"	7", 9"	7", 9"	
9"	30.1, CH_2	1.30, m	7"	8"	7", 8"	
10"-12"	29.8-31.0, CH_2	1.28-1.35, m	[e]	[e]	[e]	
13"	44.5, CH_2	1.44, m	14", 15"/16"	[e]		
14"	71.3, C					
15"/16"	29.0, CH_3	1.16, s	13", 14", 15"/16"			
1"'	99.3, CH	5.57, d (1.7)	3"', 5"', 7	2"'	2"'	6, 8,
2"'	71.6, CH	4.03, dd (1.8, 3.3)	1"', 3"', 4"'	1"', 3"'	1"', 3"', 4"', 5"', 6"'	3"'
3"'	72.0, CH	3.84, dd (3.3, 9.4)	2"', 4"', 5"'	2"', 4"'	2"', 4"', 5"', 6"'	2"', 5"'
4"'	73.5, CH	3.47, t (9.4)	2"', 3"', 5"', 6"'	3"', 5"'	2"', 3"', 5"', 6"'	6"'
5"'	71.1, CH	3.57, m	1"', 3"', 4"', 6"'	4"', 6"'	2"', 3"', 4"', 6"'	3"'
6"'	18.0, CH_3	1.24, d (6.4)	4"', 5"'	5"'	2"', 3"', 4"', 5"'	4"'

[a]acquired at 125 MHz, referenced to solvent signal $MeOD_4$ at δ 49.15 ppm. [b]acquired at 500 MHz, referenced to solvent signal $MeOD_4$ at δ 3.31 ppm. [c]proton showing HMBC correlation to indicated carbons. [d]proton showing COSY correlations to indicated protons. [e]overlapped signals [f]proton showing TOCSY correlations to indicated protons. [g]proton showing ROESY correlations to indicated protons.

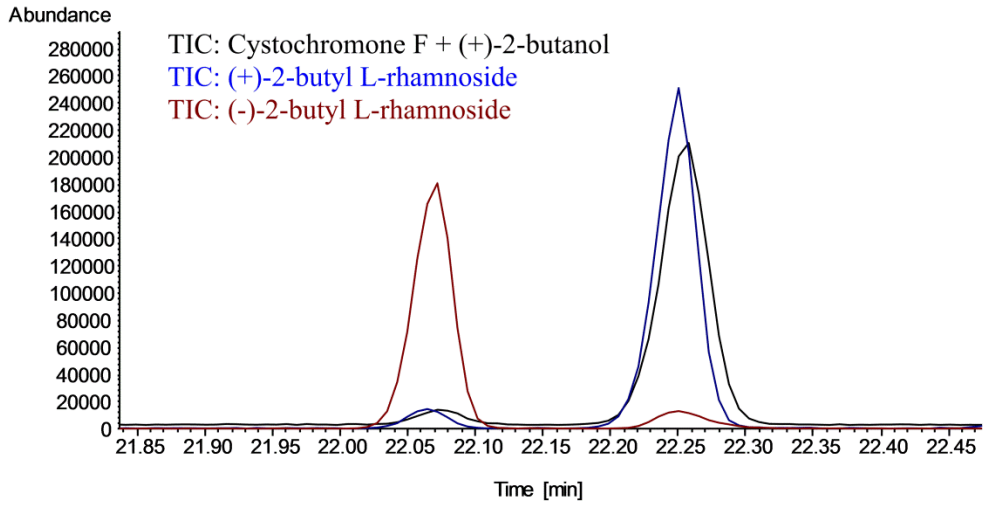

Figure S4.3 Overlapped GC-MS chromatogram of trimethylsilylated derivatives of (+)-2-butyl – rhamnoside of cystochromone F (**6**), and authentic (+)-2- and (-)-2-butyl –L-rhamnoside

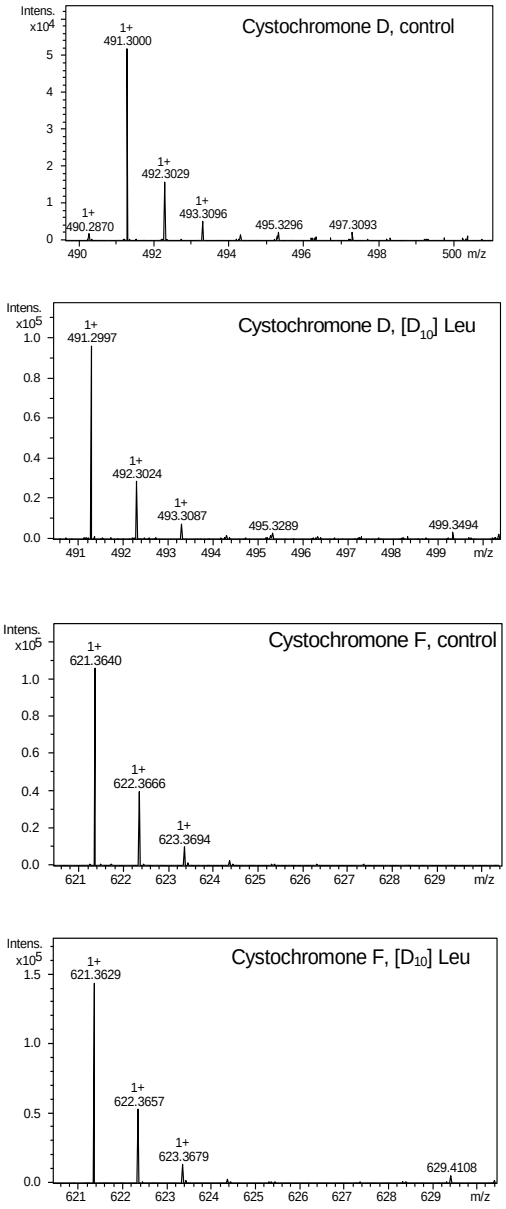

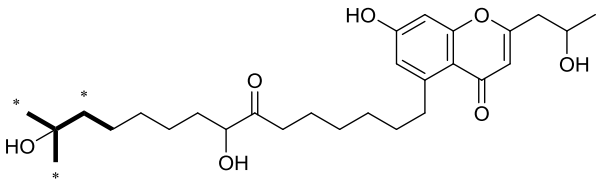

Cystochromone D (4)

Control: $[M+H]^+$ $C_{28}H_{43}O_7$
Exact Mass: Calcd - 491.3003
Measd - 491.3000

$[D_{10}]$ Leu fed:
(D_8 incorporated) $[M+H]^+$ $C_{28}H_{35}D_8O_7$
Exact Mass: Calcd - 499.3505
Measd - 499.3494

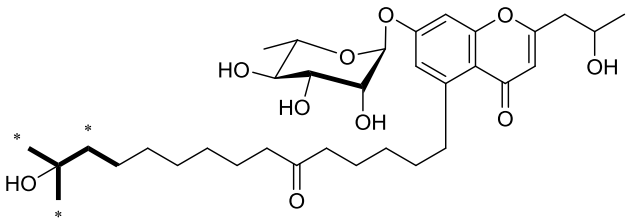

Cystochromone F (6)

Control: $[M+H]^+$ $C_{34}H_{53}O_{10}$
Exact Mass: Calcd - 621.3639
Measd - 621.3640

$[D_{10}]$ Leu fed:
(D_8 incorporated) $[M+H]^+$ $C_{34}H_{45}D_8O_{10}$
Exact Mass: Calcd - 629.4135
Measd - 629.4108

Figure S4.4 HR-ESI isotopic peak pattern of cystochromone D (**4**) and F (**6**) indicating the incorporation of labeled leucine. Observed mass shift suggested the incorporation of eight deuterium atoms, due to the transamination of leucine to $[D_9]$-α-ketoisocaproic acid and oxidation at C-14".

Table S4.6 NMR spectroscopic data for di-(*S*)-MTPA ester of 4a

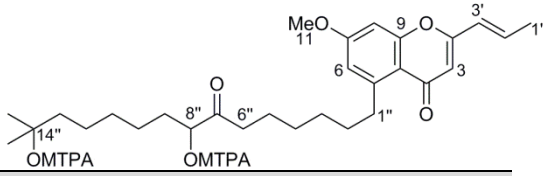

pos	δ_C,[a] type	δ_H[b] (*J* in Hz)	HMBC[c]	COSY[d]
2	161.9, C			
3	110.1, CH	6.04, s	2, 3', 4	
4	181.5, C			
5	148.0, C			
6	117.0, CH	6.75, d (2.3)	1"	
7	164.6, C			
8	99.6, CH	6.93, d (2.3)	4, 7, 9	
9	161.8, C			
10	116.0, C			
11	56.2, CH_3	3.90, s	7	
1'	18.5, CH_3	1.98, m	2', 3'	2'
2'	137.7, CH	6.91, m	1', 2	1', 3'
3'	124.3, CH	6.28, m	1', 2	2'
1"	35.9, CH_2	3.18, t (7.5)	2", 5, 10	2"
2"	32.4, CH_2	1.56, m		
3"-4"	30.3-30.7, CH_2	1.31-1.40, m	*f*	*f*
5"	24.0, CH_2	1.58/1.62*, m		6"
6"	39.0, CH_2	2.38/2.53*, m	7"	5"
7"	206.9, C			
8"	81.0, CH	5.22/5.24*, m	9"	9"
9"	30.0, CH_2	1.68/1.76*; 1.82*, m		8"
10"-13"	*e*	*e*		
14"	87.5, C			
15"/16"	25.8, CH_3	1.51, s	14"	

[a]acquired at 175 MHz, referenced to solvent signal $MeOD_4$ at δ 49.15 ppm. [b]acquired at 700 MHz, referenced to solvent signal $MeOD_4$ at δ 3.31 ppm. [c]proton showing HMBC correlation to indicated carbons. [d]proton showing COSY correlation to indicated protons. [e]not observed [f]overlapped signals. [*]second split signals

5. Discussions

5.1. General Scope of the Work

The overall goal of this thesis was to discover novel secondary metabolites from myxobacteria. In this regard, chemical screening has been performed on the extract of a number of myxobacterial strains including the ones possessing bioactivity, novel strain isolates as well as the underexplored ones. As a result, three strains MSr9139, MCy9135 and MCy9104 were chosen due to the presence of novel metabolites in their respective extracts.

In particular, chemical analyses of the myxobacterial strains MCy9135 and MSr9139 belonging to underexplored species *H. minutum* and *Jahnella* sp., respectively, was performed by hyphenated techniques. LC-MS/SPE-NMR based dereplication of these strains suggested the presence of novel structures at an early stage of the isolation period, which were further isolated and characterized as new metabolites hyalachelins and a new derivative of marine-derived microsclerodermin, respectively. Furthermore, the existence of a family of new compounds, cystochromones, in the crude extract of the *Cystobacter* sp. MCy9104 was revealed by using standard LC-MS screening method combined with the myxobacterial compound database "Myxobase".

Column chromatographies as well as semi-preparative and preparative HPLC coupled with MS were the main tools to perform the purification of target metabolites. Although the final yield of the studied compounds were most of the case very low, the use of high field NMR spectrometer equipped with a cryogenically cooled probe allowed to acquire full 2D-NMR data with small amounts of material (<1 mg). On the basis of comprehensive NMR data, the structures were elucidated and further supported by HR-MS/MS fragmentation experiments. Moreover, the biosynthetic precursors of cystochromones have been studied by feeding experiments with D- and ^{13}C-labeled precursors.

5.2. Microsclerodermins – Marine Natural Products Rediscovered from Terrestrial Myxobacteria

The methanol crude extract of strain MSr9139 *Jahnella* sp., showing potent antifungal activity, was analyzed by LC-MS/SPE-NMR coupled with bioactivity guided fractionation (Figure 1.7). Strong bioactivity against *Candida albicans* was traced to cyclic peptides pedein A,[1] microsclerodermin D,[2] and its new derivative, termed microsclerodermin L.

Microsclerodermins are cyclic peptides bearing characteristic chlorinated tryptophan, complex β-amino acid (3-amino-8-phenyl-2,4,5-trihydroxy-oct-7-enoic acid (APTO) as in microsclerodermin D and L) and unusual pyrrolidone moiety.[3] 1D and 2D NMR data of microsclerodermin L were closely resembled to that of microsclerodermin D, possessing additional methoxy functionality located on C-39. (Figure 5.1, Table S2.2) Relative and absolute stereochemical configurations were analyzed for the myxobacterial isolates by applying the previously utilized methods reported for other microsclerodermins[3] (chemical degradations followed by Marfey analysis and acetonide formation followed by ROE analysis) and the result revealed the same configurations as the known marine microsclerodermins. Microsclerodermins differ in their substitution of the β-amino acid, modifications of the tryptophan moiety and oxidation state of the pyrrolidone ring.

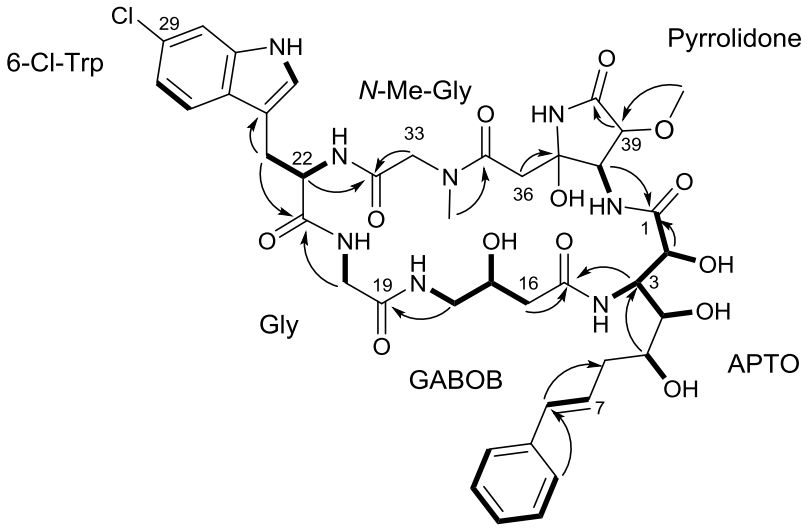

Figure 5.1 Key HMBC (arrow) and COSY (bold line) correlations of new derivative microsclerodermin L

Microsclerodermins were originally reported from the lithistid marine sponges *Microscleroderma* and *Theonella*, which are known to be excellent sources of a variety of natural products. The structural analogues, the pedeins, were discovered in parallel from the terrestrial myxobacterium *Chondromyces pediculatus*, suggesting that the biosynthetic origin of these antifungal natural compounds could be bacterial sponge symbionts.[1] Furthermore, the biosynthesis of microsclerodermin was studied by a retro-biosynthetic approach (investigated by co-authors Dr. T. Hoffmann and S. Müller) in the genome of *Jahnella* sp. strain MSr9139 and *Sorangium cellulosum* So ce38, which provided the access to the biosynthesis of the marine natural product.

There are a number of examples where marine sponge-derived natural products exhibit structural similarity to terrestrial myxobacterial compounds. For instance, the macrolide apicularen produced by *Chondromyces* sp.[4] is closely related to the marine sponge isolate salicylihalamide.[5] Moreover, renieramycin and its analogue saframycin MX1 were discovered from a *Reniera* sponge[6] and a

myxobacterium of the genus *Myxococcus*.[7] (Figure 5.2) Another noticeable example is the investigation of bengamide E, which was isolated from both terrestrial myxobacterium *Myxococcus virescens*[8] and sponge *Jaspis coriacea*.[9] Even though it is very rare to find an example demonstrating that bacterial symbiont is the real producer of the sponge-derived compounds.[10]

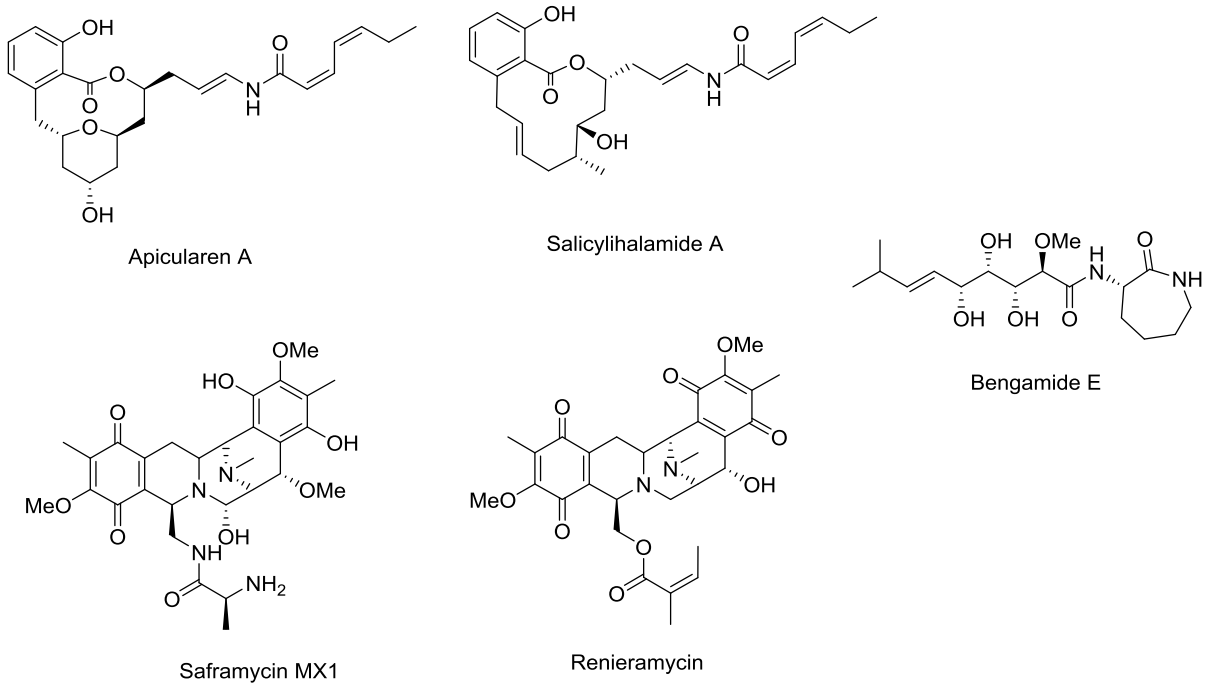

Figure 5.2 Analogues isolated in parallel from marine sponges and terrestrial myxobacteria

Furthermore, unexplored *Jahnella* sp. belongs to the myxobacterial family *Polyangiaceae*, which is known as the source of many remarkable secondary metabolites.[11] Further chemical studies of *Jahnella* sp. has resulted in a family of linear peptides (Drs. A. Plaza, T. Klefisch and Prof. R. Müller, unpublished data) together with the novel cyclic peptides jahnellamides A and B that contain an α-keto-β-methionine residue.[12]

Although a discovery of exactly the same compound from both marine sponge and terrestrial habitats is quite uncommon, our findings reinforce the theory that bacterial symbionts indeed are the producer of diverse sponge metabolites. Discovery of marine sponge derived microsclerodermins from terrestrial myxobacteria provides alternative sources for these powerful antifungal molecules. Accessibility to a sustainable microbial producer allows performing further biotechnological development such as production optimization and structural modification towards therapeutic application.

5.3. Unusual Catecholate type Siderophores – Hyalachelins

The *Hyalangium* is an underexplored myxobacterial genus and so far two groups of bioactive natural products have been isolated. Hyaladione, a chlorinated cyclic hexadiene derivative, was isolated via bioactivity guided fractionation approach using *S. aureus* as indicator strain and shows significant antibacterial activity.[13] A family of polyketides bearing either furanone (hyafurones), pyrroline (hyapyrrolines), or pyrone rings (hyapyrones) was isolated from the type strain *H. minutum* NOCB-2^T and show slight antibacterial activity.[14] (Figure 5.3, A)

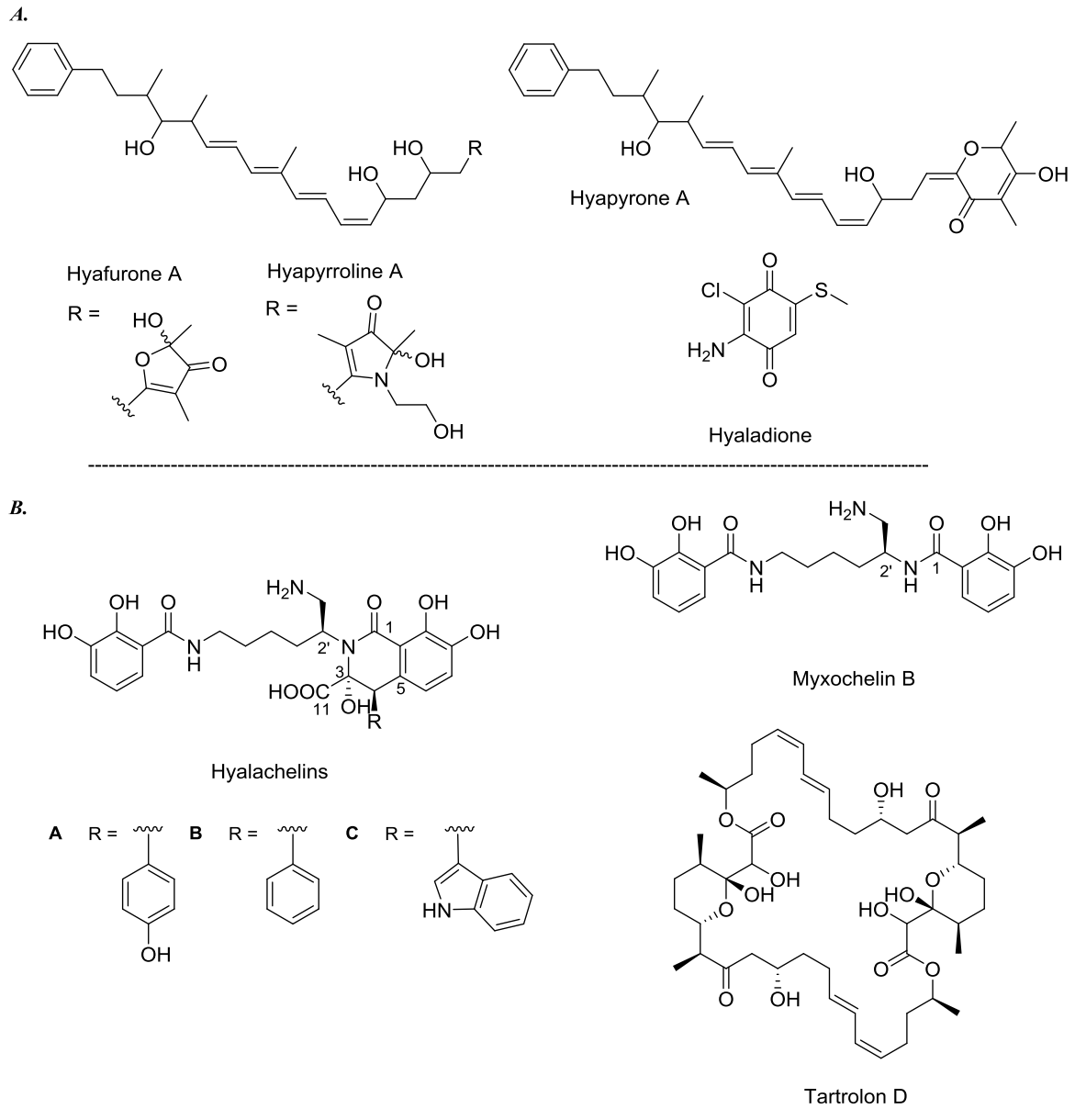

Figure 5.3 Secondary metabolites produced by *H. minutum* A) isolated from the type strain NOCB-2^T and B) identified from the strain MCy9135

During further study of this genus aimed at the discovery of novel metabolites, the strain MCy9135 was investigated since the preliminary bioactivity screening exhibited antibacterial activity against Gram-positive organisms. The strain MCy9135 was isolated in 2008 (by Dr. R. Garcia) from a soil sample collected in Xiamen, China. Its 16S rDNA analysis revealed it to be phenotypically and phylogenetically related to the unexplored species *H. minutum*. The strain was fermented and chemical composition of the extract was assessed using LC-MS coupled with SPE-NMR. Subsequently, the result allowed determining the presence of three new metabolites hyalachelins A-C together with the known compounds hyafurones, myxochelin B and tartrolon D. (Figure 5.3, B) As a consequence of stepwise chromatographic fractionations, the latter one was linked to the antibacterial activity of the crude extract.[15]

Isolation of new metabolites has been performed from water/acetone crude extract of both adsorber resin XAD-16 and cell mass. Preparative LC-MS was employed for the initial fractionation which facilitated the rapid collection of target compounds according to online mass detection. Target enriched fractions were subsequently subjected to semi-preparative HPLC as final purification step which yielded the pure hyalachelins. Planar structures were elucidated by means of 1D- and 2D-NMR data together with high resolution ESI^+-MS/MS fragmentation experiments.

Hyalachelins are characterized by possessing an unusual isoquinoline ring bearing an oxo group at C-1 and α-hydroxy acid at C-3, altogether forming unprecedented unit 3,7,8-trihydroxy-1-oxo-1,2,3,4-tetrahydroisoquinoline-3-carboxylic acid. They differ in their side chain either bearing phenyl, phenol or indol rings. (Figure 5.3, B)

Due to the absence of useful proton in the structure which could show diagnostic NOE correlation with H-4 (for the assignment of the relative configuration at C-3 and C-4) and low yield of isolated compounds, full elucidation of the stereochemical configuration was carried out by collaborators Dr. G. Lauro and Prof. G. Bifulco (University of Salerno, Italy) using quantum mechanical (QM) calculation of NMR parameters and CD spectra.[16] [17]

The NMR chemical shifts provide valuable information regarding the structure of the molecule. Despite the planar structure elucidation, the relative configuration of the molecule under examination is predicted by means of chemical shifts. Based on this, universal NMR database has been developed for the assignment of relative configuration.[18] Besides this, theoretical NMR parameters (^{13}C, ^{1}H chemical shifts and *J*-coupling values) can be readily obtained by QM calculation of all possible stereoisomers.[17] Subsequent comparison to the experimental data suggests the relative configuration for the compound under examination. Significant computational developments on QM calculations brought this approach more applicable by consuming less time and resulting more accurate data.[16] This widely applied method was used for the determination of relative configuration of hyalachelin B

in the laboratory of Prof. Bifulco. Both calculated chemical shifts and $^{3}J_{C3\text{-}H4}$ value of isomer 2'*S**,3*S**,4*R** were obtained with significant lowest mean absolute error (MAE) values, thus the relative configuration of hyalachelin B was assigned as 2'*S**,3*S**,4*R**.

Comparison of calculated and experimentally obtained CD spectra is an excellent tool for the assignment of absolute configuration and it is being used extensively for many complex natural compounds. Since the chiroptical behavior of a chiral compound depends on the spatial orientation of its chromophoric group, the CD spectrum is conformation dependent and clearly demonstrates the absolute configuration of chiral molecule.[19] Accordingly, the Boltzmann-weighted CD spectra were calculated for all possible stereoisomers of hyalachelin B (2'*S*,3*R*,4*R;* 2'*S*,3*S*,4*R;* 2'*S*,3*R*,4*S* and 2'*S*,3*S*,4*S*) and their enantiomers after optimization of the minimum energy conformers. Direct comparison demonstrated the CD curve of isomer 2'*S*,3*S*,4*R* closely fits to the experimental one and suggested the absolute configuration as 2'*S*,3*S*,4*R* (Figure 3.5). Moreover, the absolute configuration of structurally related myxochelin was determined as *S* on C-2'[20] thus further supports our findings. In contrast, calculated CD spectra of other isomers showed no significant similarity as depicted in Figure S3.5.

High structural resemblance of the hyalachelins to that of myxochelin possessing even same absolute configuration implied they might have common biosynthetic pathways. The structure of hyalachelins suggested that they could be formed from myxochelin by incorporation of tyrosine, phenylalanine or tryptophan. Hypothetically this amino acid incorporation occurred from a series of biochemical reactions, such as transamination to eliminate the amino group from the incorporated amino acid, hydroxylation on its α position and unusual C-C bond formation between C-4 and C-5 of hyalachelins (Figure 5.4). Another possible biosynthetic pathway for hyalachelins is that they are assembled from a distinct gene cluster than myxochelin showing high similarity to the one of myxochelin. The gene cluster for hyalachelin should contain additional genes that are responsible for incorporation of the aromatic amino acids and carry out the above mentioned biochemical reactions.

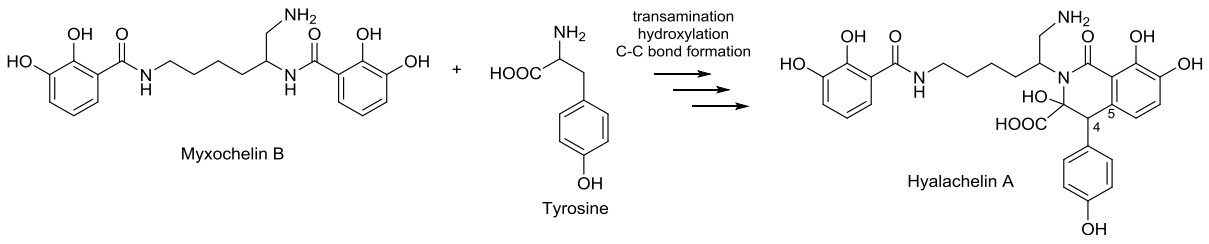

Figure 5.4 Postulated biosynthesis of hyalachelin A generated from myxochelin B

However, the challenging issue of the hyalachelin project was their very low final titer (15-30 μg/L). Various experiments were performed towards the yield enhancement, including different growth

media, production MD1G medium with various concentrations of ingredients as well as different cultivation flasks (baffled and normal glass Erlenmeyer flasks as well as plastic cultivation bottles). Highest production was observed in the plastic cultivation bottle Ultra Yield Flask™ (Thomson Instrument Company, USA) in which the cell grows in suspension and with higher velocity in comparison to the glass flasks (data not shown). Observation of higher yield might be related to the chelating property of hyalachelins because their production is regulated by the present iron amount and the normal glass wares contain glass-bound iron.

Thus, it was assumed that iron-limiting conditions could lead to an improved hyalachelin yield. In order to create such appropriate conditions, various experiments were performed by treating the growth medium with Chelex 100 resin beads or washing the cultivation flask with Chelex before usage. Unfortunately, no cell growth was observed under resin treated condition suggesting that the Chelex removed most of the iron and the remaining iron in the medium is insufficient for the growth. Therefore, $FeCl_3$ (5-200 μM) was added to the Chelex treated medium and LC-MS data showed no production enhancement.

Once the growth conditions were optimized, the cultivation was performed 16 times in 12 Ultra Yield Flask™ bottles each contained 800 mL production media to accumulate enough amount of pure compounds. During the purification procedure, it was found out that the hyalachelins were unstable when exposed to light. Assumingly, it might happen due to the presence of unstable and highly reactive hemi-aminal functionality which could lead to the opening of the isoquinoline ring.

There are over 500 different siderophores, of which 270 have been structurally characterised.[21] This promising group of compounds shows diverse important biological activities in clinical use as mentioned before (Chapter 1.2.2). The identification of the new unusual siderophore hyalachelins is another contribution to this intriguing class of molecules. The uncommon structural feature of hyalachelins is the multisubstituted isoquinoline ring which is not reported from natural products to date. Although, the structurally related catecholate type myxochelin occurs often in many myxobacteria,[22] [23] [24] the more complex hyalachelins were described for the first time in current study from the underexplored species *H. minutum*. Discovery of this new siderophores also demonstrates the biosynthetic capability of myxobacteria is being exploited to produce unusual novel natural compounds.

5.4. Cystochromones - Structures and Insights into the Biosynthesis

The genus *Cystobacter* is well-known among myxobacteria for its biosynthetic potential producing diverse bioactive secondary metabolites such as the protein synthesis inhibitor althiomycin,[25] the potent antifungal metabolite melithiazol,[26] and the antibiotic roimatacene active against Gram-negative bacteria,[27] as few examples. The strain MCy9104 was isolated in 2006 (by Dr. R. Garcia,

HIPS) from a soil sample collected in Manila, Philippines and is classified as *Cystobacter* sp. on the basis of the morphological and phylogenetic analysis.

In the course of chemical screening of myxobacteria aimed at the discovery of novel metabolites, crude extract of the strain MCy9104 was appealing due to the existence of unknown compounds, whose isolation and characterization are described in the present thesis. Cultivation of the strain in the complex growth medium CLF has triggered the biosynthesis of a family of new metabolites, termed cystochromones. Dereplication of the new compounds has been done by means of the LC-MS data in comparison to the in-house myxobacterial compound database "Myxobase". XAD-16 was used to capture the metabolites from the culture supernatant and subsequent extraction procedure guided by solvent polarity (apolar to polar) led to an enrichment of cystochromones in the ethyl acetate extract. Size exclusion chromatography on Sephadex LH-20 was performed as initial fractionation and cystochromones enriched fractions were further subjected to semi-preparative HPLC to obtain pure metabolites.

Cystochromone A occurred as the main metabolite in the highest titer (ca. 500 μg/L) while the others were produced in much lower yield (ca. 25-60 μg/L). $CDCl_3$ was the proper NMR solvent for most nonpolar cystochromone A, B and F whereas methanol-d_4 was used for the others to acquire good NMR data since they are not soluble in $CDCl_3$. Accordingly, planar structures were elucidated by means of comprehensive NMR data.

The name "cystochromones" was derived by merging the name of the producer strain *Cystobacter* with "chromone" that represents the core scaffold. Chromone C-2 bears either a propan-2-one moiety (cystochromone A-C and G) or its reduced analogue propan-2-ol (cystochromone D-F). C-7 of the chromone ring is substituted with a hydroxyl group in all cystochromones while cystochromone F carries an L-rhamnose residue at this position. C-5 is substituted with various saturated long alkyl chains differing in their oxidation state, and length of the chain (C_{14} – C_{15}). Careful analysis of comprehensive 2D NMR data and tandem HR-MS experiment suggested the oxidation occurred at C-7" and C-8" of cystochromone D, forming 8,14-dihydroxy-14-methylpentadecan-7-one residue while cystochromone F possesses a single oxidation at C-6". (Figure 5.5)

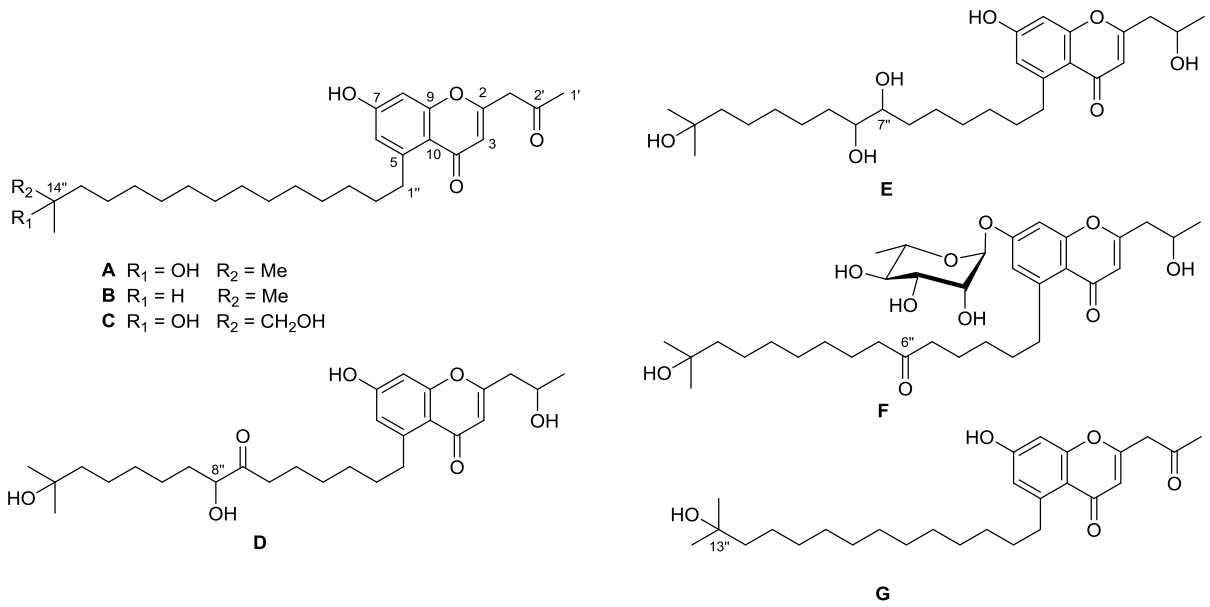

Figure 5.5 Novel metabolites cystochromones A-G isolated from *Cystobacter* sp.

The absolute configuration of the α-rhamnose residue was determined as L from a GC analysis of the (+)-2-butyl derivative in comparison to the one of the authentic sample (Figure S4.3). This was supported by the diagnostic ROESY correlations as shown in Figure 5.6.[28]

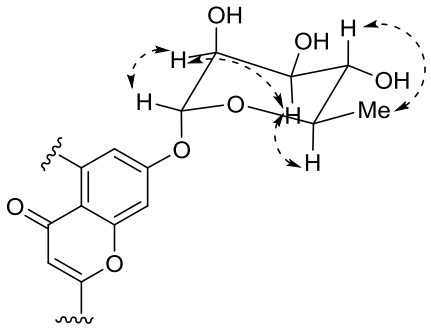

Figure 5.6 ROESY correlations supporting the L configuration of α-rhamnose of cystochromone F

Assignment of the absolute configurations of the secondary alcohols at C-2' and C-8" of cystochromone D was attempted by the modified Mosher's method.[29] The esterification reaction was performed using (*S*)- and (*R*)-MTPA, and LC-MS data revealed the presence of di-MTPA esters instead of expected 2', 8", 14"-tri esters, indicating a elimination of one MTPA residue. Corresponding di-esters were obtained in small amount (<0.1 mg, ca. 30% yield) after the purification by HPLC. The NMR data demonstrated that an MTPA residue was eliminated from C-2' and resulted in a *trans*-$\Delta^{2'}$ unsaturation (Figure 5.7). Therefore it was impossible to determine the configuration at C-2'.

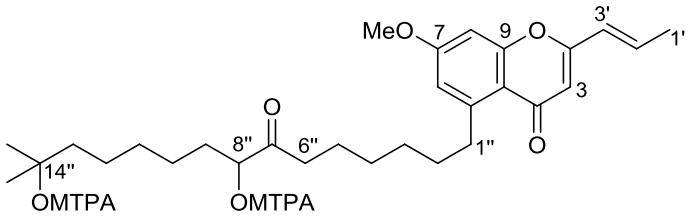

Figure 5.7 8", 14"-di-MTPA ester of cystochromone D

Moreover, NMR data showed the presence of split signals corresponding to the diagnostic protons (H-5" – H-9") that interfered with the absolute configuration assignment of C-8". It was anticipated that this might happen due to the keto-enol tauromerization on C-7"/C-8". Therefore the configuration of C-8" remained elusive. Due to the fact that the cystochromones were obtained in very low yield, the stereochemistry of the secondary alcohols of cystochromones D-E remained unsolved.

To gain insights into the biosynthetic origin of cystochromones, feeding experiments have been carried out with isotopically labeled precursors. Indeed ^{13}C labeled acetate fed experiments have revealed incorporation of intact acetate units for the carbon skeleton of chromone ring including C-1' – C-3' as well as C-1" – C-11". Moreover, LC-MS data of the [D_{10}]leucine fed culture indicated the rest of the molecule C-12" – C-16" was originated from leucine-derived starter unit (Figure 5.8) as seen by mass shift of 8 daltons.

With this data in hand, a biosynthetic pathway for the cystochromones have been proposed (Figure 5.8). Assumingly, a hybrid fatty acid and polyketide synthase (FA/PKS) pathway initiates with transamination of a leucine to the corresponding α-ketoisocaproate which is further converted to isovaleryl-CoA.[30] Furthermore, six elongation steps with malonate take place to generate 15-methylhexadecanoic acid. The latter serves as the starter unit for the second part of the biosynthesis - PKS with malonate as extender.

The resulting polyketide chain is further cyclized/aromatized to generate a 7-hydroxy-chromone ring bearing a 2-methylpentadecane chain at position 5 as well as 3-oxobutanoic acid residue at position 2. Interestingly, the ^{13}C NMR spectrum of cystochromone A derived from $^{13}C_2$ labeled acetate indicated the resonance corresponding to C-1' as singlet, although it was labeled as 2-^{13}C acetate. This finding suggested a decarboxylation from 3-oxobutanoic acid resulting in propan-2-one.

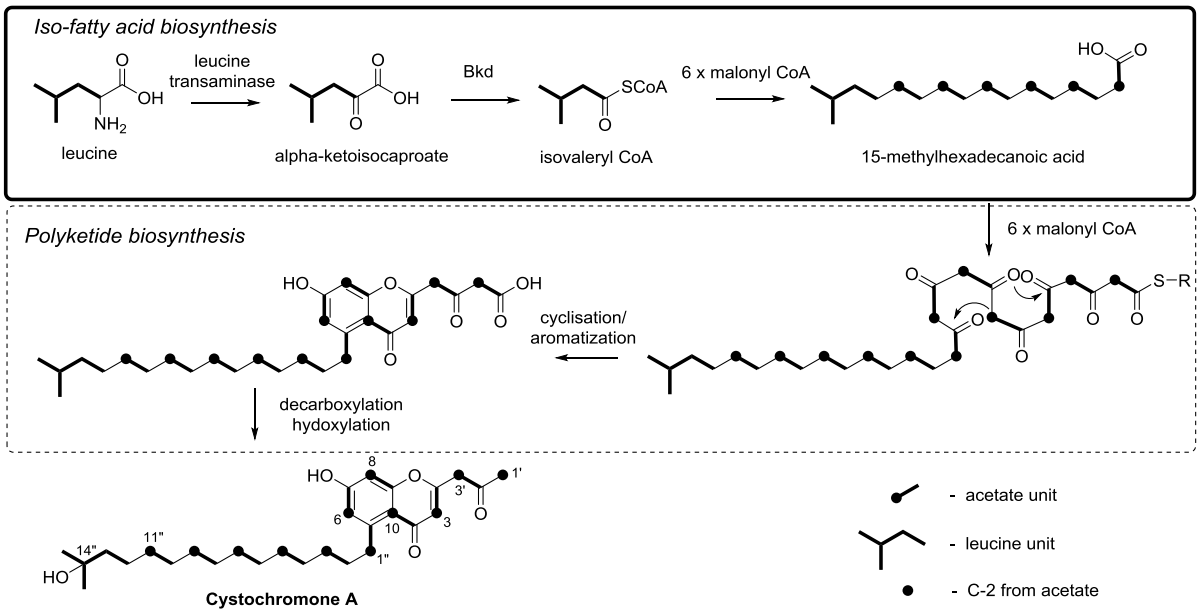

Figure 5.8 Biosynthesis of representative cystochromone A showing the incorporation of intact acetate and leucine precursors. Box with bold line illustrates iso-FA pathway and box with dashed line illustrates PKS

Biosynthesis of an iso-FA resulting from a branched chain amino acid is well known pathway from myxobacteria.[30] [31] Valine, leucine and isoleucine are converted into respective α-keto acids by separate transaminases and then oxidatively decarboxylated by the Bkd complex (branched chain keto acid dehydrogenase), resulting in the coenzyme A esters of isobutyric acid (IBA), isovaleric acid (IVA) and 2-methyl butyric acid (2MBA). These primers are employed in the iso-FA biosynthesis such as the IBA generates iso-even FA and IVA generates iso-odd FA while 2MBA creates ante-iso FA.[32]

The fact that formation of iso-even FAs from the iso-odd FAs occur by α-oxidation[31] suggests that aliphatic chain of cystochromone G (one methylene unit less) could be generated from 15-methylhexadecanoic acid in the early stage of the biosynthesis of cystochromones. However, a "pure" PKS pathway shouldn't be excluded for the biosynthesis of cystochromones.

Various branched amino acid derived iso-FA containing metabolites have been reported from myxobacteria such as the lipopeptide cystomanamides,[33] as well as the antifungal lipopeptide cyrmenins.[34] Moreover, these modified precursors are not only utilized for FA synthesis but many myxobacterial polyketides employ them as starter units, e.g. the electron-transfer chain inhibitors myxothiazols[35] [32] and myxalamids[36] [37] (Figure 5.9).

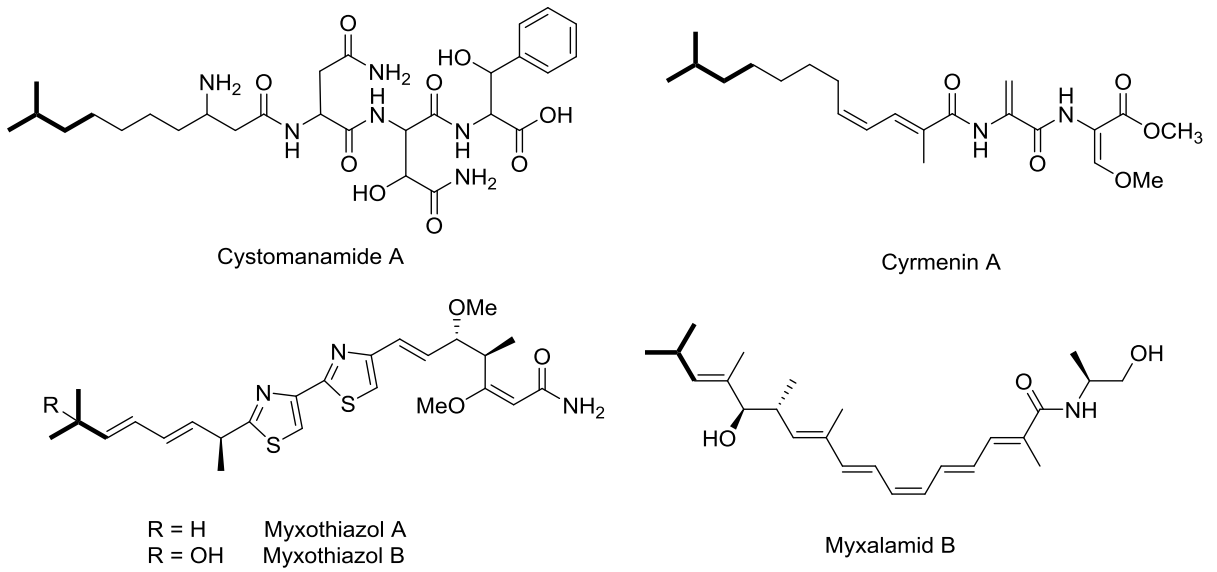

Figure 5.9 Myxobacterial metabolites possessing branched chain FA, bold line indicated the part derived from branched chain amino acid via iso-FA pathway

The most remarkable feature of the cystochromones is the unprecedented substitutional position of the pentadecyl moiety that attached to the C-5 of the chromone ring. Among known chromone ring-bearing molecules, the long chain substitution is usually located on C-2, as observed in myxobacterial stigmatellins.[38] Many other plant derived chromone derivatives have been reported that bear various substitutions on position C-2 of the chromone ring such as aromatic side chain as in aquilarone I from resinous wood of *Aquilaria sinensis*[39] or branched aliphatic chain as in urachromone B isolated from aerial part of *Hypericum henry*.[40] Pestalotiopsones A-F are chromones isolated from Chinese Mangrove plant *Rhizophora mucronata*, having both an alkyl side chain substituted at the C-2 and a free or substituted carboxyl group at the C-5.[41] (Figure 5.10)

On top of that, cystochromone F appears as the first example of a chromone derivative that bears the deoxysugar rhamnose on position C-7 whereas glucose is a common sugar residue found in the chromone family.[42]

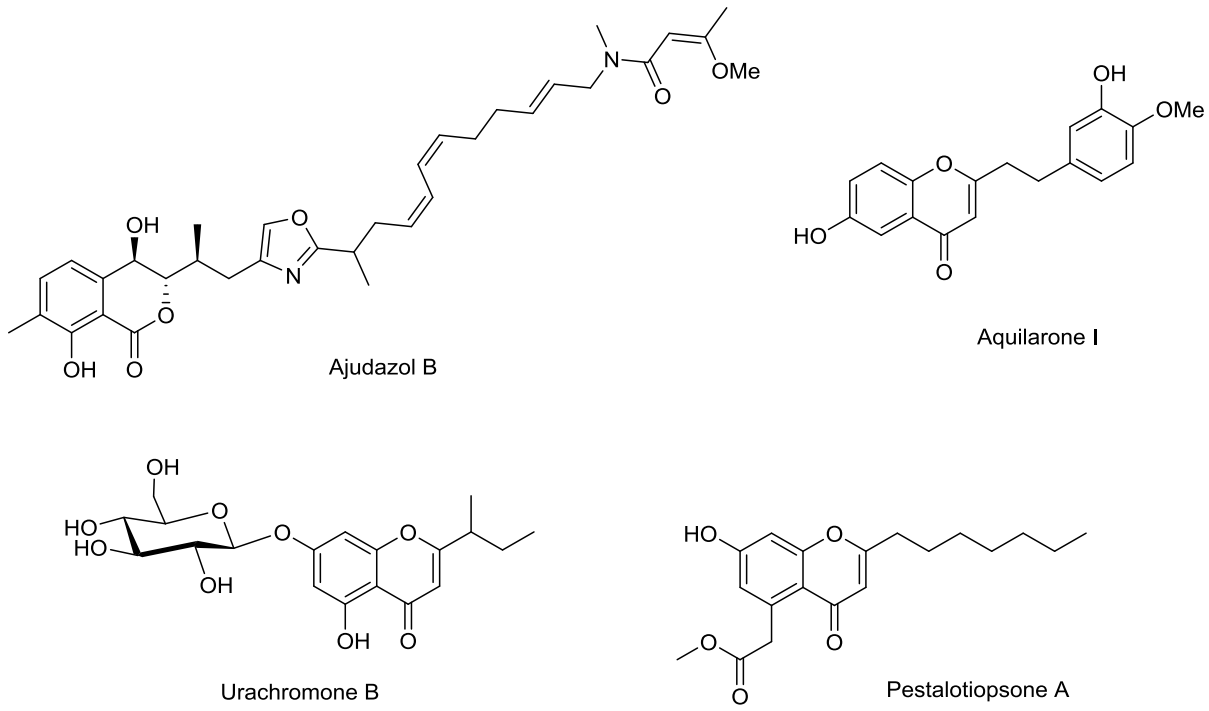

Figure 5.10 Chromone bearing natural products isolated from different bacteria and plants

From the biosynthetic point of view, the intriguing part of the cystochromone structure is the chromone ring. Biosynthesis of the structurally related myxobacterial metabolites, the isochromanone ajudazole[43] (Figure 5.10) and the chromone ring-breaing stigmatellins[44] (Figure 1.3) were intensively investigated. In general, bacterial type III PKS is capable of producing both aromatic and linear structures.[45] [46] Surprisingly, stigmatellin is encoded by an unusual type I PKS, which is generally known to produce non-aromatic compounds.[45] [47] Moreover, the chromone ring of stigmatellin is formed by a novel type of cyclase domain (Cy) located at the end of the assembly line.[38] In the case of ajudazol, the AjuTE domain, a novel class of type I TE, plays a role as the accelerator in the spontaneous formation of the isochromanone ring.[48] Both cyclisation/aromatization seem plausible for the chromone ring formation in the cystochromones. In addition, a type II PKS-like ring closing mechanism[49] should not be excluded and further investigation should be carried out to clarify this intriguing biochemistry.

Bioactivity test evaluation of cystochromone A was performed with different bacteria, fungi and cell lines and no significant inhibition was observed. However, chromone is a powerful core for bioactive secondary metabolites obtained from both plants and microorganisms.[50] Diverse significant therapeutic activities have been attributed to simple chromone ring-bearing molecules and analogues. Among them, anti-inflammatory, anticancer, antibacterial, diuretics and antioxidant activity have been described. Moreover, since the chromone is a promising scaffold for medicinal chemistry, huge effort has been put in synthetic chemistry for drug development against various diseases.[42]

Although the genus *Cystobacter* is rather broadly studied well-known source of diverse natural products, the discovery of cystochromones suggests that the screening of newly isolated strain belonging to "well-studied genus" is worthy for the exploration of novel natural molecules.

Summary

The main achievement of this work was the discovery of two new families of compounds, hyalachelins and cystochromones together with a new derivative of the sponge-derived peptide microsclerodermins from myxobacteria. These results provide another evidence that these gram negative bacteria are warranted sources of novel secondary metabolites and further exploration into myxobacterial natural products has the potential to find new molecules bearing unique chemical structures.

5.5.References

[1] B. Kunze, B. Bohlendorf, H. Reichenbach, G. Höfle, *J. Antibiot.* **2008**, *61*, 18–26.

[2] E. W. Schmidt, D. J. Faulkner, *Tetrahedron.* **1998**, *54*, 3043–3056.

[3] C. A. Bewley, C. Debitus, D. J. Faulkner, *J. Am. Chem. Soc.* **1994**, *116*, 7631–7636.

[4] B. Kunze, R. Jansen, F. Sasse, G. Höfle, H. Reichenbach, *J. Antibiot.* **1998**, *51*, 1075–1080.

[5] K. L. Erickson, J. A. Beutler, J. H. Cardellina, M. R. Boyd, *J. Org. Chem.* **1997**, *62*, 8188–8192.

[6] H. Y. He, D. J. Faulkner, *J. Org. Chem.* **1989**, *54*, 5822–5824.

[7] H. Irschik, W. Trowitzsch-Kienast, K. Gerth, G. Höfle, H. Reichenbach, *J. Antibiot.* **1988**, *41*, 993–998.

[8] T. A. Johnson, J. Sohn, Y. M. Vaske, K. N. White, T. L. Cohen, H. C. Vervoort, K. Tenney, F. A. Valeriote, L. F. Bjeldanes, P. Crews, *Bioorg. Med. Chem.* **2012**, *20*, 4348–4355.

[9] M. Adamczeski, E. Quinoa, P. Crews, *J. Am. Chem. Soc.* **1989**, 111, 647-654.

[10] E. W. Schmidt, A. Y. Obraztsova, S. K. Davidson, D. J. Faulkner, M. G. Haygood, *Marine Biology* **2000**, *136*, 969–977.

[11] R. Garcia, R. Müller in *The Prokaryotes* E. Rosenberg, E. DeLong, S. Lory, E. Stackebrandt, F. Thompson, Eds.; Springer-Verlag: Berlin Heidelberg, **2014**.

[12] A. Plaza, K. Viehrig, R. Garcia, R. Müller, *Organic letters* **2013**, *15*, 5882–5885.

[13] P. W. Okanya, K. I. Mohr, K. Gerth, H. Steinmetz, V. Huch, R. Jansen, R. Müller, *J. Nat. Prod.* **2012**, *75*, 768–770.

[14] P. W. Okanya, K. I. Mohr, K. Gerth, W. Kessler, R. Jansen, M. Stadler, R. Müller, *J. Nat. Prod.* **2014**, *77*, 1420–1429.

[15] H. Irschik, D. Schummer, K. Gerth, G. Höfle, H. Reichenbach, *J. Antibiot.* **1995**, *48*, 26–30.

[16] G. Bifulco, P. Dambruoso, L. Gomez-Paloma, R. Riccio, *Chem. Rev.* **2007**, *107*, 3744–3779.

[17] S. D. Micco, M. G. Chini, R. Riccio, G. Bifulco, *Eur. J. Org. Chem.* **2010**, *8*, 1411-1432.

[18] Y. Kobayashi, C. H. Tan, Y. Kishi, *Angew. Chem. Int. Ed.* **2000**, *39*, 4279.

[19] G. Bringmann, T. Bruhn, K. Maksimenka, Y. Hemberger, *Eur. J. Org. Chem.* **2009**, *17*, 2717-2727.

[20] S. Miyanaga, T. Obata, H. Onaka, T. Fujita, N. Saito, H. Sakurai, I. Saiki, T. Furumai, Y. Igarashi, *J. Antibiot.* **2006**, *59*, 698–703.

[21] R. C. Hider, X. Kong, *Nat. Prod. Rep.* **2010**, *27*, 637–657.

[22] B. Kunze, N. Bedorf, W. Kohl, G. Höfle, H. Reichenbach, *J. Antibiot.* **1989**, *42*, 14–17.

[23] Y. Li, K. J. Weissman, R. Müller, *J. Am. Chem. Soc.* **2008**, *130*, 7554–7555.

[24] B. Silakowski, B. Kunze, G. Nordsiek, H. Blöcker, G. Höfle, R. Müller, *Eur. J. Biochem.* **2000**, *267*, 6476–6485.

[25] B. W. Bycroft, R. Pinchin, *J. Chem. Soc., Chem. Commun.* **1975**, 121–122.

[26] B. Böhlendorf, M. Herrmann, H. J. Hecht, F. Sasse, E. Forche, B. Kunze, H. Reichenbach, G. Höfle, *Eur. J. Org. Chem.* **1999**, *10*, 2601–2608.

[27] W. Zander, K. Gerth, K. l. Mohr, W. Kessler, R. Jansen, R. Müller, *Chem-Eur J* **2011**, *17*, 7875–7881.

[28] B. Ohlendorf, W. Lorenzen, S. Kehraus, A. Krick, H. B. Bode, G. König, *J. Nat. Prod.* **2009**, *72*, 82–86.

[29] T. R. Hoye, C. S. Jeffrey, F. Shao, *Nat. Protoc.* **2007**, *2*, 2451–2458.

[30] H. B. Bode, J. S. Dickschat, R. M. Kroppenstedt, S. Schulz, R. Müller, *J. Am. Chem. Soc.* **2005**, *127*, 532–533.

[31] J. S. Dickschat, H. B. Bode, R. M. Kroppenstedt, R. Müller, S. Schulz, *Org. Biomol. Chem.* **2005**, *3*, 2824–2831.

[32] T. Mahmud, H. B. Bode, B. Silakowski, R. M. Kroppenstedt, M. Xu, S. Nordhoff, G. Höfle, R. Müller, *J. Biol. Chem.* **2002**, *277*, 23768–32774.

[33] L. Etzbach, A. Plaza, R. Garcia, S. Baumann, R. Müller, *Org. Lett.* **2014**, *16*, 2414–2417.

[34] T. Leibold, F. Sasse, H. Reichenbach, G. Höfle, *Eur. J. Org. Chem.* **2004**, *2*, 431–435.

[35] G. Thierbach, H. Reichenbach, *Biochim. Biophys. Acta.* **1981**, *638*, 282–289.

[36] K. Gerth, R. Jansen, G. Reifenstahl, G. Höfle, H. Irschik, B. Kunze, H. Reichenbach, G. Thierbach, *J. Antibiot.* **1983**, *36*, 1150–1156.

[37] B. Silakowski, G. Nordsiek, B. Kunze, H. Blöcker, R. Müller, *Chem. Biol.* **2001**, *8*, 59–69.

[38] N. Gaitatzis, B. Silakowski, B. Kunze, G. Nordsiek, H. Blöcker, G. Höfle, R. Müller, *J. Biol. Chem.* **2002**, *277*, 13082–13090.

[39] D. Chen, Z. Xu, X. Chai, K. Zeng, Y. Jia,D. Bi, Z. Ma, P. Tu, *Eur. J. Org. Chem*. **2012**, *27*, 5389-5397.

[40] X.-Q. Chen, Y. Li, X. Cheng, K. Wang, J. He, Z.-H. Pan, M.-M. Li, L.-Y. Peng, G. Xu, Q.-S. Zhao, *Chem. Biodiversity*. **2010**, *7*, 196-204.

[41] J. Xu, J. Kjer, J. Sendker, V. Wray, H. Guan, R. Edrada, W. Lin, J. Wu, P. Proksch, *J. Nat. Prod.* **2009**, *72*, 662–665.

[42] A. Gaspar, M. J. Matos, J. Garrido, E. Uriarte, F. Borges, *Chem. Rev.* **2014**, *114*, 4960–4992.

[43] B. Kunze, R. Jansen, G. Höfle, H. Reichenbach, *J. Antibiot.* **2004**, *57*, 151–155.

[44] B. Kunze, T. Kemmer, G. Höfle, H. Reichenbach, *J. Antibiot.* **1984**, *37*, 454–461.

[45] D. E. Cane, *Chem. Rev.* **1997,** *7*, 2463-2464.

[46] B. Shen, *Top. Curr. Chem.* **2000**, *209*, 1–51.

[47] J. Staunton, B. Wilkinson in *Topics in Current Chemistry*. A. Meijere, K. Houk, H. Kessler, J. Lehn, S. Ley, S. Schreiber, J. Thiem Eds.; Springer Verlag: Berlin, **1998**.

[48] K. Buntin, K. J. Weissman, R. Müller, *Chem. Bio. Chem.* **2010**, *11*, 1137–1146.

[49] C. Hertweck, A. Luzhetskyy, Y. Rebets, A. Bechthold, *Nat. Prod. Rep.* **2007**, *24*, 162–190.

[50] S. Khadem, R. J. Marles, *Molecules.* **2011**, *17*, 191–206.

Author's Contribution in the Work Presented in this Thesis

Chapter 2

The author carried out the cultivation of the strain MSr9139 and performed the extraction, purification as well as the NMR data acquisition of microsclerodermin D and L. Further the author assigned the structure of microsclerodermins based on the NMR data. The author carried out the cultivation of the strain MSr9139 in the presence of various halogenated salts and analyzed the corresponding LC-MS data.

Chapter 3

The author involved in the LC-NMR screening of the strain MCy9135 and dereplication process. Further the author performed the cultivation of the strain, isolated the hyalachelins and acquired the NMR data. The author elucidated the planar structures of hyalachelins and performed the CAS assay.

Chapter 4

The author performed the screening of the strain MCy9104, cultivation in production medium, planned the strategy of the purification and isolated the cystochromones. The author acquired the NMR data, elucidated the structures and carried out the Mosher analysis as well as methoxylation reaction. Further, the author performed the feeding experiment and analyzed the LC-MS and ^{13}C-NMR data.

6. Appendix

6.1. Microsclerodermins

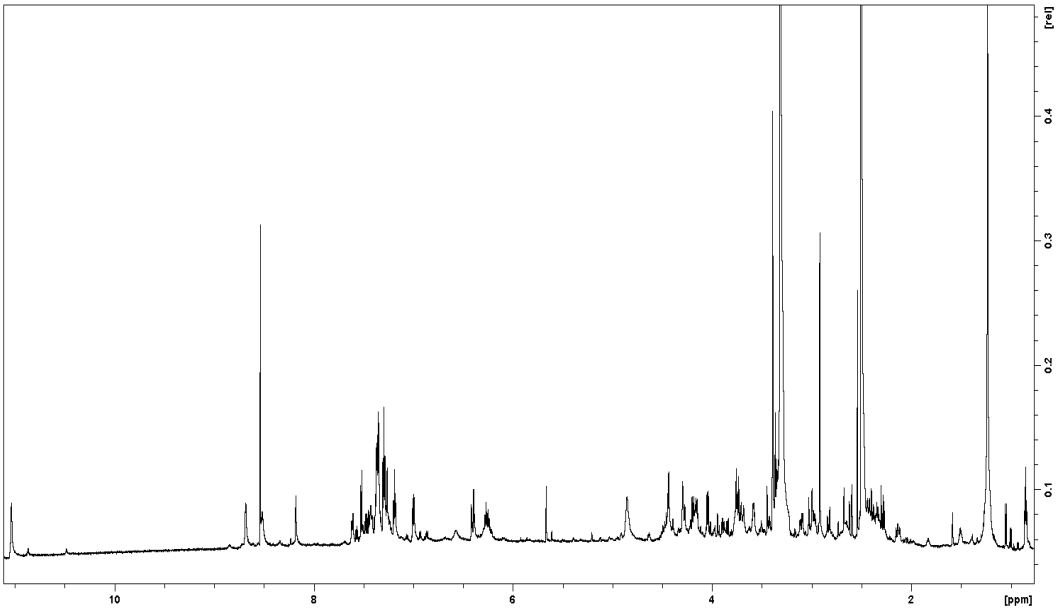

^{1}H NMR spectrum of microsclerodermin L in DMSO-d_6

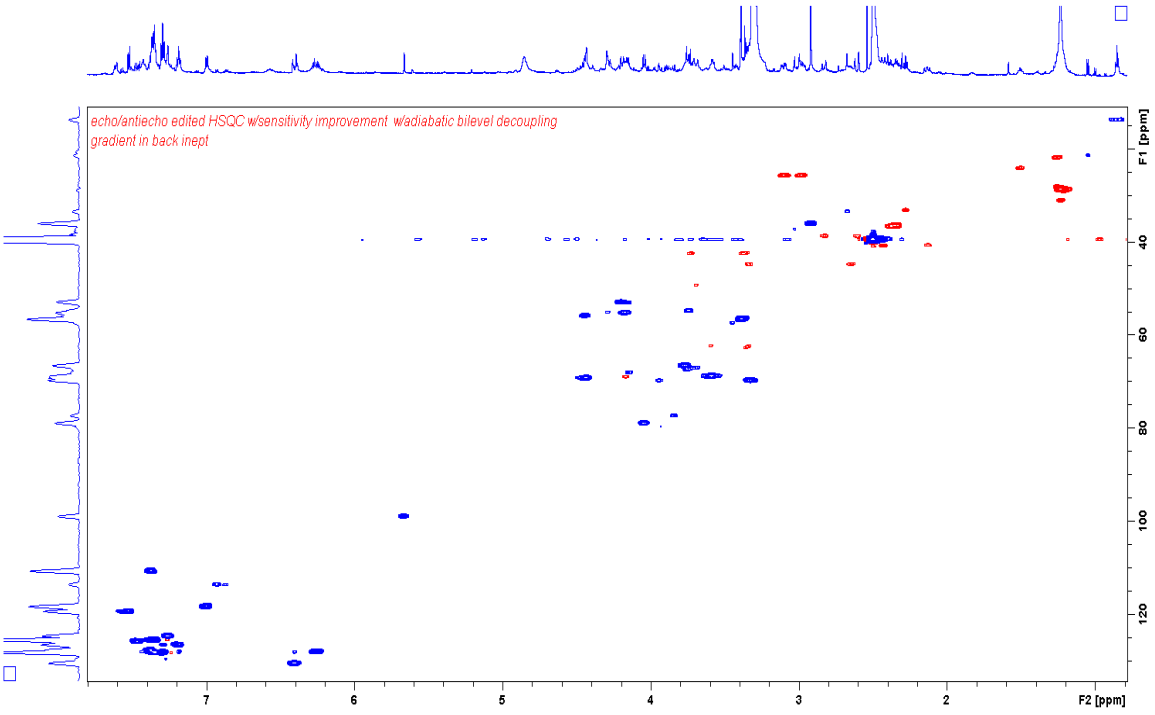

HSQC spectrum of microsclerodermin L in DMSO-d_6

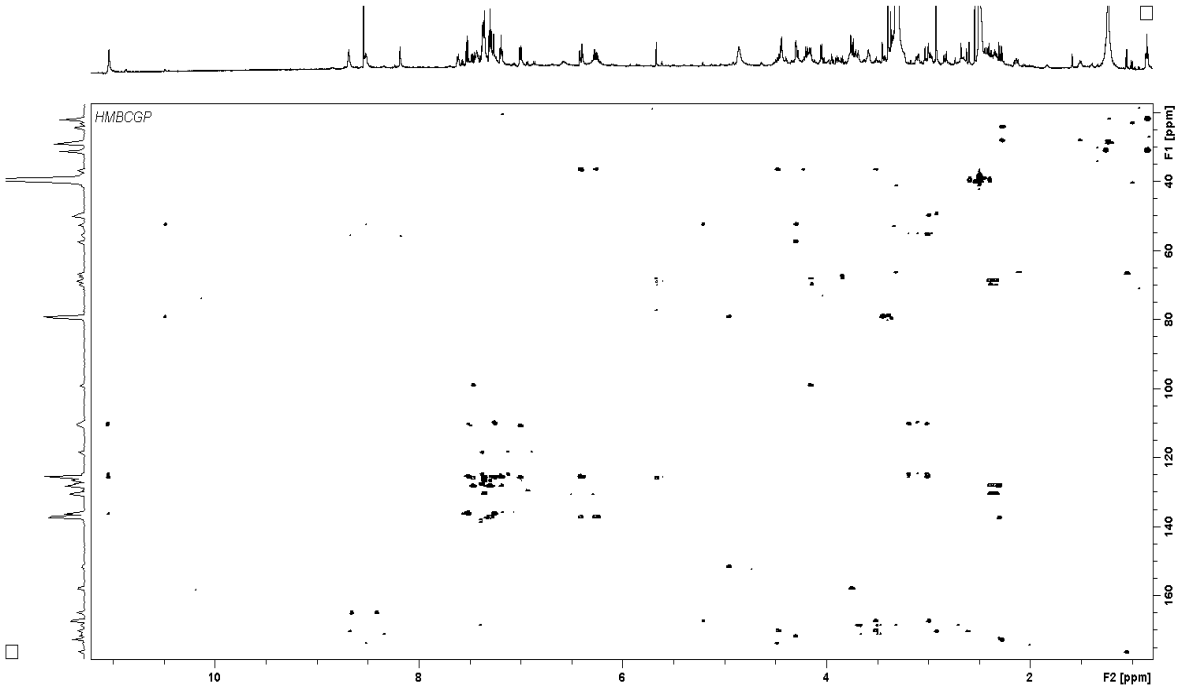

HMBC spectrum of microsclerodermin L in DMSO-d_6

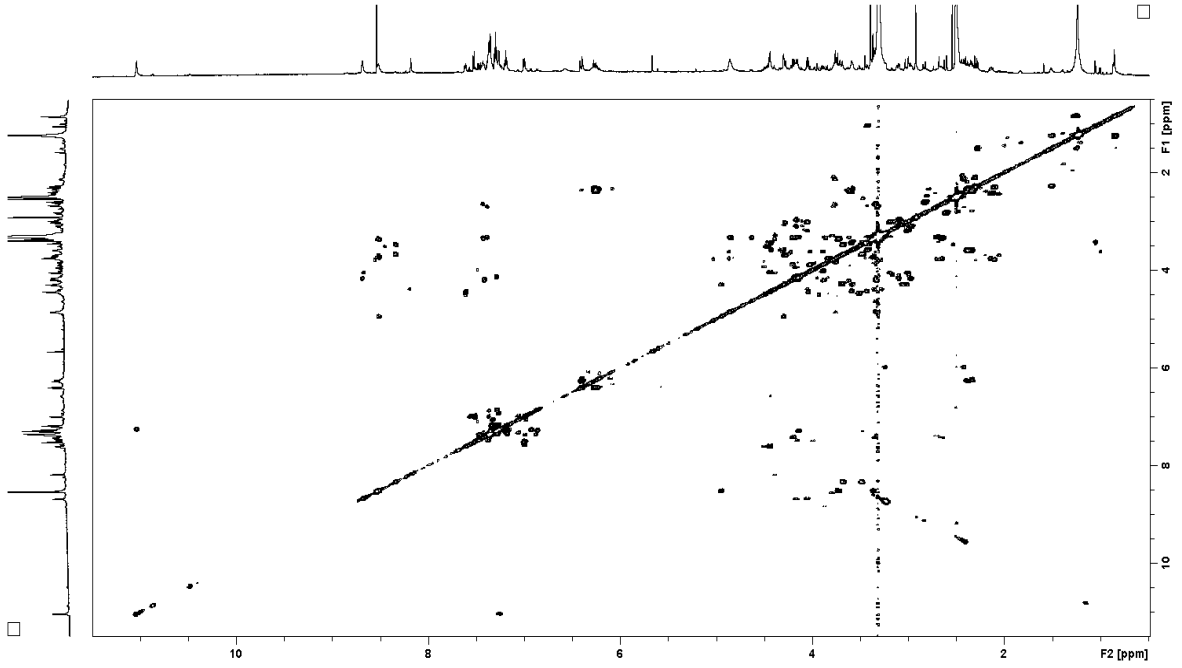

COSY spectrum of microsclerodermin L in DMSO-d_6

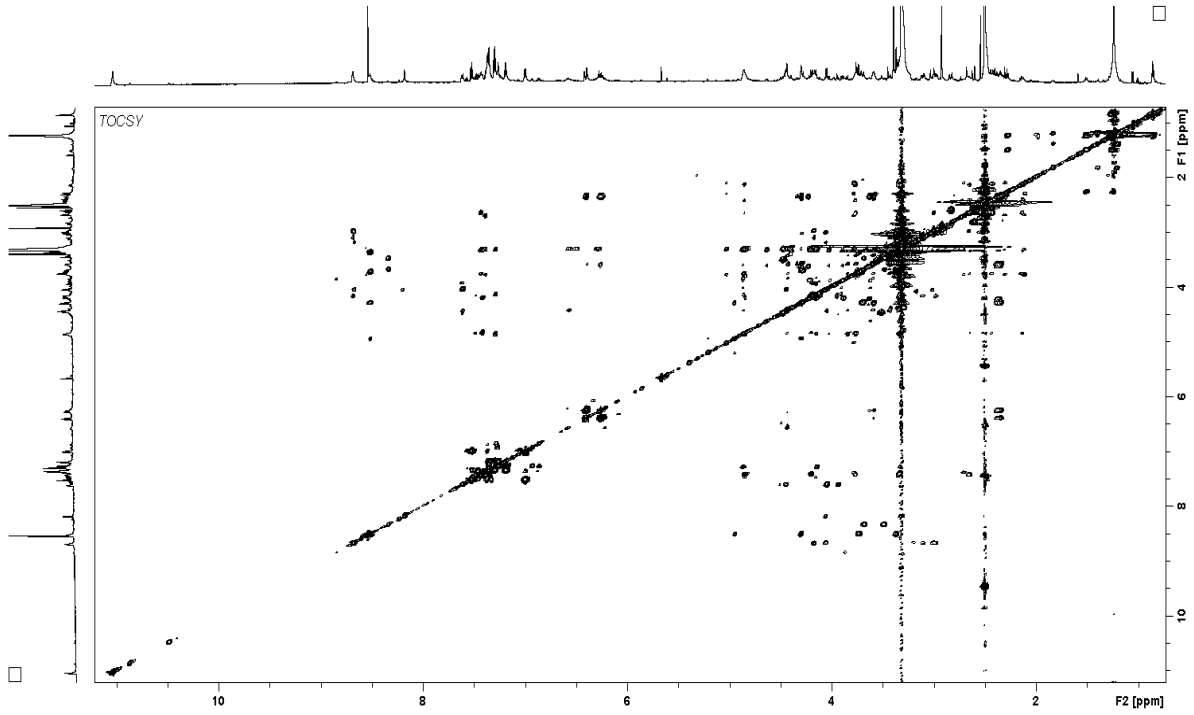

2D TOCSY spectrum of microsclerodermin L in DMSO-d_6

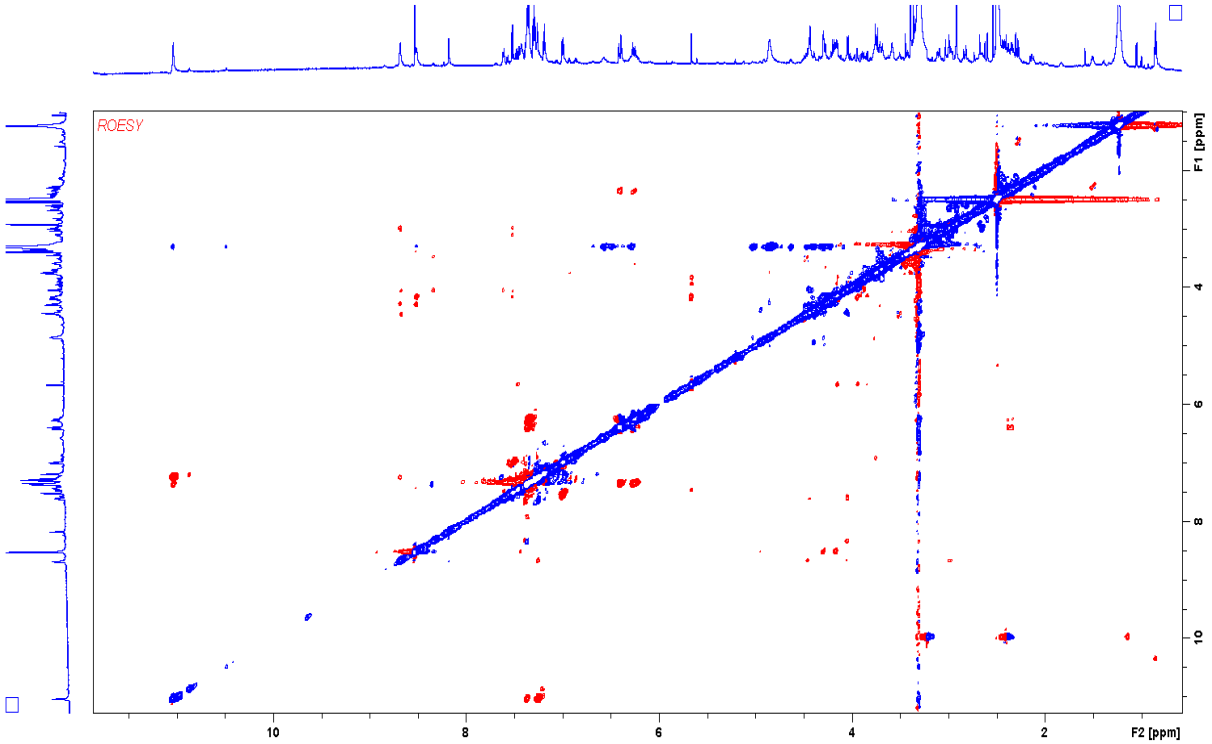

ROESY spectrum of microsclerodermin L in DMSO-d_6

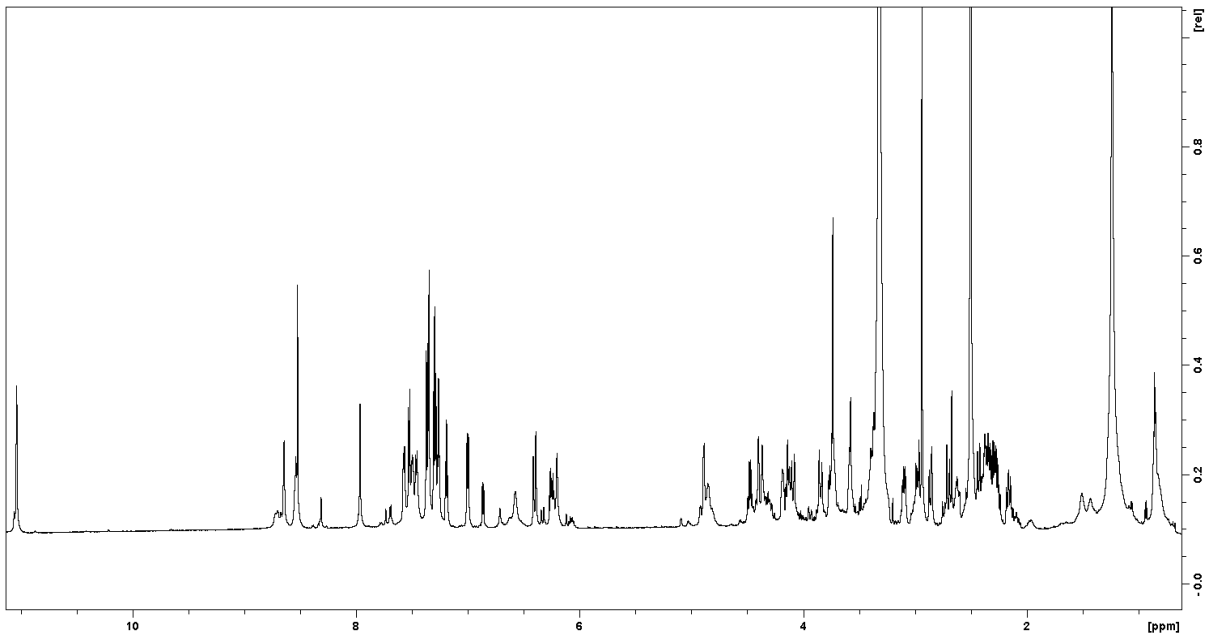

^{1}H NMR spectrum of microsclerodermin D in DMSO-d_6

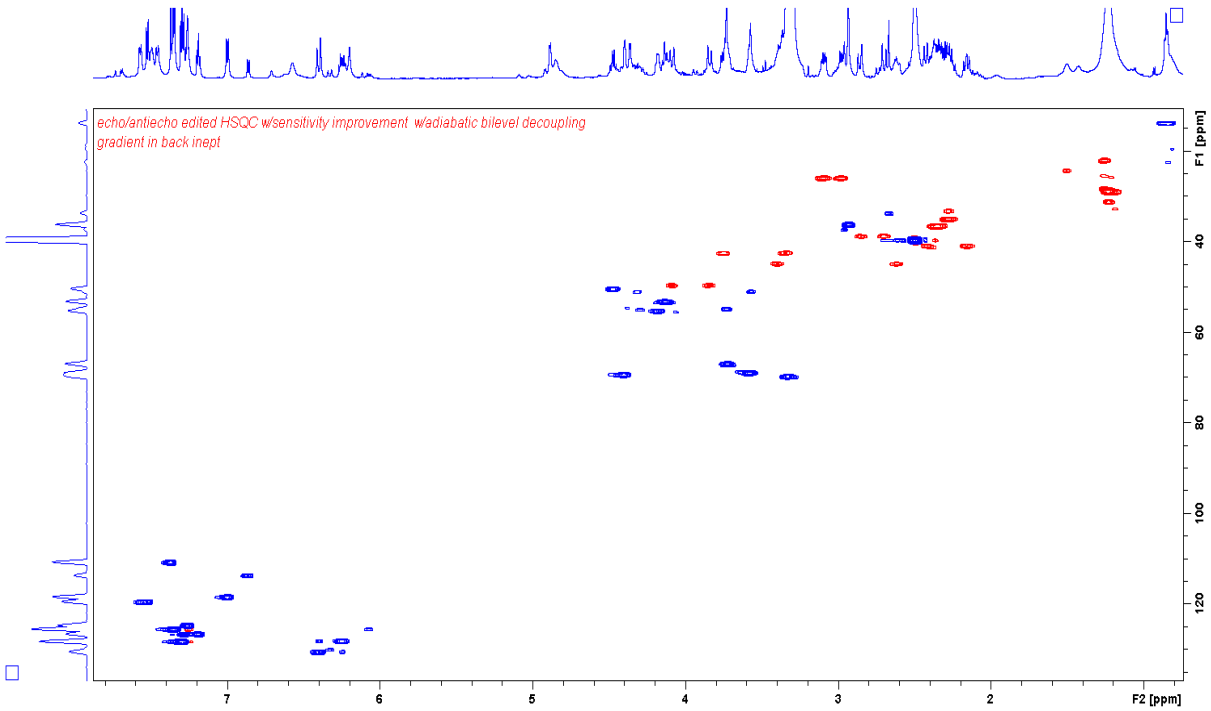

HSQC spectrum of microsclerodermin D in DMSO-d_6

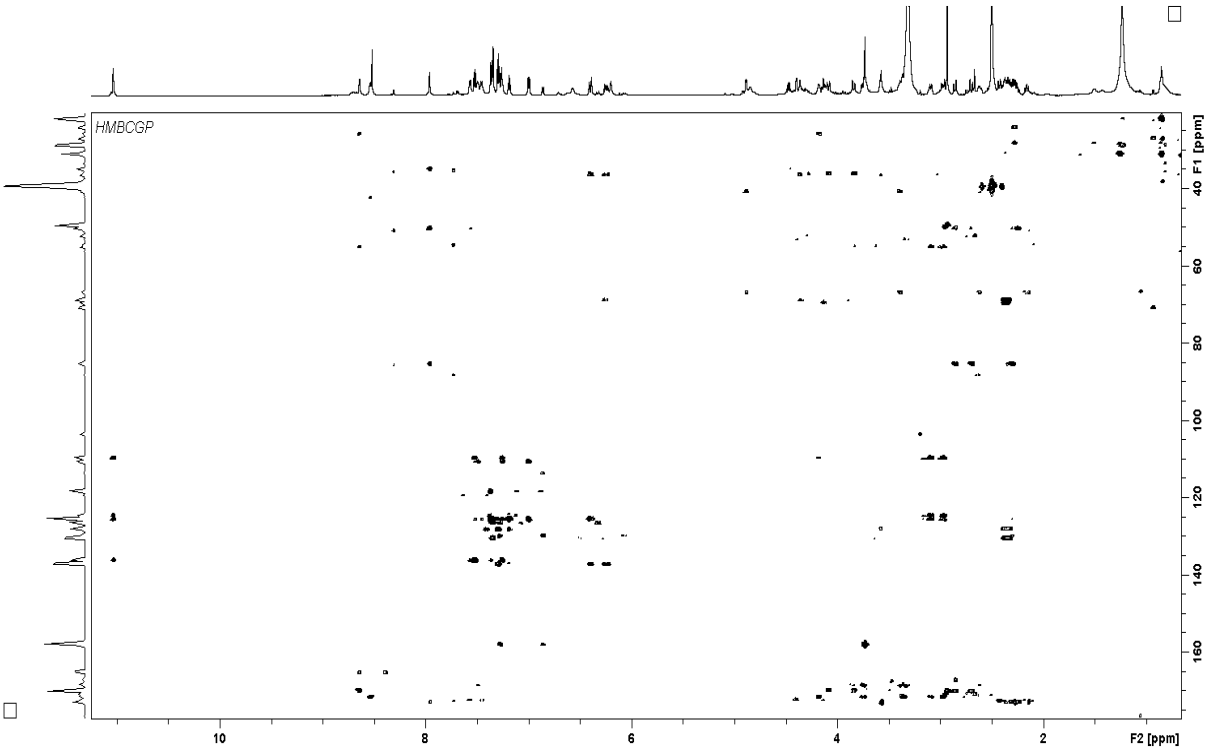

HMBC spectrum of microsclerodermin D in DMSO-d_6

6.2.Hyalachelins

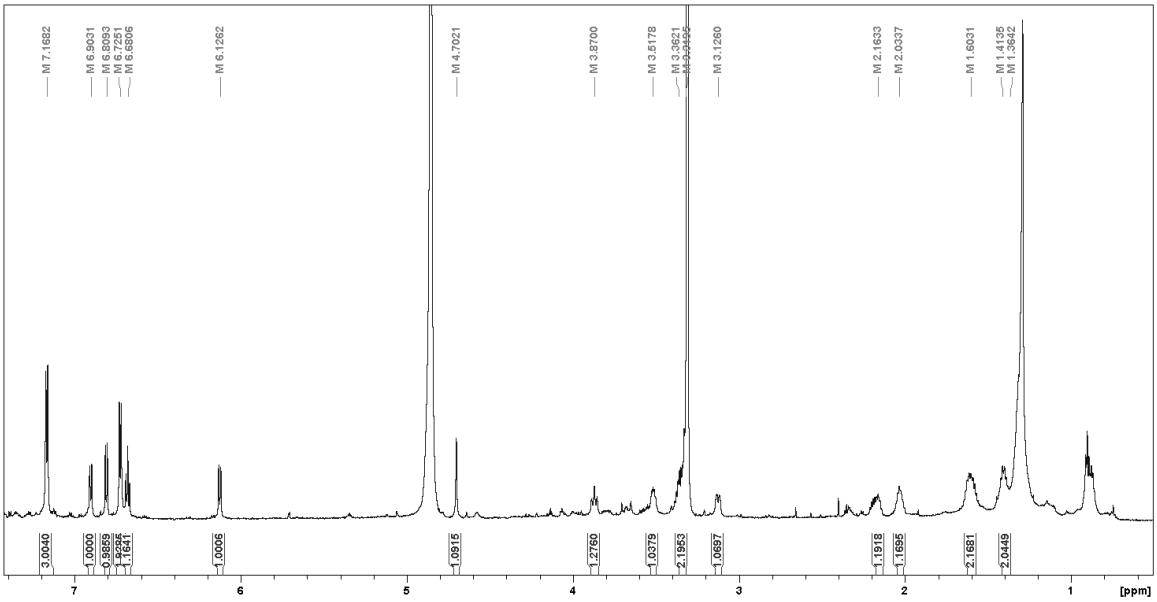

^{1}H-NMR spectrum of hyalachelin A in CD_3OD (700MHz)

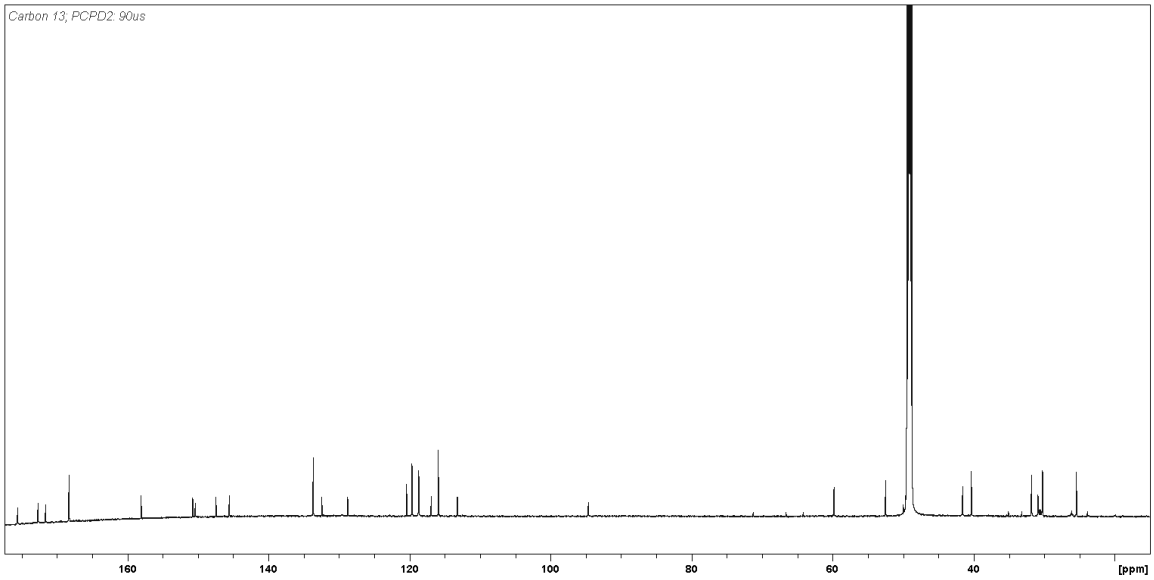

^{13}C-NMR spectrum of hyalachelin A in CD_3OD (175MHz)

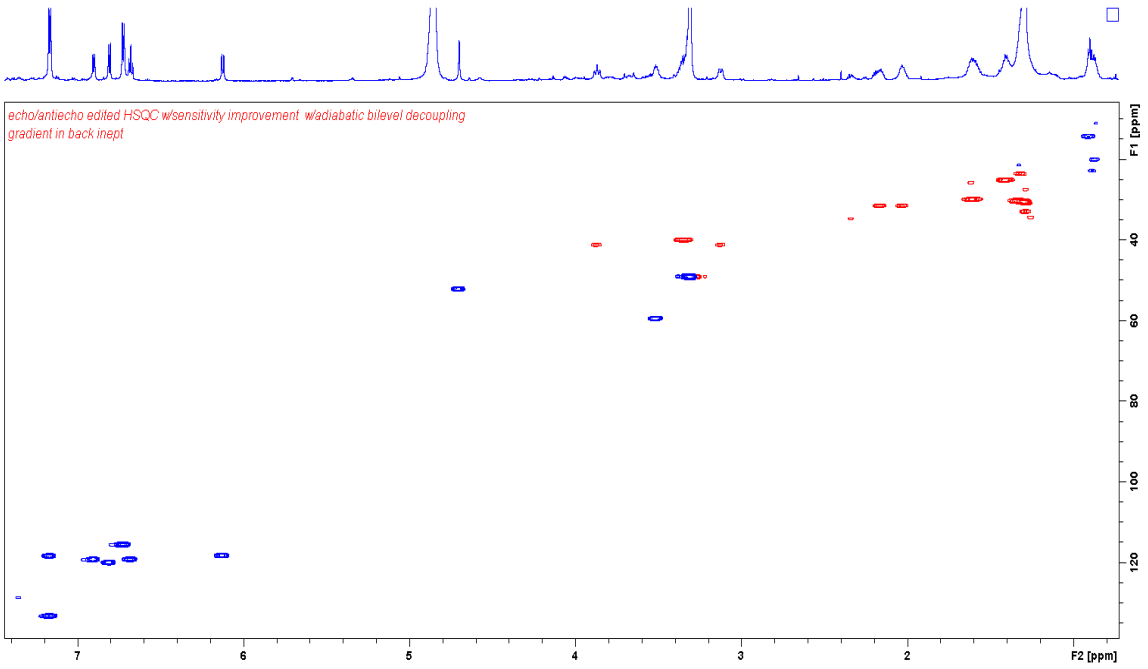

HSQC spectrum of hyalachelin A in CD_3OD (700MHz)

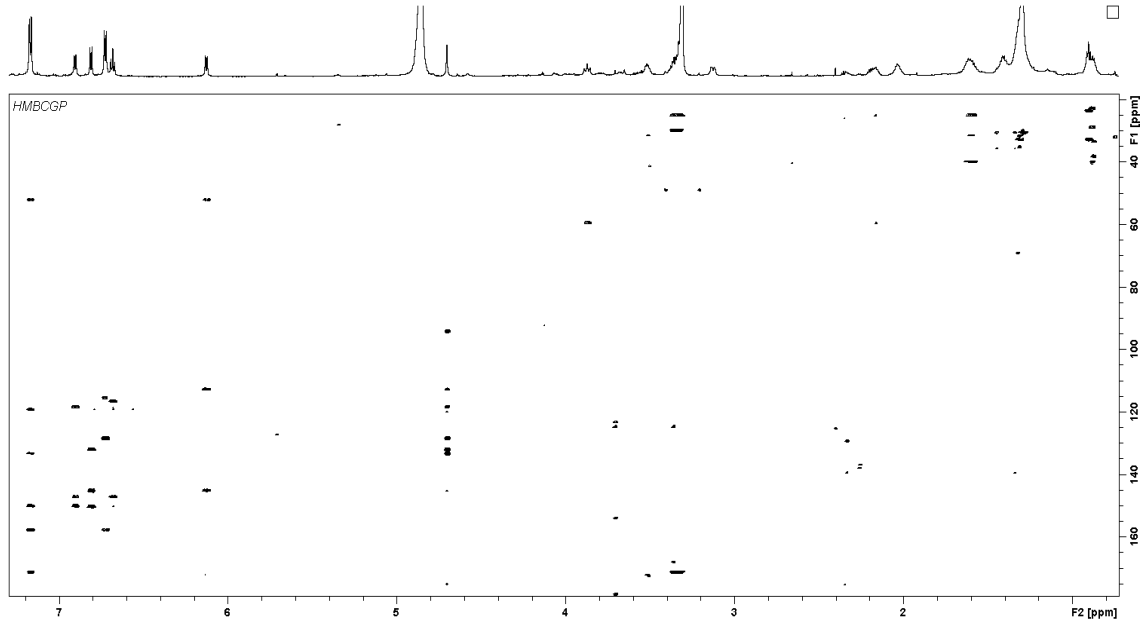

HMBC spectrum of hyalachelin A in CD_3OD (700MHz)

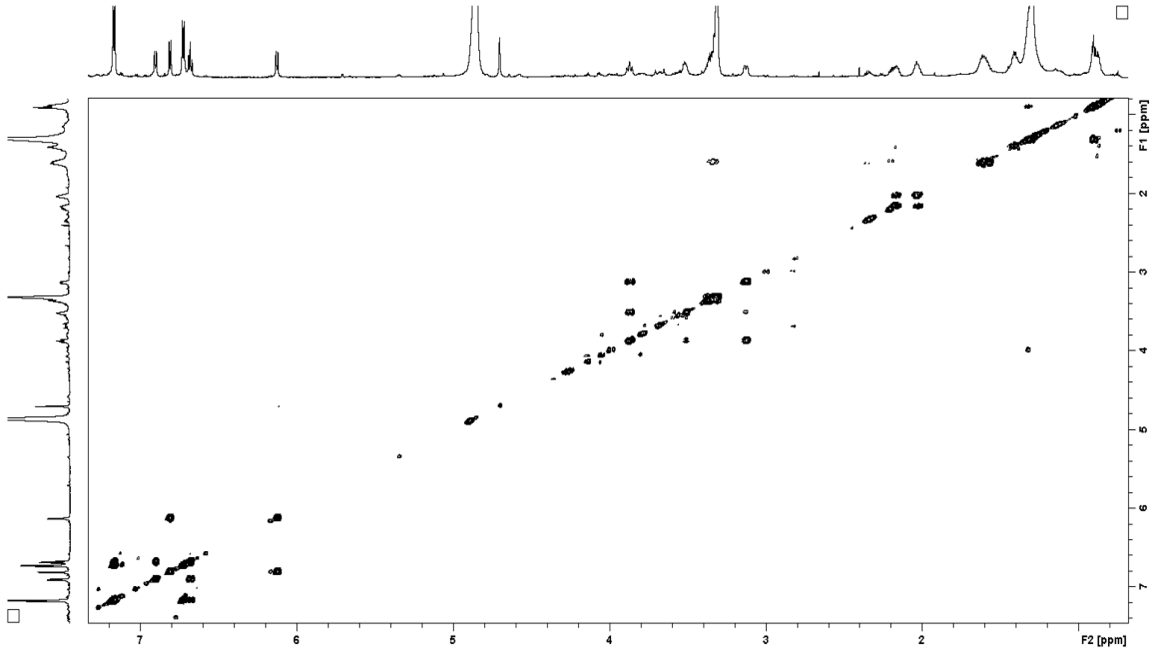

COSY spectrum of hyalachelin A in CD_3OD (700MHz)

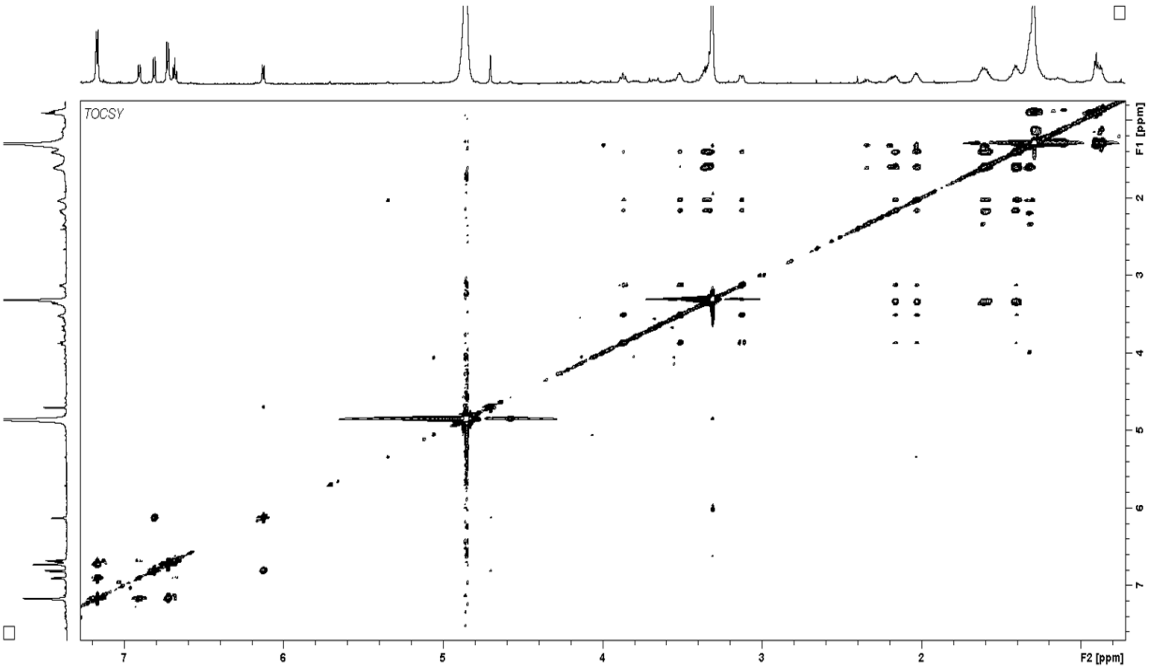

2D-TOCSY spectrum of hyalachelin A in CD_3OD (700MHz)

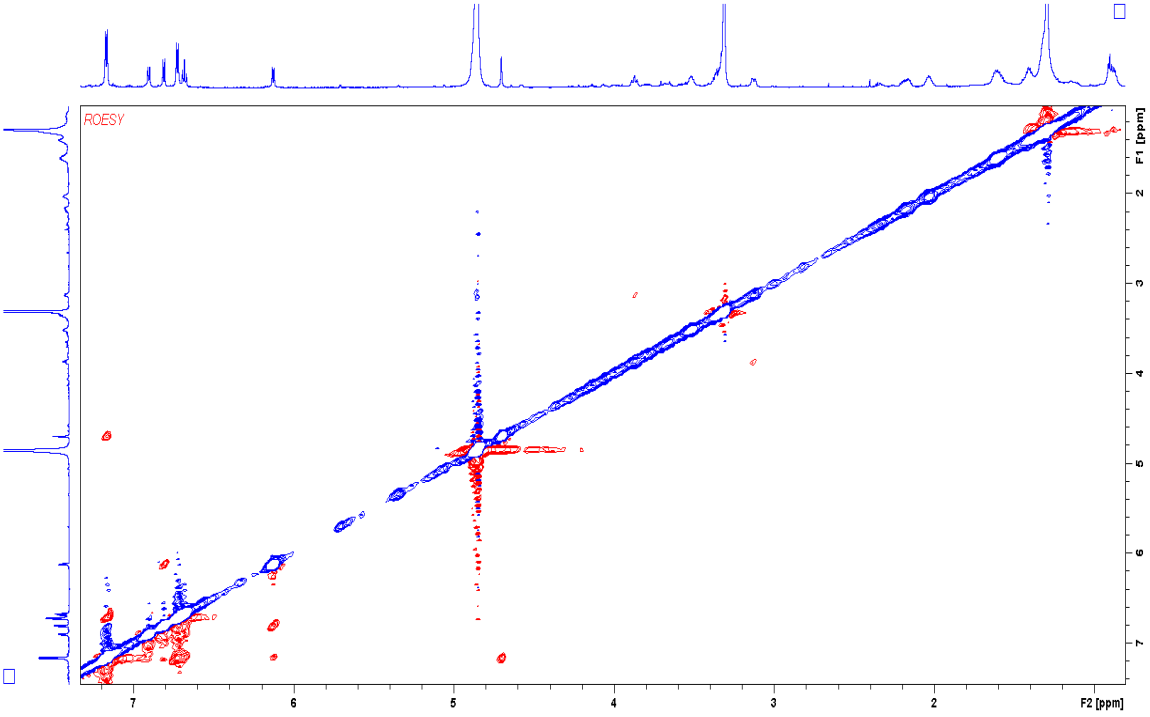

ROESY spectrum of hyalachelin A in CD_3OD (700MHz)

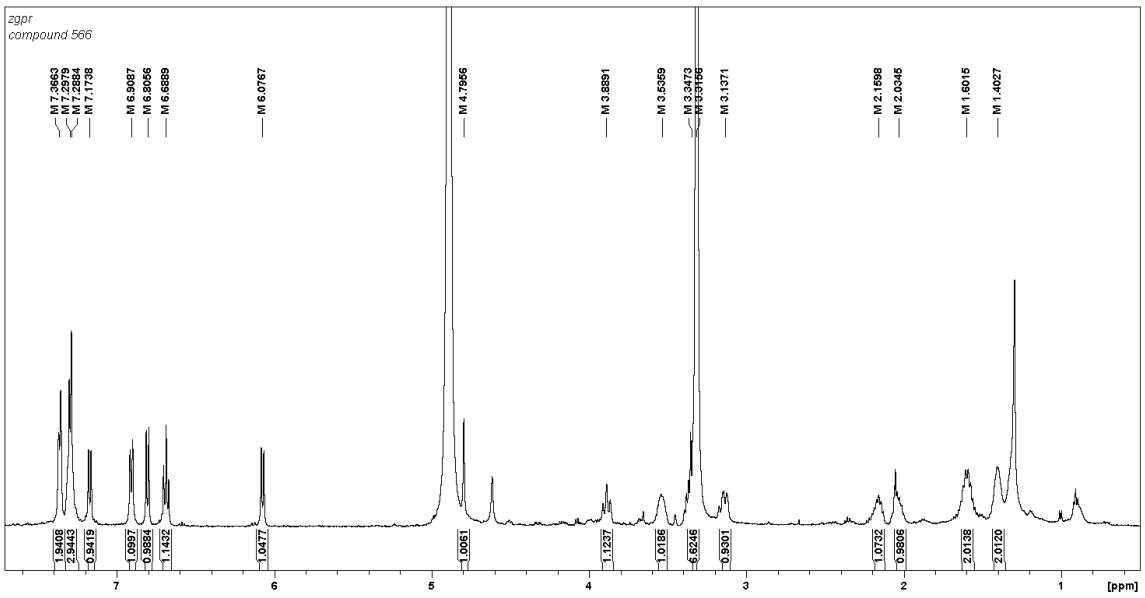

^{1}H-NMR spectrum of hyalachelin B in CD_3OD (500MHz)

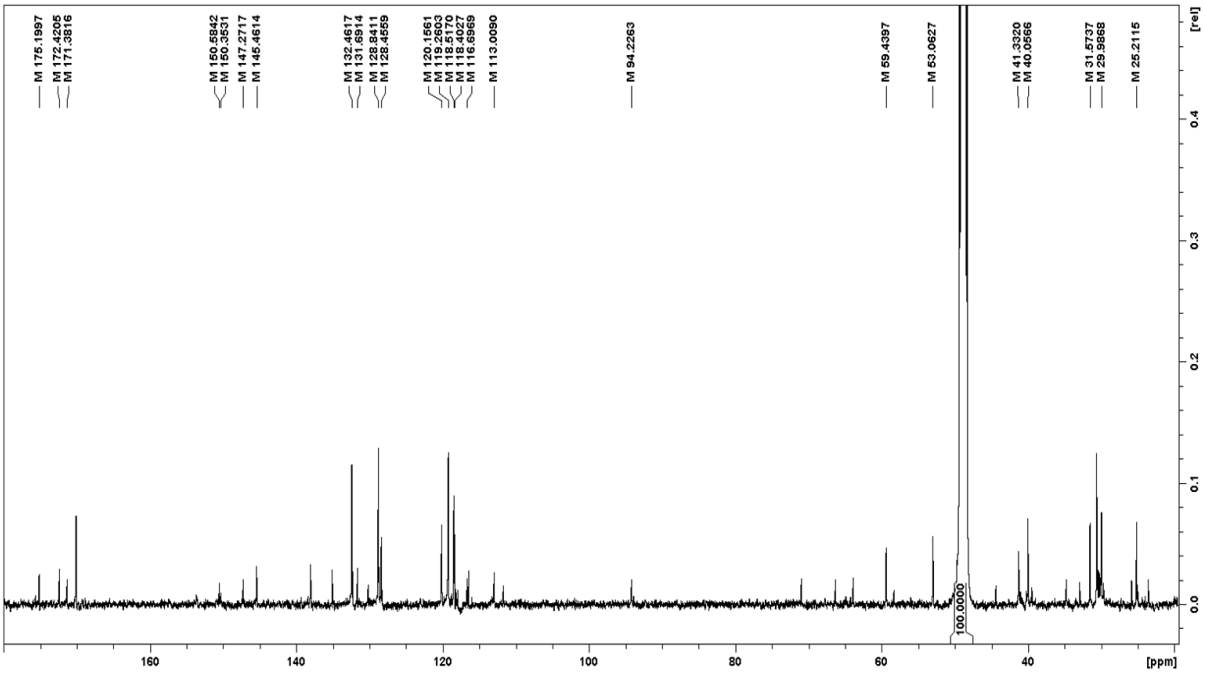

^{13}C-NMR spectrum of hyalachelin B in CD_3OD (125MHz)

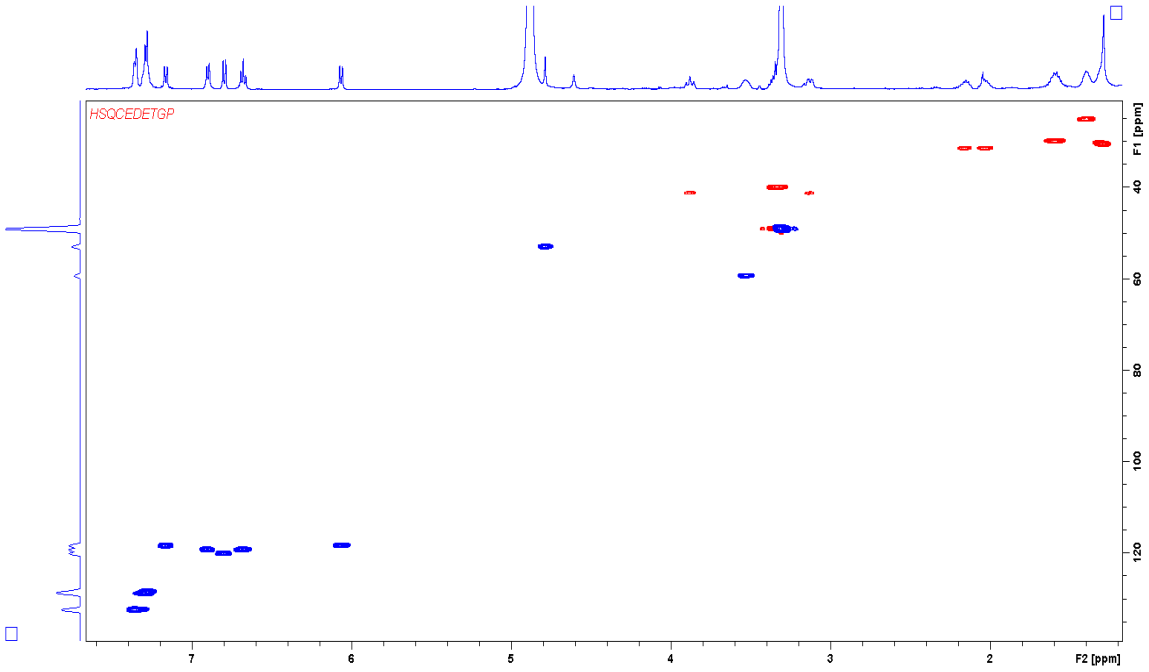

HSQC spectrum of hyalachelin B in CD_3OD (500MHz)

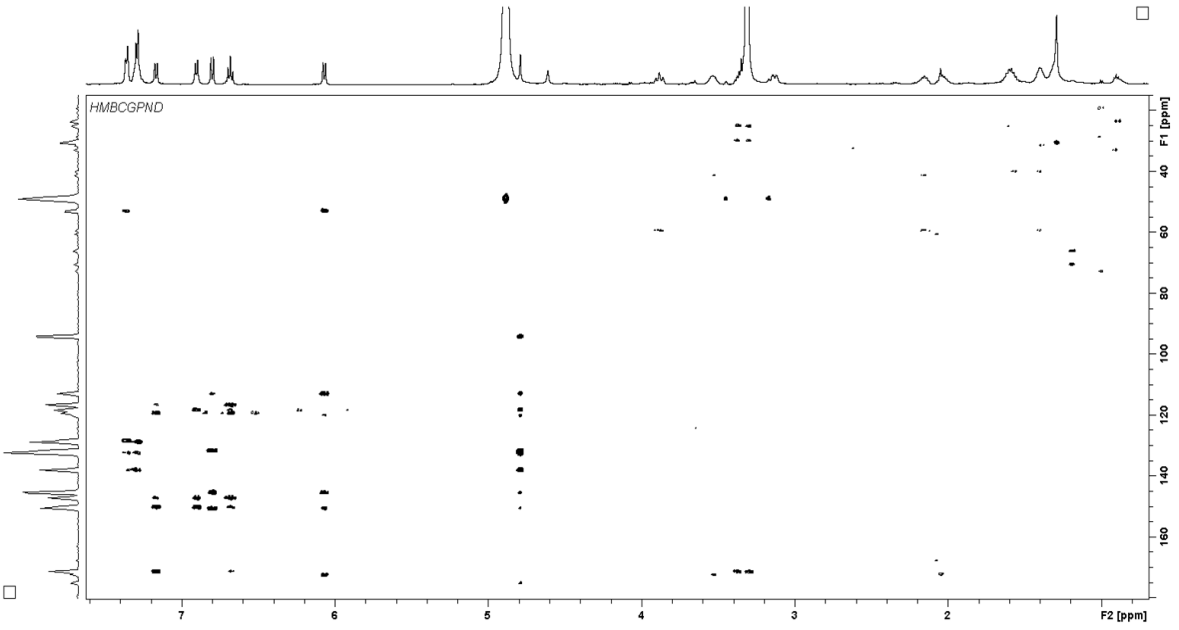

HMBC spectrum of hyalachelin B in CD_3OD (500MHz)

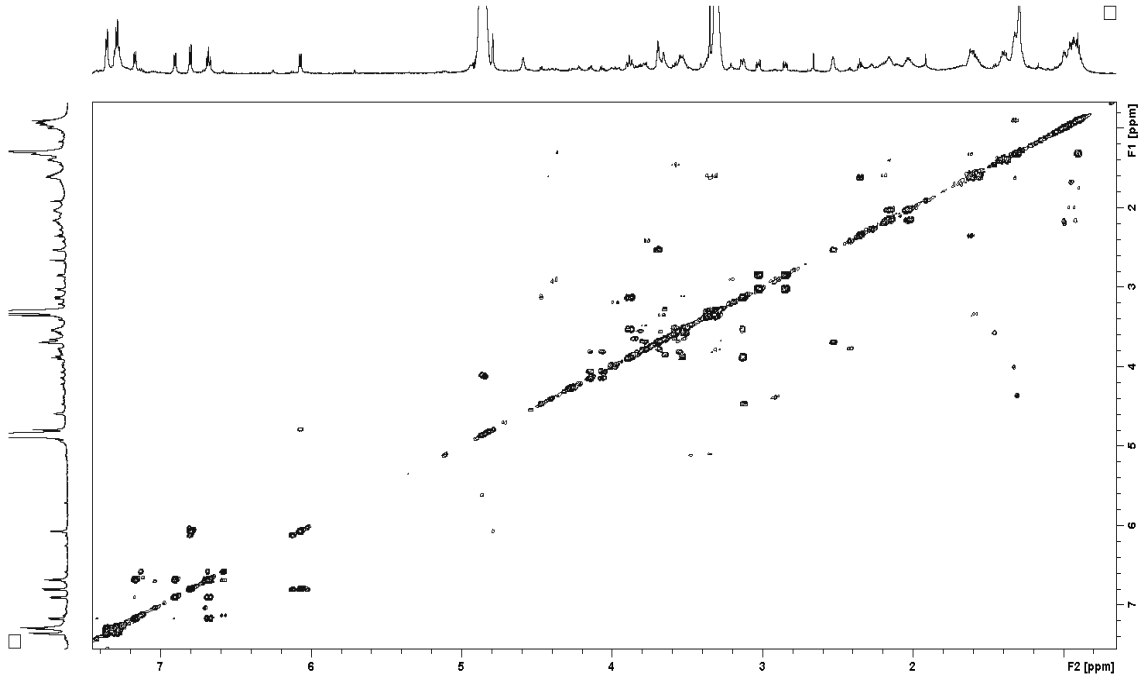

COSY spectrum of hyalachelin B in CD_3OD (700MHz)

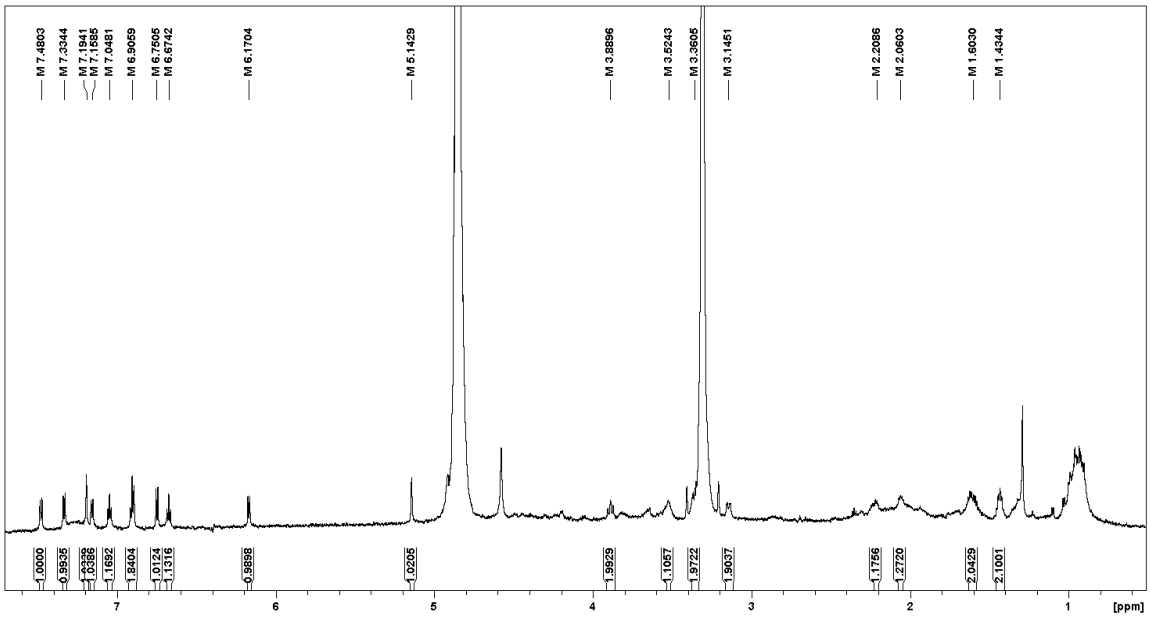

^1H NMR spectrum of hyalachelin C in CD_3OD (700 MHz)

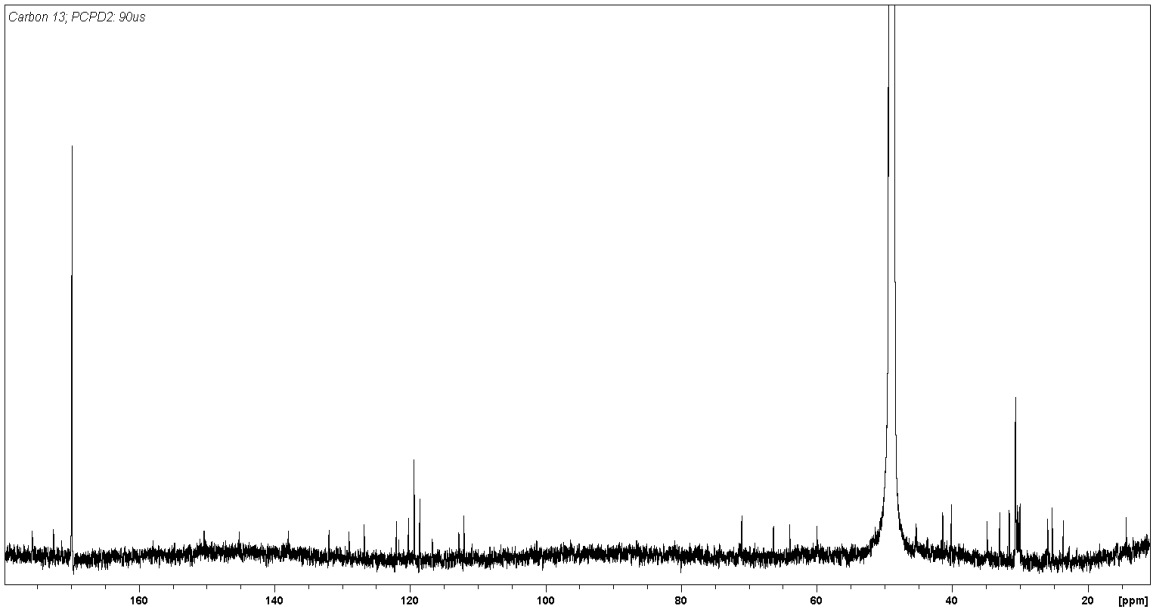

^{13}C-NMR spectrum of hyalachelin C in CD_3OD (175MHz)

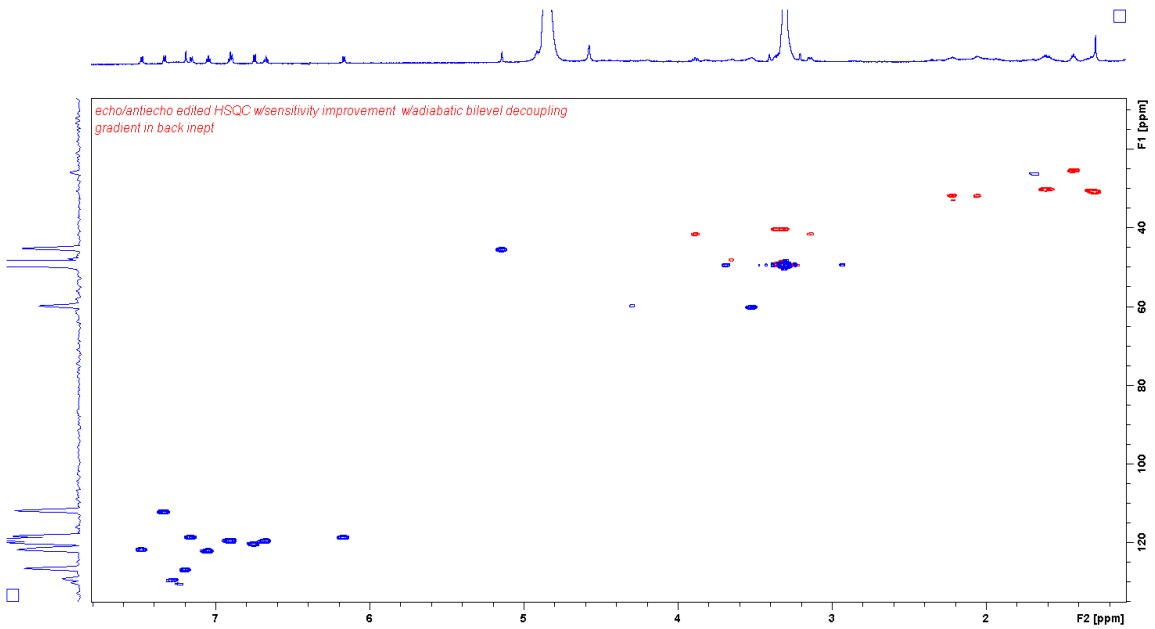

HSQC spectrum of hyalachelin C in CD_3OD (700 MHz)

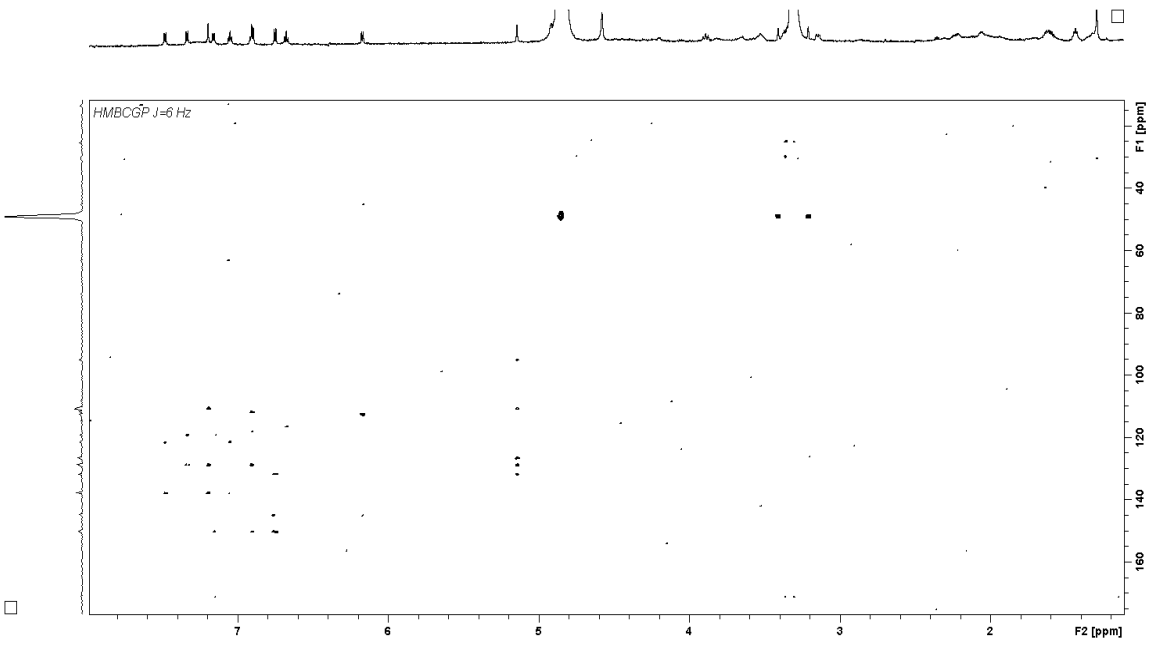

HMBCspectrum of hyalachelin C in CD_3OD (700 MHz)

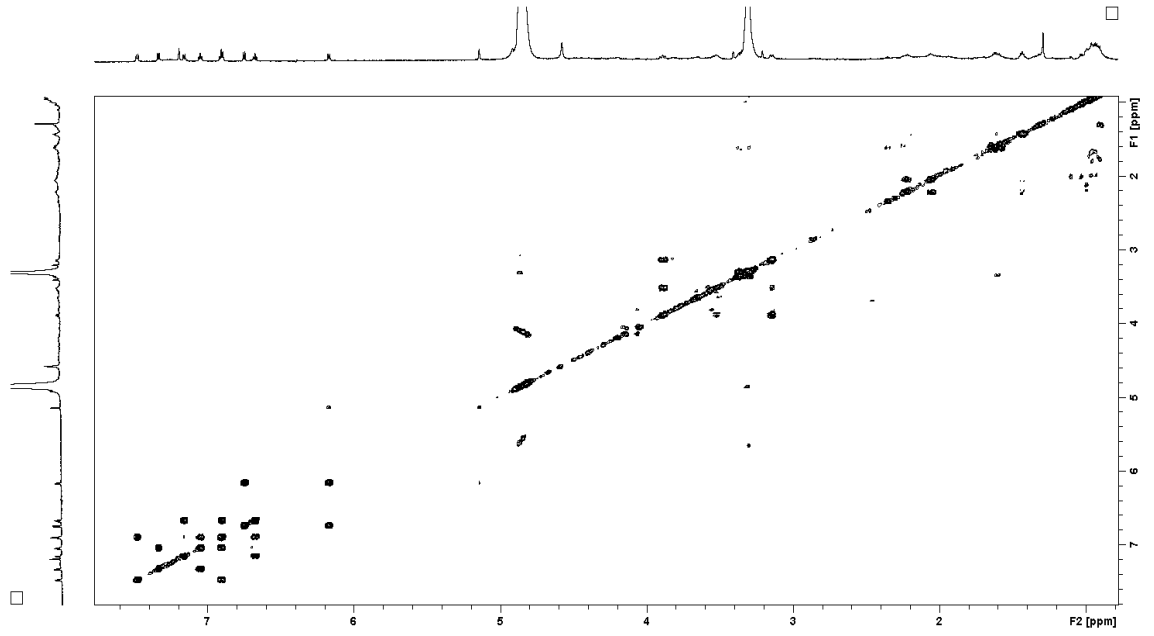

COSY spectrum of hyalachelin C in CD_3OD (700 MHz)

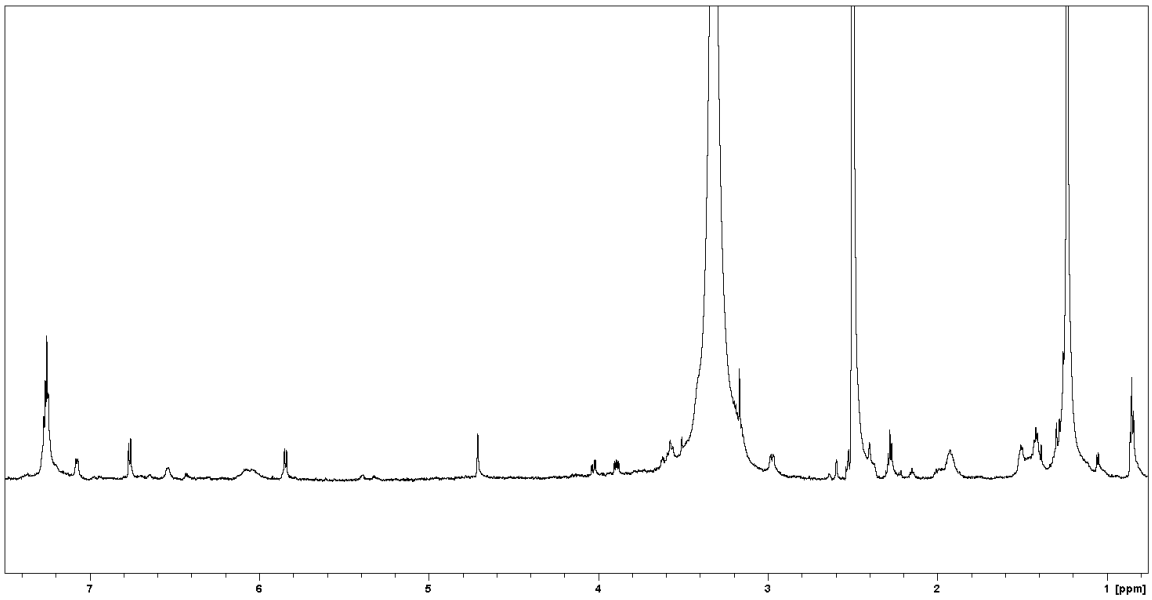

^{1}H-NMR spectrum of hyalachelin B in DMSO-d_6 (700 MHz)

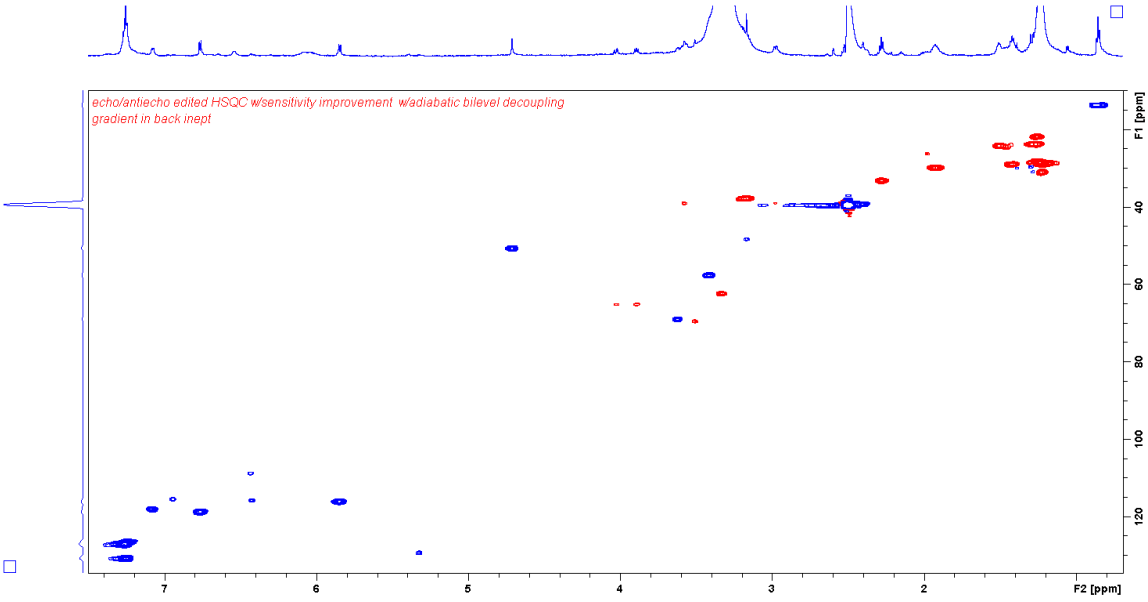

HSQC spectrum of hyalachelin B in DMSO-d_6 (700 MHz)

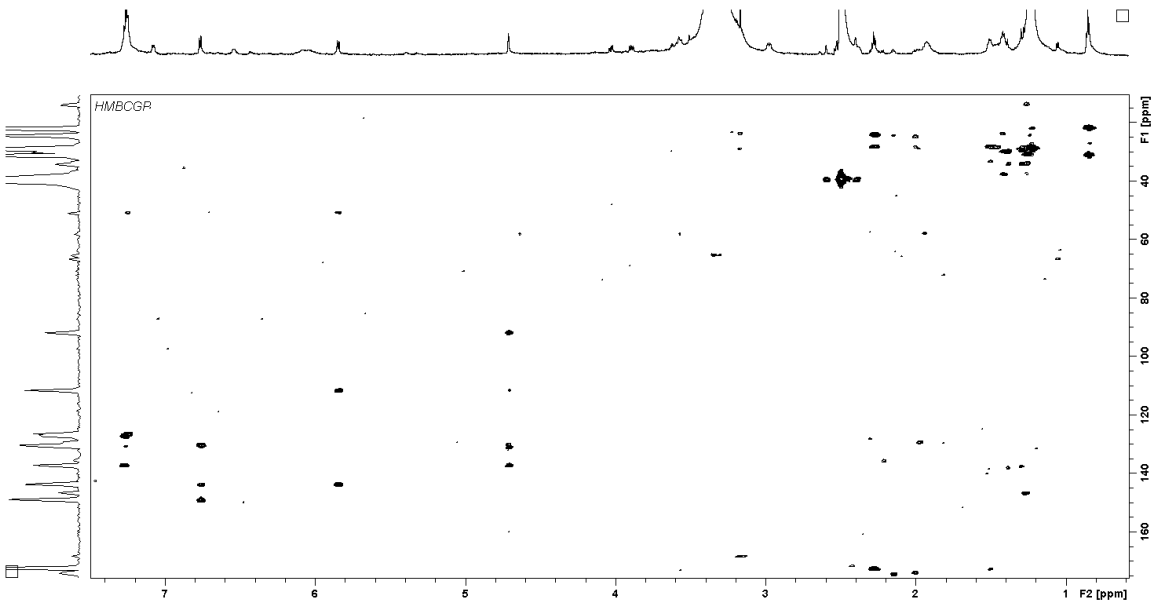

HMBC spectrum of hyalachelin B in DMSO-d_6 (700 MHz)

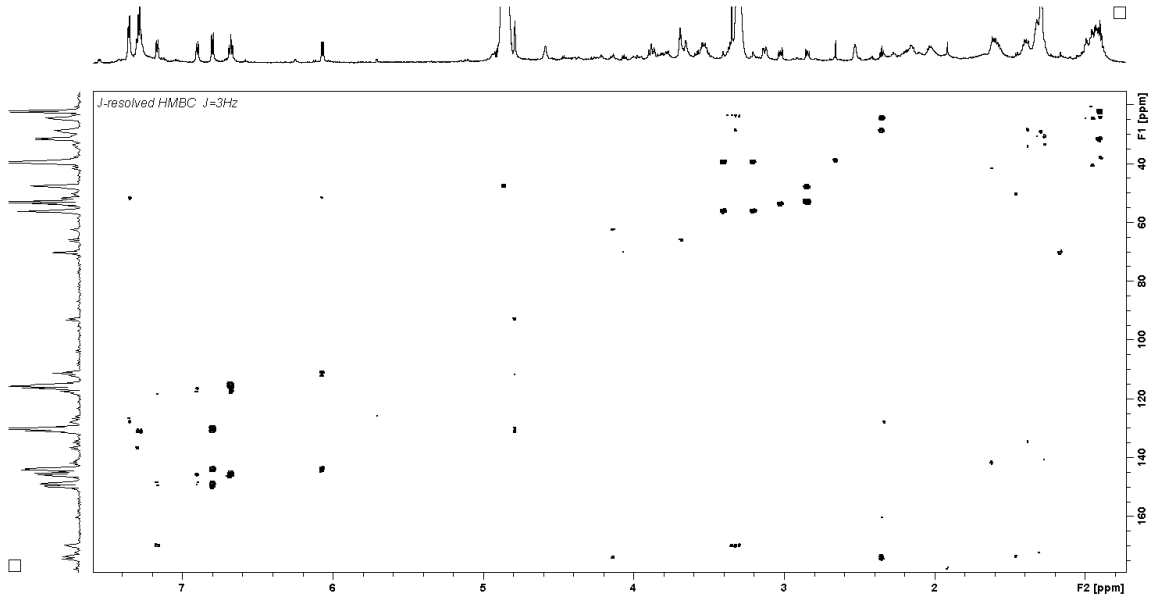

J-resolved HMBC spectrum of hyalachelin B in CD_3OD (700 MHz)

6.3. Cystochromones

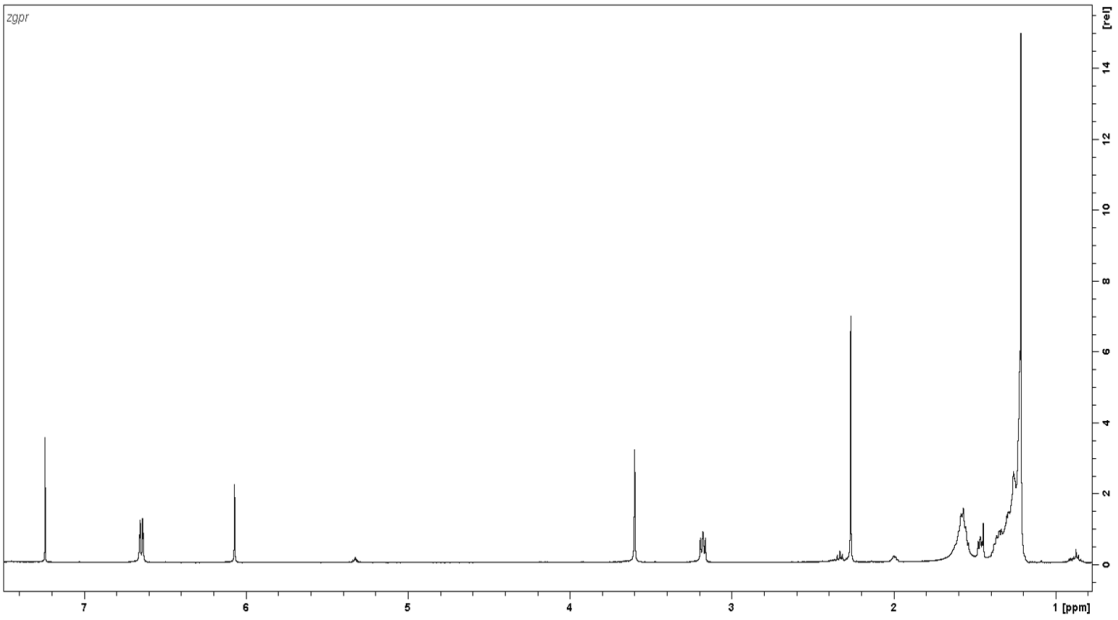

^{1}H-NMR spectrum of cystochromone A in $CDCl_3$ (500 MHz)

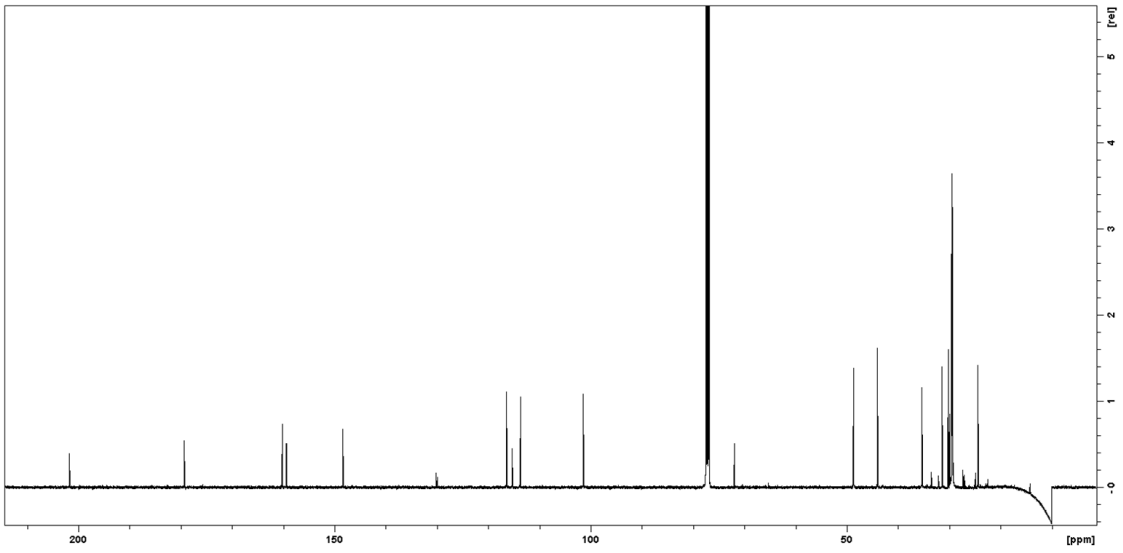

^{13}C-NMR spectrum of cystochromone A in $CDCl_3$ (500 MHz)

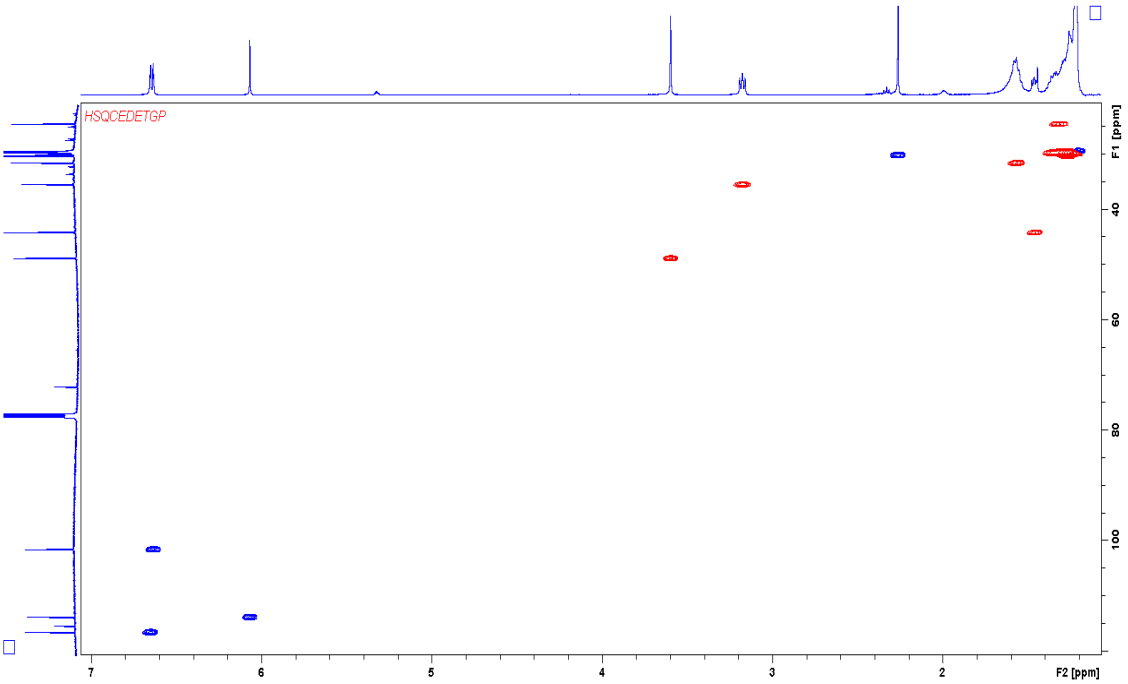

HSQC spectrum of cystochromone A in $CDCl_3$ (500 MHz)

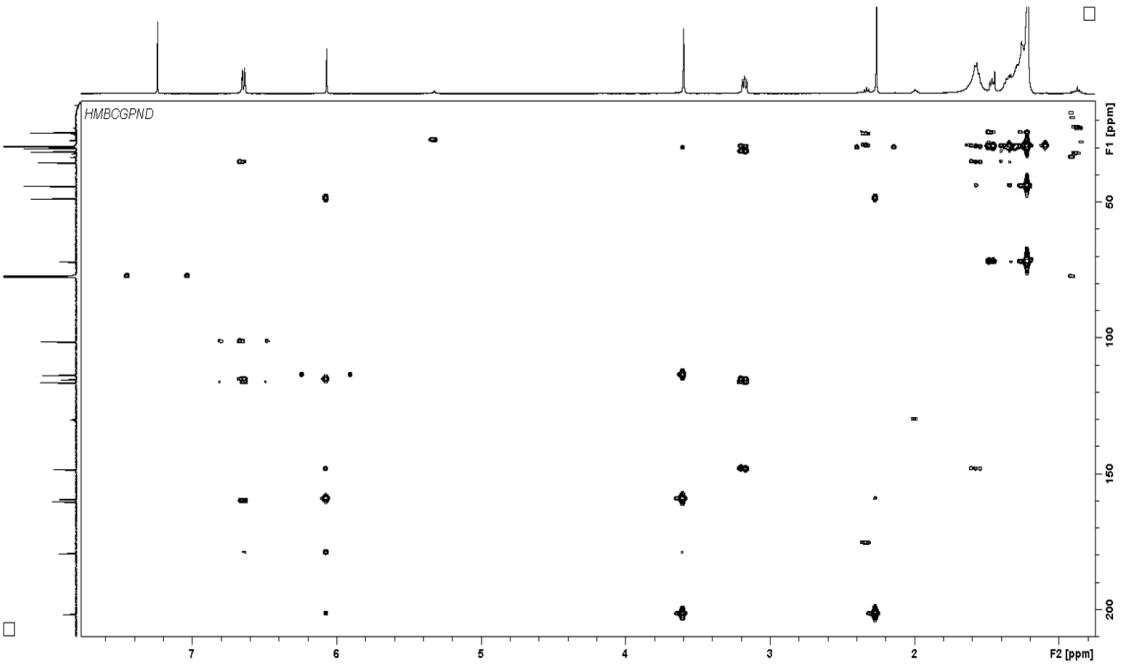

HMBC spectrum of cystochromone A in $CDCl_3$ (500 MHz)

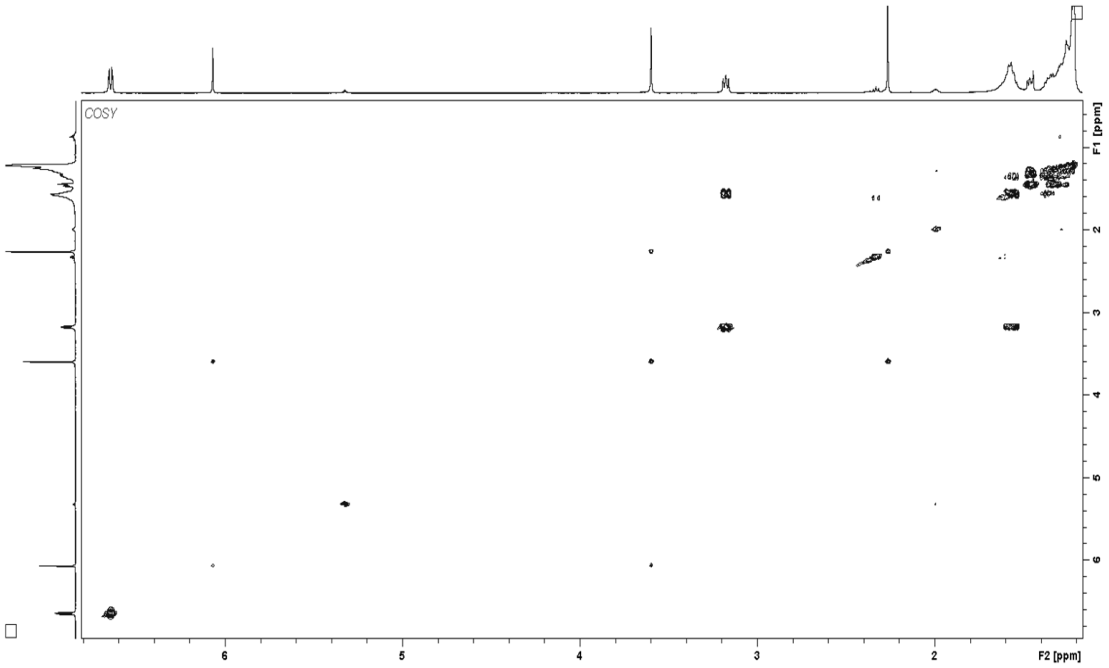

COSY spectrum of cystochromone A in $CDCl_3$ (500 MHz)

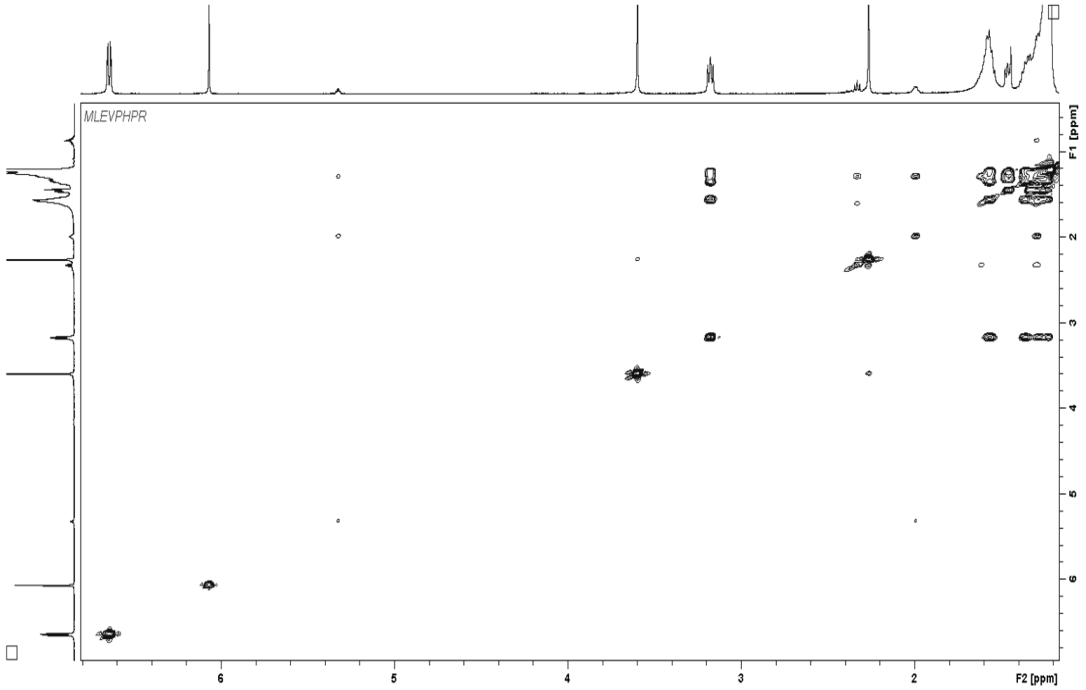

TOCSY spectrum of cystochromone A in $CDCl_3$ (500 MHz)

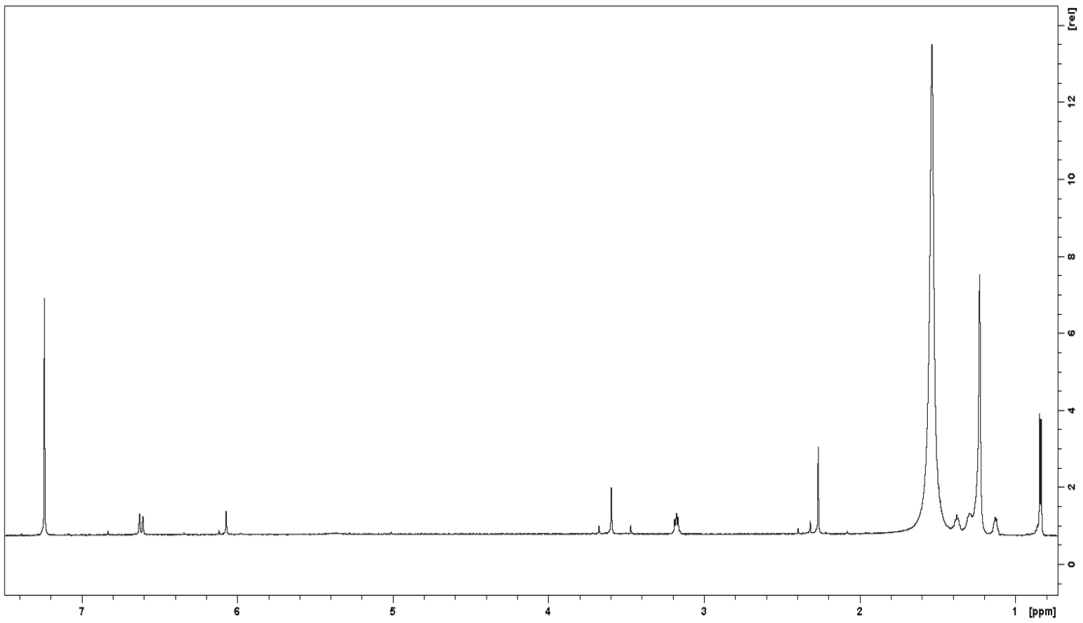

^{1}H-NMR spectrum of cystochromone B in $CDCl_3$ (700 MHz)

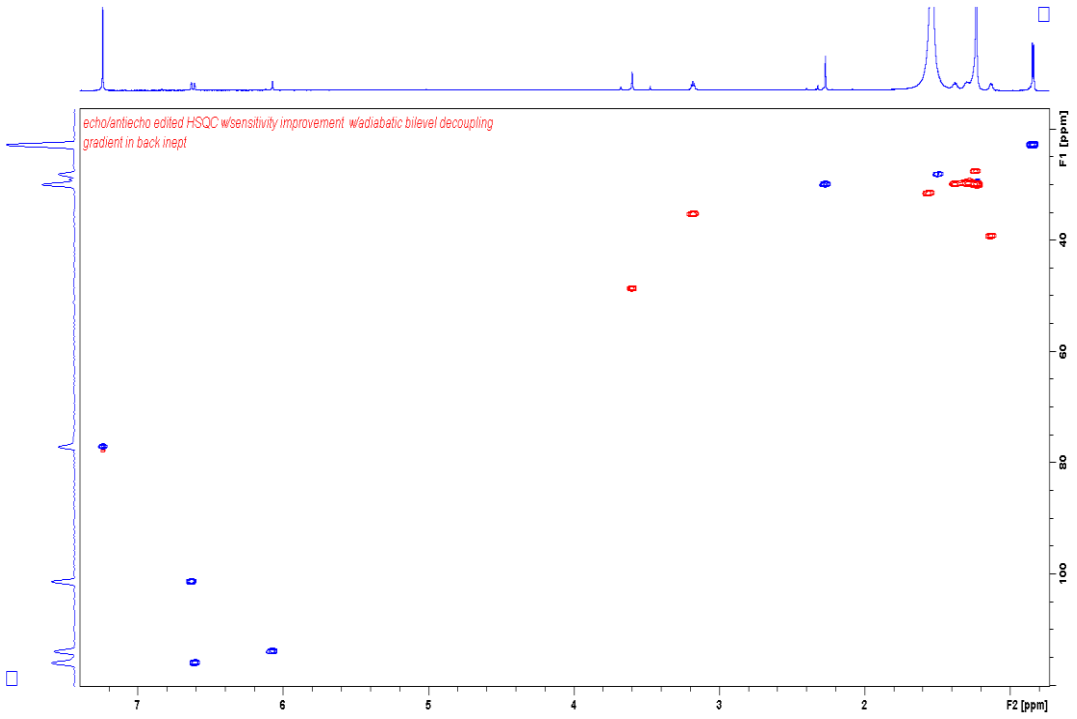

HSQC spectrum of cystochromone B in $CDCl_3$ (700 MHz)

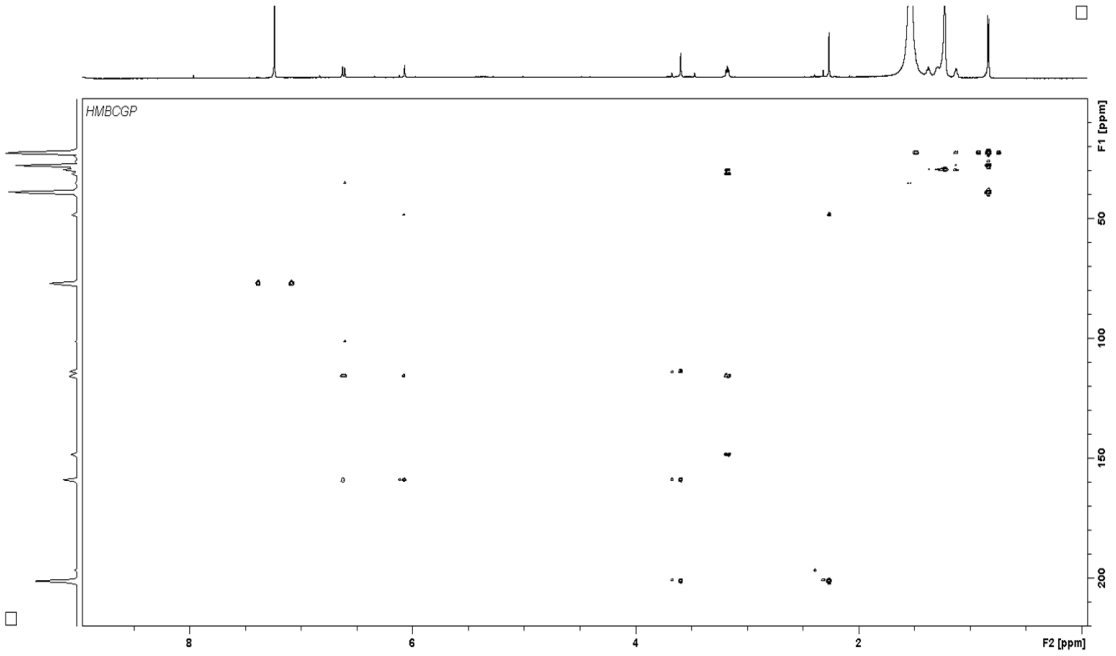

HMBC spectrum of cystochromone B in $CDCl_3$ (700 MHz)

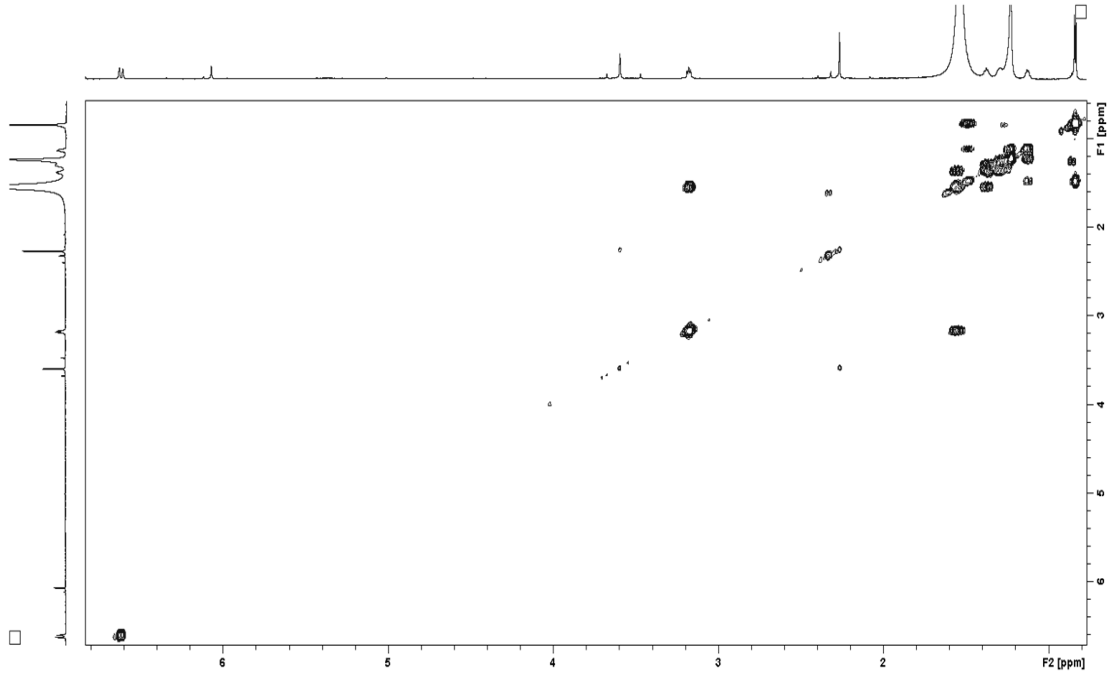

COSY spectrum of cystochromone B in $CDCl_3$ (700 MHz)

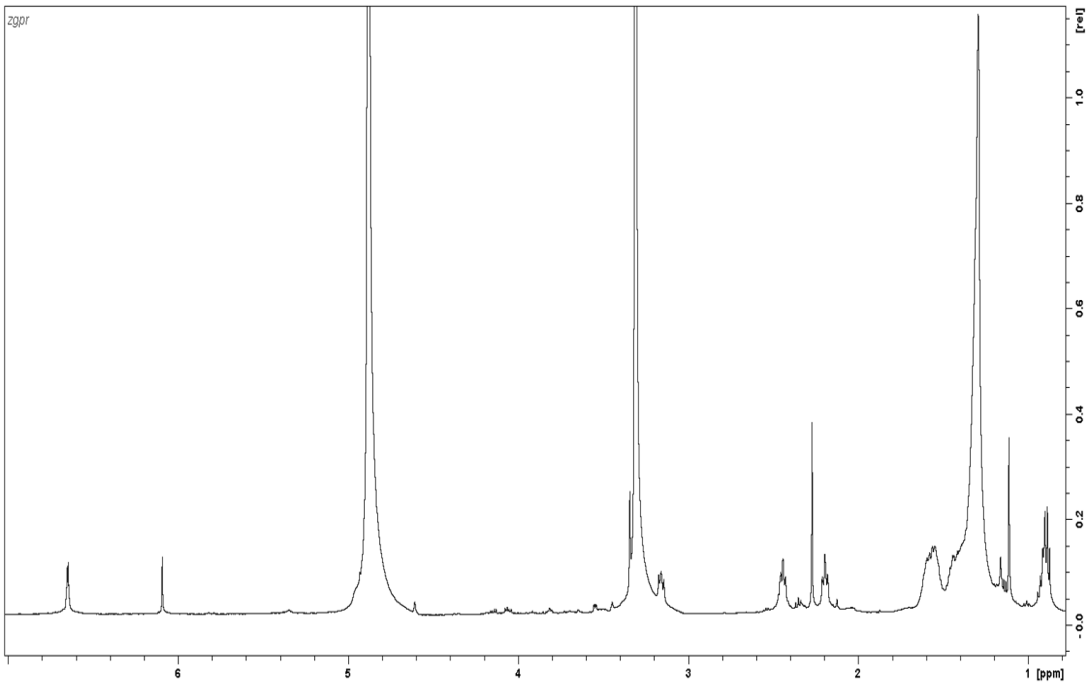

^{1}H-NMR spectrum of cystochromone C in $MeOD_4$ (500 MHz)

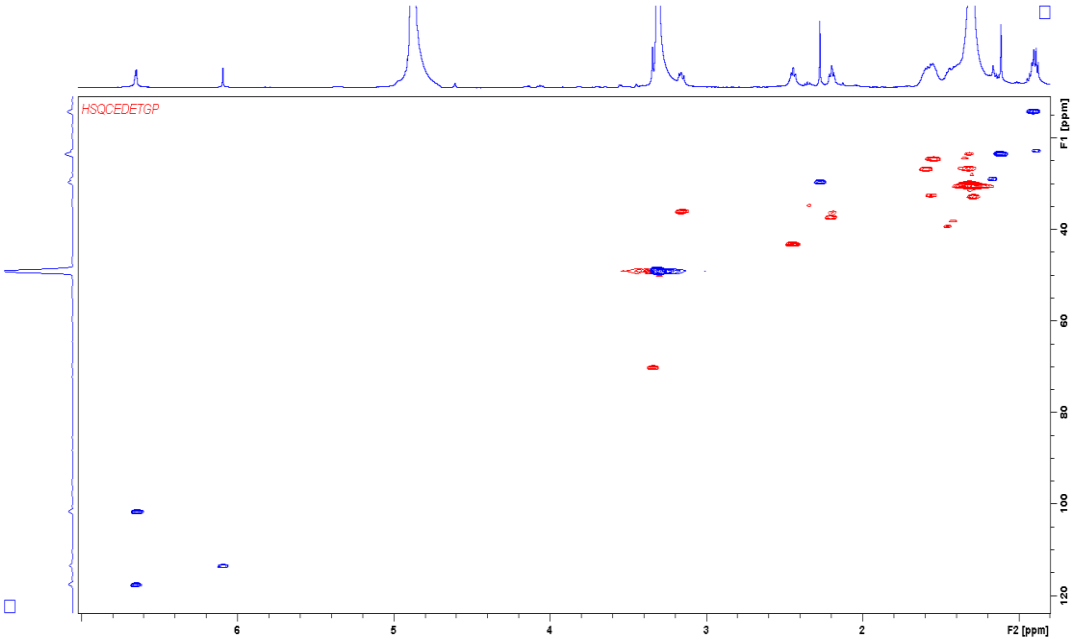

HSQC spectrum of cystochromone C in $MeOD_4$ (500 MHz)

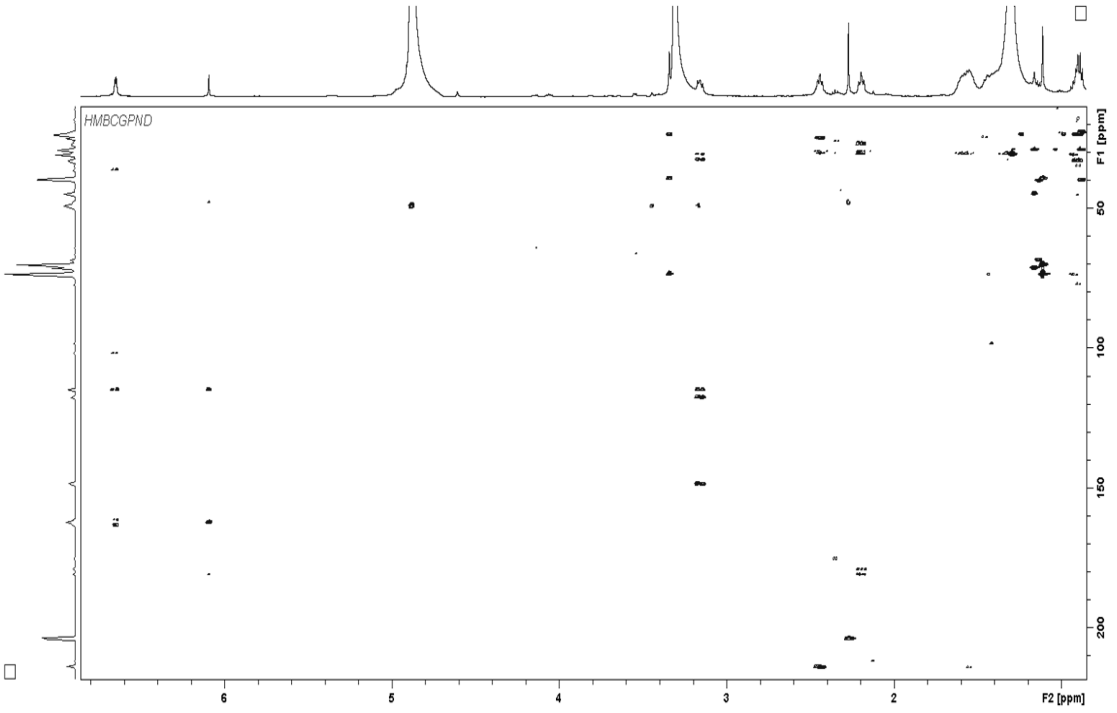

HMBC spectrum of cystochromone C in $MeOD_4$ (500 MHz)

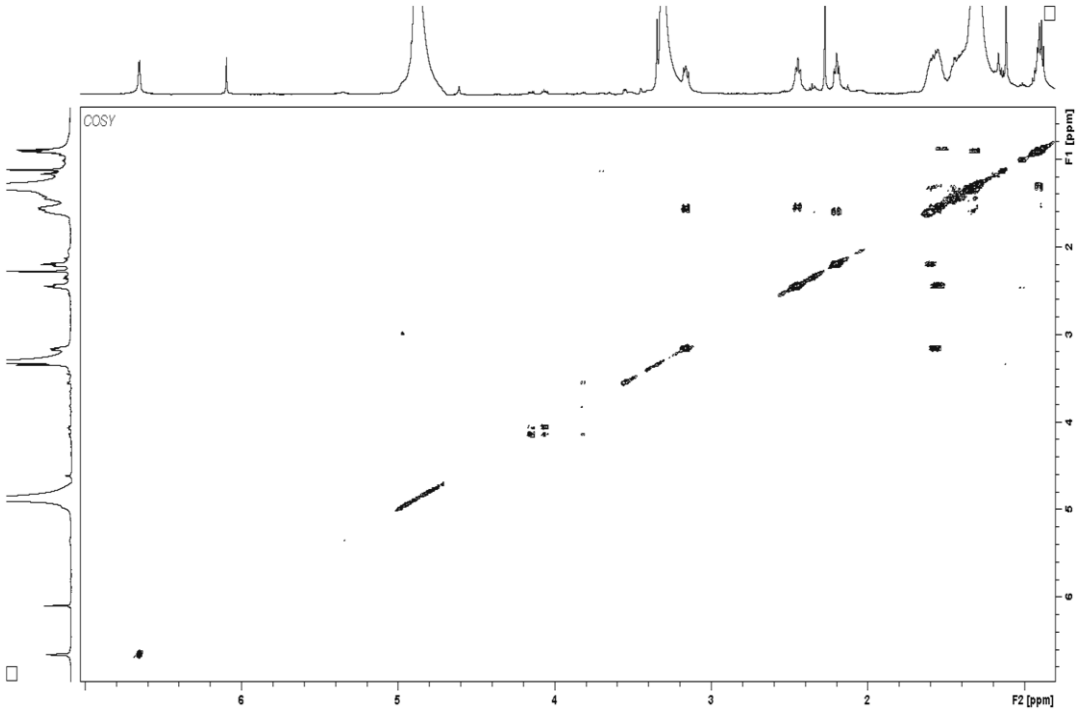

COSY spectrum of cystochromone C in $MeOD_4$ (500 MHz)

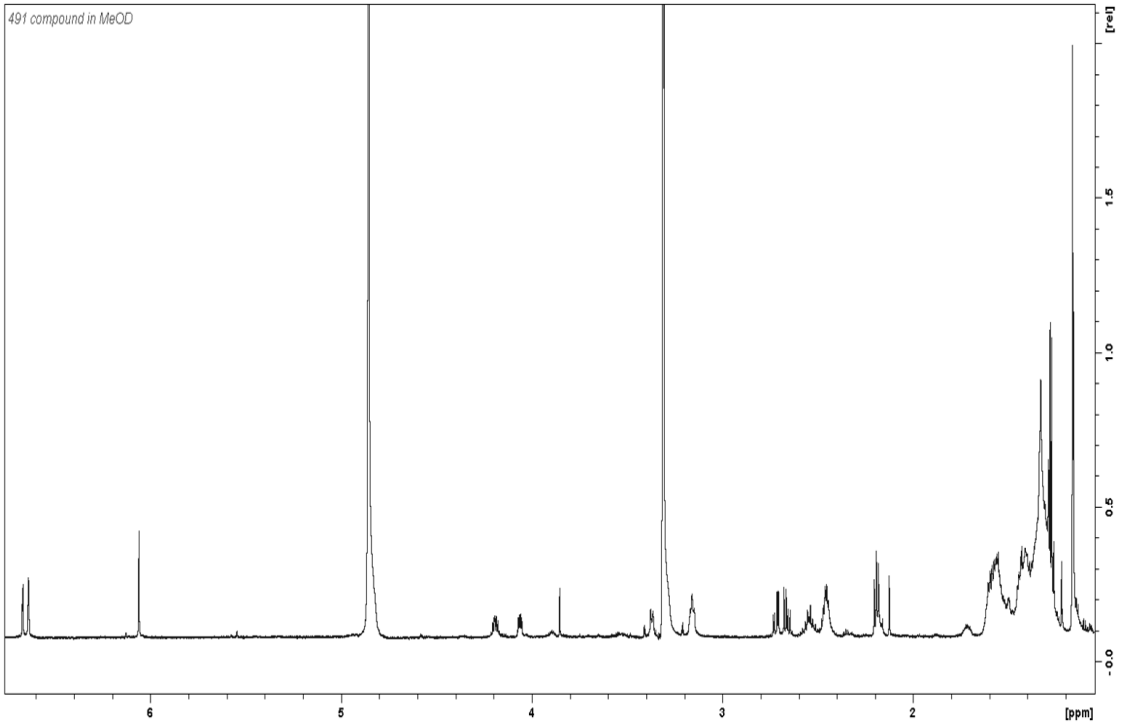

^{1}H-NMR spectrum of cystochromone D in $MeOD_4$ (700 MHz)

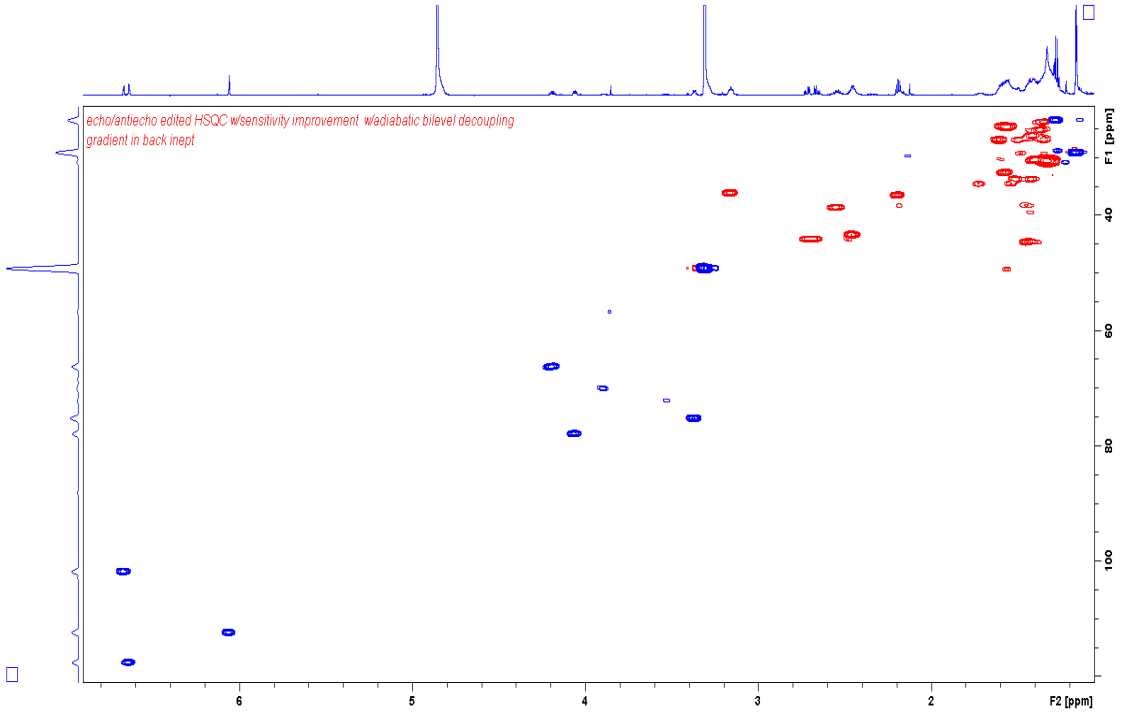

HSQC spectrum of cystochromone D in $MeOD_4$ (700 MHz)

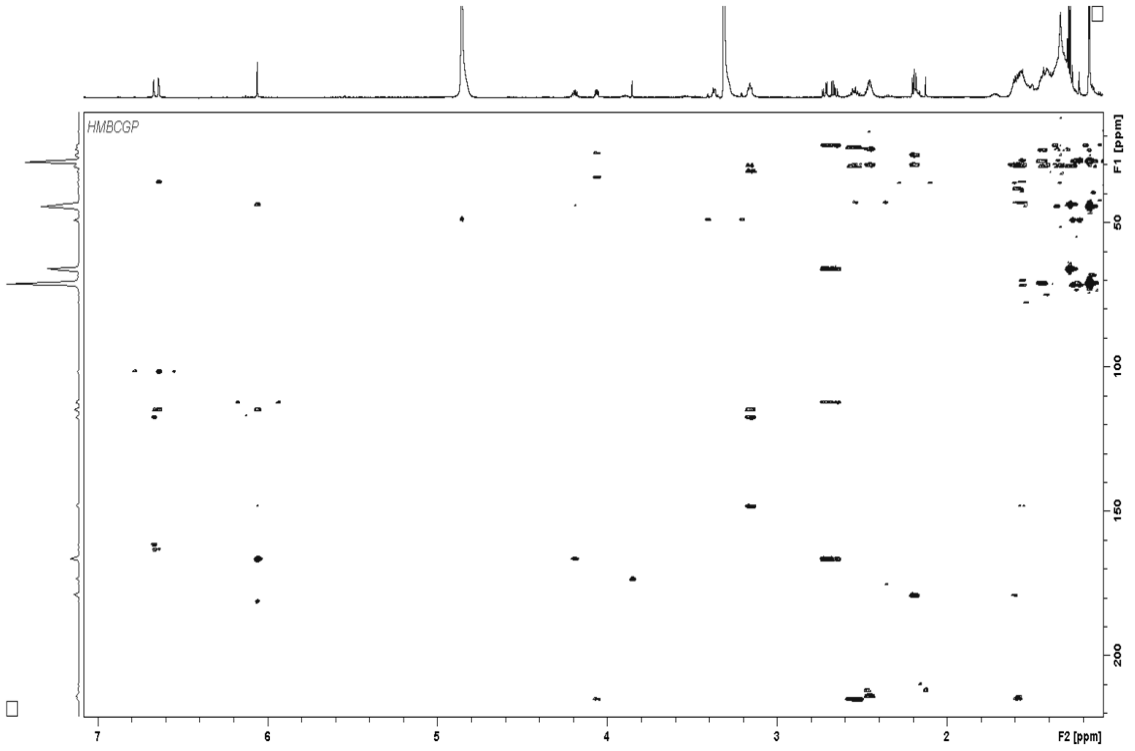

HMBC spectrum of cystochromone D in $MeOD_4$ (700 MHz)

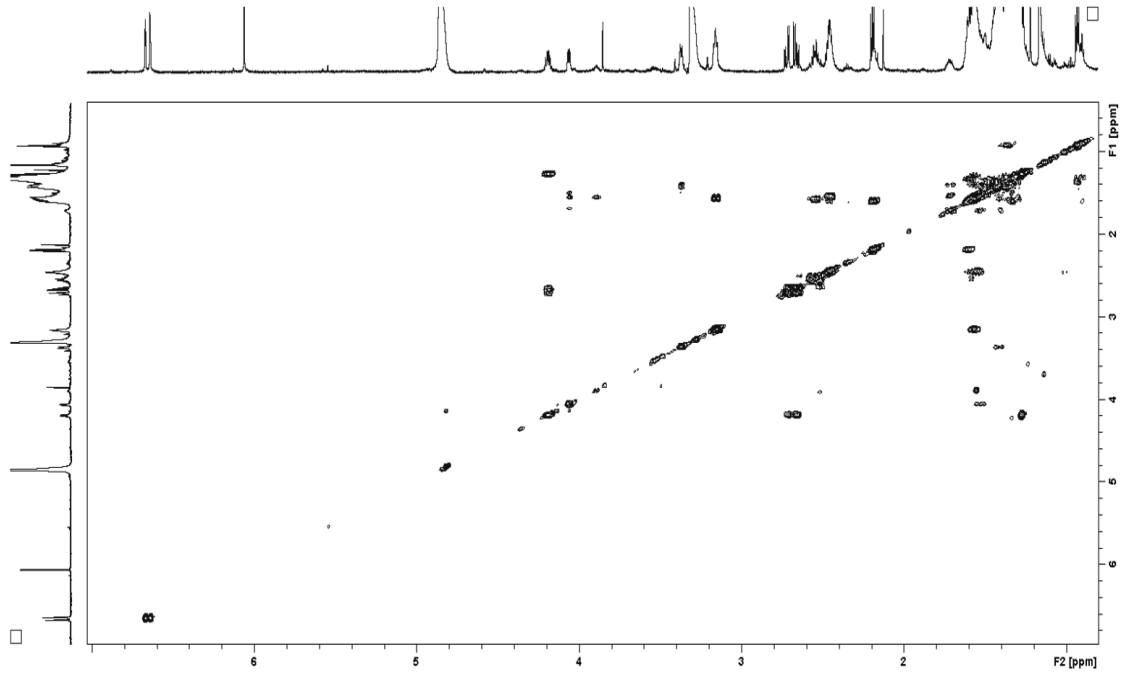

COSY spectrum of cystochromone D (4) in $MeOD_4$ (700 MHz)

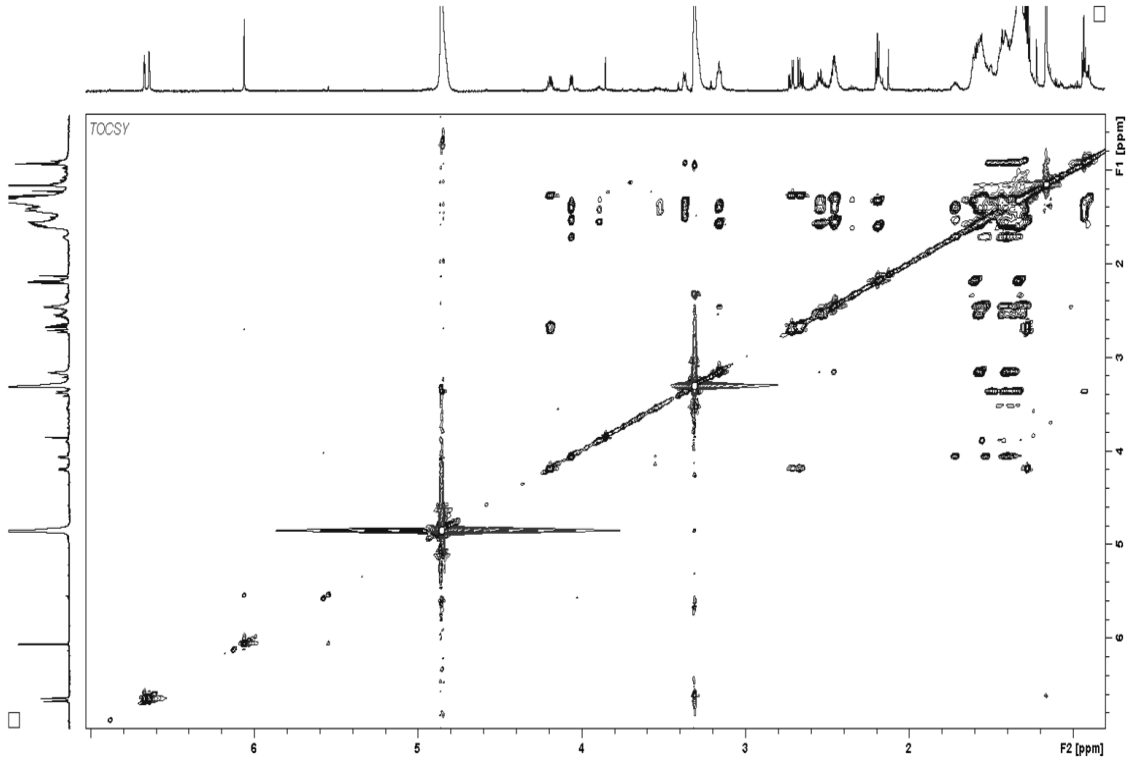

TOCSY spectrum of cystochromone D in $MeOD_4$ (700 MHz)

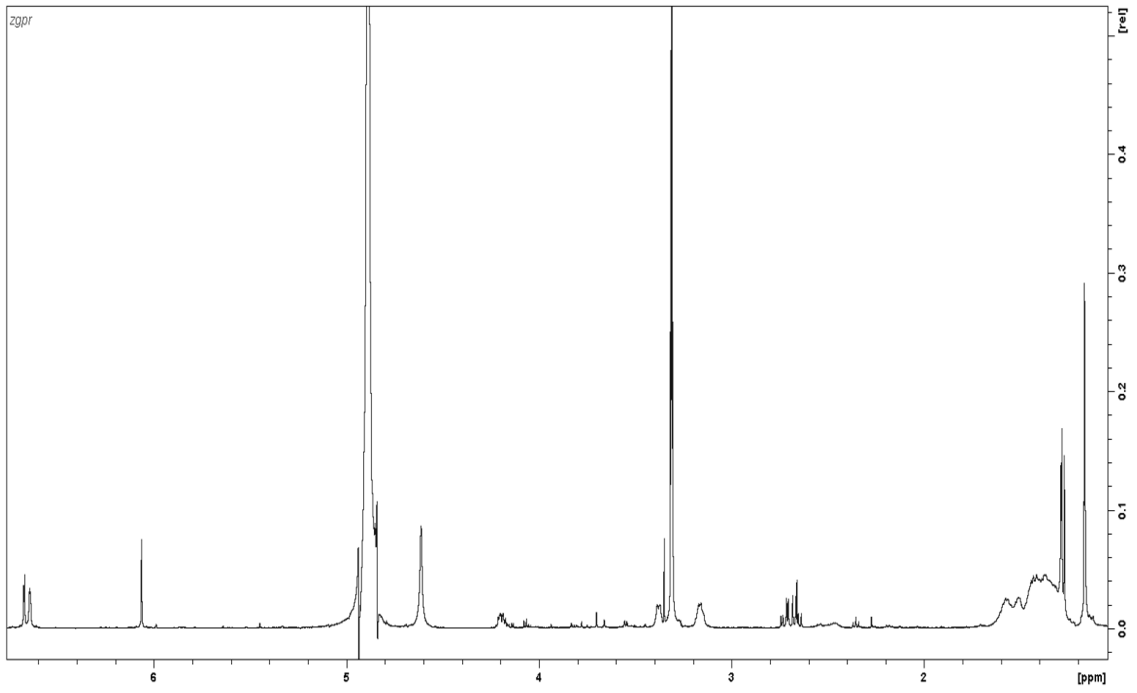

^{1}H-NMR spectrum of cystochromone E in $MeOD_4$ (500 MHz)

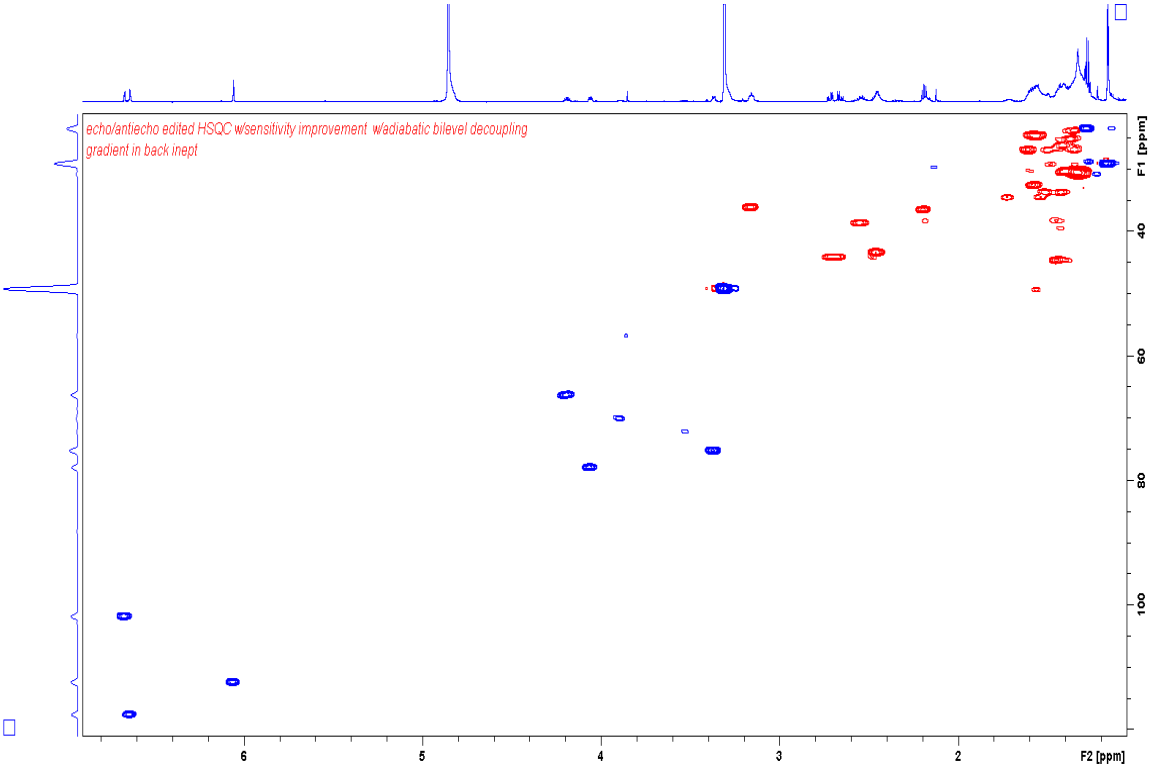

HSQC spectrum of cystochromone E in $MeOD_4$ (500 MHz)

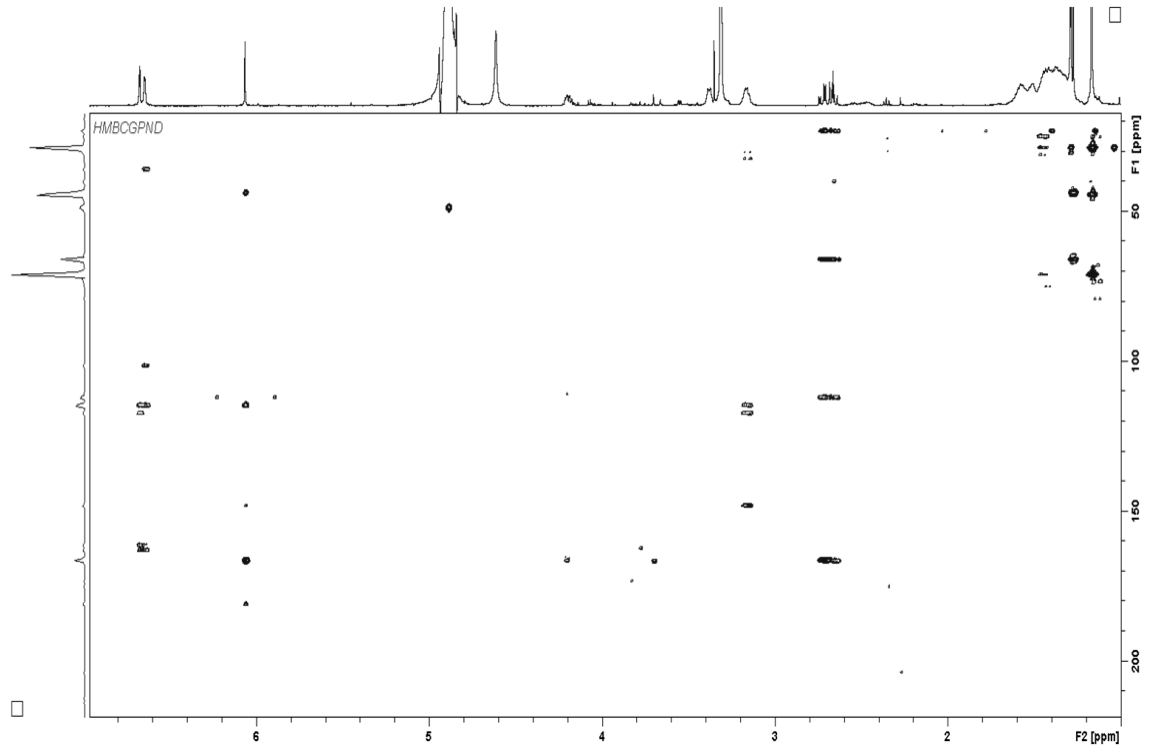

HMBC spectrum of cystochromone E in $MeOD_4$ (500 MHz)

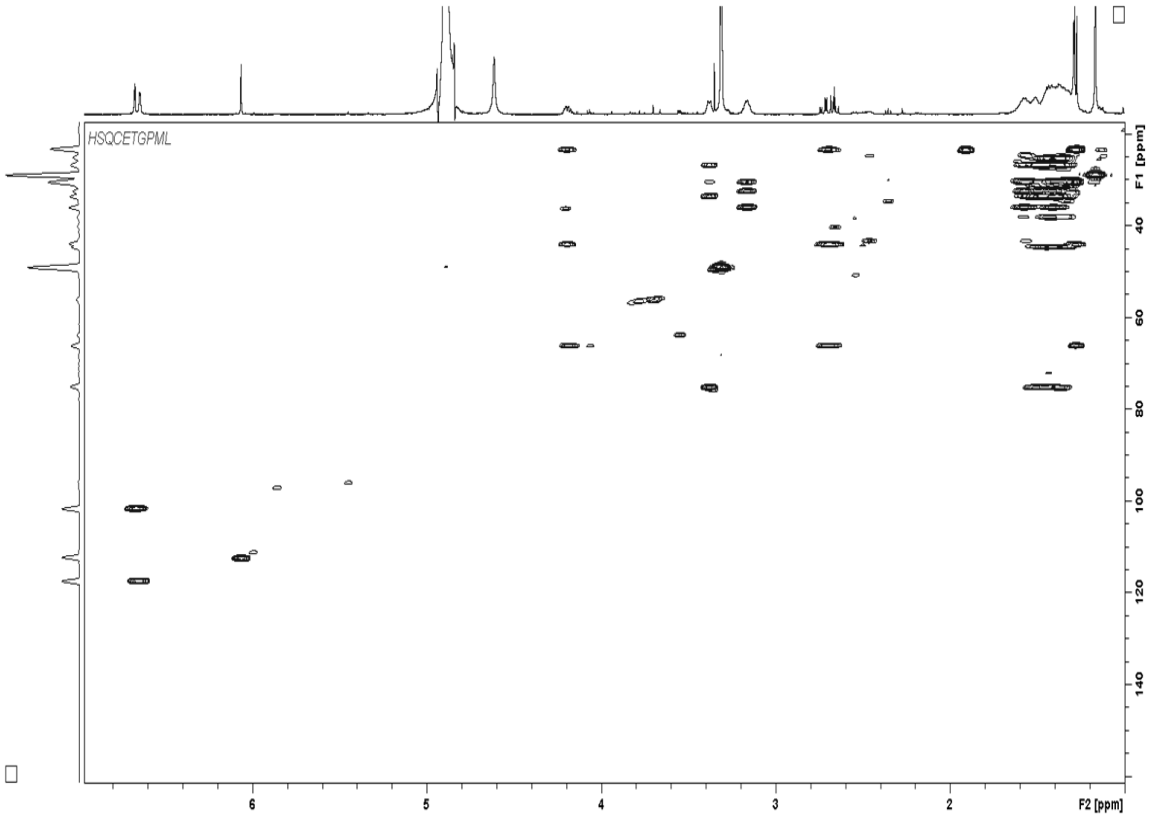

HSQC-TOCSY spectrum of cystochromone E in $MeOD_4$ (500 MHz)

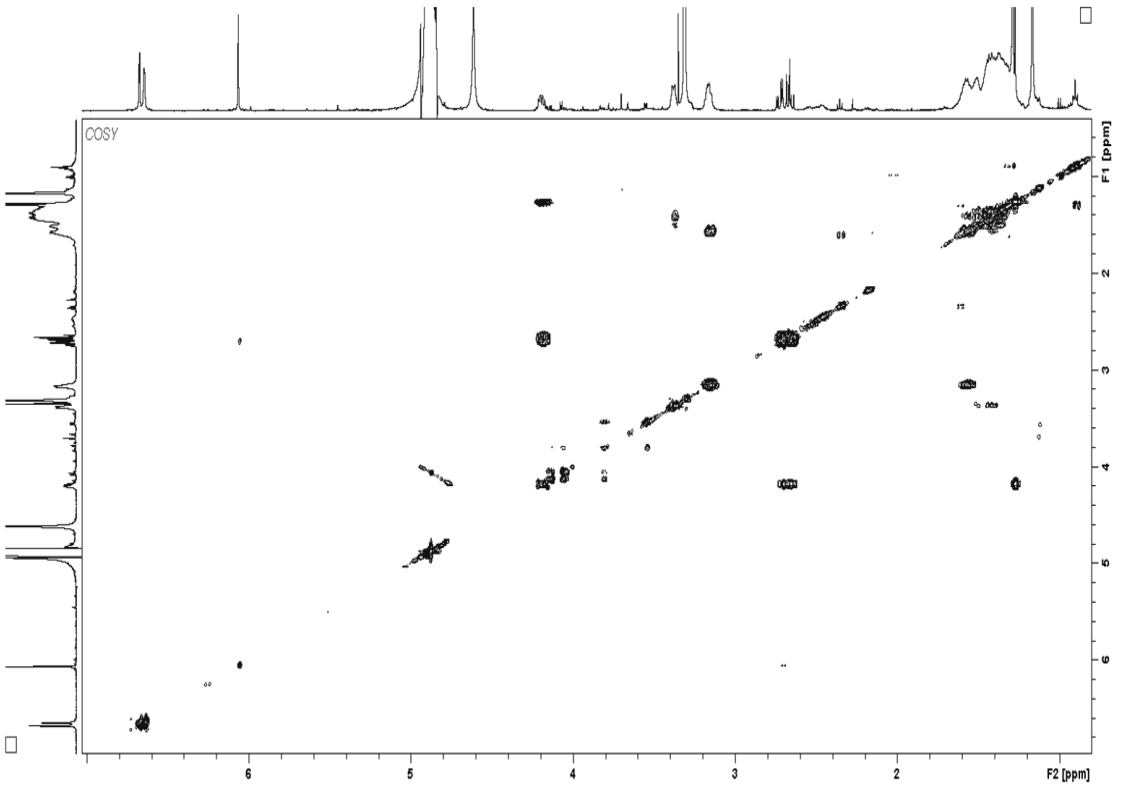

COSY spectrum of cystochromone E in $MeOD_4$ (500 MHz)

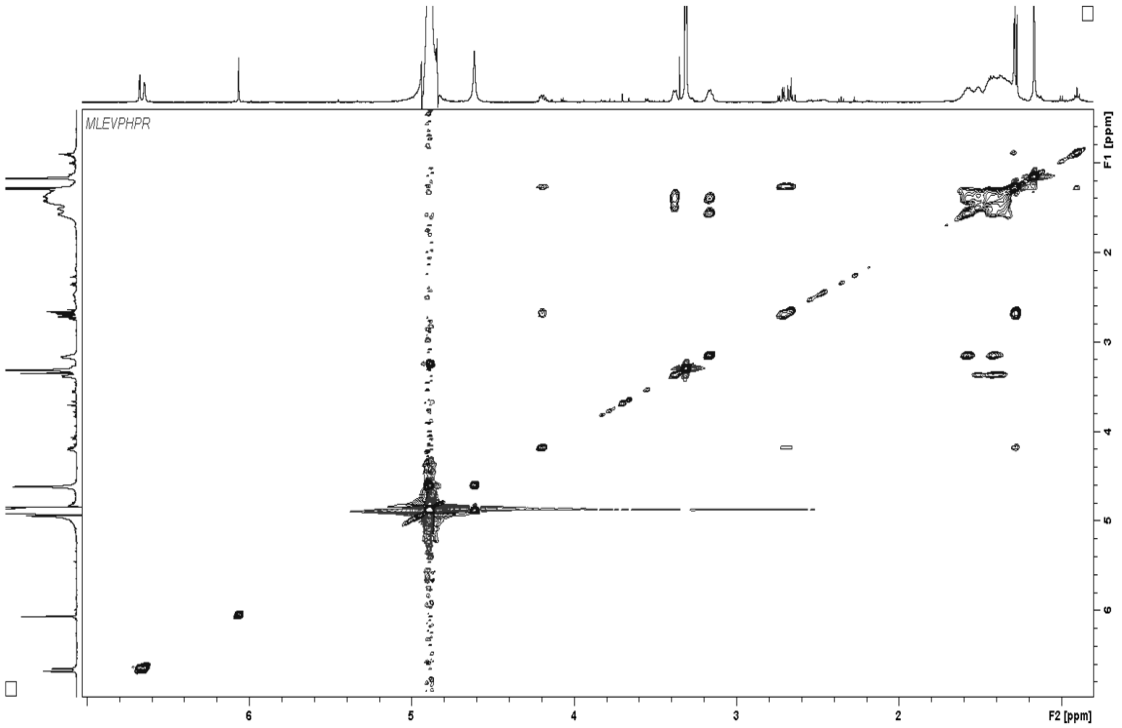

TOCSY spectrum of cystochromone E in $MeOD_4$ (500 MHz)

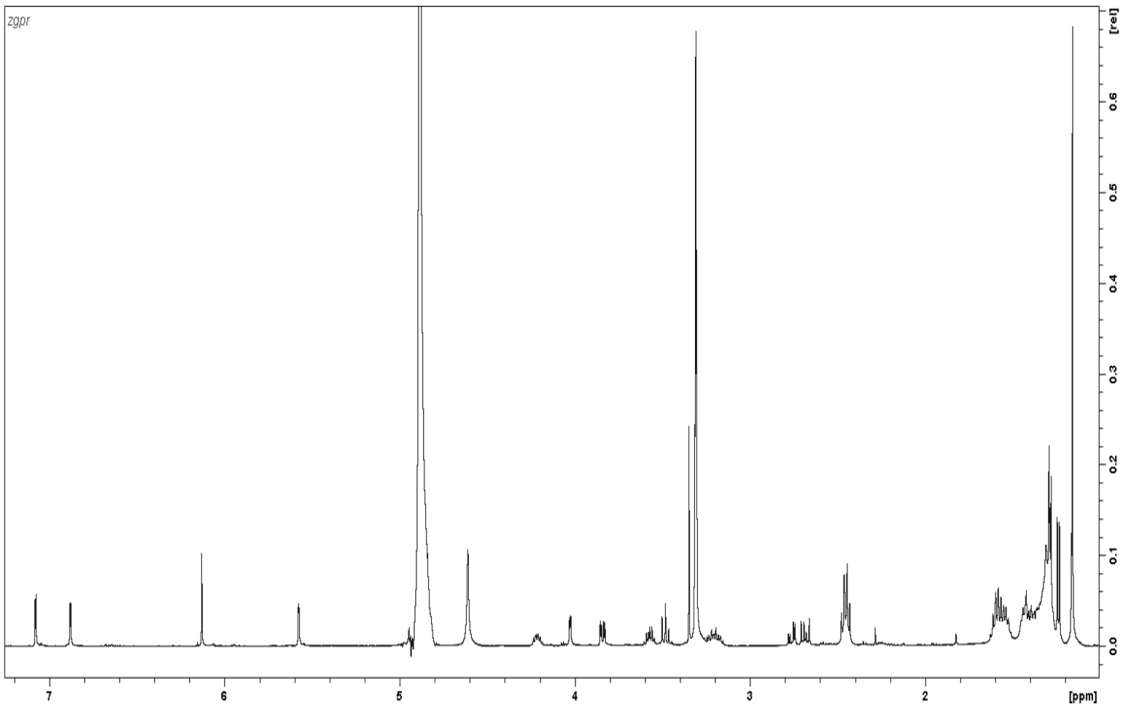

^{1}H-NMR spectrum of cystochromone F in $MeOD_4$ (500 MHz)

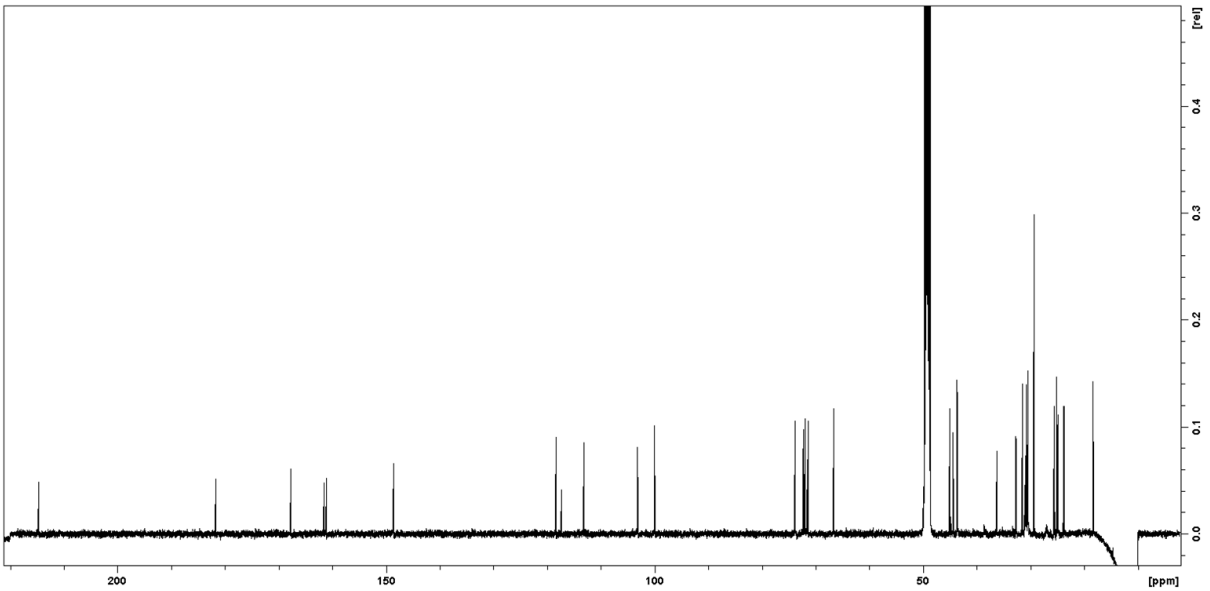

^{13}C-NMR spectrum of cystochromone F in $MeOD_4$ (500 MHz)

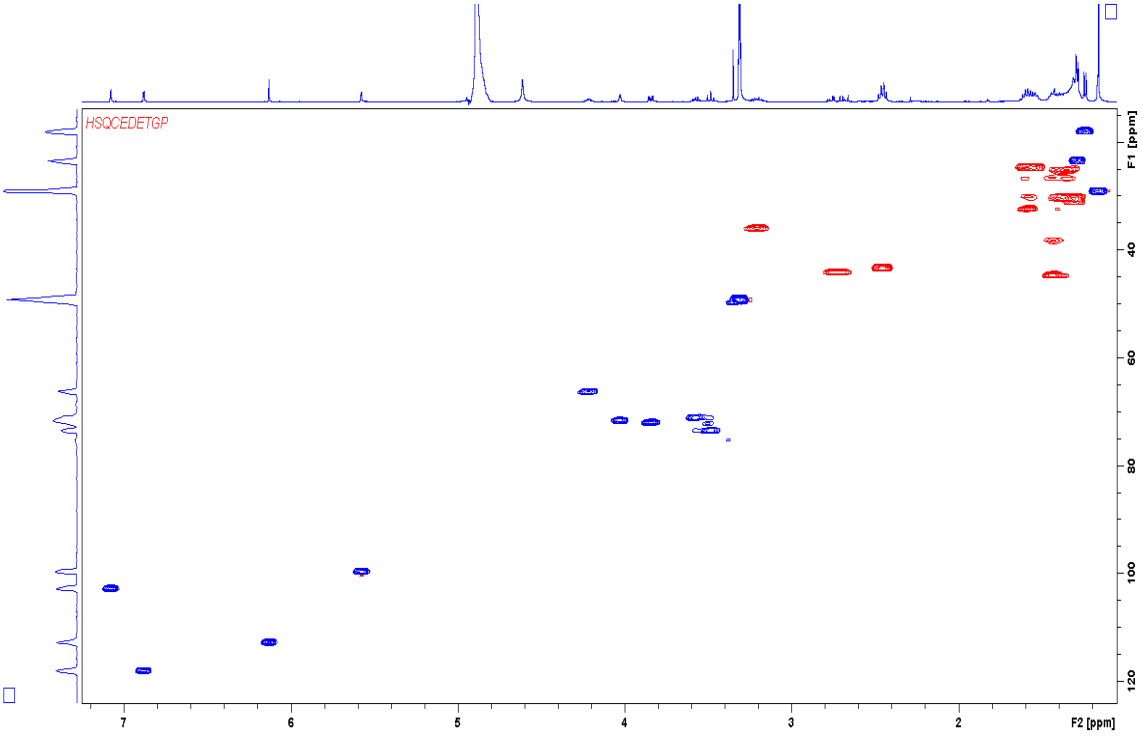

HSQC spectrum of cystochromone F in $MeOD_4$ (500 MHz)

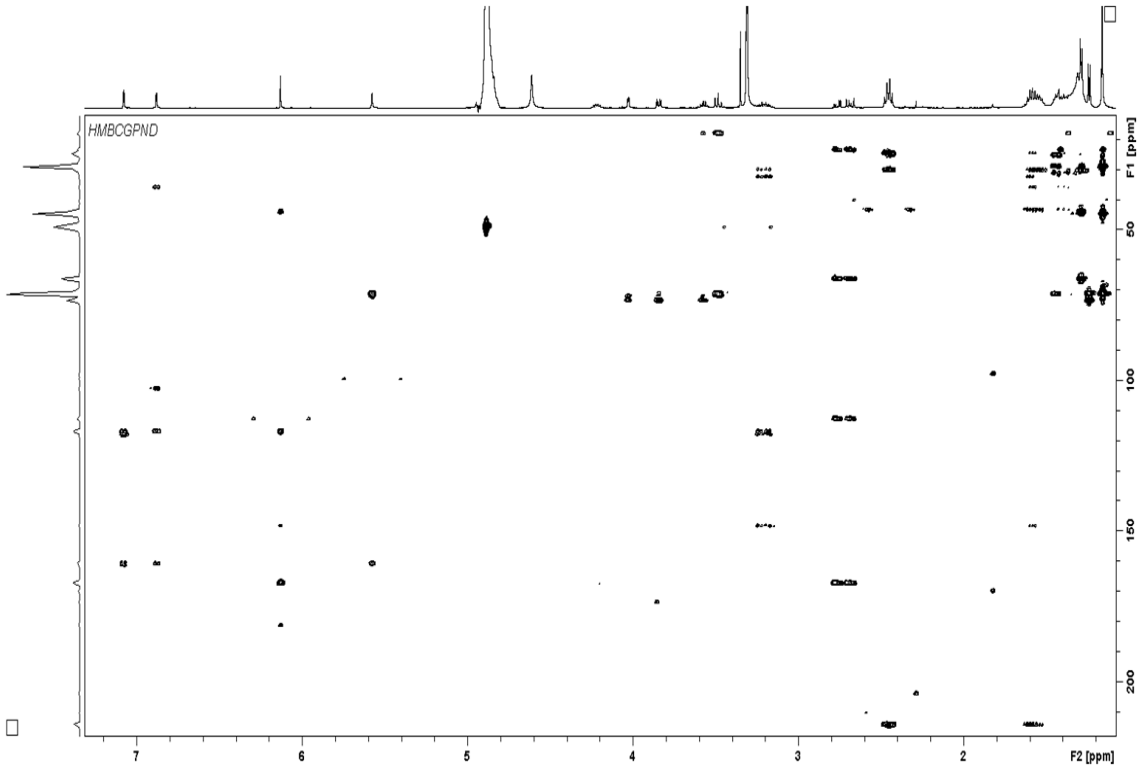

HMBC spectrum of cystochromone F in $MeOD_4$ (500 MHz)

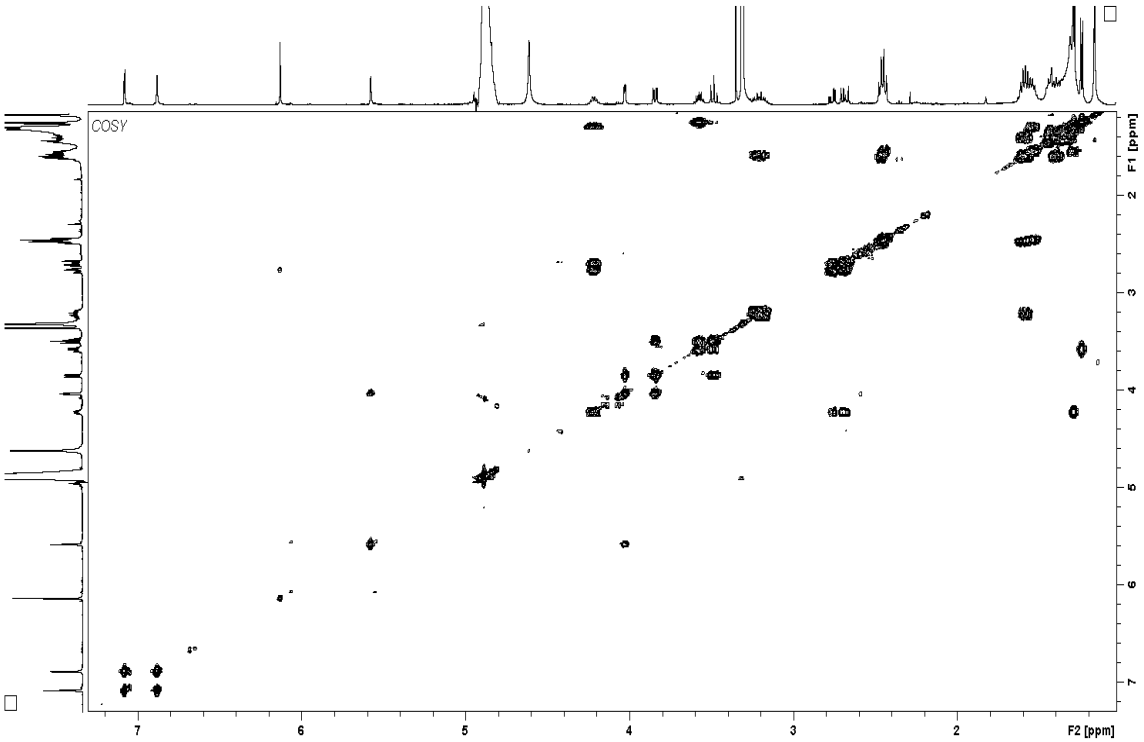

COSY spectrum of cystochromone F in $MeOD_4$ (500 MHz)

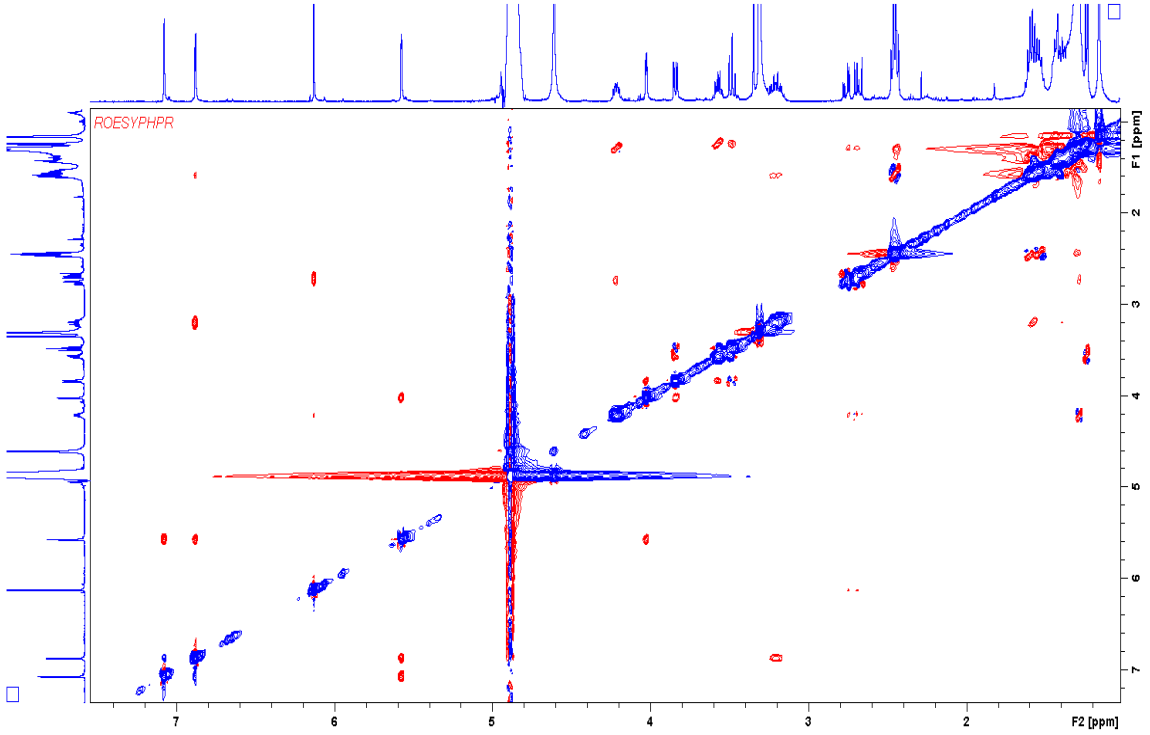

ROESY spectrum of cystochromone F in $MeOD_4$ (500 MHz)

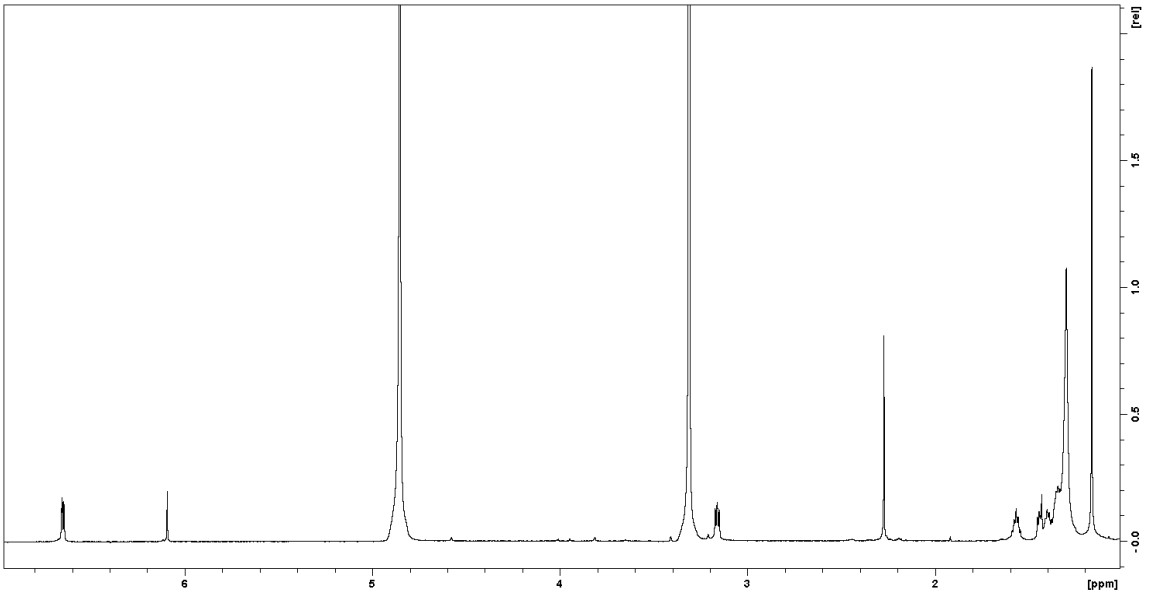

^{1}H-NMR spectrum of cystochromone G in $MeOD_4$ (700 MHz)

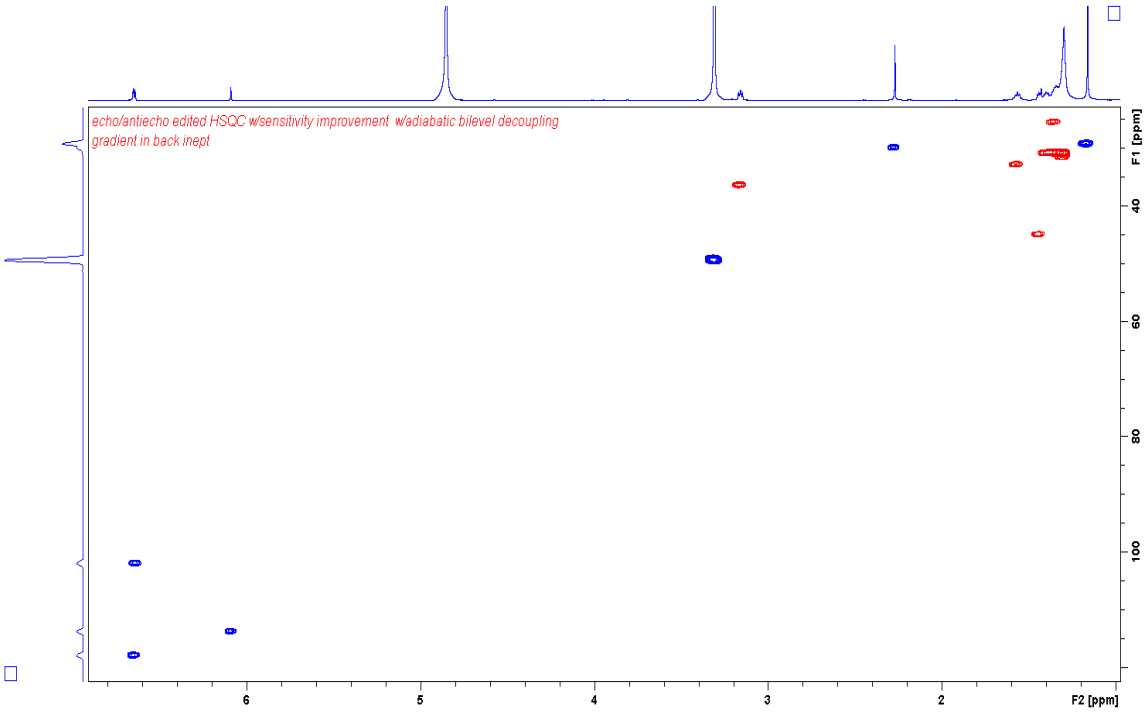

HSQC spectrum of cystochromone G in $MeOD_4$ (700 MHz)

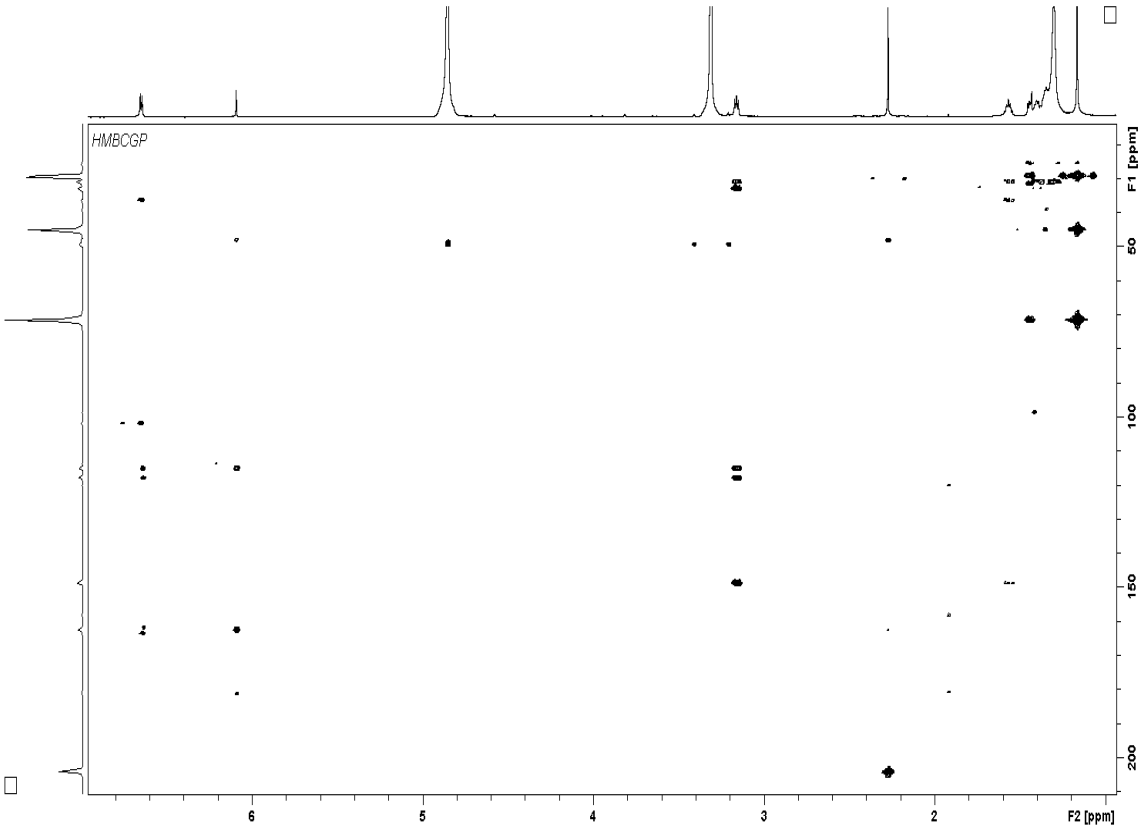

HMBC spectrum of cystochromone G in $MeOD_4$ (700 MHz)

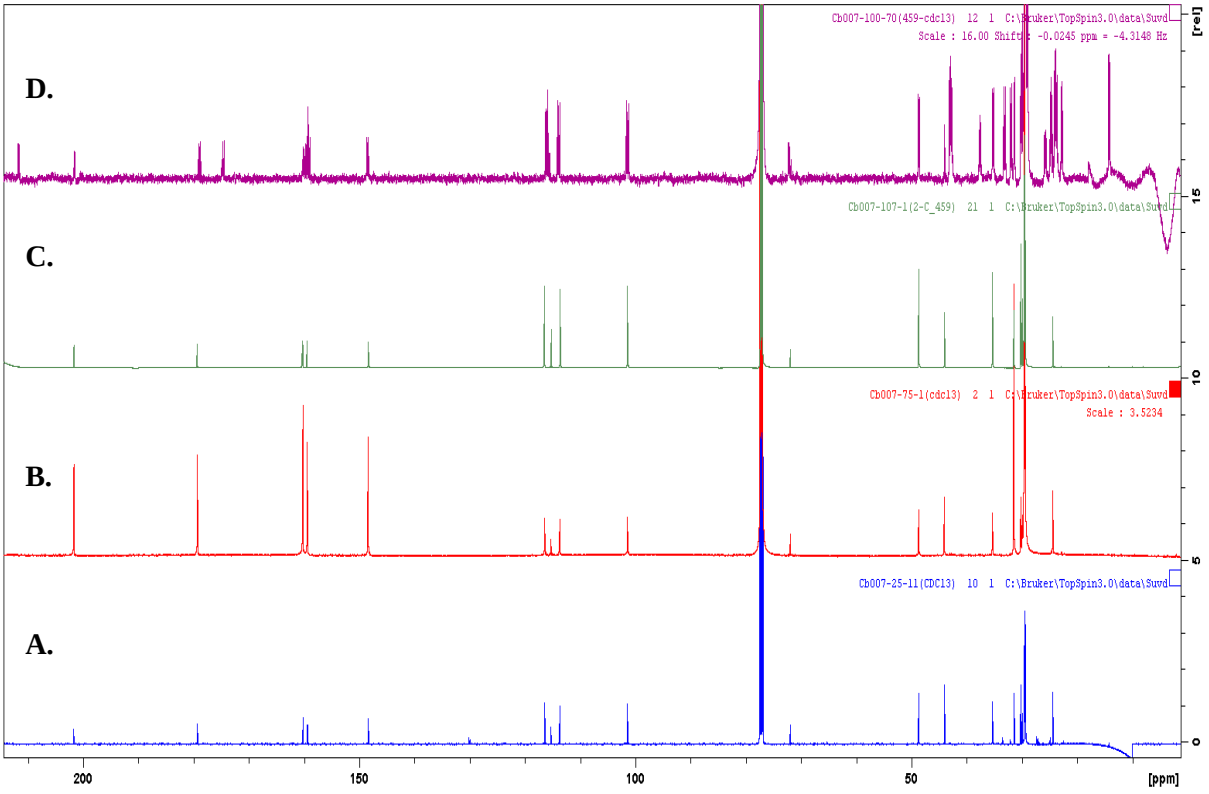

^{13}C-NMR spectrum of cystochromone A in $CDCl_3$enriched with a) non labeled, b) [1-^{13}C]-acetate, c) [2-^{13}C]-acetate and d) [1,2-^{13}C]-acetate (normalized with non-labeled signal at δ 44.1)

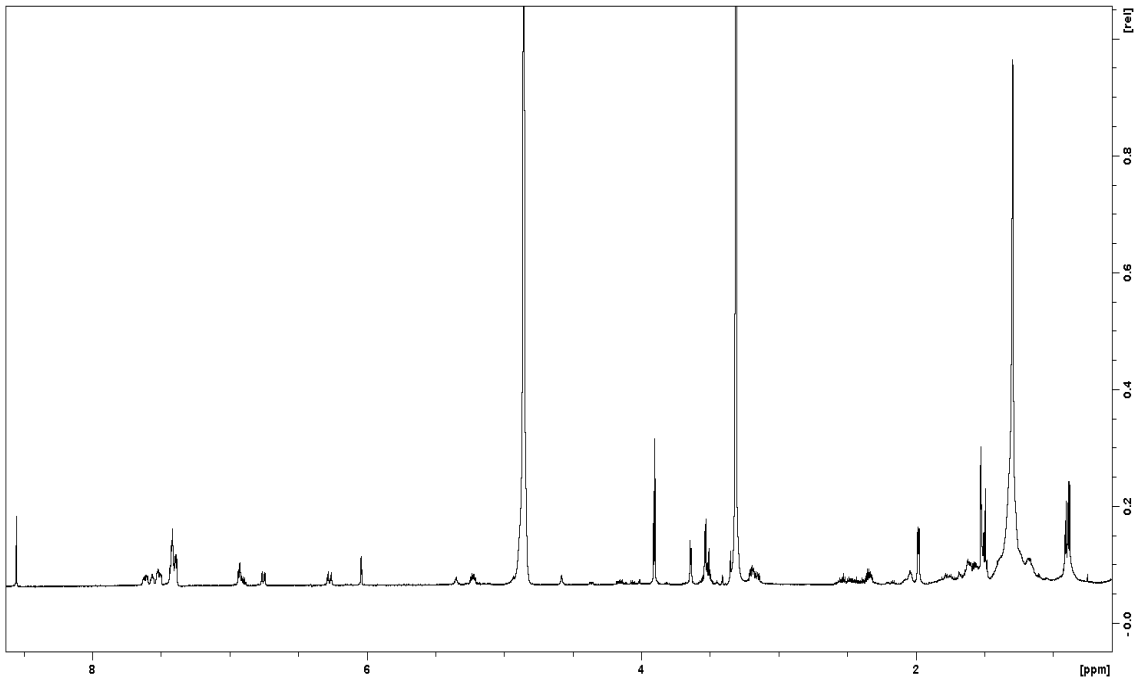

^{1}H-NMR spectrum of di-(*S*)-MTPA ester of 7-OMe-cystochromone D in $MeOD_4$ (700 MHz)

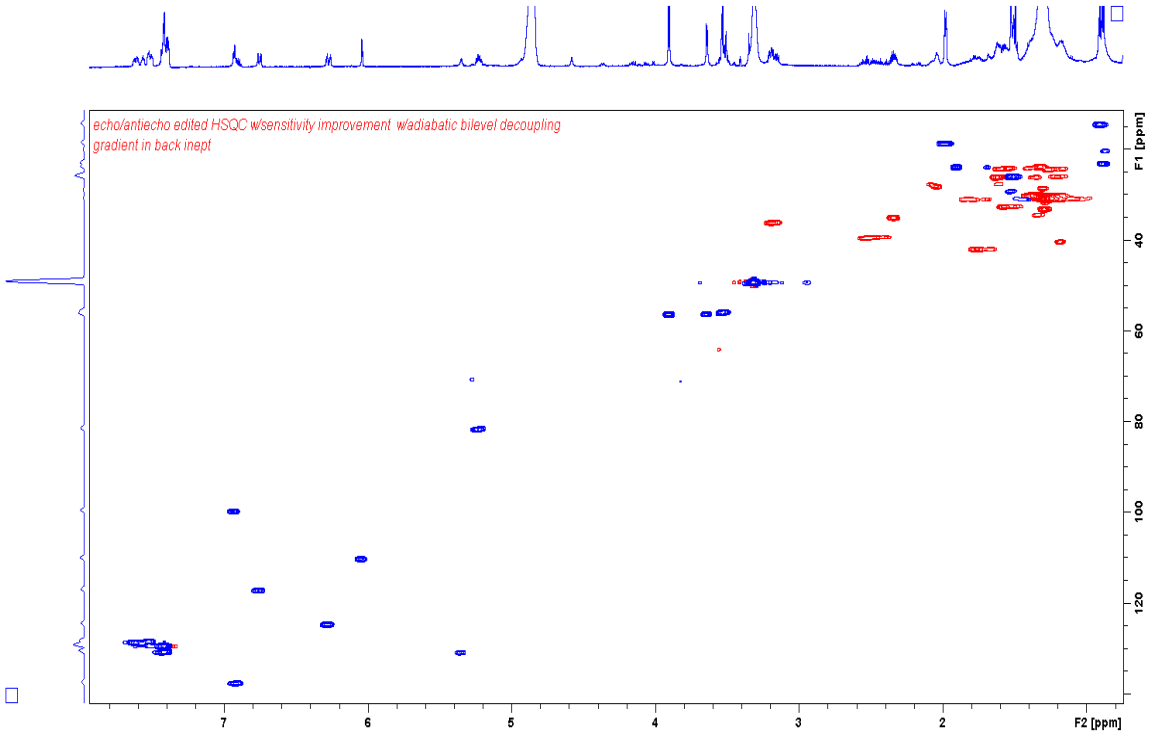

HSQC spectrum of di-(*S*)-MTPA ester of 7-OMe-cystochromone D in $MeOD_4$ (700 MHz)

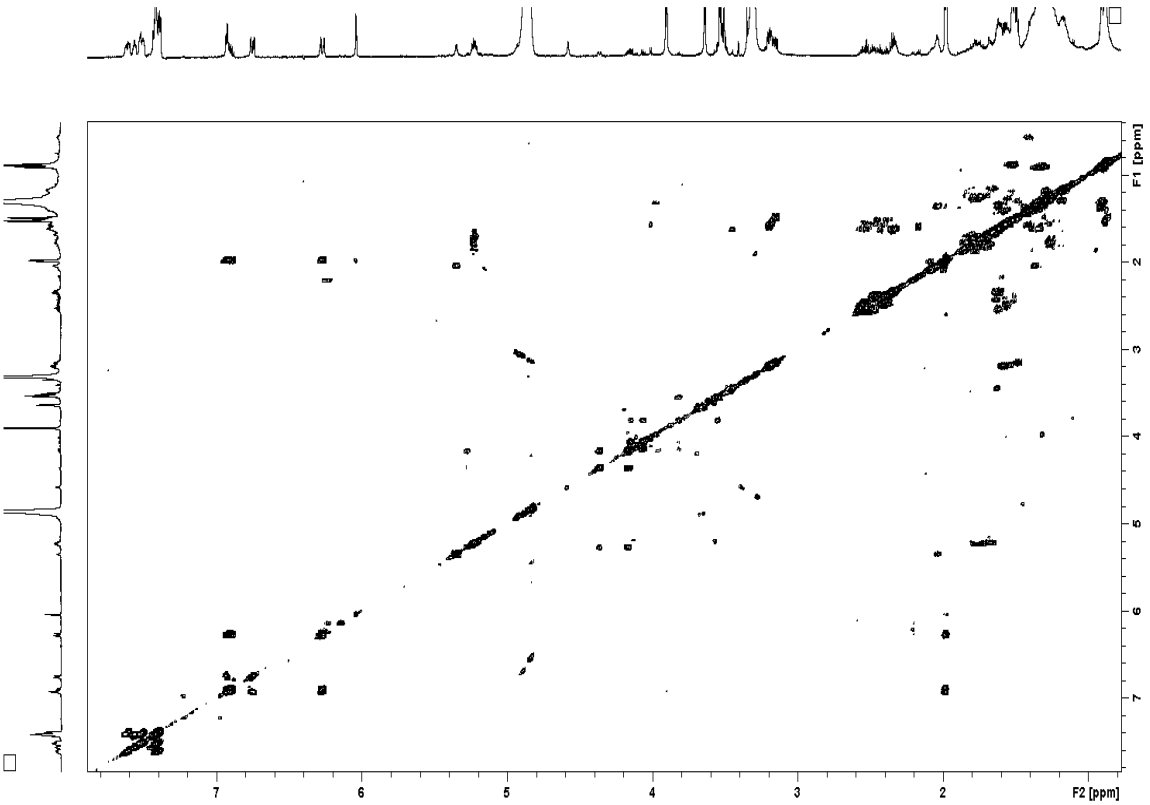

COSY spectrum of di-(*S*)-MTPA ester of 7-OMe-cystochromone D in $MeOD_4$ (700 MHz)

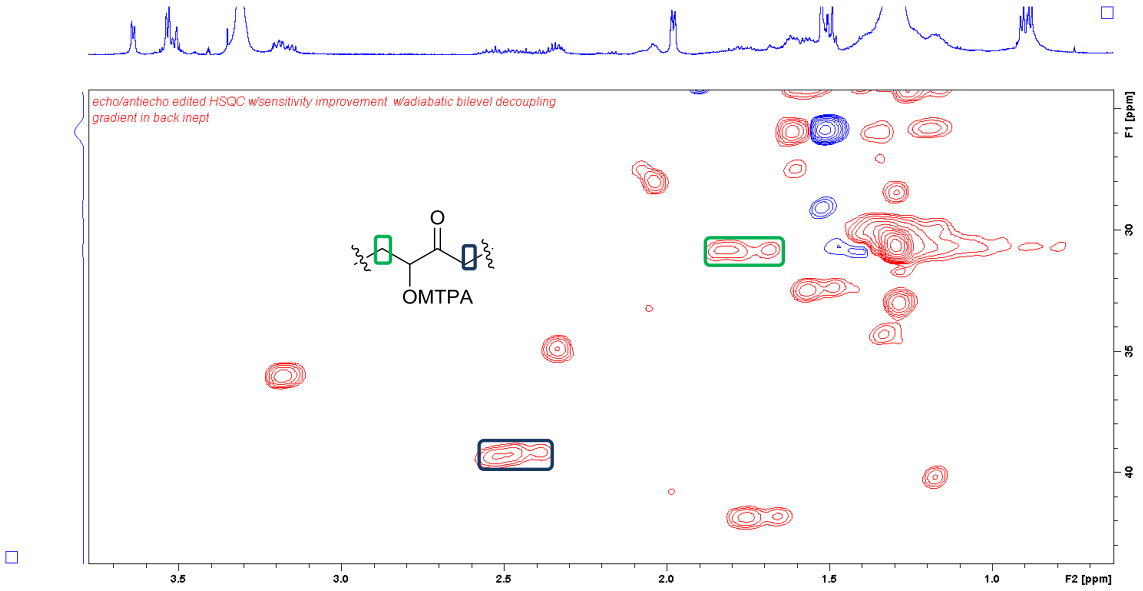

Expanded HSQC spectrum of di-(*S*)-MTPA ester of 7-OMe-cystochromone D showing two sets of methylene signals

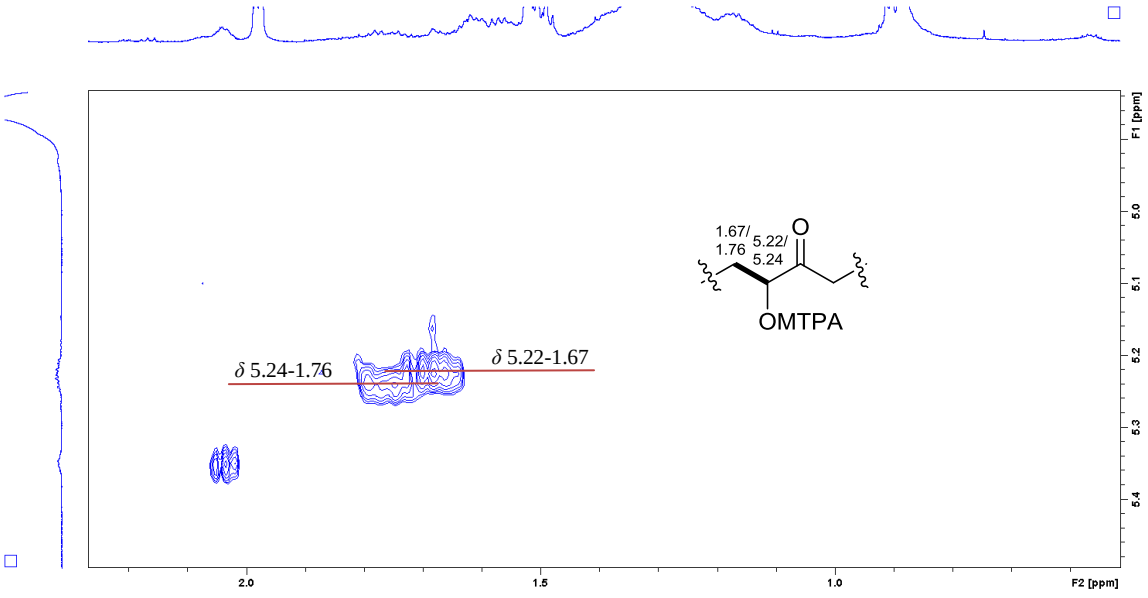

Expanded COSYspectrum of di-(*S*)-MTPA ester of 7-OMe-cystochromone D showing two sets of COSY correlations corresponding to single signal

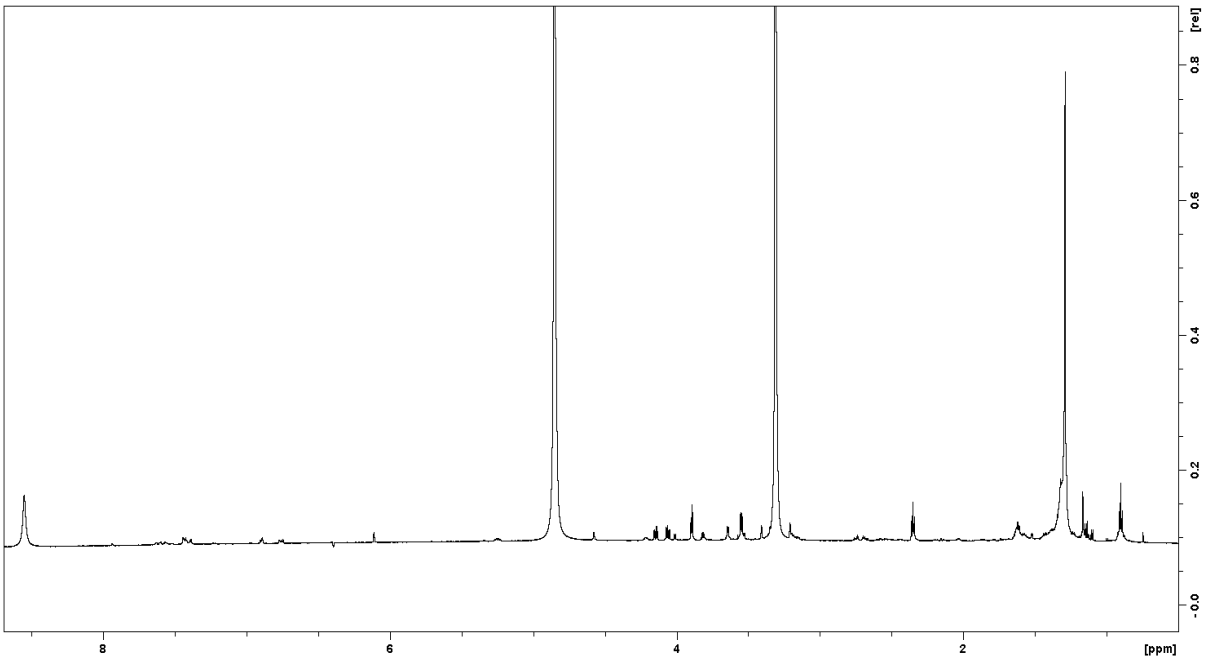

^{1}H-NMR spectrum of di-(*R*)-MTPA ester of 7-OMe-cystochromone D (**4a**) in $MeOD_4$ (700 MHz)

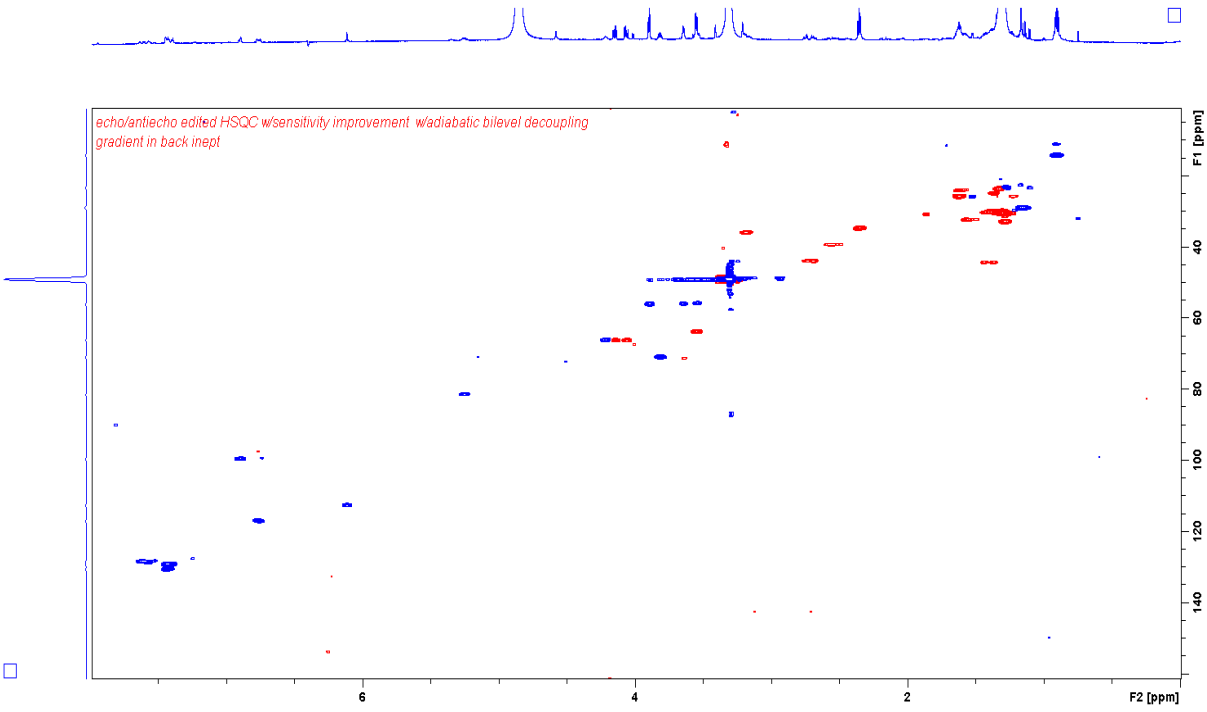

HSQC spectrum of di-(*R*)-MTPA ester of 7-OMe-cystochromone D (**4a**) in $MeOD_4$ (700 MHz)

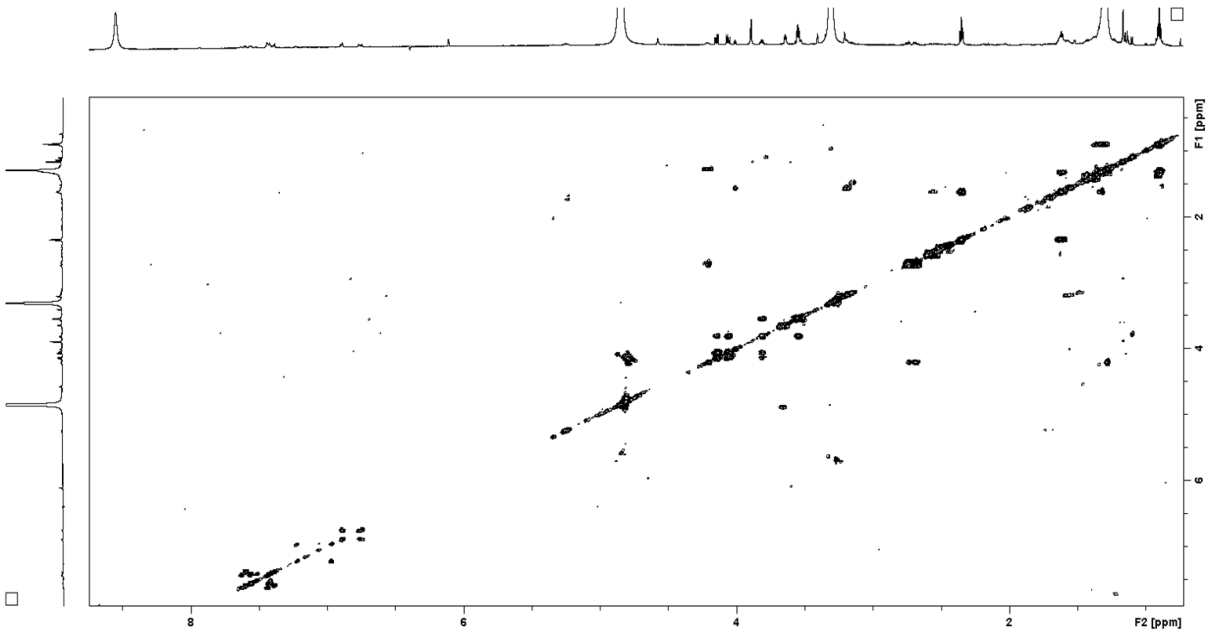

COSY spectrum of di-(*R*)-MTPA ester of 7-OMe-cystochromone D (**4a**) in $MeOD_4$ (700 MHz)